

Biological effects of iron-based nanomaterials evaluated from single species to complex microbial communities

PhD THESIS

May 2018

PhD student: MSc. **Nhung H. A. Nguyen**

Supervisor: RNDr. Alena Ševců, Ph.D.

Address: Studentská 1402/2
461 17 Liberec 1
Czech Republic
Tel: +420 485 353 612

Email: nhung.nguyen@tul.cz

Liberec, May 2018

Biologický účinek nanomateriálů na bázi železa na jednotlivé druhy mikroorganismů i na mikrobiální komunitu

Disertační práce

May 2018

Studijní program: P 3901 Aplikované vědy v inženýrství
Studijní obor: 3901 V055 Aplikované vědy v inženýrství

Autor práce: MSc. Nhung H.A. Nguyen
Školitel: RNDr. Alena Ševců, Ph.D

Liberec, May 2018

Preface

The study in this PhD thesis was performed at Faculty of Mechatronic, Informatics and Interdisciplinary Studies and most of laboratory work at the Institute for Nanomaterials, Advanced Technology and Innovation (CxI), Technical University of Liberec, and the Faculty of Science, department F.-A. Forel for Environmental and Aquatic Sciences, Université de Genève. It was conducted from February 2013 to March 2018 under the supervision of RNDr. Alena Ševců, Ph.D.

The thesis is framed in two parts: (1) an introductory review containing the main findings of my research (2) whole articles dealing with toxicity studies of iron-based materials. A list of all my publications with impact factor (IF) can be found [here](https://scholar.google.com/citations?user=JOKPmA4AAAAJ) (<https://scholar.google.com/citations?user=JOKPmA4AAAAJ>).

Toxicity studies of iron-based NMs/NPs

1. **Nhung H. A. Nguyen**, Roman Spanek, Vojtech Kasalicky, David Ribas, Denisa Vlkova, Hana Reháková, Pavel Kejzlar, and Alena Sevcu (2018). Different effects of nano-scale and micro-scale zero-valent iron particles on planktonic microorganisms from natural reservoir water. *Environmental Science: Nano*. DOI: 10.1039/C7EN01120B. **IF 6.047**
2. **Nhung H. A. Nguyen**, Nadia R. von Moos, Vera I. Slaveykova, Katrin Mackenzie, Rainer U. Meckenstock, Silke Thummler, Julian Bosch, and Alena Sevcu (2018). Biological effect of four iron-containing materials developed for nanoremediation on green alga *Chlamydomonas* sp. *Ecotoxicity and Environmental Safety*, 154, 36-44. **IF 3.743**
3. **Nhung H. A. Nguyen**, Mohamed S. A. Darwish, Ivan Stibor, Pavel Kejzlar, and Alena Sevcu (2017). Magnetic Poly(N-isopropylacrylamide) nanocomposites: Effect of preparation method on antibacterial properties. *Nanoscale Research Letters*, 12, 571-582. **IF 2.833**

4. Rune Hjorth, Claire Coutris, **Nhung H. A. Nguyen**, Alena Sevcu, Julian Alberto Gallego-Urrea, Anders Baun, and Erik J. Joner (2017). Ecotoxicity testing and environmental risk assessment of iron nanomaterials for sub-surface remediation – Recommendations from the FP7 project NanoRem. *Chemosphere*, 182, 525-531. **IF 4.208**

5. Mohamed S. A. Darwish, **Nhung H. A. Nguyen**, Alena Sevcu, Ivan Stibor, and Stoyan K Smoukov (2016). Dual-modality self-heating and antibacterial polymer-coated nanoparticles for magnetic hyperthermia. *Materials Science and Engineering: C*, 63, 88-95. **IF 4.164**

6. Mohamed S. A. Darwish, **Nhung H.A. Nguyen**, Alena Sevcu, and Ivan Stibor (2015). Functionalized magnetic nanoparticles and their effect on *Escherichia coli* and *staphylococcus aureus*. *Journal of Nanomaterials*, Article ID 416012, doi:10.1155/2015/416012. **IF 1.871**

7. Claire Coutris, **Nhung H. A. Nguyen** and Rune Hjorth (2015). Environmental impact of reactive nanoparticles - Dose reponse relationships, Matrix effects on Ecotox. Report number: EU 7th FP NanoRem, Project Nr. 309517, Deliverable 5.1. NANOREM - Nanotechnology for Contaminated Land Remediation.

Toxicity study of other NMs/NPs

8. Margarita Esquivel-Gaon, **Nhung H. A. Nguyen**, Mauro F. Sgroi, Daniele Pullini, Flavia Gili, Davide Mangherini, Alina Iuliana Prunad, Petra Rosicka, Alena Sevcu, and Valentina Castagnola (2018). *In vitro* and environmental toxicity of reduced graphene oxide as additive in automotive lubricants. *Nanoscale*, DOI: 10.1039/C7NR08597D. **IF 7.367**

9. **Nhung H. A. Nguyen**, Vinod Vellora Thekkae Padil, Vera I. Slaveykova, Miroslav Cernik, and Alena Sevcu (2018). Green synthesis of metal and metal oxide nanoparticles and their effect on the unicellular alga *Chlamydomonas reinhardtii*. *Nanoscale Research Letters*, Accepted 25.04.2018. **IF 2.833**

10. Petra Rosicka, **Nhung H.A. Nguyen**, Alena Sevcu, Tomas Lederer, and Miroslava Rysova (2016). Ecotoxicity of organometal halide perovskites tested on *Pseudomonas putida*. *Research and Application, NANOCON*, ISBN 978-80-87294-71-0, 606-611.
11. Stanisław Waclawek, Vinod Vellora Thekkae Padil, **Nhung H. A. Nguyen**, Jean-Francois Calais, Alena Sevcu, and Miroslav Cernik (2016). Behaviour of Ag and Si-Graphite nanomaterials in environmental and extreme conditions. *Research and Application, NANOCON*, ISBN 978-80-87294-71-0, 643-650.
12. Vinod Vellora Thekkae Padil, **Nhung H. A. Nguyen**, Rozek, Zbigniew, Sevcu, Alena, and Miroslav Cernik (2015). Synthesis, fabrication and antibacterial properties of a plasma modified electrospun membrane consisting of gum Kondagogu, dodecanyl succinic anhydride and poly (vinyl alcohol). *Surface and Coatings Technology*, 271, 32-38. **IF 2.589**
13. Vinod Thekkae Vellora Padil, **Nhung H. A. Nguyen**, Alena Sevcu, and Miroslav Cernik (2014). Properties of electrospun membrane composed of gum karaya, polyvinyl alcohol, and silver nanoparticles. *Journal of Nanomaterials*, Article ID 750726, 10 pages, 2015. doi:10.1155/2015/750726. **IF 1.871**

Declaration (Prohlášení)

Byl jsem seznámen s tím, že na mou disertační práci se plně vztahuje zákon č. 121/2000 Sb. o právu autorském, zejména § 60 – školní dílo.

Beru na vědomí, že Technická univerzita v Liberci (TUL) nezasahuje do mých autorských práv užitím disertační práce pro vnitřní potřebu TUL.

Užiji-li disertační práci nebo poskytnu-li licenci k jejímu využití, jsem si vědom povinnosti informovat o této skutečnosti TUL; v tomto případě má TUL právo ode mne požadovat úhradu nákladů, které vynaložila na vytvoření díla, až do jejich skutečné výše.

Disertační práci jsem vypracoval samostatně s použitím uvedené literatury a na základě konzultací se školitelem.

Současně čestně prohlašuji, že tištěná verze práce se shoduje s elektronickou verzí, vloženou do IS STAG.

V Liberci dne:

Podpis:.....

Acknowledgements

Introduction

In starting this section on acknowledgements, I would at the beginning like to thank the Technical University of Liberec in general term for allowing me the great opportunity to come to the Czech Republic and learn not only interesting academic but also important life lessons. Both types of learning have really changed my life in a positive way, and I always think that I have been very fortunate in coming so far in my personal and career development, especially when I compare my situation now with my earlier life in the Vietnamese countryside on my parents' smallholding. I come from a tropical climate, where the sun is shining and the climate hot all through the year, the very opposite of what I encountered on arrival in Liberec. It was very hard for me to adapt to a new climate, especially on arrival in the middle of winter, when it was $-23\text{ }^{\circ}\text{C}$ and mostly dark on the day I arrived. Moreover, the culture shock that I experienced in the following months was also an added problem in my new life in Liberec. Professionally, when I came to the Institute for Nanomaterials at TUL in 2013 I did not have any background neither in nanomaterials nor nanotoxicology. In addition, when I arrived at the institute in February 2013, I had to learn everything from scratch. I went through some pessimistic moments during this early time, but I had great support from all my colleagues, both academically and personally, and I was grateful for the opportunity given to me to learn and progress, and in personal terms I always reminded myself during this time that "where there's a will, there's a way".

And now after 5 years, I have to say that I am very happy to have come here because I have learned a lot of life lessons, got to know another country and culture, which I very much appreciate, and thanks to the university community, I have developed so much professionally and academically, and am now on the cusp of completing my post-graduate work in finishing this doctoral thesis. In the limited space available in this section on acknowledgements I cannot describe all the lessons I have learned and the experiences I have undergone, but as a result of my academic and personal journey I feel humble and grateful, and based on my experiences I would definitely now want to help others in their own academic and personal paths.

Individual acknowledgments

I owe enormous and ongoing gratitude to my supervisor, *Dr. Alena Ševců*. I feel grateful to her for having given me the opportunity to come and work in an academic environment. In addition, she opened the door for me to change my life, giving me the chance both to learn about a new scientific field and also a new culture. For the past five years, she has been a great and constant supporter and a person I feel comfortable working with. Additionally, my praise goes to *Prof. Miroslav Černík*, my ‘big boss’, who has also supported me, even though I have not worked directly with him.

During the years of undertaking this study, I have had the opportunity and pleasure of participating in various European projects, where I have attended project meetings, and met and become acquainted with many researchers. Moreover, I have also visited and worked in other laboratories. These opportunities have been instrumental to my research. I sincerely want to thank the people I have collaborated and co-authored with during this time. I own huge gratitude to *Prof. Vera I. Slaveykova* and my friend *Dr. Nadia R. von Moos* from Geneva University, who gave me the opportunity to learn a new method, flow cytometry. I would also like to express my thanks to *Mohamed S. A. Darwish* and *Dr. Vinod Vellora Thekkae Padil* at Technical University of Liberec, who provided me with materials/particles at the beginning of my study. Moreover, I would never forget *Dr. Katrin Mackenzie* from Helmholtz Centre in Germany, who gave me great advice on reacting to the reviewers’ comments. I also would like to thank to my new friend *Dr. David Ribas* from Catalonia University, who I met in a working project, who was always ready for cooperation. Moreover, I have to thank *Dr. Vojtěch Kasalický* from the Institute of Hydrobiology in the Czech Republic, who helped me to understand the first results in next-generation sequencing.

Next, I would like to thank all the kind people in the institute, who have helped me in practical conditions, such as advising me on how to survive the hard winters, translating Czech documents, especially my thanks to Ms. Milena Maryšková, who translated my thesis abstract. Additionally, they let me join in Czech activities, where I have learned about Czech culture. Moreover, my thanks go to all people in the lab, who have helped me to perform various small experiments whenever I asked them.

I would also like to express my thanks to various projects which have supported me during this study: NanoREM project from the European Union's 7th FR for research, technological development and demonstration under Grant Agreement no. 309517; FutureNanoNeeds project from the European 7th FP project (no 604602); Nanobiowat project from the Technology Agency of the Czech Republic (no. TE01020218), and the SGS from the Ministry of Education of the Czech Republic within the SGS project no. 21066/115 at the Technical University of Liberec.

As a special acknowledgement, I would like to give thanks to my parents, Yen and Cuc. They are my strength, and have always made me try harder and harder, and do my best to achieve a better life. They have always reminded me be a harmonized, kind and pleasant person to everyone, wherever I go.

Last, but not least, my gratitude goes to my partner John, who has supported me in all aspects without any hesitation or any conditions. He has corrected the English language of this thesis.

Thanks to everyone for your help and support, with my appreciation.

Nhung H. A. Nguyen

Liberec, May 2018

Summary

The first article on the toxicity of engineered nanomaterials (ENMs) was published in 2004, a time considered to be as the birth of nano(eco)toxicology. More than a decade later now, almost three thousand articles have been published on this topic, but challenges in this study field still remain. More and more studies are being produced with focus on (1) new released ENMs, (2) commercial ENMs, (3) understanding toxicity mechanisms, (4) getting closer to target application conditions, and (5) studying more about the composition of ENMs. Additionally, ENMs change their own properties and behaviour during exposure conditions, e.g. they agglomerate, aggregate, sediment, interact with biomolecules and change colour. The standard OECD methods for the toxicity assessment of chemicals have been adapted for the toxicity testing of ENMs. However, they are difficult to apply in realistic conditions. Therefore, seeking or employing appropriate methods in nano(eco)toxicology is still an urgent need.

This thesis summarises the impacts of iron-based nanomaterials (NMs)/nanoparticles (NPs), including functional magnetic (Fe_3O_4) and zero-valent iron (ZVI) NMs/NPs. The study not only contributes to the toxicity data of iron-based NMs/NPs, but also brings some new modified methods and employs advanced methods to the study of toxicity. A notable outcome was that my study moved from single microorganism strains to natural microbial communities.

First, functional Fe_3O_4 -based NMs/NPs were used for obtaining toxicity methods on a lab scale and on single bacterial strains. The particles/materials were functionalized for bio applications. The biological effects of these particles on microorganisms were applied to two single bacterial strains: Gram-negative *Escherichia coli* and Gram-positive *Staphylococcus aureus*. The basic methods were modified for Fe_3O_4 particle studies including bacterial growth rate, cell viability and morphology, as well as DNA damage. The growth rate method was the main method carried out in this study. It was a feasible, economic and less time-consuming method and gave useful data: growth inhibition or effective concentration (EC). Combining all methods was found to be the most efficient frame for interpreting the toxicity results. The negative effects of Fe_3O_4 materials were selected on types of chemical functionalized roots, bacterial strains, as well as synthesis methods.

Secondly, the toxicity study of iron zero-valent (ZVI) NMs/NPs was performed and deemed truly necessary because these NMs/NPs are put into the environment for various purposes. The ZVI particles have potential for the remediation of contaminated soil or groundwater or surface water

due to their strongly reactive properties. The ZVI particles were modified to improve their properties in *in situ* applications to effect lower aggregation, and higher mobility. The target microorganisms for my ZVI toxicity study were investigated (1) in lab conditions with particular soil Gram-negative *Pseudomonas putida* (under aerobic condition), Gram-positive *Clostridium perfringens* (anaerobic condition), and unicellular green alga *Chlamydomonas* sp., and (2) in *in-situ* conditions with natural microbial communities in freshwater and groundwater. The methods/endpoints involved the growth rate of bacteria/algae, viable bacteria, bacterial morphology, algal membrane integrity, ROS formation for lab scale and the effects on whole bacterial communities in freshwater. Notably, as far as is known this study was the first to apply next-generation sequencing to environmental samples.

Through this study I found that in terms of methods: (1) to be able to interpret the results correctly, it is necessary to carry out combined methods for toxicity; (2) it is more useful to select methods which apply from the lab to *in-situ* study. The functionalized Fe₃O₄ NMs/NPs showed more negative effects on Gram-positive compared to Gram-negative bacteria, and these effects depended on functional modifications as well as techniques of synthesis. The studied ZVI caused effects depending on their properties (size, shape, surface charge, modifiers) and the proportion of reactive Fe(0). ZVI had negative effects on anaerobic than aerobic bacteria in 24h in lab study. *Chlamydomonas* sp. was more sensitive to the ZVI after 2h compared to 24h. The ZVI effect was positive *in-situ* in a long-term experiment, which could indicate that the ZVI reduces concentrations of pollutants and thus facilitates bioremediation processes. The effects of ZVI in underground and reservoir water often showed toxicity at the beginning application and the ZVI concentration quickly decreased due to its reaction with existing organic compounds and oxygen in the water. The ZVI impact on natural microbial communities is thus low and shortlived.

Keywords: toxicity, nanomaterials, ZVI, functional Fe₃O₄-based materials, *Escherichia coli*, *Staphylococcus aureus*, *Chlamydomonas* sp., *Clostridium perfringens*, bacterial communities

Abstrakt

První článek o toxicitě syntetických nanomateriálů („engineered nanomaterials“, ENMs) byl publikován v roce 2004 a je považován za zrod nano(eko)toxikologie. Více než deset let poté vzniklo téměř tři tisíce publikací na toto téma. Stále více studií se zabývá (1) nově vytvořenými ENMs, (2) komerčně dostupnými ENMs, (3) porozuměním mechanismu jejich toxicity, (4) vytvořením podmínek pro jejich aplikace a (5) detailnějším studiem složení ENMs. Typickou vlastností ENMs je, že v průběhu testování toxicity mění své chování, tj. aglomerují, tvoří agregáty, sedimentují, interagují s biomolekulami a dochází ke změnám zabarvení prostředí. Standardní OECD metody pro stanovení toxicity chemických látek byly upraveny pro hodnocení ENMs, avšak je poměrně obtížné aplikovat tyto metody v reálných podmínkách, což je důvodem pro snahu najít lepší metody pro nano(eko)toxikologii.

Tato dizertační práce shrnuje dopady materiálů na bázi železa, konkrétně částic z magnetického Fe_3O_4 a nula-mocného železa („zero-valent iron“, ZVI), studiem toxicity těchto částic a zavedením některých nově modifikovaných a pokročilých metod. Důležitým výstupem této práce je přechod ze studia jednotlivých mikroorganismů k přirozeně se vyskytujícím mikrobiálním společenstvům.

Nejprve byly vybrány Fe_3O_4 materiály připravené pro bioaplikace, na nichž byly použity toxikologické metody laboratorního měřítka a to na jednotlivých bakteriálních kmenech. Biologický efekt těchto částic/materiálů byl sledován na dvou bakteriálních kmenech: gram-negativní *Escherichia coli* a gram-pozitivní *Staphylococcus aureus*. Základní metody modifikované pro Fe_3O_4 částice zahrnovaly stanovení rychlosti růstu, buněčné životaschopnosti, změny morfologie a poškození DNA. Metoda sledování rychlosti růstu byla stěžejní metodou především proto, že je snadno realizovatelná, levná a méně časově náročná ve srovnání s ostatními metodami, přičemž poskytuje užitečné informace o inhibici růstu a efektivní koncentraci („effective concentration“, EC). Kombinace všech metod poskytla velmi dobrý nástroj pro popis výsledků toxicity. Účinek Fe_3O_4 materiálů byl výsledkem typu jejich funkcionalizace, metody syntézy a vybraného bakteriálního kmene.

Dále byla sledována toxicita částic/materiálů z nula-mocného železa (ZVI), které je ve formě částic využíváno díky jejich vysoké reaktivitě pro remediaci znečištěné půdy, a podzemních nebo povrchových vod. Testované ZVI částice byly speciálně upravené pro *in situ* aplikace snížením tendence k agregování a zvýšením jejich mobility, přičemž jejich toxicita byla sledována na (1)

půdní gram-negativní *Pseudomonas putida* v laboratorních podmínkách (aerobně), gram-pozitivní *Clostridium perfringens* (anaerobně) a jednobuněčné zelené řase *Chlamydomonas* sp.; (2) *in situ* na přirozeně se vyskytujících mikroplanktonních společenstvech. Testovací metody zahrnovaly stanovení rychlosti růstu bakterií/řas, životaschopnosti a změny morfologie bakterií, membránové integrity řas, vznik reaktivních kyslíkových radikálů („reactive oxygen species“, ROS) a celkový vliv na bakteriální společenstva ve spodní a povrchové vodě. Nutno zdůraznit, že v této práci bylo na environmentálních vzorcích poprvé použito sekvencování příští generace.

Při výzkumu bylo dosaženo těchto znalostí z hlediska použitých metod: (1) pro stanovení toxicity je nutné kombinovat metody, aby bylo dosaženo správné interpretace získaných výsledků; (2) je lepší vybrat takové metody, které lze převést z laboratoře i na výzkum *in situ*. Fe_3O_4 materiály vykazovaly výraznější negativní efekt na gram-pozitivních bakteriích oproti gram-negativním, a to jak v důsledku funkčních modifikací, tak v důsledku technologie přípravy těchto materiálů. Působení ZVI částic záviselo na jejich vlastnosti a podílu reaktivního Fe(0). Navíc bylo v rámci 24 hodinového laboratorního experimentu zjištěno, že ZVI částice měly negativní efekt především na anaerobní bakterie. V případě dlouhodobého *in situ* experimentu ZVI částice prokázaly určitý pozitivní účinek, tím že snižují vysoké koncentrace polutantů a tím umožňují bioremediační procesy. Účinek ZVI v podzemní a zásobní vodě v počátku aplikace často ukazoval na jejich toxicitu, ale jelikož koncentrace ZVI rychle klesla díky reakcím s přítomnými organickými sloučeninami a přítomným kyslíkem, lze tvrdit, že jejich dopad na přirozeně se vyskytující mikrobiální komunity je velmi malý a spíše krátkodobý.

Key words: toxicita nanomateriálů, ZVI, Fe_3O_4 materiály, *Escherichia coli*, *Staphylococcus aureus*, *Chlamydomonas* sp., *Clostridium perfringens*, mikrobiální společenstva

Table of contents

Preface.....	3
Declaration (Prohlášení)	6
Acknowledgements.....	7
Summary	10
Abbreviations	15
1. Background and aims	16
2. Materials	19
2.1 Iron-based NMs/NPs.....	19
2.2 Microorganisms	21
3. Methods	23
4. Characterizations of NMs/NPs	24
5. Results and discussion	25
5.1 Lessons learnt from (nano)toxicity methods	25
5.2 Toxicity of iron-based NMs/NPs on single bacterial species (prokaryotic cells).....	27
5.3 Toxicity of iron-based NMs/NPs on unicellular alga (eukaryotic cells)	30
5.4 Effect of iron-based NMs/NPs on complex microbial communities	33
5.5 Behaviour of iron-based NMs/NPs in tested media.....	34
6. List of whole papers	36
Paper 1	36
Paper 2	50
Paper 3	60
Paper 4	72
Paper 5	80
Paper 6	89
Paper 7	100
7. Conclusions	108
8. References	114

Abbreviations

ENMs	engineered nanomaterials
ENPs	engineered nanoparticles
NMs	nanomaterials
NPs	nanoparticles
nZVI	nano zero-valent iron particles
mZVI	micro zero-valent iron particles
APTS	aminopropyltriethoxysilane
PEG	polyethylene glycol
TEOS	tetraethoxysilane magnetite
OA	oleic acid
PEI	polyethyleneimine
PEI-nC	polyethyleneimine-methyl cellulose
PNIPAAm	N-isopropylacrylamide
ORP	oxidation reduction potential
ROS	reactive oxygen species
AU	absorbance unit
OD	Optical density
QY	quantum yield
FCM	flow cytometry
PCR	polymerase chain reaction
qPCR	quantitative PCR
NGS	next-generation sequencing
EC	effective concentration
OECD	Organisation for Economic Co-operation and Development
ISO	International Organization for Standardization

1. Background and aims

Nanotechnology is the study of materials and particles in nanoscale. A nanomaterial is defined as a "natural, incidental or manufactured material containing particles, in an unbound state or as an aggregate or as an agglomerate and where, for 50 % or more of the particles in the number size distribution, one or more external dimensions is in the size range 1 nm-100 nm" (<https://ec.europa.eu/jrc/en/science-update/jrc-report-reviews-measurement-methods-nanoparticle-sizing>). The nanoscales of materials or particles that are engineered for purposed applications, are called engineered nanomaterials (ENMs). They have been found to have outstanding advantages due to their distinct properties. In parallel, there have been concerns about whether they pose potential risks to health and the environment.

In 2004, the first paper was published on the toxicity of ENMs (Oberdörster, 2004). At the same time, a major review of the opportunities and uncertainties of nanotechnologies (RS/RAE 2004) was released by the Royal Society and the Royal Academy of Engineering, which highlighted the potential risks to health and the environment that may arise from exposure to nanomaterials, especially nanoparticles (ISBN 0 85403 604 0, 2004). Therefore, this time marked the birth of ENM toxicity assessment.

In a pool of new ENMs, iron-based materials, including magnetic (Fe_3O_4) and ZVI materials, have attracted a high level of interest because of their merits: easy and cheap synthesis. In particular, magnetic iron oxide particles have been employed in an increasing number of applications (Ali et al., 2016; Mohammed et al., 2017) because of their biocompatibility, superparamagnetic behaviour and chemical stability, which are primarily suitable for biological and biomedical applications (Liu et al., 2013; Mahdavi et al., 2013). The magnetic particles also show as adsorbents in water treatment, providing a convenient approach for separating and removing the contaminants (metals) by applying external magnetic fields (Carlos et al., 2013). ZVI has great reactivity, and has been used for cleaning up a wide range of contaminants in soil and groundwater, including metals, non-metal inorganic species, halogenated aliphatics, halogenated aromatics and other organic compounds (Yan et al., 2013; Mueller et al., 2012; Ševců et al., 2017; Němeček et al., 2015). On the other hand, iron materials/particles need to improve their properties by functionalizing or synthesizing for desired utilizations (Li et al.,

2006; Blaney, 2007; Yan et al., 2013; Ribas et al., 2016; Waclawek et al., 2017).

With an increasing number of applications being conducted with iron-based, engineering aspects related to their functions, the toxicological impacts of iron materials have received increasing attention. The toxicity of the materials depends on (1) their characteristics, such as chemical composition, size, shape, modification, life stage; (2) exposure conditions regarding sterilized nutrient medium, natural environmental medium, temperature, pH; (3) the behaviour of materials in exposure conditions: aggregation, agglomeration, sedimentation and interaction with organic compounds; (4) the studied (micro)organisms on different trophic levels: for example, bacteria, algae, plants, animals, or whole communities; (5) the accuracy of the methods; and (6) the chosen endpoints. Therefore, the study of material toxicity should take all of these issues into account.

Tests on single strain bacteria, algae, earthworms, plants, fish have often been carried out in lab scale in a variety of growth media and have been one of the most common strategies in the field of nanomaterial toxicity assessment. These studies are often based on standard methods (OECD, ISO) and are very important for setting up modified or new methods, more appropriate for nanomaterials.

A complex microbial community in a natural environment can be studied to evaluate the toxicity of nanomaterials in environmental applications and during accidental spills. There have been several studies on ZVI impacts on soil or groundwater microbial communities (Fajardo et al., 2012; Nguyen et al., 2018). These studies are more complex because many factors in natural conditions are involved, such as organic compounds, pH, oxygen concentration, redox potential amongst others.

Overall, the assessment of nanomaterials toxicity is still urgently needed due to the increasing use of nanomaterials in synthesis and applications. In particular, iron-based materials have great properties and a wide range of applications from biological sciences and medicine to the environment. In parallel, the nanotoxicity study of iron-based materials is challenging because their properties change depending on the exposure scenarios.

The biological effects of iron-based NMs/NPs in this study are addressed in line with the aims of this thesis, which are listed below and illustrated in Figure 1.

- Establishing suitable toxicity methods depending on the target microorganisms and environment (papers 1 to 7).

- Comparing the toxicity of Gram-negative and Gram-positive bacteria (prokaryotic cells) through various biological endpoints such as growth rate, viability, morphology and DNA integrity (Papers 3, 5, 6).
- Studying the toxicity of algal *Chlamydomonas* sp. (eukaryotic cells) by different endpoints such as algal growth rate, membrane integrity, ROS formation and photosynthesis efficiency (Papers 2, 4, 7).
- Studying the toxicity of microbial communities in natural freshwater, namely Harcov reservoir water, utilizing a range of different methods from cultivation to next-generation sequencing (Paper 1).

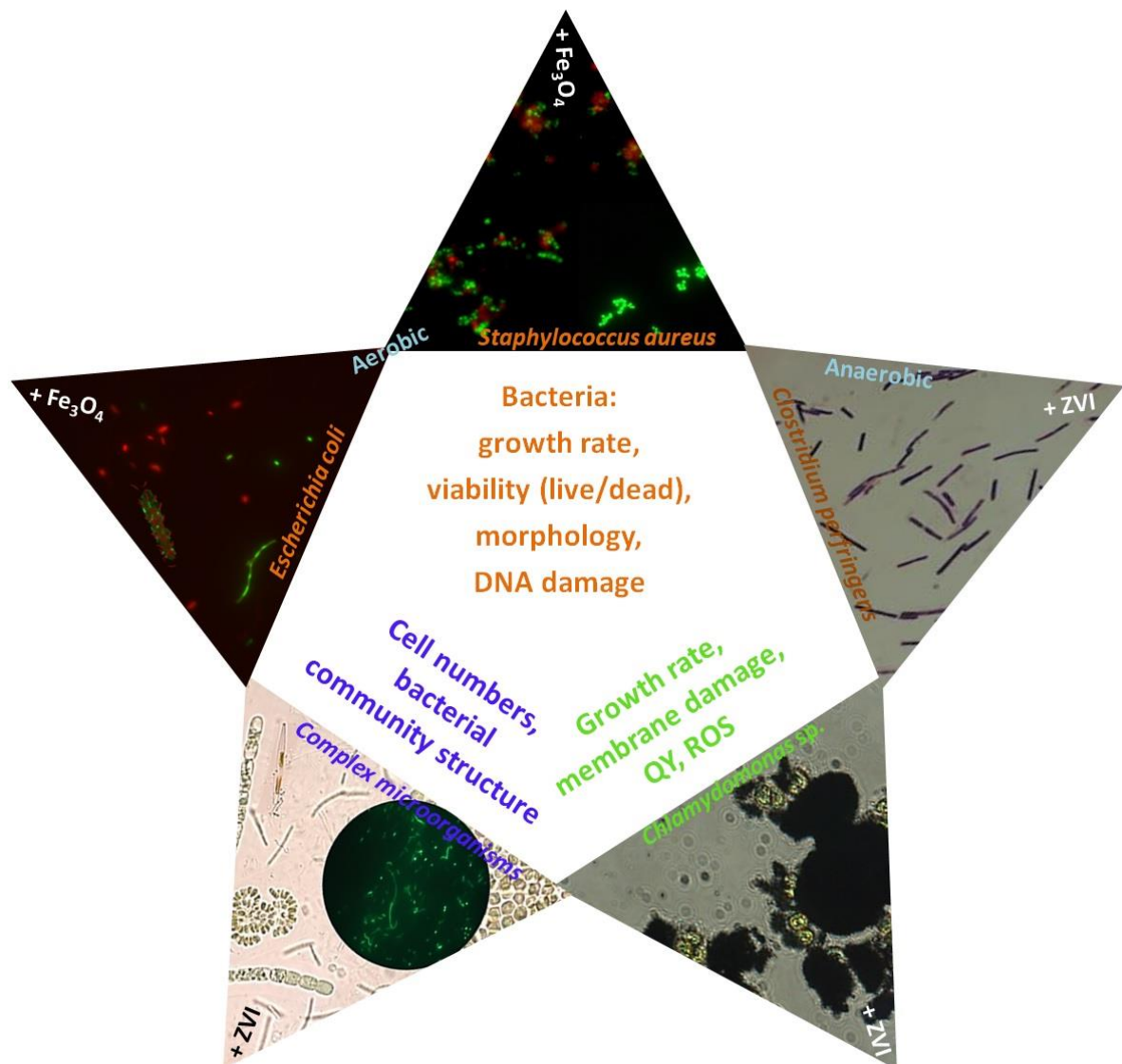


Figure 1: Summary of the study of the impacts of iron-based NMs/NPs on microorganisms in this thesis.

2. Materials

2.1 Iron-based nanomaterials/nanoparticles

Table 1 summarises the iron-based NMs/NPs tested in this study. They can be divided into two groups: (1) functionalized Fe_3O_4 particles/materials, which were synthesised for bio applications and where the research aimed to describe their biological effects or antibacterial properties; (2) modified ZVI particles of different sizes, which were used for cleaning contaminated soil and groundwater and where the focus was on single microorganisms commonly present in the environment and on the natural microbial community present in reservoir water.

The functionalized Fe_3O_4 particles were synthesized by Dr. Darwish, a postdoctoral researcher at the Technical University of Liberec. The Fe_3O_4 NMs/NPs were produced and functionalized by different methods to achieve the best functionalized Fe_3O_4 NMs/NPs. This internal cooperation resulted in papers 3, 5 and 6.

Part of the ZVI NMs/Nps was provided by the NanoREM project partners. These were synthesised to unlock the potential of nanoremediation in soil and groundwater (<http://nanorem.eu/>). The ZVI particles were obtained from UVR-FIA (Germany), GmH-UFZ (Germany) and the University of Duisburg-Essen (Germany). This international cooperation led to joint papers number 2, 4 and 7. The nZVI and mZVI particles were provided by Dr. Ribas from the Technical University of Catalonia (Spain) and Hepure Technologies (USA), respectively. These particles were aimed at application in environmental remediation. This cooperation contributed to paper 1.

Table 1. Summary of all iron-based NMs/NPs used in this study.

Materials	Properties	Article No.
Functionalized Fe₃O₄ NMs/NPs		
APTS-Fe ₃ O ₄ , PEG-Fe ₃ O ₄ , TEOS-Fe ₃ O ₄	APTS PEG TEOS	6
OA-MNP, PEI-MNP, PEI-mC-MNP	OA PEI PEI-mC	5
Fe ₃ O ₄ -PNIPAAm-1, Fe ₃ O ₄ -PNIPAAm-2, Fe ₃ O ₄ -PNIPAAm-3	PNIPAAm synthesized by different methods: (1) emulsion polymerization, (2) <i>in-situ</i> precipitation, (3) physical addition.	3
Iron-based NMs/NPs		
FerMEG12 (Milled-Fe)	Fe(0) \approx 80 wt%, <40 μ m, <100 nm thick, 13 – 18 m ² /g, Flakes	2, 4, 7
Carbo-Fe [®]	Fe ⁰ \approx 20%, Fe _{total} = 30.3 wt%, AC _{total} = 55%, \sim 1 μ m, 550 - 650 m ² /g, sphere-like fragments	2, 4, 7
Trap-Ox [®] Fe-Zeolite	Si = 38%, Al = 1.8%, Fe(II/III) = 1.3% , spheres	2, 4, 7
Fe-oxide (Nano-Goethite)	Fe(III) \approx 60%, humic acid coated, 400 nm, 135 m ² /g, sphere-like fragments	2, 4, 7
nZVI	Fe(0) \approx 74%, C = 2.7%, iron oxide = 23.3%, \sim 100 nm, 29.6 m ² /g	1
mZVI	Fe(0) \approx 95%, C = 1.8%, \sim 4 μ m, 0.487 m ² /g	1

2.2 Microorganisms

The microorganisms were selected depending on the target NMs/NPs applications. The microorganisms were maintained in growth media and conditions specified by the providers' guidelines. The Gram-negative and Gram-positive bacteria *E. coli* and *S. aureus* were used for testing the toxicity of Fe₃O₄ NMs/NPs due to their use in bio applications (papers 3, 5 and 6). Gram-negative *P. putida*, Gram-positive *C. perfringens* and green unicellular alga *Chlamydomonas* sp. were used for testing the toxicity of ZVI NMs/NPs, which are applied in environmental remediation (papers 2, 4, and 7). The complex microbial community in reservoir water was chosen to compare the nano- and microscale effect of ZVI particles (paper 1). Details of the studied microorganisms are shown below as Table 2.

Table 2. Summary of microorganisms used in this study

Microorganisms	Characteristics, source	Growth conditions	Article No.
Bacteria (Prokaryotic cells)			
<i>Escherichia coli</i> (<i>E. coli</i>)	Gram-negative, CCM 3954	Aerobic, 37°C, soya broth medium	3, 4, 5, 6
<i>Staphylococcus aureus</i> (<i>S. aureus</i>)	Gram-positive, CCM 3953	Aerobic, 37°C, soya broth medium	3, 5, 6
<i>Pseudomonas putida</i> (<i>P. putida</i>)	Soil, Gram-negative, CCM 1977	Aerobic, 27°C, soya broth medium	7
<i>Clostridium perfringens</i> (<i>C. perfringens</i>)	Soil, Gram-positive, CCM 4435	Anaerobic, 37°C, anaerobic basal medium	7
Unicellular green alga (Eukaryotic cells)			
<i>Chlamydomonas</i> sp.	Planktonic, motile; Biology Centre CAS, Institute of Hydrobiology, České Budějovice, Czech Republic.	Aerobic, 22°C, light/dark regime (16h/8h), WC	2, 7
Mixture of Prokaryotic and Eukaryotic cells			
Microorganisms in reservoir water	Harcov reservoir, Liberec, Czech Republic.	Late summer, natural water	1

CCM – Czech Collection of Microorganisms, Masaryk Univ., Brno, Czech Republic.

WC medium components (cf. Guillard et al., 1972)

3. Methods

All methods used in this study are listed in Table 3. The chosen methods depended on the available instruments in our own laboratory or in laboratories we cooperated with. Typically, a combination of several methods was employed in one study, for example cell cultivation, optical microscopy and next-generation sequencing (paper 1); fluorometry and flow cytometry (paper 2); optical density (OD), optical microscopy and comet assay (paper 3); OD and fluorometry (paper 4); OD and optical microscopy (papers 5, 6). The endpoints of the methods are given in Table 3.

Table 3. Summary of all methods and endpoints investigated in this study.

Methods	Endpoints	Article No.
Cultivation	Viability of cultivable bacteria (CFU)	1
Optical density (OD)	Bacterial growth rate	3, 4, 5, 6, 7
Fluorescence microscopy	Viability, reactive oxygen species (ROS), membrane integrity (Sytox, PI)	2, 3, 5, 6
Comet assay	DNA damage	3
Optical microscopy	Cell morphology, cell numbers	3
Fluorometry (QY)	Photosystem II efficiency	2, 3, 7
Flow cytometry	Cell numbers, fluorescence of chlorophyll, membrane integrity, ROS formation	2
Next-generation sequencing (NGS)	Bacterial community structure	1

4. Characterization of NMs/NPs

A proper characterisation of iron-based NMs/NPs was necessary for the evaluation of toxicity. The methods that were used for the characterization of NPs and obtained parameters are shown in Table 4. For example, ZVI at micro- and nano-size tended to be more aggregated in centrifuged freshwater compared to filtered water and DI water. In the freshwater, the pH and ORP values of nZVI were higher and significantly changed compared to mZVI (paper 1). FerMEG12 showed positive surface charge in algal medium (WC), while Carbo-Iron[®], Fe-zeolites and Nano-Gothite showed negative charge during 24h-exposure. These four iron-based materials also aggregated to form larger sizes after 2h in WC medium (paper 2). In addition, the pH and ORP values of APTS-/PEG- and TEOS-NPs in bacterial media were comparable to the controls (paper 6).

Table 4. Summary of all methods and measurement parameters of particles

Method	Parameter
SEM	Shape of particles
BET	Specific surface area
ICP-OES	Concentration of chemical compounds and dissolved metals
DLS in combination with electrophoresis	Size distribution Zeta potential
Differential centrifugal sedimentation (DCS)	Size distribution
pH, ORP, dissolved O ₂	Physical-chemical parameters

5. Results and discussion

5.1 Lessons learnt from (nano)toxicity methods

The development of new test strategies has received much recent attention due to (1) the constraints of (nano)toxicity testing, (2) the inability of (nano)toxicity tests to adequately assess risk, and (3) the limitations of the studies in realistic conditions. In this thesis I established and used numerous methods (Table 3) depending on the target microorganisms and conditions for toxicity study. Moreover, I found that it is important to use a multi-method approach to elucidate toxicity mechanisms, the influence of NP interactions with media/organisms, and ultimately to identify artifacts and appropriate endpoints for nanotoxicity study (Sørensen et al., 2016; Jung et al., 2013; Hjorth et al., 2017).

The biological effects of iron-based materials were investigated using different strategies for different endpoints. The most common method in this study, bacterial growth rate, was used to evaluate the bacterial growth as well as to extrapolate data on effective concentration (EC). The key is to measure cell turbidity by wavelength absorption, here using a microplate reader. It is a feasible, economical, and reachable method. Bacterial growth rate is a good method to indicate the tolerance of bacteria to nanoparticles. Fast-growing bacteria, for example, are more susceptible to NPs than slow-growing bacteria (Bayer, 1989; Mah and Toole, 2001). However, iron-based materials/particles can aggregate and sediment, and can cause shading effect; all these are interfering factors, which should be taken into account. To obtain reliable data, negative controls with only NMs/NPs should be screened before the experiments begin, which means that absorbance of various concentrations of NMs/NPs without cells in exposure medium are measured. The absorbance of NPs should be constant during the whole experiment. The tested concentrations should be chosen (1) within the constant absorbance values; (2) or the absorbance values of NMs/NPs should be subtracted by the absorbance values of NMs/NPs and cells; (3) or there should be a combination of (1) and (2). This method was applied from lab scale to large scale study (Nguyen et al., 2017; Darwish et al., 2015; Darwish et al., 2016; Hjorth et al., 2017; Coutris et al., 2015).

Following bacterial growth rate assay, cell viability assay using fluorescence staining and a microplate reader was applied. The principle of this method is to measure the fluorescence staining cells by a suitable wave length Excitation (Ex)/Emission (Em). In this method, the negative controls of MNs/NPs with staining in the same incubation conditions as the experiment were always carried out. The fluorescence values of negative controls should not be detectable or scored at very low values with any tested NM/NP concentration; otherwise, materials/particles might react with the fluorescent probes. In this case, they should be replaced by other suitable probes. For example, live/dead kit (L7007, Thermofisher) did not interfere with the tested materials in number of studies (Nguyen et al., 2017; Darwish et al., 2016; Darwish et al., 2015; Oukarroum et al., 2012; Naik et al., 2014; Fajardo et al., 2012; Liu et al., 2013).

Fluorescence microscopy is a very good method for the observation of cell morphology and cell viability. The disadvantage of this method is that it is time-consuming even if an image analysis tool is used. However, it can give direct evidence, which can always be visually presented. The method was used to evaluate cell length and biofilm cluster formation in the effects of Fe₃O₄ on *E. coli* and *S. aureus*, respectively. To obtain adequate data, a large number of cells and images should be taken, e.g. at least some hundreds of cells (Nguyen et al., 2017; Darwish et al., 2015).

The single cell gel electrophoresis assay (SCGE, known as comet assay) is a method to obtain genotoxicity data. It is commonly used in eukaryotic cells. Basically, this method serves to measure the comet length of tail and head. In our study, the method was adapted to prokaryotic cells (bacteria), which represents a DNA damage study. The amount of DNA strand breaks should be related to the effect of NMs/NPs. The obtained data are very useful if they are combined with other methods (bacterial growth, cell viability, cultivation). However, this method is hugely time-consuming and cannot be applied to a large number of samples and a complex microbial community. The method is employed in many genotoxicity studies of eukaryotic cell lines, whilst there are few studies on bacterial genome including the one in this thesis (Nguyen et al., 2017; Cotelle and Fe, 1999; Karlsson, 2010; Omidkhoda et al., 2007; Gaharwar and Paulraj, 2015; Naik et al., 2014).

Aquapen is a practical small instrument used for measuring the efficiency of photosystem II of algae. It is fast and economic, and useful data can be obtained about single algal cultures as well as environmental water samples. The method should be performed in parallel with other methods to produce more endpoints for a broader view of toxicity assessment. In this study, the

use of Aquapen was limited by the colour of iron-based NMs. In the case of ZVI particles, it could only measure up to 50 mg/L, or in the case of Nano-Goethite the maximum tested concentration could be 100 mg/L. Some other researchers have successfully used this method for nanotoxicity study on algae (Oukarroum et al., 2012; Ralph et al., 2007; Baselga-Cervera et al., 2016; Gerloff-Elias et al., 2005).

Flow cytometry (FC) is an advanced method, combined with fluorescent probes for investigating multi-endpoints in toxicity study. The principle is to separate differently stained fluorescent cells (bacteria, algae or cell lines), which depend on the tested endpoints. For example, the algal cells were stained with SYTOX Green and propidium iodide (PI) for detecting damaged cell membranes (Nguyen et al., 2018). FC will separate damaged cells by blue channel with 533/30 nm (SYTOX) and red channel 585/40 nm (PI). This instrument has a good reputation in the nanotoxicity field since it is applied in many studies in both lab scale and large scale (Nguyen et al., 2018; von Moos et al., 2015; Cheloni et al., 2016; Melegari et al., 2013; Ghosh et al., 2012).

Next-generation sequencing is a highly advanced method and is still a new method applied in nanotoxicity research. It is a very good method for the metagenomics of soil or water microbial communities from environmental samples. Its disadvantages are that it is expensive to run the experiments, and it is time-consuming to analyse and interpret the data. There have been several studies of soil samples with iron-based NMs/NPs, but as far as is known, this thesis is first study of metagenomics in natural freshwater samples (Nguyen et al., 2018).

5.2 Toxicity of iron-based NMs/NPs on single bacterial species (prokaryotic cells)

The number of nanotoxicity studies focusing on microorganisms is increasing; however, these have mainly been limited to a single species grown in an adequate nutrient medium (Auffan et al., 2008; Saccà et al., 2013; Kim et al., 2010; Fajardo et al., 2013; Jiang et al., 2015; El-Temsah et al., 2016; Semerád and Cajthaml, 2016). In these studies, the experiments have been performed in carefully controlled, sterilized conditions. Therefore, the obtained data should be reproducible and easier to interpret and easier to understand the toxic mechanism. Another benefit of lab study is that the experiments can be repeated in the same conditions on different bacterial strains, and the results compared. In this thesis, the aim was to study the biological

effects of different functionalized Fe₃O₄ materials which were produced for bio applications. The experimental conditions were set up in constant conditions. The bacteria *E. coli* and *S. aureus* were used as microorganism models.

The biological study of modified APTS-, TEOS- and PEG-Fe₃O₄ on *E. coli* and *S. aureus* is presented in paper 6 (Darwish et al., 2015). The *E. coli* responded to stress conditions when in contact with APTS-Fe₃O₄ by prolonged cells. The effective concentration (EC10) of *E. coli* affected by APTS-, PEG- and TEOS-Fe₃O₄ was in the order 0.17, 0.5 and 0.35 g/L compared to unmodified Fe₃O₄ at 0.6 g/L. The EC10 of *S. aureus* on APTS-, PEG- and TEOS-Fe₃O₄ was 0.1, 0.25 and 0.12 g/L compared to unmodified Fe₃O₄ with NOEC < 1 g/L. The functional groups of APTS, TEOS and PEG played more or less an antibacterial role on both bacteria, especially the APTS-Fe₃O₄ affected Gram-positive *S. aureus* at EC10 of 0.1 g/L. In general, *S. aureus* was found to be more sensitive than *E. coli* to the three tested modified Fe₃O₄ NPs. APTS-magnetite NPs displayed a degree of antimicrobial activity, allowing their use in bio applications such as drug nanocarriers, where bacterial growth is undesirable (Darwish et al., 2015).

Next, the effects of three coatings: OA, PEI and PEI-mC of Fe₃O₄ particles (MNP) on *E. coli* and *S. aureus* were compared (paper 5) (Darwish et al., 2016). The bacterial growth rate method was applied as described in Darwish et al., 2015. Additionally, biofilm formation and viable cells assays were investigated. PEI-MNP and PEI-mC-MNP displayed the highest effect on *S. aureus* (0.077 and 0.146 g/L) and *E. coli* (0.552 and 0.145 g/L), while OA-MNP showed the least effect on both bacteria, *S. aureus* (0.2 g/L) and *E. coli* (> 1g/L). Following another assay, the percentage of dead cells of *E. coli* were 24% (P= 0.02) when it was grown with PEI-mC-MNP, while those of *S. aureus* were significant at P < 0.001 with all MNP materials at concentrations of more than 0.5 g/L. All functionalized Fe₃O₄ inhibited the formation of biofilms of *S. aureus*. *S. aureus* was again more affected by all three functionalized Fe₃O₄ than *E. coli* cells. PEI-mC Fe₃O₄ was found to be most effective against both *S. aureus* and *E. coli* (EC10 of 0.15 g/L), while PEI-Fe₃O₄ had the most inhibiting properties on *S. aureus* (EC10 of 0.077 g/L). The functionalized magnetite nanoparticles are promising agents for hyperthermia, as well as for further work on hyperthermic drug release (Darwish et al., 2016).

The last types of functionalized Fe₃O₄ were synthesized by three different methods: emulsion polymerisation (Fe₃O₄-PNIPAAm-1), Fe₃O₄-PNIPAAm-2 (*in-situ* precipitation) and physical addition (Fe₃O₄-PNIPAAm-3). The biological effects were studied by multi-endpoint approaches (growth rate, viability cells, cell morphology and damaged DNA) (paper 4: Nguyen

et al., 2017). The EC10 was found to be almost similar in Fe₃O₄-PNIPAAm-1 and Fe₃O₄-PNIPAAm-2, being 0.1 and 0.14 g/L for *E. coli* and 0.05 and 0.05 g/L for *S. aureus*. A significant increase in the length of *E. coli* cells was caused by Fe₃O₄-PNIPAAm-1 and Fe₃O₄-PNIPAAm-2, while biofilm cluster was increased in Fe₃O₄-PNIPAAm-2 and Fe₃O₄-PNIPAAm-3. However, the PNIPAAm itself had a significant effect on both *E. coli* length cells and biofilm clusters. Fe₃O₄-PNIPAAm-1 displayed stronger biological effects on both bacterial strains than Fe₃O₄-PNIPAAm-2 and Fe₃O₄-PNIPAAm-3 (Fig. 2). *S. aureus* was more sensitive than *E. coli* to all three magnetic PNIPAAm nanocomposites. Emulsion polymerisation was the most effective method for synthesising of PNIPAAm magnetites nanocomposites, which displayed the strongest antibacterial property (Nguyen et al., 2017).

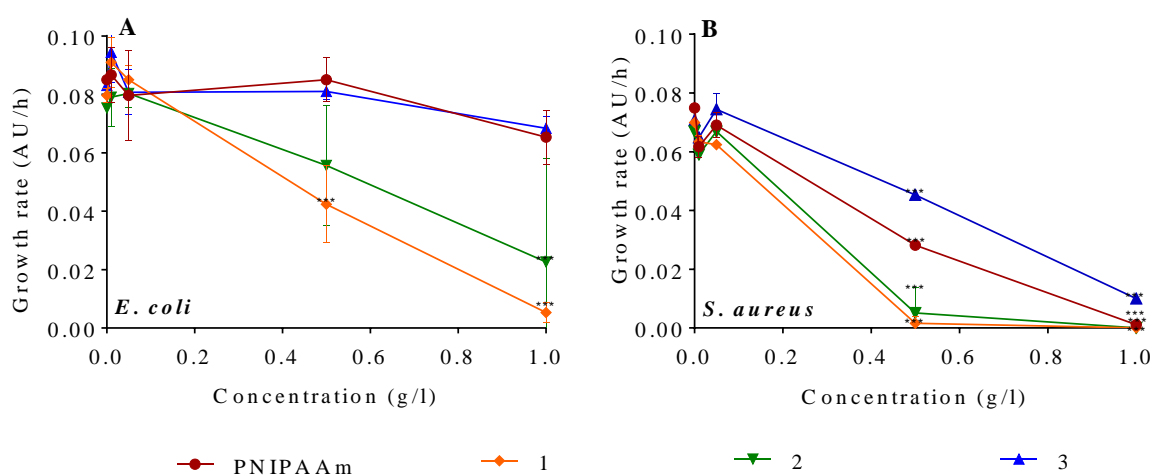


Figure 2. Example of bacterial growth rate study of *E. coli* (A) and *S. aureus* (B) with PNIPAAm (red circles), Fe₃O₄-PNIPAAm-1 (orange diamonds [1]), Fe₃O₄-PNIPAAm-2 (green triangles [2]) and Fe₃O₄-PNIPAAm-3 (blue triangles [3]). The error bars show SD calculated from n = 3. Significance level ***P < 0.001 (Nguyen et al., 2017).

The antibacterial properties of functionalized Fe₃O₄ materials were also investigated in other studies. Chitosan coated IONPs had antibacterial properties against *Bacillus subtilis* and *E. coli* using BacLight fluorescence assay, bacterial growth kinetic and CFU (Arakha et al., 2015). Glycerol iron oxide nanoparticles (GIO-NPs) were obtained by an adapted coprecipitation method and the GIO-NPs showed antibacterial property. These results indicate that the biofilm inhibition of Gram-negative *P. aeruginosa* 1397 was higher than Gram-positive *E. faecalis* ATCC 29212 at concentrations from 0.01 to 0.625 g/L (Iconaru et al., 2013). The antibacterial

activities of IONPs, synthesized by laser ablation in liquid, were tested against Gram-positive *S. aureus* and Gram-negative *E. coli*, *P. aeruginosa* and *Serratia marcescens*. The results of zone inhibition showed a notable inhibition on both bacterial strains, and the synthesized magnetic nanoparticles were used to rapidly capture *S. aureus* cells under the magnetic field effect (Ismail et al., 2015). Fe₃O₄ NPs were synthesized through the chemical combustion method, and their antibacterial property was strongly revealed against Gram-positive *S. aureus*, *Xanthomonas* and Gram-negative *E. coli* and *Proteus vulgaris* (Prabhu et al., 2015).

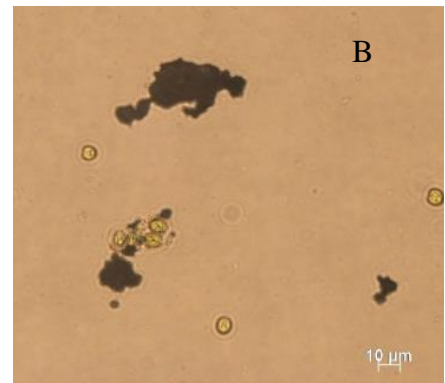
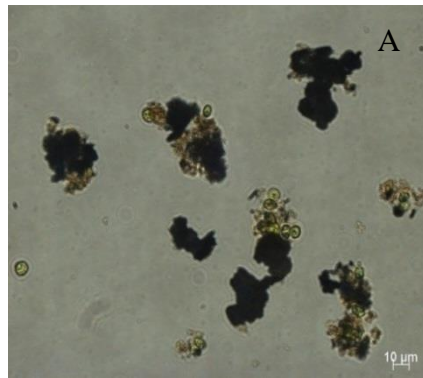
5.3 Toxicity of iron-based NMs/NPs on unicellular alga (eukaryotic cells)

The unicellular alga, *Chlamydomonas* sp. served in this thesis as a model for eukaryotic cells. Four new iron-based materials developed for groundwater remediation were tested: (i) FerMEG12 - pristine flake-like milled Fe(0) nanoparticles; (ii) Carbo-Iron® - Fe(0)-nanoclusters containing activated carbon (AC) composite; (iii) Trap-Ox® Fe-BEA35 (Fe-zeolite) - Fe-doped zeolite; and (iv) Nano-Goethite - 'pure' FeOOH. Toxicity study of these materials was necessary before they could be released into the environment. A whole test battery consisting of eight micro(organisms) bacteria (*V. fischeri*, *E. coli*), algae (*P. subcapitata*, *Chlamydomonas* sp.), crustaceans (*D. magna*), worms (*E. fetida*, *L. variegatus*) and plants (*R. sativus*, *L. multiflorum*) was applied by the project partners. *E. coli* and *Chlamydomonas* sp. was investigated by the author. A ball milled FerMEG12 showed toxicity in the test battery at concentrations up to 100 mg/L, which is the cut-off for hazard labelling in chemicals regulation in Europe (paper 3: Hjorth et al., 2017). The alga *Chlamydomonas* sp. was chosen for further investigation of different biological endpoints. The results also confirmed that FerMEG12 caused the most damage to algal cells and flow by Carbo-Iron®, Fe-zeolite and Nano-Goethite (paper 2: Nguyen et al., 2018). An example of algal cells exposed to the four iron-based materials observed under microscope is shown in Fig. 3.

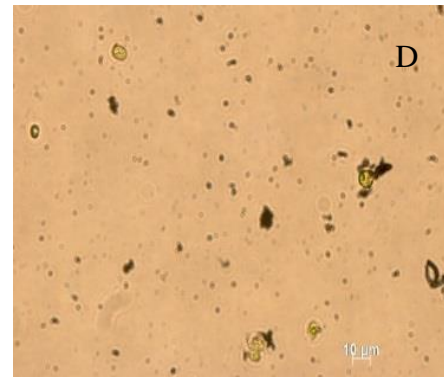
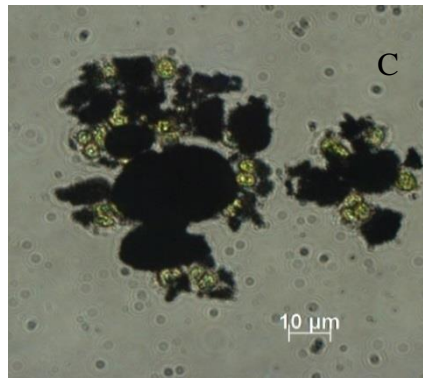
2 h

24 h

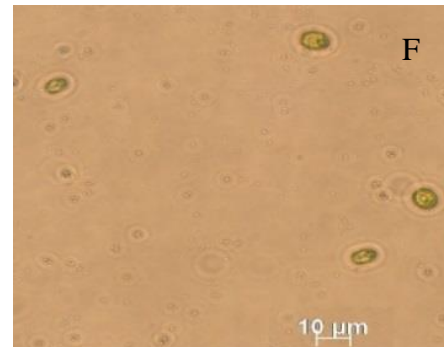
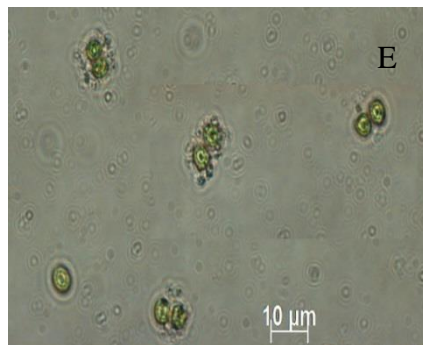
Algae +
FerMEG12



Algae +
Carbo-
Iron[®]



Algae +
Fe-zeolites



Algae +
Nano-
Goethite

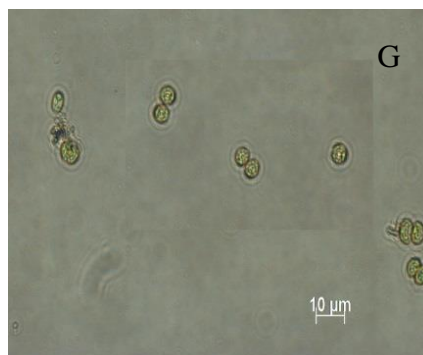


Figure 3. Example images of *Chlamydomonas* with FerMEG12 (A, B), Carbo-Iron[®] (C, D), Fe-zeolites (E, F) and Nano-Goethite (G, H). The images were taken using a bright field Zeiss microscope (mag. 400 x; scale bar = 10 μ m) (Nguyen et al., 2018).

Each of the iron-based materials has its own specific and unique properties for targeted application purposes. Some of these characteristics may not favour the target microorganisms; hence, they should be taken into account when undertaking toxicity studies. These unfavourable factors were listed as lessons learnt in paper 3 (Hjorth et al., 2017). The green algae take in light for their essential life elements; therefore, the dark colour of FerMEG12 and Carbo-Iron[®], and the colouration of Nano-Goethite at higher concentrations (500mg/L) resulted in shading of the algal cells. The larger size of FerMEG12 and Carbo-Iron[®] (original state or due to agglomeration) and consequent sedimentation reduced their effect on *Chlamydomonas* sp. The constituents of iron-based materials, including the percentage of the Fe(0), glycerol, humic acid or other added chemicals, may also need to be considered in toxicity studies. In the case of Fe-zeolites, these have two phases of in-situ application: a sorption phase following particle injection to the aquifer, and, after sorption is complete, a flush of H₂O₂ is applied, which leads to hydroxyl radical formation (Fenton-like reaction), which then regenerates the particles and oxidises the contaminant. Even though there was no specific evidence, the shape of FerMEG12 with rough, sharp edges on the surface, could be involved in damage to algal membranes (Nguyen et al., 2018).

As one of the transition metals, ZVI can participate in one-electron oxidation-reduction reactions producing ROS, which can have direct toxic effects on living organisms (Ševců et al., 2011). FerMEG12, for example, with 80% Fe(0), was without surface passivation and displayed higher toxicity to *Chlamydomonas* sp. than the other Fe-containing materials. This could be due to higher release of Fe(II) followed by higher uptake by algal cells, causing oxidative stress via the classic Fenton reaction (Lee et al., 2008; Ševců et al., 2011). ZVI toxicity strongly depends on the percentage of ZVI used and on the surface coating (El-Temsah and Joner, 2012).

FerMEG12 had the most negative effect on the tested micro(organisms), and therefore was remodified. The hypothesis concerned whether the adverse effect was caused by humic acid, a surfactant used for stabilizing FerMEG12, or if humic acids would reduce the toxicity of FerMEG12 particles on organisms by reducing their bioavailability. The experiment compared the toxicity of ZVI alone, ZVI with humic acid, humic acid alone and remodified FerMEG12.

No adverse effect of remodified FerMEG12 was found in either anaerobic *C. clostridium* or aerobic *P. subcapitata*. Humic acid decreased bacterial growth only at 1000 mg/L (Coutris et al., 2015).

5.4 Effect of iron-based NMs/NPs on complex microbial communities

There have been few studies focused on the effects of NMs on whole bacterial communities. The iron-based materials tended to be applied to soil, groundwater or freshwater environments, where natural microbial communities are present. Up to the present time, studies on the effects of ZVI on microbial communities have been scarce and it is difficult to replicate field-relevant exposure conditions; however ecotoxicity studies for these materials are urgently needed (Kocur, 2015).

The nano-scale ZVI caused changes in the diversity of Eubacteria in groundwater microcosms, but no change in abundance was detected (Kirschling et al., 2010). Another study found that nZVI enhanced bacterial growth but did not influence the bacterial community structure (Barnes et al., 2010) in aquatic microbial microcosms. An experiment of nZVI in soil mesocosms revealed that nZVI has the potential to inhibit microbial functions because of the changes in soil bacterial community composition and reduction of the activity of chloroaromatic mineralizing microorganisms (Tilston et al., 2013). In a recent study using next-generation amplicon pyrosequencing, nZVI/CMC addition stimulated growth of dehalogenating bacteria in a long-term field study of microbial communities (Kocur et al., 2016). The most advanced results in this thesis were obtained from next-generation sequencing (paper 1). When comparing nano and microparticles nZVI and mZVI, samples of natural reservoir microplankton were studied. Total bacterial species richness and less common bacteria increased significantly when treated with mZVI compared to nZVI. The abundance of *Limnohabitans* (*Betaproteobacteria*), *Roseiflexus* (*Chloroflexi*), *hgcl_clade* (*Actinobacteria*) and *Comamonadaceae_unclassified* (*Betaproteobacteria*) increased under nZVI treatment, while mZVI enhanced *Opitutae_vadinHA64* (*Verrucomicrobia*) and the *OPB35_soil_group* (*Verrucomicrobia*) (Fig. 4). mZVI had no significant effect on algal cell number, though cyanobacteria numbers increased slightly. Algae were only marginally affected by nZVI after seven days, and cyanobacteria numbers remained unaffected after 21 days. nZVI increased the cultivable bacteria, which increased significantly and shaped the bacterial community both directly, through the release of

Fe(II)/Fe(III), and indirectly, through rapid oxygen consumption and the establishment of reductive conditions (Nguyen et al., 2018).

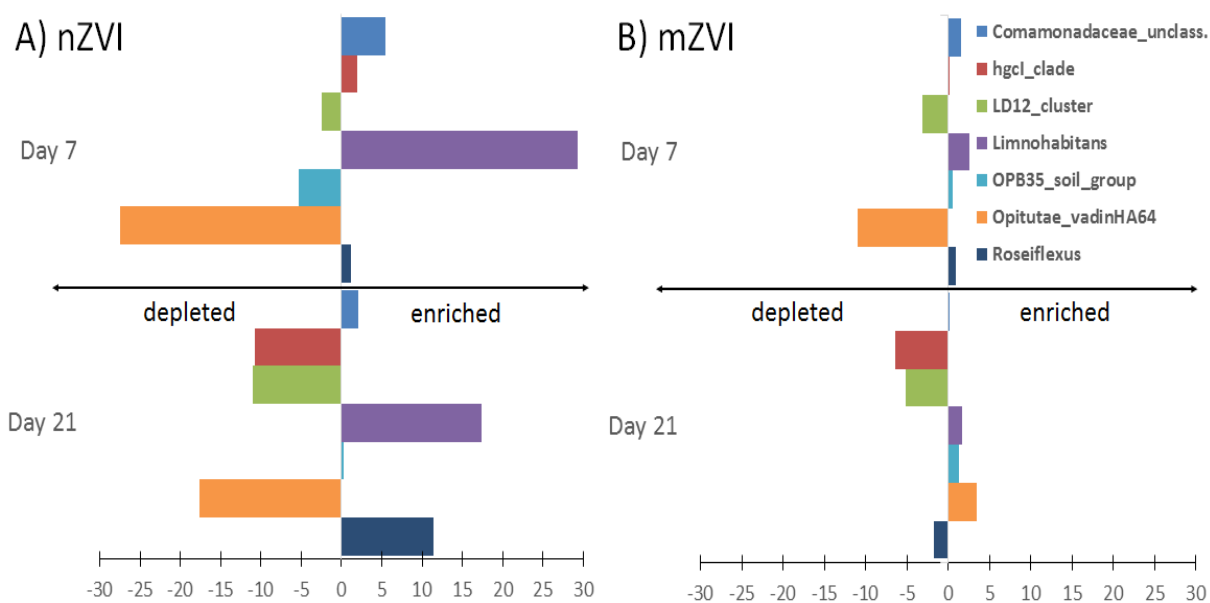


Figure 4: Example of effects of (A) nZVI and (B) mZVI on most abundant bacterial groups in reservoir water after 21 days (Nguyen et al., 2018)

5.5 Behaviour of iron-based NMs/NPs in tested media

It was necessary to study the behaviour of iron-based NMs/NPs in the test conditions or media to be able to interpret the data of the toxicity study such as size distribution, surface charge, agglomeration, and sedimentation, and also other chemical parameters (pH, ORP) and dissolved oxygen. These parameters could some extent explain the causes of toxicity. The smaller NPs may cause a more toxic effect on the cells compared to larger NPs (Diao and Yao, 2009; Phenrat et al., 2009; Lei et al., 2016). The agglomeration of NPs could change their properties, which may reduce the toxicity toward microorganisms (Keller et al., 2012) due to the consequent sedimentation. The shading effect of NPs might lead to distorted results in studies involving algae (Hjorth et al., 2017). NPs were found to be more stable in a higher pH value, and magnetic NPs were more stable compared to ZVI (Auffan et al., 2008). The ZVI aggregation rate was greater in seawater (pH 8.1) than in freshwater (pH 7.5) and uncoated ZVI aggregated faster than coated ZVI (Keller et al., 2012). In the environment, NPs undergo different ways of transformations: (a) chemical, (b) physical (aggregation), (c) biological, and

(d) interaction with macromolecules (Lowry et al., 2012). The listed transformation of NPs could also happen in growth media. The biotic and abiotic degradation processes occurring in situ may progressively remove nanoparticle coating, thus modifying nZVI behaviour and overall toxicity (Lefevre et al., 2015). In algal growth medium (WC), iron oxide (Nano-Goethite) was more stable than Fe-zeolites compared to unstable ZVI (FerMEG12 and Carbo-Iron) during 24 h (paper 2). The mZVI and nZVI aggregated quickly in centrifuged freshwater compared to filtered freshwater (pH 8) (paper 1).

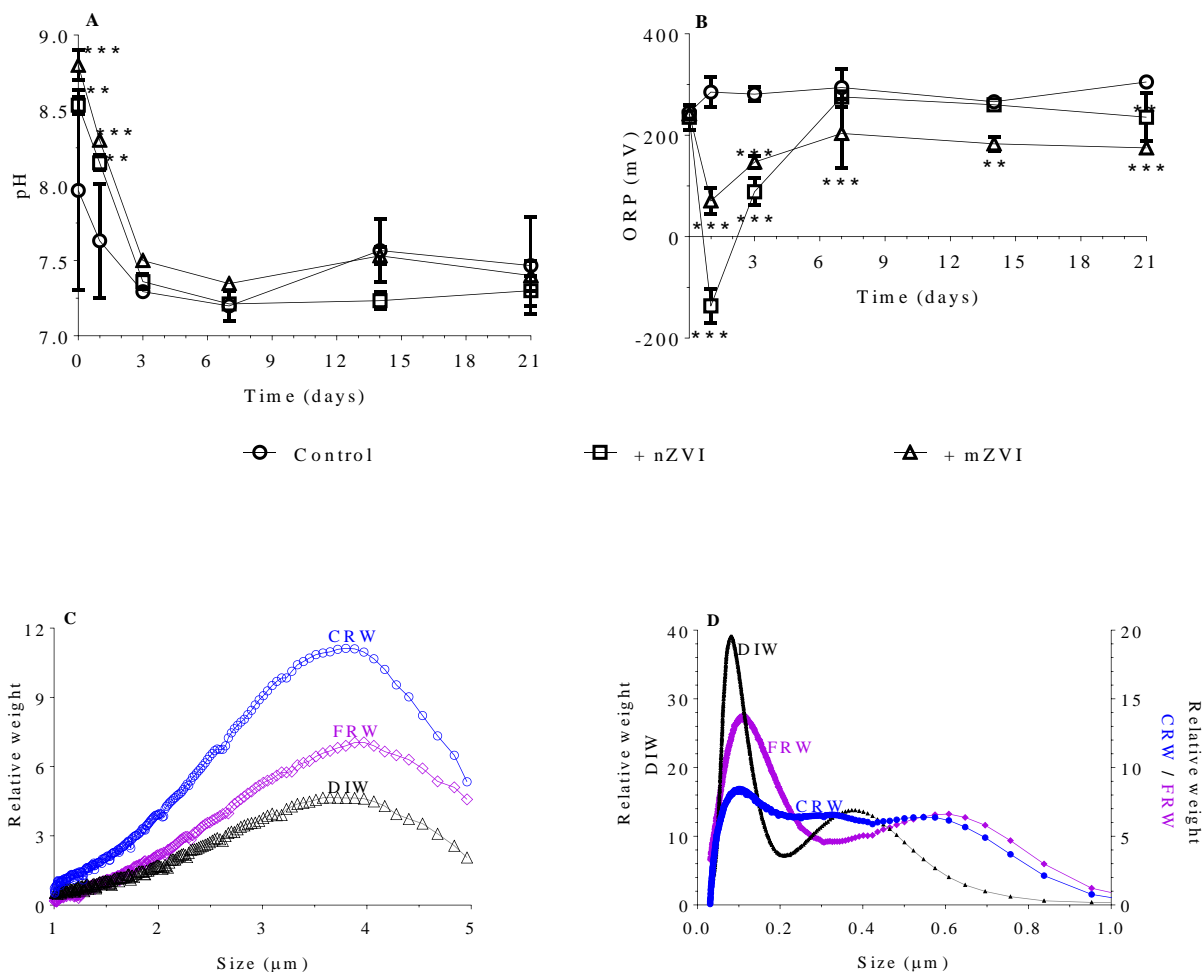


Figure 5. Example of physio-chemical parameters monitored over the 21-day experiment with mZVI and nZVI in reservoir water. (A) pH, (B) oxidative reductive potential, (C) size distribution determined by differential centrifugal sedimentation with samples mZVI in centrifuged reservoir water CRW, filtered reservoir water (FRW) and deionized water (DIW), and (D) size distribution determined by differential centrifugal sedimentation with samples nZVI in CRW, FRW and DIW. Error bar n = 3; * P < 0.05, ** P < 0.01 and *** P < 0.001 (Nguyen et al., 2018).

6. List of whole papers

Paper 1

Nhung H. A. Nguyen, Roman Spanek, Vojtech Kasalicky, David Ribas, Denisa Vlkova, Hana Reháková, Pavel Kejzlar, and Alena Sevcu (2018). Different effects of nano-scale and micro-scale zero-valent iron particles on planktonic microorganisms from natural reservoir water.

Environmental Science: Nano. DOI: 10.1039/C7EN01120B. **IF 6.047**



Cite this: DOI: 10.1039/c7en01120b

Different effects of nano-scale and micro-scale zero-valent iron particles on planktonic microorganisms from natural reservoir water†

Nhung H. A. Nguyen,^{*ab} Roman Špánek,^{ab} Vojtěch Kasalický,^c David Ribas,^d Denisa Vlková,^a Hana Řeháková,^a Pavel Kejzlar^a and Alena Ševců^{†*ab}

While nano-scale and micro-scale zero-valent iron (nZVI and mZVI) particles show high potential for remediation of polluted soil aquifers and elimination of cyanobacterial blooms, this has required their release into the environment. This study compares the impact of 100 mg L⁻¹ of nZVI and mZVI on natural planktonic microorganisms from a reservoir, incubated in 1.5 L batches over 21 days. In addition to counting cyanobacterial and algal cell numbers, bacterial community structure was assessed using Ion Torrent sequencing and the number of cultivable bacteria determined using standard cultivation methods. Surprisingly, while mZVI had no significant effect on algal cell number, cyanobacteria numbers increased slightly after 14 days ($P < 0.05$). Algae were only marginally affected by nZVI after seven days ($P < 0.05$), while cyanobacteria numbers remained unaffected after 21 days. Total species richness and less common bacteria increased significantly when treated with mZVI (compared to nZVI). The abundance of *Limnohabitans* (*Betaproteobacteria*), *Roseiflexus* (*Chloroflexi*), hgcL-clade (*Actinobacteria*) and Comamonadaceae_unclassified (*Betaproteobacteria*) increased under nZVI treatment, while mZVI enhanced *Opiritae_vadinHA64* (*Verrucomicrobia*) and the OPB35_soil_group (*Verrucomicrobia*). Interestingly, the number of cultivable bacteria increased significantly after three days in water with nZVI, and further still after seven days. nZVI shaped bacterial community both directly, through release of Fe(0)/Fe(II), and indirectly, through rapid oxygen consumption and establishment of reductive conditions. The strong physico-chemical changes caused by nZVI proved temporary; hence, it can be assumed that, under natural conditions in resilient reservoirs or lakes, microbial plankton would recover within days or weeks.

Received 24th November 2017,
Accepted 16th March 2018

DOI: 10.1039/c7en01120b

rsc.li/es-nano

Environmental significance

Nanoscale zerovalent iron (nZVI) has been the subject of great interest over the last decade as it is a highly reactive material, capable of rapidly assimilating toxic pollutants (e.g. chlorinated ethenes) in soil and underground waters. To date, however, most field studies have been performed in contaminated underground environments. As nZVI have been postulated as a possible treatment for harmful cyanobacterial blooms, this study focuses on the effect of nZVI on natural pelagic microplankton in a freshwater reservoir. Moreover, we aim to distinguish between the effect of nano- and micro-ZVI particles on the natural microbial community.

1. Introduction

Zero-valent iron (ZVI) has a long tradition of environmental application due to its high capacity to clean-up a wide range

of pollutants, including chlorinated organic compounds and toxic metal cations.^{1–3} Initially applied as granules (>50 μm), and more recently as a micro-scale ZVI (mZVI) material,⁴ ZVI is now more often applied as nano-scale ZVI particles (nZVI).^{5–9} Due to their high specific surface area, micro- and nano-scale materials are more reactive than granular materials, while their small particle size means they can be used for more diverse applications.¹⁰ In addition to the above-mentioned applications, a number of laboratory studies have suggested that nZVI could also prove useful for prevention of cyanobacterial blooms.^{11,12}

Unfortunately, the high capability of ZVI for cleaning-up pollutants in groundwater and soils^{7,13,14} may also have an

^a Institute for Nanomaterials, Advanced Technologies and Innovation, Technical University of Liberec (TUL), Studentská 2, 46117 Liberec, Czech Republic.

E-mail: nhung.nguyen@tul.cz, alena.sevcu@tul.cz

^b Faculty of Mechatronics, Informatics and Interdisciplinary Studies, Technical University of Liberec (TUL), Studentská 2, 46117 Liberec, Czech Republic

^c Biology Centre of the Czech Academy of Sciences, Institute of Hydrobiology, České Budějovice, Czech Republic

^d Department of Chemical Engineering, Technical University of Catalonia (UPC), ETSEIB, Av. Diagonal, 647, E-08028, Barcelona, Spain

† Electronic supplementary information (ESI) available. See DOI: 10.1039/c7en01120b



effect on indigenous microorganisms mediating fundamental ecosystem processes as they are the first to be exposed to the particles. Hence, there is an urgent need for the evaluation of potential risks relating to ecosystem function changes when using ZVI materials.

Two main mechanisms of direct effect on microbial cells have been identified for ZVI: generation of reactive oxygen species (ROS) and the potential to physically damage bacterial or algal cells due to its strong affinity to cell surfaces,¹⁵ which can lead to a significant decrease in mobility.^{16,17} It is well known that ZVI particles have the potential to release Fe(n) into the surrounding environment, converting less reactive hydrogen peroxide (H₂O₂) into harmful ROS, e.g. hydroxyl radicals (•OH), via the Fenton reaction.^{18,19} ROS are normally scavenged by antioxidants and enzymes; however, elevated concentrations in microbial cells can result in oxidative stress and damage to lipids, proteins and DNA. In addition, the physical interaction of nZVI and microbial cells could cause damage to outer membranes or physical inactivation of cells.^{16,21} Indirect effects of nZVI on microorganisms include a decrease in dissolved oxygen concentration, along with a subsequent decrease in oxidation reduction potential,^{1,22} which could potentially harm aerobic microorganisms. On the other hand, ZVI oxidation or reduction processes could be beneficial for iron-oxidising bacteria.²³

A careful risk assessment of ZVI particles requires different ecotoxicity studies targeting organisms on different ecosystem levels. Consequently, the number of ecotoxicity studies focusing on microorganisms is increasing; however, these have mainly been limited to a single species grown in adequate nutrient media,^{16,24–30} a situation far from relevant to natural environment conditions. Despite this, such studies are important for better understanding more complex studies on microbial communities under natural conditions.

Generally speaking, all studies on ZVI effects to aquifer and soil bacterial communities describe shifts in community structure.^{9,15,31–34} The first toxicity study on a whole bacterial community from the River Thames showed no negative effect from ZVI particles (100 mg L⁻¹, nZVI majority of Fe(0), with 27% of boron on the surface, 30–90 nm; and mZVI 99.5% of Fe(0), 1.5–6.8 μm), the number of bacteria even increasing after 40 days.¹⁵ Similarly, no deleterious effect of nZVI (100 mg L⁻¹, 24–32% Fe(0) and 33% Fe(0) modified with polyaspartate) was observed on total bacterial abundance in a series of microcosm experiments³³ nor prolonged toxicity on dechlorinating microorganism during a 300 day anaerobic column experiment (Nanofer 25, 20% suspension of Fe(0) in water).³⁵ Recently, Němeček *et al.* (2014) showed that the long-term effect of nZVI (Nanofer 25, 20% suspension of Fe(0) in water) on indigenous prokaryotic microorganisms may be neutral, or even positive, as the reduction in toxic pollutants allows further biodegradation.³⁴ This finding was further supported by repeated *in situ* application of nZVI (first round Nanofer STAR, second round Nanofer 25S, 1 g L⁻¹ and 2 g L⁻¹ of 20% suspension in water, respectively) to combat

contamination by hexavalent chromium Cr(vi) and chlorinated ethenes, which resulted in significant stimulation of iron-reducing, sulphate-reducing and chloro-respiring bacterial growth over the 13-month study.⁹ Moreover, no evidence for any negative effect on soil microbial activity was observed when comparing nZVI (ball-milled Fe(0) in 0.18% polyacrylic acid) with mZVI (>98.3% Fe in 0.18% polyacrylic acid) toxicity.³⁶ On the other hand, high levels of mZVI (25 g L⁻¹, >90% Fe(0)) were seen to change anaerobic sludge bacterial community composition,³⁷ with *Flavobacteriaceae*, *Comamonadaceae* and several unclassified iron-reducing bacteria increasing in abundance, considered positive for degradation of toxic flame retardants.³⁷ Velimirovic *et al.* reported five types of mZVI as positively stimulating a CAH-degrading mixed bacterial culture at concentrations up to 500 mg L⁻¹, while 1–15 g L⁻¹ resulted in inhibition depending on mZVI size.³⁸ mZVI in general has a lower impact on microbes than nZVI, though comprehensive studies on natural freshwater communities have yet to be published.

Studies on impact of nZVI on algae or cyanobacteria are still scarce and are generally limited to single-species cultures, while on mZVI effect have yet to be undertaken. A cyanobacterial bloom, dominated by *Microcystis aeruginosa*, was strongly affected by nZVI (Nanofer 25S, >90% Fe(0)) after 24 h exposure (EC50: 50 mg L⁻¹), with the effect significantly higher than on *Desmodesmus subspicatus*.¹¹ Two different nZVI types, Nanofer 25S and Nanofer STAR (70–90% Fe(0) and 10–30% iron oxides), affected the growth rate of freshwater *Pseudokirchneriella subcapitata* at concentrations >8 mg L⁻¹ and ≥12 mg L⁻¹, respectively.¹⁹ Likewise, ball-milled nZVI (FerMEG12, 15–30% Fe(0) in monoethylene glycol) had a negative effect on *P. subcapitata* and *Chlamydomonas* sp. at concentrations <100 mg L⁻¹,^{30,39} while the monoethylene glycol dispersant alone had no effect.³⁰

The major objective of this study was to examine the effect of nZVI and mZVI particles on planktonic microorganisms. The study was carried out on natural freshwater from a reservoir, sampled in late summer in order to include a fully developed phytoplankton community. ZVI inevitably oxidises into Fe-oxides naturally present in the environment at concentrations ranging from 0.1 to 194.7 mg L⁻¹ in rivers⁴⁰ and from 20 to 40 g kg⁻¹ in soils.⁴¹ Hence, we used a concentration of 100 mg L⁻¹ as this was considered relevant to concentrations in the vicinity of ZVI application, where ZVI suspension quickly dilutes^{42–44} and as this is the limit for hazard labelling in EU chemical regulations. Centrifuged and filtered reservoir water was used when assessing the size distribution of both ZVI materials in order to reveal possible differences due to sample preparation. We describe the effect of nZVI and mZVI particles on prokaryotic (bacteria, cyanobacteria) and eukaryotic (algae) microorganisms by determining the number of cultivable bacteria and the number of cyanobacterial and algal cells. For the first time, we apply 16S rRNA amplicon sequencing in order to describe the effect of nZVI and mZVI on the development of a natural bacterial community.



2. Material and methods

2.1. ZVI particles

A suspension of nZVI in deionised water was obtained from the Polytechnic University of Catalonia, Spain. The material was produced using a novel wet-ball milling process utilising alumina abrasive and monoethylene glycol (MEG; Scharlab S. L.) as the grinding media. The nZVI particles had a mean diameter of 160 nm, a maximum size of 540 nm (determined by scanning electron microscopy [SEM]), a specific surface area of $29.6 \text{ m}^2 \text{ g}^{-1}$ and contained 74.0% Fe(0), 2.7% carbon and 23.3% of iron oxide.⁴⁵ The mZVI reactive powder (no: 72052910) was provided by Hepure Technologies (USA) and had a specific surface area of $0.487 \text{ m}^2 \text{ g}^{-1}$, 95% Fe(0), 1.8% carbon, <1% oxygen, 1% silicon, 0.1% phosphorus and 1% sulphur. A 10 g L^{-1} stock suspension of ZVI in deionised water was freshly prepared before the experiment. Images of the pristine particles are presented in Fig. S1.†

2.2. Experimental design and sampling of reservoir water

Water samples were obtained from Harcov reservoir (50.7702097N, 15.0755733E; Czech Republic) one metre from the reservoir bank and from a point 10 cm below the surface on 22 August 2016. The water was immediately transported in sterile containers (20 L) to the laboratory and the experiment started immediately after arrival. The following variants were prepared in triplicate in sterile 1.5 L glass bottles: fresh reservoir water mixed with stock suspension of either nZVI or mZVI at a final concentration of 100 mg L^{-1} and fresh reservoir water only (control without ZVI). Additionally, sterilised reservoir water and sterilised reservoir water mixed with nZVI were prepared in parallel as reference controls. The bottles, illuminated with two 3 metre light tubes emitting visible light at 670–800 lux (GOSSEN, Germany), were slowly mixed manually for one minute a day and the position of the bottles randomly changed each day. Sub-samples (160 mL) were taken after 0, 1, 3, 7, 14 and 21 days for determination of cultivable bacteria, either as colony forming units (CFU) or number of cyanobacterial and algal cells. Aliquots for DNA extraction and 16S rRNA amplicon sequencing were sampled during days 0, 7 and 21.

2.3. Physico-chemical analysis of reservoir water

The reservoir water (1 L) was sampled separately, in triplicate, for analysis of chemical parameters (Table S1†), determined using iron chromatography (IC; ThermoFisher) and inductively coupled plasma spectrometry (ICP-OES) on an OPTIMA 2100 DV (Perkin Elmer) spectrophotometer, and total organic carbon (TOC) using a multi N/C 2100S analyser (Analytik Jena, Germany).

Concentration of dissolved Fe at 0 and 21 days was measured using ICP-OES. Water samples with nZVI and mZVI (10 mL) were centrifuged for 30 minutes at 4600 rpm (ROTANTA 460R, Hettich, Germany), the supernatant then being passed through Amicon Ultracel 3K ultra-filtration filters with a 3

kDa molecular weight cut-off (Millipore, USA) to separate Fe ions from the particles.

The pH, ORP and dissolved oxygen concentration was measured directly at the reservoir and during the laboratory experiment using a Multi 3430 multi-parameter portable probe (WTW, Germany).

2.4. Characterisation of ZVI particles in reservoir water

The nZVI and mZVI particles (100 mg L^{-1}) were suspended for 24 h in (1) centrifuged reservoir water prepared by spinning for 30 minutes at 6000 rpm, (2) filtered reservoir water prepared by filtration over a $1.4 \mu\text{m}$ membrane filter (Whatman, Life Sciences) and (3) deionised water as a control. The nZVI and mZVI particles were characterised using a Zeiss Ultra Plus field-emission SEM (Zeiss, Germany). The samples were fixed onto aluminium stubs using double-sided carbon tape and cleaned with RF plasma (Evactron) for 10 min before SEM analysis. SEM images were acquired at an accelerating voltage of 5 kV at low probe current (about 15 pA) using an InLens secondary electron detector with SmartSEM software. Subsamples were further analysed for size distribution using differential centrifugal sedimentation (DCS) on a DC24000 centrifuge (CPS Instruments, UK) at a maximum operational speed of 2500 rpm for mZVI and 24 000 rpm for nZVI. In addition, colloidal particles of natural organic compounds were concentrated by centrifugation of filtered ($1.4 \mu\text{m}$) reservoir water for 45 minutes at 6000 rpm, with maximum operational speed set at 10 000 rpm. This protocol was adapted from Barnes *et al.* (2010).¹⁵

2.5. DNA extraction

Reservoir water samples (150 mL) treated with nZVI and mZVI and untreated reservoir water (control) were pre-filtered with $20 \mu\text{m}$ filter papers (Whatman, GE Healthcare Life Science, China) and then filtered through a Hydrophilic Durapore PVDF $0.22 \mu\text{m}$ membrane (Merck Millipore, Germany) for DNA extraction. Briefly, DNA was extracted from the filter using a FastDNA Spin Kit for Soil (MP Biomedicals, CA, USA) according to the manufacturer's protocol, with the Bead Blaster 24 homogenisation unit (Benchmark Scientific, NJ, USA) employed for cell lysis. Extracted DNA concentration was quantified using a Qubit 2.0 fluorometer (Life Technologies, USA) (further details in Dolinová *et al.*, 2016).⁴⁶

2.6. PCR amplification and next-generation sequencing (NGS)

All isolated DNA samples for bacterial and cyanobacterial community analysis were sequenced in duplicate, with two consecutive polymerase chain reactions (PCR) performed per sample to amplify DNA from the V4 region (normal and barcode fusion primers used). *In silico* analysis of primers was performed in order to cover as much diversity as possible while keeping the amplicon size below 400 bp. Amplification of the V4 region of the eubacterial 16S rRNA gene was performed with primers 515F (5'-TGCCAGCMGCGG-3')⁴⁷ and barcode 802R (5'-TACNVGGGTATCTAATCC-3').⁴⁸ A



MOCK community (collection of 6 bacterial genomes prepared in-house) was subsequently sequenced in order to verify data evaluation (Fig. S2†). PCR cycle conditions were as follows: first PCR 95 °C for 3 min; 10 cycles at 98 °C for 20 s, 50 °C for 15 s and 72 °C for 45 s, with a final extension at 72 °C for 1 min; second PCR 95 °C for 3 min; 35 cycles at 98 °C for 20 s, 50 °C for 15 s and 72 °C for 45 s, with a final extension at 72 °C for 1 min. The concentration of purified PCR products was measured with a Qubit 2.0 fluorometer (Life Technologies, USA). Barcode-tagged amplicons from different samples were then mixed in equimolar concentration. Sequencing of bacterial amplicons was performed on the Ion Torrent platform (Life Technologies, USA), the raw Ion Torrent reads being processed with Mothur software.⁴⁹ Low quality reads were removed and sequences were assigned to each sample. Chimeric sequences were identified using UCHIME⁵⁰ and subsequently removed. Sequences exceeding 400 bases were trimmed and sequences shorter than 180 bases removed. Sequences were classified against Silva database v. 123 with a bootstrap value set at 80%. A cut-off value of 97% was used for clustering sequences into operational taxonomic units (OTUs). Sequence data were normalised to group with the least sequences by randomly selecting a selected number of sequences from each sample. Cluster analysis by Bray–Curtis dissimilarity was undertaken using Vegan in the *R* statistical package.⁵¹

2.7. Abundance of ferroxidase enzyme

Ferroxidase enzyme (EC1.16.3.1) abundance in prokaryotes was conducted using metabolic inference (preferably, but not exclusively, using NGS) on 16S rRNA gene libraries using Paprica software,⁵² based on the phylogenetic placement approach. Paprica uses pathways/enzymes shared between the members of all clades on a reference tree to determine which pathways/enzymes are likely to be associated with a phylogenetically placed read. Paprica accepts reads pre-processed by Mothur software, allowing removal of low quality reads, short reads and contaminants (e.g. mitochondria, chloroplasts).

2.8. Determination of cultivable bacteria

The number of cultivable bacteria was determined in nZVI and mZVI treated reservoir water by counting CFUs in 1 mL of undiluted and 10-fold diluted samples spread on plate count agar (BIO-RAD, France) in sterile Petri dishes, with CFUs counted after seven days incubation at 20 ± 2 °C. Cultivable bacterial abundance is expressed as CFU per mL.

2.9. Microscopy analysis of phytoplankton

Determination of cell number and filament measurement was based on Czech standard methodologies (CSN 75 77 17). Disintegration of the algal and cyanobacterial colonies into individual cells was undertaken by addition of potassium hydroxide (KOH; 0.1 M), then sucking and releasing a 10 mL sample twenty times using a syringe. The cells were then counted in a Cytus I chamber (0.01 mL) using an Olympus

BX43 fluorescence microscope (Olympus, Japan) with a blue excitation filter for algae and a green excitation filter for cyanobacteria.

2.10. Calculation and statistical analysis

For improved comparison, all data were converted into a fold change, calculated by dividing the numbers of cells at day 1, 3, 7, 14 and 21 (D_n) by the number of cells at day 0 (D_0). The differences between treatments and control were compared using ANOVA and Dunnett's test (GraphPad PRISM, USA). Significance levels were set at $*P < 0.05$, $**P < 0.01$ and $***P < 0.001$.

Three diversity metrics were used to compare the impact of ZVI particles on bacterial community composition, as described in Newton and McLellan (2015).⁵³ Species were described using richness, the most abundant taxa/groups within samples were described using the inverse Simpson index and the tail statistic was used to describe the diversity of rare community members. The Mann–Whitney *U* test was used to examine whether composition of bacterial community exposed to mZVI differed significantly from those exposed to nZVI.

3. Results

3.1. Characterisation of ZVI particles in reservoir water

nZVI and mZVI particles were exposed to two differently prepared reservoir water (centrifugation and filtration) samples with the aim of removing microorganisms and debris that disable characterisation of the particles. Particles exposed to deionised water were considered as a control. Both nZVI and mZVI tended to aggregate in centrifuged reservoir water (Fig. 1A and 2A) and filtered reservoir water (Fig. 1B and 2B), but not in deionised water (Fig. 1C and 2C). mZVI particles had a normal (Gaussian) distribution from 1 to 5 μm , with the maximum ranging from 3.8 to 4 μm in all samples of reservoir and deionised water, as determined by DCS. In contrast, nZVI particles were split into two 'populations', with a dominant peak around 110 nm in centrifuged reservoir water and 120 nm in filtered reservoir water. The smaller population always appeared around 600 nm in both variants. In deionised water, the larger population was detected at around 100 nm and the smaller around 380 nm (Fig. 1D; see SEM images of pristine particles in Fig. S1† for comparison). Compared to centrifuged reservoir water, colloidal particles of natural organic compounds in filtered reservoir water were completely missing at fractions < 60 nm, while relatively few particles were observed at > 60 nm (Fig. S3†).

3.2. Physical–chemical parameters of reservoir water

Temperature remained more or less constant (22.5 ± 0.2 °C) over the 21 day experiment, with the exception of day 0 (sampling in reservoir; 18 °C; Fig. 3A). While the initial pH was 8.0 in untreated reservoir water (control), addition of ZVI particles caused an immediate significant increase in reservoir



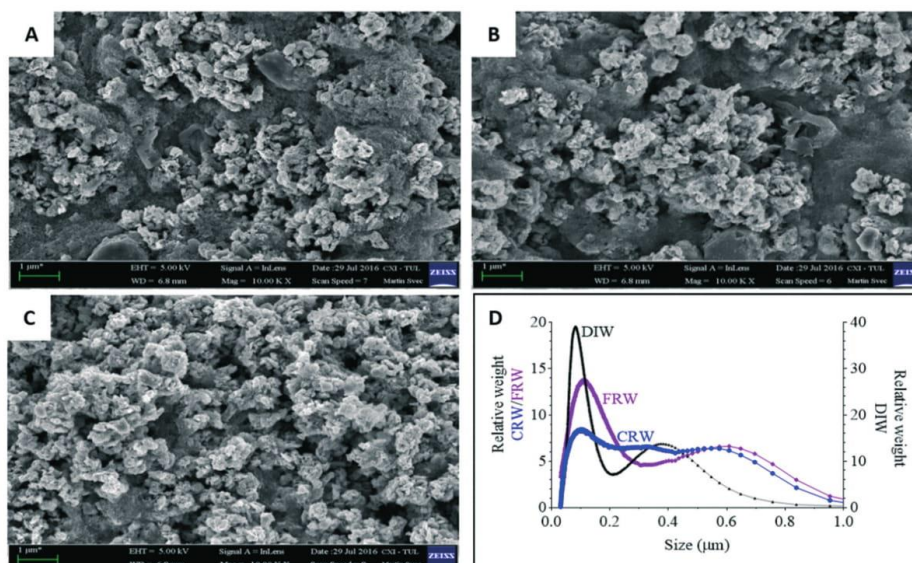


Fig. 1 Scanning electron microscopy images of nZVI exposed for 24 h in reservoir water: (A) nZVI in centrifuged reservoir water (CRW); (B) nZVI in filtered reservoir water (FRW); (C) nZVI in deionised water (DIW) used as a control; scale bar = 1 µm; (D) size distribution of nZVI in CRW, FRW and DIW determined by differential centrifugal sedimentation.

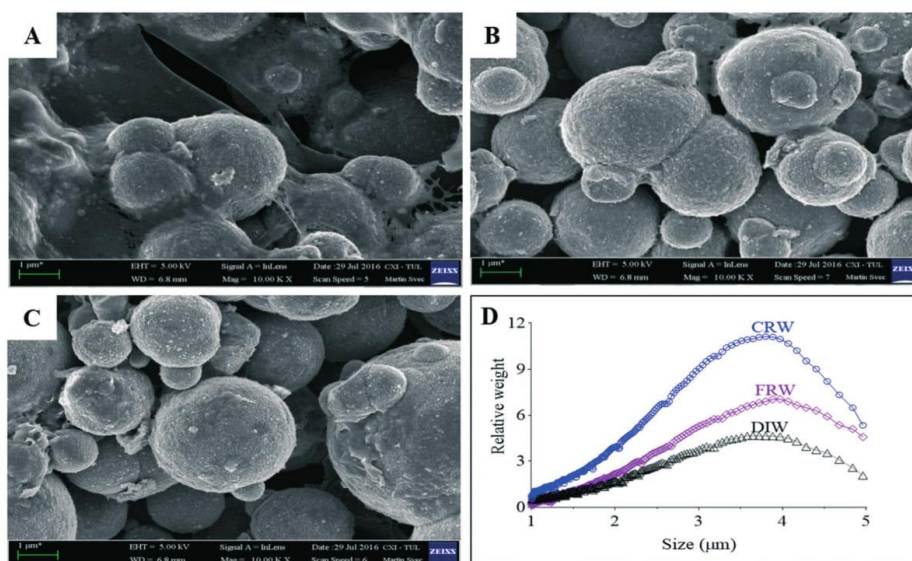


Fig. 2 Scanning electron microscopy images of mZVI exposed for 24 h in reservoir water: (A) mZVI in centrifuged reservoir water (CRW); (B) mZVI in filtered reservoir water (FRW); (C) mZVI in deionised water (DIW) used as a control; scale bar = 1 µm; (D) size distribution of mZVI in CRW, FRW and DIW determined by differential centrifugal sedimentation.

water treated with mZVI (pH 8.8; $P < 0.001$) and nZVI (8.5; $P < 0.01$). The pH then decreased slightly to 7.6 (reservoir water), 8.2 (nZVI) and 8.3 (mZVI), but remained significantly

higher than the control after one day and thereupon remained between 7.2 and 7.6 (with or without ZVI; not significant) until the end of the experiment (Fig. 3B). The ORP



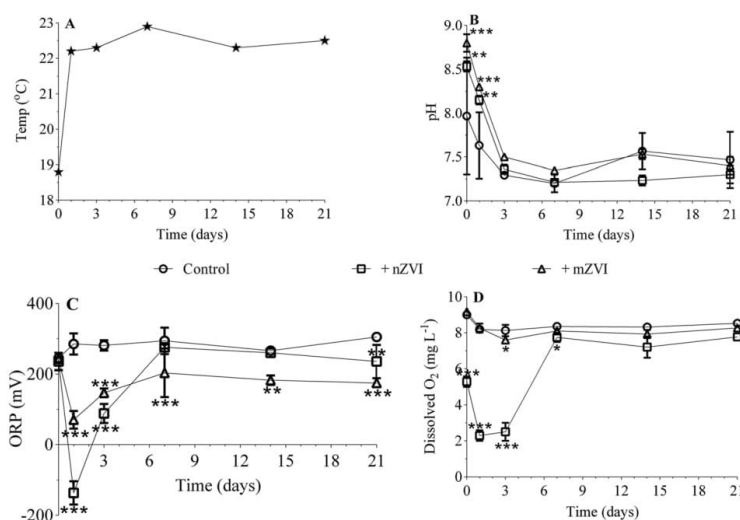


Fig. 3 Physio-chemical parameters monitored over the 21 day experiment with mZVI and nZVI in reservoir water. (A) Temperature, (B) pH, (C) oxidative reductive potential and (D) dissolved oxygen. Error bar $n = 3$. Statistically significant differences (* $P < 0.05$, ** $P < 0.01$ and *** $P < 0.001$) compare the treatment to the control.

of reservoir water was 245 mV at the beginning of the experiment and fluctuated around 300 mV until the end (Fig. 3C). The ORP of reservoir water with nZVI decreased to -136 mV ($P < 0.001$) and to 70 mV ($P < 0.001$) with mZVI after one

day. ORP gradually increased to 88 mV with nZVI ($P < 0.001$) and 148 mV with mZVI reservoir water ($P < 0.001$) after three days, after which there was no significant difference from the control with nZVI while mZVI ORP remained lower (175–200

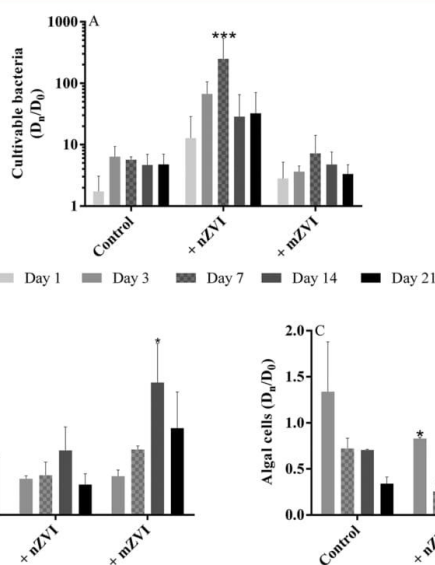


Fig. 4 Abundance of planktonic microorganisms (fold change of D_n/D_0) over the 21 day experiment using reservoir water with nZVI (+ nZVI), reservoir water with mZVI (+ mZVI), and reservoir water only as a control; (A) cultivable bacteria, (B) cyanobacterial number and (C) green algae number. Note: different scales for the y axis. Error bars $n = 3$. Statistically significant differences (* $P < 0.05$, ** $P < 0.01$ and *** $P < 0.001$) compare the treatment to the control. The actual number of cells is provided in the ESI† (Table S2).



mV, $P < 0.01$) over the next 21 days (Fig. 3C). Dissolved oxygen in the control and mZVI sample was around 9 mg L^{-1} at the beginning of the experiment and decreased slightly to $\sim 8 \text{ mg L}^{-1}$ over 21 days. In comparison, nZVI caused a decline to 5.3 mg L^{-1} at day 0, declined further to 2.3 and 2.5 mg L^{-1} after one day and after three days ($P < 0.001$), respectively, then increased to 7.8 mg L^{-1} ($P < 0.05$) after seven days; this situation lasting until the end of the experiment (Fig. 3D). A reddish-brown colour appeared in bottles containing nZVI from day 2, demonstrating presence of oxidised Fe. The reddish colour was observed in reservoir water with both nZVI and mZVI at the end the experiment (Fig. S4†).

3.3. Effect of mZVI and nZVI on planktonic microorganisms

Compared to the untreated control samples, the number of cultivable bacteria in the nZVI treatment increased geometrically, with a maximum at day 7 yielding $171 \times 10^3 \text{ CFU mL}^{-1}$ ($P < 0.001$), but then decreased slowly up to day 21, though still remaining about 3–4 times higher than the control (Fig. 4A, Table S2A†). Both the control and the mZVI treatments displayed a similar number of CFU with no significant difference.

Changes in the number of cyanobacterial cells were recorded in the presence of ZVI particles (Fig. 4B; Table S2B†), with numbers increasing over time with mZVI (significantly higher than the control at day 14; $P < 0.05$) but remaining comparable to the control with nZVI. The dominant cyanobacterial species at the beginning of the experiment was the colony-forming *Microcystis aeruginosa*, followed by *M. flos-aquae* and *Woronichinia naegeliana* at lower abundance, and the genus *Anabaena* sp. rarely recorded. *M. aeruginosa* was still dominant after 7 days, while *M. flos-aquae* and *W. naegeliana* became dominant after 14 days, especially in reservoir water with mZVI.

Early in the experiment, small green algae (*Chlorophyta*) dominated the phytoplankton, especially colony-forming *Planktosphaeria* sp. followed by *Staurastrum* sp., *Scenedesmus* sp., *Tetraedron* sp., *Monoraphidium* sp., *Oocystis* sp. and *Botryococcus braunii*. *Bacillariophyta*, *Dinophyta* and *Cryptophyta* taxa were only rarely recorded, as were ciliates and flagellates. The number of small green algae in nZVI was reduced compared with the control after three days, with this effect remaining significant for up to seven days ($P < 0.05$), while abundance of algae in mZVI remained similar to the control throughout the study (Fig. 4C, Table S2C†).

3.4. Bacterial community composition

NGS was used to characterise bacterial communities in the control and in samples with nZVI and mZVI at day 0, 7 and 21. Diversity tests revealed samples with mZVI as having higher species richness than nZVI ($P < 0.05$), particularly as regards rare community members (tail) ($P < 0.05$, Table 1). Moreover, significant differences were observed at both the family and genus levels when comparing mZVI and nZVI, being more important towards the end of the experiment (day

Table 1 Comparison of diversity indices for reservoir water (control) and reservoir water with nZVI and mZVI. The numbers in brackets represent the standard deviation of duplicate samples

	Richness	Inverse Simpson	Tail
Control	161 (28)	10 (1)	20 (4)
nZVI	147 (18)	11 (3)	18 (2)
mZVI	184 (34)	14 (3)	24 (6)
Mann-Whitney <i>U</i>	Richness	Inverse Simpson	Tail
mZVI-nZVI	31 ^a	29 n.s.	32 ^a

^a Indicates significance at $P < 0.05$; n.s. not significant.

21; family: $P < 0.05$, genus: $P < 0.001$). Statistically significant changes were also detected between the control and nZVI/mZVI samples at genus level by day 21 ($P < 0.05$, Table 2).

At the beginning of the experiment, untreated epilimnion water displayed a typical freshwater bacterial community, being represented in all treatments by the phyla *Proteobacteria* (*Alpha*-, *Beta*- and *Deltaproteobacteria*; together 38%), *Actinobacteria* (23%), *Bacteroidetes* (19%), *Verrucomicrobia* (10%), *Cyanobacteria* (4%) and *Chloroflexi* (2%) (Fig. 5). At day 7, the relative abundance of *Actinobacteria* and *Alphaproteobacteria* had decreased in all treatments, being compensated for by an increase in *Verrucomicrobia* and *Deltaproteobacteria* (control and mZVI) or *Betaproteobacteria* (nZVI). After an additional two weeks (day 21), the abundance of *Actinobacteria* and *Deltaproteobacteria* had recovered while *Verrucomicrobia* stayed enriched and *Alphaproteobacteria* reduced in the control and mZVI treatments. In nZVI, *Betaproteobacteria* (still dominating the bacterioplankton) were reduced by an increase in *Chloroflexi* and *Deltaproteobacteria* at day 21. *Bacteroidetes* and *Cyanobacteria* were not, or only weakly, affected by the treatment over time.

At the family level, bacterial community structure was also typical for a freshwater reservoir, consisting of *Microbacteriaceae* and *Sporichthyaceae* (both *Actinobacteria*), *Burkholderiaceae* and *Comamonadaceae* (both *Betaproteobacteria*), *Acetobacteraceae*, *Caulobacteraceae*, *Pelagibacteriaceae*, *Rhodospirillaceae* (all *Alphaproteobacteria*), *Opitutae* (*Verrucomicrobia*), *Flavobacteriaceae* and *Saprosiraceae* (both *Bacteroidetes*), and *Roseiflexaceae* (*Chloroflexi*) (Fig. 6). Cluster analysis supported the existence of three sample groups: i) starting samples, ii) mZVI and control samples and iii) nZVI samples. Starting samples were dominated by members of the *Pelagibacteriaceae* (LD12 cluster; 23%), *Sporichthyaceae* (hgcl_clade; 20%), *Flavobacteriaceae* (genus *Flavobacterium*; 7%), *Comamonadaceae* (genus *Limnohabitans*; 3%), *Microbacteriaceae* ('*Candidatus Limnoluna*'; 2%) and *Roseiflexaceae* (genus *Roseiflexus*; 1.4%). While trends differed in the presence of nZVI compared to the control, there was no shift in structure in mZVI samples. For example, while the *Comamonadaceae* and *Flavobacteriaceae* families were gradually reduced in mZVI and the control, the family-like group

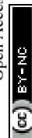


Table 2 Differences between control, nZVI and mZVI treatments at the genus and family levels, evaluated using the standard Mann-Whitney *U* test

Genus level	Day 0	Day 7	Day 21
Control/mZVI	n.s.	n.s.	*
Control/nZVI	n.s.	n.s.	*
mZVI/nZVI	n.s.	**	***
Family level			
Control/mZVI	n.s.	n.s.	n.s.
Control/nZVI	n.s.	n.s.	n.s.
mZVI/nZVI	n.s.	*	*

Significance levels: * $P < 0.05$, ** $P < 0.01$ and *** $P < 0.001$; n.s. not significant.

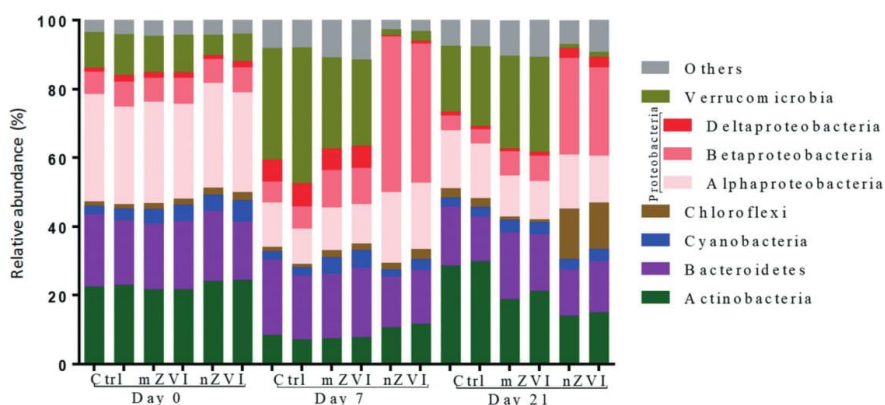


Fig. 5 Phylum and class composition of bacterial populations in the control, mZVI and nZVI treatments. The phylum *Proteobacteria* is represented by *Alfa*-, *Beta*- and *Delta*-classes. Phyla with less than 2% abundance are shown as unclassified. Samples without ZVI particles are used as a control (Ctrl). Note that each sample was sequenced in duplicate.

Opiritae_vadinHA64 increased continuously up to day 21. In the presence of nZVI, however, *Comamonadaceae* increased remarkably after seven days, then decreased after 21 days. *Opiritae_vadinHA64* decreased continuously while *Sporichthyaceae* declined and remained at the same low level from day 7 to the end of the experiment (Fig. 6).

At the genus level, a comparison of relative abundance in the nZVI and mZVI treatments with the control revealed seven groups with >5% change in total bacterial population (Fig. 7). In general, the addition of nZVI particles resulted in more dynamic population shifts (up to 29%) than the addition of mZVI (<11%). A decline in the LD12 cluster and an increase in *Limnohabitans* and in the *Comamonadaceae_unclassified* read tags was observed as a common effect of both materials. *Roseiflexus* showed a continuous increase over days 0, 7, but not day 21, following mZVI treatment, while the opposite trend was observed in the tribe *Opiritae_vadinHA64*. The *hgcI* clade abundance remained steady until day 7, but was reduced by day 21. The tribe *OPB35_soil_group* was enriched from its initial abundance in nZVI and mZVI treatments, including the control; however, population growth in nZVI treatment was 5% lower

than in control after 7 days. Other genus-like groups also showing 3–5% differences from the control were *Azospirillum*, *Brevundimonas*, *Desulfomonile*, *Flavobacterium*, the NS11-12_marine_group, *Polynucleobacter*, *Roseomonas* and the *Bacteria_unclassified* group. *Flavobacterium*, *Polynucleobacter* and *Roseomonas* all profited from nZVI treatment over both sampling days, while the NS11-12_marine_group was always depleted. A notable decrease in population size was observed for *Desulfomonile* and the *Bacteria_unclassified* group in nZVI at day 7. *Desulfomonile* was also reduced in mZVI at day 7.

3.5. Ferroxidase enzyme

Abundance of enzymes related to iron metabolism in bacteria was calculated using the Paprica⁵² pipeline, which conducts a metabolic inference from 16S rRNA gene sequence libraries. Specifically, we extracted pathway and time changes in abundance of ferroxidase enzyme (EC1.16.3.1).

Compared to the control, the abundance of ferroxidase changed in the presence of nZVI and mZVI over the 21 day experiment (Fig. S5†), with the enzyme gradually increasing in *Roseiflexus* sp. and the species *Roseiflexus castenholzii* but



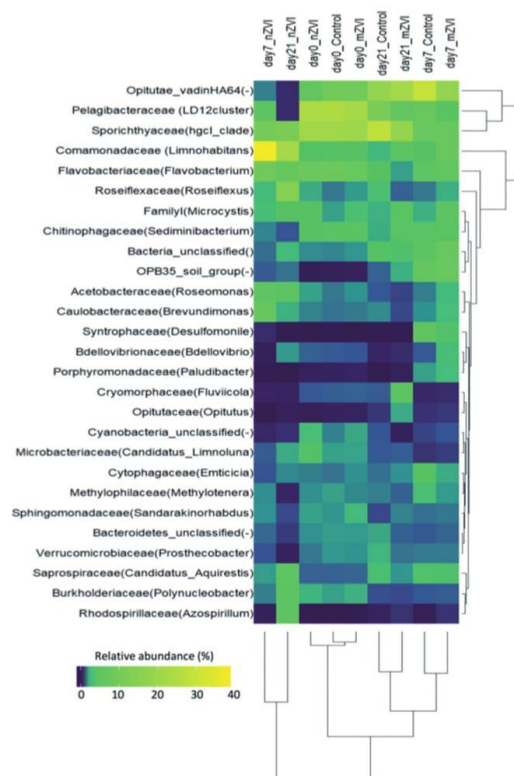


Fig. 6 Heatmap indicating the relative abundance of the major bacterial families for days 0, 7 and 21. The relationship of the bacterial composition in each sample is depicted with a cluster dendrogram based on Bray-Curtis dissimilarity among samples and among families. The dominant genus rank is provided in parentheses after the family name (dash '-'), when unclassified at genus level. Only those families with a relative abundance >2% are shown. Data are means from duplicate samples.

decreasing in *Fluviicola taffensis* (Fig. S6†). Based on our data, there was no indication of ferroxidase enzyme in the genus *Sediminibacterium*.

4. Discussion

The use of commercially produced ZVI particles for remediation of polluted aquatic habitats has resulted in questions regarding their impact on naturally occurring microbial communities.^{15,54,55} Microbial communities are important in aquatic habitats as they are responsible for dissolved carbon transfer to higher trophic levels (the microbial food web concept). They have also been described as key players in the self-purification of lakes and reservoirs,⁵⁶ and as such possess high ecological potential. In contrast to previous studies,³³ we opened a black box and identified freshwater heterotrophic bacteria that were affected by nZVI and mZVI particles.

4.1. Effect of ZVI on phytoplankton and associated bacteria

We observed different effects of nZVI and mZVI on freshwater reservoir microorganisms (Fig. 4 and 5). Presence of nZVI, for example, significantly stimulated growth of cultivable bacteria but reduced the number of algae on day 3 and day 7, compared to the control (Fig. 4A and C). On the other hand, addition of mZVI resulted in a slight increase in cyanobacteria, which was rather surprising (Fig. 4B and 5). While the use of nZVI has been suggested for prevention of harmful cyanobacterial blooms,^{11,12} our study revealed no significant effect of nZVI on cyanobacteria.

The association of distinct bacterial consortia with specific algae is known as the "phycosphere". In our study, we found similar bacterial clades as described for the *M. aeruginosa* phycosphere in plateau lake,⁵⁷ i.e. *Brevundimonas*, the OM27 clade and *Roseomonas*. The genus *Brevundimonas* (*Caulobacteraceae*) has been described as a keystone species in particle-associated bacterial communities during *M. aeruginosa* blooms⁵⁷ and, while information on clade OM27 is limited, *Roseomonas* sequences have been detected in freshwater bacterial communities associated with cyanobacterial blooms in four Swedish lakes.⁵⁸

Additionally, we also observed that cyanobacterial colonies of *M. aeruginosa* (cells 4–5 μm) dominant up to day 7 in mZVI, were then outcompeted by *M. flos-aquae* and *W. naegelianiana* (cells 2–3 μm). Small-cell colonies were most probably more capable of competition for nutrients, because similar trends were observed in nZVI and control as well. Increasing proportion of disintegrated and partly decayed cyanobacterial cells towards the end of the experiment could be caused by depletion of nutrients, and, moreover algicidal bacteria (e.g. *Brevundimonas*, Fig. 6) might work against cyanobacteria. Algicidal bacteria that can associate with cyanobacteria have the capability to control their proliferation in fresh water and even to lyse them.⁵⁹

The reduction of small green algae after seven days in nZVI was most probably due to unfavourable conditions due to decline in ORP and depletion of bioavailable phosphorus,^{11,12} while the decrease of algal number over the 21 days of the experiment in nZVI, mZVI as well as in control strongly suggests the nutrient limitation. Consequently, bacteria decomposing algal cell walls were favoured by the availability of polysaccharides. We speculate that the increase in relative abundance in the OPB35_soil_group (*Verrucomicrobia*, Fig. 7) could be linked to the decay of algae due to its capability for active polysaccharide degradation (laminarin and xylose) of the closely-related genus *Limnisphaera*.⁶⁰

4.2. Oxygen and ORP drive microbial community composition

Compared with the control and mZVI samples, nZVI reductive reactivity resulted in a significant drop in dissolved oxygen and ORP at the start of the experiment (Fig. 3). Consequently, the strictly aerobic genus *Sediminibacterium* (*Chitinophagaceae*)⁶¹ population decreased with nZVI, but not



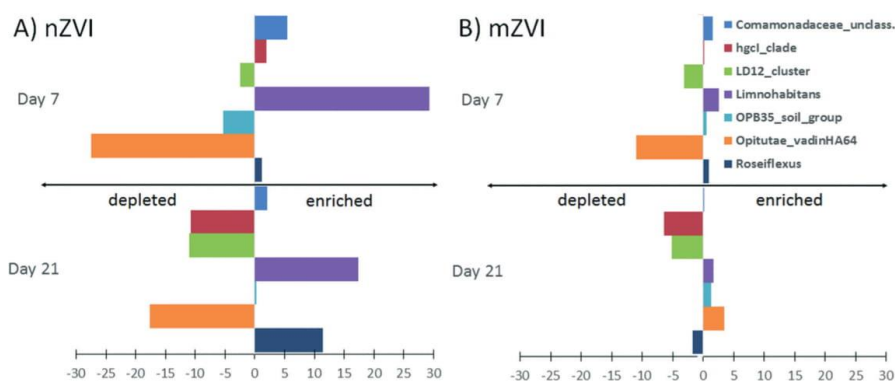


Fig. 7 Impact of ZVI particles on the development of genus-like groups of the most abundant bacteria from the Harcov reservoir. Values were calculated as differences in relative abundance in A) nZVI and the control, or B) mZVI and the control, after 7 and 21 days. The values are means from duplicate measurements. Only those genera or tribes with a relative difference >5% are shown.

in the control or with mZVI (Fig. 6). Moreover, the low dissolved oxygen concentration most probably affected phagotrophic protists, such as heterotrophic flagellates and ciliates. Both these protist groups are efficient grazers on bacteria and, as such, exhibit “top-down” control.⁶² As grazing on bacteria was found to be negligible under anoxic conditions,⁶³ absence of oxygen probably released bacteria from grazing pressure and shifted the community from small-size grazing-resistant prokaryotes to fast-growing opportunists.⁶⁴ In support of our hypothesis, the addition of nZVI strongly favoured growth of *Limnohabitans* (*Betaproteobacteria*), facultative anaerobes^{65,66} and fast growing bacteria that often dominate in bacterivore-free (<0.8 μm) treatments.⁶⁷ In contrast, the freshwater LD12 cluster (*Alphaproteobacteria*) and *Verrucomicrobia*, with their slow-growth life strategy, were depleted in the same treatments. The lesser decrease in ORP (though persistent over the 21 days) caused by mZVI resulted in *Opirituae_vadinHA64* and *OPB35_soil* (*Verrucomicrobia*) being slightly enriched. *Opirituae_vadinHA64* have recently been recorded in the epilimnion of freshwater lakes with higher dissolved oxygen concentrations,⁶⁸ similar to that in the mZVI treatment, and thus we can assume that this cluster prefers aerobic conditions. Unfortunately, *Verrucomicrobia* are still poorly understood, many publications have noted that different members of this group have different oxygen requirements, some being strict aerobes while others are facultative anaerobes or strict anaerobes.^{69–72}

4.3. Response of rare bacterial taxa

Rare bacteria have been proposed as drivers of key functions in aquatic systems as they outnumber the dominant group diversity and each represents a specific metabolic combination.⁷³ Their appearance in samples after experimental manipulation suggests that conditions differed from *in situ* reservoir conditions, where they were almost absent. Our experiment promoted growth of the biofilm-forming taxa

Azospirillum (*Rhodospirillaceae*, *Alphaproteobacteria*) and *Paludibacter* (*Porphyromonadaceae*, *Bacteroidetes*), both having a negligible relative abundance at day 0 but increasing dramatically over the next three weeks of the experiment (Fig. 6). *Azospirillum* bacteria are diazotrophs with the capacity for sulphur-chemolithotrophy.⁷⁴ The strictly anaerobic *Paludibacter* has previously been reported as the most abundant genus on biofilms forming on particles of 0.02–0.2 mm under static conditions.⁷⁵ Similarly, the genus *Desulfomonile*, which bloomed after seven days but then vanished up until day 21 in both treatments (Fig. 6), has previously been reported as a rare taxa from acidic peatlands responding to sulphate incubation.⁷⁶ Populations of the filamentous bacteria ‘*Candidatus Aquirestis*’ (LD2/SOL cluster, *Bacteroidetes*) benefitted from the experimental setup and established strong populations in nZVI and reservoir water after 21 days. These bacteria primarily inhabit the pelagic zone of non-acidic stagnant inland waters and show a strong spring peak, with minor peaks in summer and early autumn.⁷⁷ To conclude, the emergence of rare bacterial taxa indicates changes in water chemistry and the availability of nutrients. In our study, this appears to have been due to increasing nitrogen limitation, a higher availability of sulphur and iron, and the decay of algae with polysaccharide cell walls.

4.4. Oligotrophic bacteria depletion in nZVI

Manipulation experiments may lead to nutrient depletion during transfer from a dissolved to a particulate (biomass) fraction. The freshwater clusters *hgcI* (*Actinobacteria*) and LD12 (*Alphaproteobacteria*) are small slow-growing bacteria with a passive life style favoured by oligotrophic conditions.⁶⁸ We hypothesise that their relatively high abundance in the reservoir water control and mZVI treatments could serve as indicators of nutrient depletion, while their lower numbers in the nZVI treatment suggest nutrient remineralisation.



In soils, *Verrucomicrobia* generally displays an oligotrophic life strategy.⁷⁸ Currently, members of the phylum *Verrucomicrobia* are increasingly being recognised as abundant species in aquatic habitats,⁶⁸ with prevalence of cluster CL0-14 being negatively correlated with high pH and positively correlated with hydraulic retention time and temperature, as are the oligotrophic clusters LD12 (freshwater SAR11 cluster) and LD28 (*Methylopusillus* spp.).⁷⁹ Our manipulations demonstrated a striking decrease in the abundance of the *Verrucomicrobia* cluster *Opiritutae_vadinHA64* after nZVI addition, similar to that for the *hgcI* and LD12 clusters (Fig. 6). The *Opiritutae_vadinHA64* cluster represents around 80% of all *Verrucomicrobia* in the Harcov reservoir; hence, it has great potential as an indicator clade of nZVI. However, more information is still needed on its ecophysiology, distribution, phylogeny and diversity.

4.5. ZVI particles enhance growth of bacteria with ferroxidase

Typically for natural freshwaters, dissolved Fe(II) was found at very low concentrations (0.1 to 0.01 mg L⁻¹; Table S3†) in this study. On the other hand, oxidation of Fe(0) releasing soluble Fe(II), which was further converted into insoluble Fe(III), was ongoing throughout the experiment.⁸⁰ Iron oxidising bacteria may have caused the increase in cultivable bacteria, also supported by the simultaneous increase in ferroxidase enzyme, a key enzyme in Fe(II) oxidation. The most probable source in this case was the nZVI, which can supply extra Fe(II) for bacterial metabolism.

To date, all known oxygen-dependent, neutrophilic and lithotrophic iron oxidisers have been recorded within the *Proteobacteria*^{23,81} and for *Comamonadaceae* in groundwaters at neutral pH.⁸² In this study, however, we confirmed *Roseiflexus* sp. and *Roseiflexus castenholzii* as being heavily involved in the increase of ferroxidase, a fact not reported elsewhere (Fig. S5 and S6†). Similar trends were observed in a microcosm study on the River Thames, the authors presuming that the increase in total bacteria was attributable to the Fe oxidation process itself.¹⁵ In a previous study, *Sediminibacterium* was identified as an iron-oxidising bacterium actively promoting the corrosion of cast iron pipes alongside sulphur-oxidising and iron-reducing bacteria.⁸³ In our study, the comparable levels recorded in the control and mZVI treatment suggest that *Sediminibacterium* were not promoted by the addition of ZVI particles.

4.6. ZVI particle fate in the aquatic environment

The behaviour of nZVI and mZVI is strongly dependent on environmental conditions. In our case, the detection and measurement of ZVI particles was only possible after centrifugation or filtration, following the removal of large debris particles or microorganisms. As with mZVI, nZVI tended to show higher aggregation/agglomeration in centrifuged rather than filtered reservoir water (Fig. 1 and 2), most probably due to a higher content of colloids that remained after centrifugation. Hence, we believe that centrifuged reservoir water is more

comparable to natural reservoir water than filtered water. Stronger particle aggregation is often connected with higher pH values^{16,19} and, indeed, water from the Harcov reservoir was somewhat alkaline (pH 8.0). The pH increased still further up to 8.8 with ZVI as an electron donor (Fig. 3), though the pH decreased to ~7.4 over the next 21 days in both ZVI treatments. Under the oxic conditions in our study, released Fe(II) quickly oxidised to Fe(III) and most probably formed stable colloids with natural organic matter⁸⁴ that were not harmful to microorganisms. Moreover, the aggregated ZVI particles rapidly formed a sediment, which could reduce their effect on freely-swimming microorganisms in the water column, allowing them to escape direct contact.^{20,30} Oxidation of nZVI led to a decline in ORP and dissolved oxygen concentration after one day (Fig. 3), which had a strong influence on shifts in bacterial community, as described above. However, these values increased again as nZVI oxidised and reductive capacity was spent, resulting in values comparable with the control, the process being driven further by the growth and activity of the microorganisms described above.

5. Conclusions

In general, nZVI showed a stronger effect on planktonic microorganisms than mZVI, most probably due to its higher reactivity. nZVI significantly stimulated the growth of cultivable bacteria and iron-oxidising bacteria but slightly reduced the growth of algae. Phagotrophic flagellates and ciliates were most probably affected by low dissolved oxygen concentration, such conditions releasing bacteria from grazing pressure and shifting the community from small grazing-resistant prokaryotes to fast-growing opportunists. In support of this hypothesis, nZVI strongly favoured growth of the facultative anaerobe *Limnohabitans* and other opportunist bacteria that can come to dominate in bacterivore-free treatments, whereas the LD12 cluster and *Verrucomicrobia*, with slow-growing life strategies, were depleted. Unexpectedly, mZVI resulted in a slight increase in cyanobacterial number, which could be explained by increase in small-cell colonies of *M. flo-aquae*, and *W. naegeliana*. Further *in situ* studies that more realistically mimic reservoir conditions could well reveal more information on the influence of ZVI on natural microbial communities, including parts of the microbial food web not covered here such as heterotrophic flagellates and viruses.

Conflicts of interest

There are no conflicts to declare.

Acknowledgements

The research reported in this paper was financially supported by the Technology Agency of the Czech Republic within “Nanobiowat” under Project no. TE01020218, and by the Ministry of Education, Youth and Sports under the framework of targeted support for the “National Programme for



Sustainability I", the OPR & DI project (LO 1201) and Nano-Envi, Project no. LM2015073. The work of N. Nguyen was partly supported by MŠMT under SGS Project no. 21176/115 of the Technical University of Liberec. V. Kasalický was supported by Czech Science Foundation Project no. 15-12197S.

References

- 1 P. Bardos, B. Bone, M. Černík, D. W. Elliott, S. Jones and C. Merly, *Remediation*, 2015, **26**, 101–108.
- 2 Y. S. El-Temseh and E. J. Joner, *Chemosphere*, 2012, **89**, 76–82.
- 3 A. Ševců, Y. S. El-Temseh, J. Filip, E. J. Joner, K. Bobčíková and M. Černík, *Environ. Sci. Pollut. Res.*, 2017, **24**, 21191–21202.
- 4 K. J. Cantrell, D. I. Kaplan and T. W. Wietsma, *J. Hazard. Mater.*, 1995, **42**, 201–212.
- 5 R. A. Crane and T. B. Scott, *J. Hazard. Mater.*, 2012, **211–212**, 112–125.
- 6 Wei-xian Zhang and W. X. Zhang, *J. Nanopart. Res.*, 2003, **5**, 323–332.
- 7 N. C. Mueller, J. Braun, J. Bruns, M. Černík, P. Rissing, D. Rickerby and B. Nowack, *Environ. Sci. Pollut. Res.*, 2012, **19**, 550–558.
- 8 S. Comba, A. Di Molfetta and R. Sethi, *Water, Air, Soil Pollut.*, 2011, **215**, 595–607.
- 9 J. Němeček, P. Pokorný, O. Lhotský, V. Knytl, P. Najmanová, J. Steinová, M. Černík, A. Filipová, J. Filip and T. Cajthaml, *Sci. Total Environ.*, 2015, **563–564**, 822–834.
- 10 F. Fu, D. D. Dionysiou and H. Liu, *J. Hazard. Mater.*, 2014, **267**, 194–205.
- 11 B. Marsalek, D. Jancula, E. Marsalkova, M. Mashlan, K. Safarova, J. Tucek and R. Zboril, *Environ. Sci. Technol.*, 2012, **46**, 2316–2323.
- 12 V. K. Sharma, L. Chen, B. Marsalek, R. Zboril, K. E. O'Shea and D. D. Dionysiou, *Water Sci. Technol.: Water Supply*, 2016, **17**, 107–114.
- 13 R. Köber, H. Hollert, G. Hornbruch, M. Jekel, A. Kamptner, N. Klaas, H. Maes, K.-M. Mangold, E. Martac, A. Matheis, H. Paar, A. Schäffer, H. Schell, A. Schiwy, K. R. Schmidt, T. J. Strutz, S. Thümmeler, A. Tiehm and J. Braun, *Environ. Earth Sci.*, 2014, **72**, 3339–3352.
- 14 P. Bardos, B. Bone, P. Daly, D. Elliott, S. Jones, G. Lowry and C. Merly, *A Risk/Benefit Appraisal for the Application of Nano-Scale Zero Valent Iron (nZVI) for the Remediation of Contaminated Sites*, WP9 NanoRem, 2014.
- 15 R. J. Barnes, C. J. van der Gast, O. Riba, L. E. Lehtovirta, J. I. Prosser, P. J. Dobson and I. P. Thompson, *J. Hazard. Mater.*, 2010, **184**, 73–80.
- 16 M. Auffan, W. Achouak, J. Rose, M. A. Roncato, C. Chanéac, D. T. Waite, A. Masion, J. C. Woicik, M. R. Wiesner and J. Y. Bottero, *Environ. Sci. Technol.*, 2008, **42**, 6730–6735.
- 17 C. Lei, L. Zhang, K. Yang, L. Zhu and D. Lin, *Environ. Pollut.*, 2016, **218**, 505–512.
- 18 A. Ševců, Y. S. El-Temseh, E. J. Joner and M. Černík, *Microbes Environ.*, 2011, **26**, 271–281.
- 19 A. Keller, K. Garner, R. J. Miller and H. S. Lenihan, *PLoS One*, 2012, **7**, 1–10.
- 20 M. Diao and M. Yao, *Water Res.*, 2009, **43**, 5243–5251.
- 21 M. L. Saccà, C. Fajardo, G. Costa, C. Lobo, M. Nande and M. Martin, *Chemosphere*, 2014, **104**, 184–189.
- 22 W. Zhang, C.-B. Wang and H.-L. Lien, *Catal. Today*, 1998, **40**, 387–395.
- 23 S. Hedrich, M. Schlömann and D. B. Johnson, *Microbiology*, 2011, **157**, 1551–1564.
- 24 M. L. Saccà, C. Fajardo, M. Nande and M. Martín, *Microb. Ecol.*, 2013, **66**, 806–812.
- 25 J. Y. Kim, H. J. Park, C. Lee, K. L. Nelson, D. L. Sedlak and J. Yoon, *Appl. Environ. Microbiol.*, 2010, **76**, 7668–7670.
- 26 C. Fajardo, M. L. Saccà, M. Martinez-Gomariz, G. Costa, M. Nande and M. Martin, *Chemosphere*, 2013, **93**, 1077–1083.
- 27 C. Jiang, X. Xu, M. Megharaj, R. Naidu and Z. Chen, *Sci. Total Environ.*, 2015, **530–531**, 241–246.
- 28 Y. S. El-Temseh, A. Sevcu, K. Bobcikova, M. Cernik and E. J. Joner, *Chemosphere*, 2016, **144**, 2221–2228.
- 29 J. Semerád and T. Cajthaml, *Appl. Microbiol. Biotechnol.*, 2016, **100**, 9809–9819.
- 30 R. Hjorth, C. Coutris, N. H. A. Nguyen, A. Sevcu, A. Baun and E. Joner, *Chemosphere*, 2017, **182**, 525–531.
- 31 C. Fajardo, L. T. Ortíz, M. L. Rodriguez-Membibre, M. Nande, M. C. Lobo and M. Martin, *Chemosphere*, 2012, **86**, 802–808.
- 32 E. L. Tilston, C. D. Collins, G. R. Mitchell, J. Princivalle and L. J. Shaw, *Environ. Pollut.*, 2013, **173**, 38–46.
- 33 T. L. Kirschling, K. B. Gregory, E. G. Minkley, G. V. Lowry and R. D. Tilton, *Environ. Sci. Technol.*, 2010, **44**, 3474–3480.
- 34 J. Němeček and J. Lhotský, *Sci. Total Environ.*, 2014, **485–486**, 739–747.
- 35 A. Schiwy, H. M. Maes, D. Koske, M. Flecken, K. R. Schmidt, H. Schell, A. Tiehm, A. Kamptner, S. Thümmeler, H. Stanjek, M. Heggen, R. E. Dunin-Borkowski, J. Braun, A. Schäffer and H. Hollert, *Environ. Pollut.*, 2016, **216**, 1–9.
- 36 L. G. Cullen, E. L. Tilston, G. R. Mitchell, C. D. Collins and L. J. Shaw, *Chemosphere*, 2011, **82**, 1675–1682.
- 37 Y.-h. Shih, H. L. Chou, Y. H. Peng and C.-y. Chang, *Bioresour. Technol.*, 2012, **108**, 14–20.
- 38 M. Velimirovic, Q. Simons and L. Bastiaens, *Chemosphere*, 2015, **134**, 338–345.
- 39 N. H. A. Nguyen, N. R. von Moos, V. I. Slaveykova, K. Mackenzie, R. U. Meckenstock, S. Thümmeler, J. Bosch and A. Ševců, *Ecotoxicol. Environ. Saf.*, 2018, **154**, 36–44.
- 40 G. V. Lowry, E. M. Hotze, E. S. Bernhardt, D. D. Dionysiou, J. A. Pedersen, M. R. Wiesner and B. Xing, *J. Environ. Qual.*, 2010, **39**, 1867–1874.
- 41 C. Colombo, G. Palumbo, J. Z. He, R. Pinton and S. Cesco, *J. Soils Sediments*, 2014, **14**, 538–548.
- 42 J. Soukupova, R. Zboril, I. Medrik, J. Filip, K. Safarova, R. Ledl, M. Mashlan, J. Nosek and M. Cernik, *Chem. Eng. J.*, 2015, **262**, 813–822.
- 43 Z. Shi, D. Fan, R. L. Johnson, P. G. Tratnyek, J. T. Nurmi, Y. Wu and K. H. Williams, *J. Contam. Hydrol.*, 2015, **181**, 17–35.



- 44 T. J. Strutz, G. Hornbruch, A. Dahmke and R. Köber, *J. Contam. Hydrol.*, 2016, **191**, 54–65.
- 45 D. Ribas, M. Cernik, V. Martí and J. A. Benito, *J. Nanopart. Res.*, 2016, **18**, 181.
- 46 I. Dolinová, M. Czinnerová, L. Dvořák, V. Stejskal, A. Ševců and M. Černík, *Chemosphere*, 2016, **157**, 276–285.
- 47 S. E. Dowd, T. R. Callaway, R. D. Wolcott, Y. Sun, T. McKeehan, R. G. Hagevoort and T. S. Edrington, *BMC Microbiol.*, 2008, **8**, 125.
- 48 M. J. Claesson, Q. Wang, O. O'Sullivan, R. Greene-Diniz, J. R. Cole, R. P. Ross and P. W. O'Toole, *Nucleic Acids Res.*, 2010, **38**, 1–13.
- 49 P. D. Schloss, S. L. Westcott, T. Ryabin, J. R. Hall, M. Hartmann, E. B. Hollister, R. A. Lesniewski, B. B. Oakley, D. H. Parks, C. J. Robinson, J. W. Sahl, B. Stres, G. G. Thallinger, D. J. Van Horn and C. F. Weber, *Appl. Environ. Microbiol.*, 2009, **75**, 7537–7541.
- 50 R. C. Edgar, B. J. Haas, J. C. Clemente, C. Quince and R. Knight, *Bioinformatics*, 2011, **27**, 2194–2200.
- 51 A. J. Oksanen, F. G. Blanchet, M. Friendly, R. Kindt, P. Legendre, D. Mcglinn, P. R. Minchin, R. B. O. Hara, G. L. Simpson, P. Solymos, M. H. H. Stevens, E. Szoecs and H. Wagner, *The Comprehensive R Archive Network*, 2016, 2.4-1, pp. 1–291, <https://github.com/vegandevs/vegan>.
- 52 J. S. Bowman and H. W. Ducklow, *PLoS One*, 2015, **10**, 1–18.
- 53 R. J. Newton and S. L. McLellan, *Front. Microbiol.*, 2015, **6**, 1–13.
- 54 A. M. I. Niyas, *J. Crit. Rev.*, 2014, **1**, 26–39.
- 55 E. Lefevre, N. Bossa, M. R. Wiesner and C. K. Gunsch, *Sci. Total Environ.*, 2015, **565**, 889–901.
- 56 M. A. Cooperstein and H. E. Canavan, *Biointerphases*, 2013, **8**, 1–12.
- 57 C. Yang, Q. Wang, P. N. Simon, J. Liu, L. Liu, X. Dai, X. Zhang, J. Kuang, Y. Igarashi, X. Pan and F. Luo, *Front. Microbiol.*, 2017, **8**, 1202.
- 58 A. Eiler and S. Bertilsson, *Environ. Microbiol.*, 2004, **6**, 1228–1243.
- 59 N. Meyer, A. Bigalke, A. Kaulfuß and G. Pohnert, *FEMS Microbiol. Rev.*, 2017, **41**, 880–899.
- 60 M. Martinez-Garcia, D. M. Brazel, B. K. Swan, C. Arnosti, P. S. G. G. Chain, K. G. Reitenga, G. Xie, N. J. Poulton, M. L. Gomez, D. E. D. D. Masland, B. Thompson, W. K. Bellows, K. Ziervogel, C.-C. C. Lo, S. Ahmed, C. D. Gleasner, C. J. Detter and R. Stepanauskas, *PLoS One*, 2012, **7**, 1–11.
- 61 Y. Kim, B. Kim, K. Kang and T.-Y. Y. Ahn, *Int. J. Syst. Evol. Microbiol.*, 2016, **66**, 4501–4505.
- 62 K. Simek, J. Pernthaler, M. G. Weinbauer, J. R. Dolan, J. Nedoma, M. Masin and K. Hornak, *Appl. Environ. Microbiol.*, 2001, **67**, 2723–2733.
- 63 A. Oikonomou, M. Pachiadaki and T. Stoeck, *FEMS Microbiol. Ecol.*, 2014, **87**, 691–703.
- 64 J. Pernthaler, *Nat. Rev. Microbiol.*, 2005, **3**, 537–546.
- 65 M. W. Hahn, V. Kasalický, J. Jezbera, U. Brandt and K. Šimek, *Int. J. Syst. Evol. Microbiol.*, 2010, **60**, 2946–2950.
- 66 V. Kasalický, J. Jezbera, K. Šimek and M. W. Hahn, *Int. J. Syst. Evol. Microbiol.*, 2010, **60**, 2710–2714.
- 67 K. Šimek, K. Horňák, J. Jezbera, J. Nedoma, P. Znachor, J. Hejzlar and J. Sed'a, *Aquat. Microb. Ecol.*, 2008, **51**, 249–262.
- 68 R. J. Newton, S. E. Jones, A. Eiler, K. D. McMahon and S. Bertilsson, *Microbiol. Mol. Biol. Rev.*, 2011, **75**, 14–49.
- 69 P. J. Cabello-Yeves, R. Ghai, M. Mehrshad, A. Picazo, A. Camacho and F. Rodriguez-Valera, *Front. Microbiol.*, 2017, **8**, 1–17.
- 70 A. De Wever, K. Van Der Gucht, K. Muylaert, S. Cousin and W. Vyverman, *Aquat. Microb. Ecol.*, 2008, **50**, 113–122.
- 71 J. Zhang, X. Zhang, Y. Liu, S. Xie and Y. Liu, *Ann. Microbiol.*, 2014, **64**, 1405–1411.
- 72 J. F. Humbert, U. Dorigo, P. Cecchi, B. Le Berre, D. Debros and M. Bouvy, *Environ. Microbiol.*, 2009, **11**, 2339–2350.
- 73 A. Jousset, C. Bienhold, A. Chatzinotas, L. Gallien, A. Gobet, V. Kurm, K. Küsel, M. C. Rillig, D. W. Rivett, J. F. Salles, M. G. A. van der Heijden, N. H. Youssef, X. Zhang, Z. Wei and W. H. G. Hol, *ISME J.*, 2017, **11**, 853–862.
- 74 Y. Kwak and J. H. Shin, *Mar. Genomics*, 2016, **25**, 21–24.
- 75 H. Fang, Y. Chen, L. Huang and G. He, *Sci. Rep.*, 2017, **7**, 1–14.
- 76 B. Hausmann, K.-H. Knorr, K. Schreck, S. G. Tringe, T. Glavina Del Rio, A. Loy and M. Pester, *ISME J.*, 2016, **10**, 2365–2375.
- 77 M. Schauer, C. Kamenik and M. W. Hahn, *Appl. Environ. Microbiol.*, 2005, **71**, 5900–5907.
- 78 G. T. Bergmann, S. T. Bates, K. G. Eilers, C. L. Lauber, J. G. Caporaso, W. A. Walters, R. Knight and N. Fierer, *Soil Biol. Biochem.*, 2011, **43**, 1450–1455.
- 79 M. M. Salcher, S. M. Neuenschwander, T. Posch and J. Pernthaler, *ISME J.*, 2015, **9**, 2442–2453.
- 80 A. J. Feitz, S. H. Joo, J. Guan, Q. Sun, D. L. Sedlak and T. D. Waite, *Colloids Surf., A*, 2005, **265**, 88–94.
- 81 D. Emerson, E. J. Fleming and J. M. McBeth, *Annu. Rev. Microbiol.*, 2010, **64**, 561–583.
- 82 M. Blöthe and E. E. Roden, *Appl. Environ. Microbiol.*, 2009, **75**, 468–473.
- 83 H. Wang, C. Hu, X. Hu, M. Yang and J. Qu, *Water Res.*, 2012, **46**, 1070–1078.
- 84 P. Liao, W. Li, Y. Jiang, J. Wu, S. Yuan, J. D. Fortner and D. E. Giammar, *Environ. Sci. Technol.*, 2017, **51**, 12235–12245.



Paper 2

Nhung H. A. Nguyen, Nadia R. von Moos, Vera I. Slaveykova, Katrin Mackenzie, Rainer U. Meckenstock, Silke Thummler, Julian Bosch, and Alena Sevcu (2018). Biological effect of four iron-containing materials developed for nanoremediation on green alga *Chlamydomonas* sp. *Ecotoxicity and Environmental Safety*, 154, 36-44. **IF 3.743**



Contents lists available at ScienceDirect

Ecotoxicology and Environmental Safety

journal homepage: www.elsevier.com/locate/ecoenv

Biological effects of four iron-containing nanoremediation materials on the green alga *Chlamydomonas* sp.



Nhung H.A. Nguyen^a, Nadia R. Von Moos^b, Vera I. Slaveykova^{b,*}, Katrin Mackenzie^c,
Rainer U. Meckenstock^d, Silke Thümmmler^e, Julian Bosch^{f,1}, Alena Ševců^{a,*}

^a Technical University of Liberec, Institute for Nanomaterials, Advanced Technologies and Innovation, Faculty of Mechatronics, Informatics and Multidisciplinary Studies, Studentská 2, 461 17 Liberec, Czech Republic

^b University of Geneva, Faculty of Sciences, Earth and Environmental Sciences, Department for Environmental and Aquatic Sciences, Uni Carl Vogt, 66 Bvd Carl Vogt, 1211 Geneva, Switzerland

^c Helmholtz Centre for Environmental Research GmbH-UFZ, Permoserstraße 15, 04318 Leipzig, Germany

^d University of Duisburg-Essen, Biofilm Centre, Universitätsstr. 5, 45141 Essen, Germany

^e TU Bergakademie Freiberg, Institute of Mechanical Process Engineering and Mineral Processing, Agricolastraße 1, 09599 Freiberg, Germany

^f Helmholtz Zentrum München, Ingolstädter Landstraße 1, 85764 Neuherberg, Germany

ARTICLE INFO

Keywords:

Biological effect
FerMEG12
Carbo-Iron
Trap-Ox Fe-zeolite
Nano-Goethite
Chlamydomonas sp.

ABSTRACT

As nanoremediation strategies for in-situ groundwater treatment extend beyond nanoiron-based applications to adsorption and oxidation, ecotoxicological evaluations of newly developed materials are required. The biological effects of four new materials with different iron (Fe) speciations [i] FerMEG12 - pristine flake-like milled Fe(0) nanoparticles (nZVI), [ii] Carbo-Iron* - Fe(0)-nanoclusters containing activated carbon (AC) composite, [iii] Trap-Ox* Fe-BEA35 (Fe-zeolite) - Fe-doped zeolite, and [iv] Nano-Goethite - 'pure' FeOOH were studied using the unicellular green alga *Chlamydomonas* sp. as a model test system. Algal growth rate, chlorophyll fluorescence, efficiency of photosystem II, membrane integrity and reactive oxygen species (ROS) generation were assessed following exposure to 10, 50 and 500 mg L⁻¹ of the particles for 2 h and 24 h. The particles had a concentration-, material- and time-dependent effect on *Chlamydomonas* sp., with increased algal growth rate after 24 h. Conversely, significant intracellular ROS levels were detected after 2 h, with much lower levels after 24 h. All Fe-nanomaterials displayed similar Z-average sizes and zeta-potentials at 2 h and 24 h. Effects on *Chlamydomonas* sp. decreased in the order FerMEG12 > Carbo-Iron* > Fe-zeolite > Nano-Goethite. Ecotoxicological studies were challenged due to some particle properties, i.e. dark colour, effect of constituents and a tendency to agglomerate, especially at high concentrations. All particles exhibited potential to induce significant toxicity at high concentrations (500 mg L⁻¹), though such concentrations would rapidly decrease to mg or µg L⁻¹ in aquatic environments, levels harmless to *Chlamydomonas* sp. The presented findings contribute to the practical usage of particle-based nanoremediation in environmental restoration.

1. Introduction

Iron (Fe)-based materials possess remarkable potential for the remediation of soil aquifers, groundwater and cyanobacterial blooms (Bardos et al., 2015; Ribas et al., 2016; Sharma et al., 2016). Numerous in-situ applications of zero-valent iron (ZVI) nanoparticles have proved a powerful tool in the clean-up of chlorinated ethenes and toxic metal

ions due to their high reductive capacity (Köber et al., 2014; Mueller et al., 2012). Further, emerging particulate materials containing Fe as Fe(0), Fe(II) and Fe(III), where the Fe species act as reductants or sorbents for metals and metalloids, have been used successfully in microbiological contaminant degradation or as heterogeneous Fenton catalysts (Bardos et al., 2015; Mackenzie et al., 2016; Gillies et al., 2017).

Abbreviations: AC, activated carbon; DLS, dynamic light scattering; FCM, flow cytometry; FE SEM, field-emission scanning electron microscopy; FU, fluorescence units; nZVI, nanoscale zero-valent iron; ORP, oxidative reductive potential; PI, propidium iodide; PSII, photosystem II; QY, quantum yield; ROS, reactive oxygen species; ZVI, zero-valent iron

* Corresponding authors.

E-mail addresses: nhung.nguyen@tul.cz (N.H.A. Nguyen), nadia.vonmoos@immeda.ch (N.R. Von Moos), vera.slaveykova@unige.ch (V.I. Slaveykova), katrin.mackenzie@ufz.de (K. Mackenzie), rainer.meckenstock@uni-due.de (R.U. Meckenstock), Silke.Thuemmmler@mvtat.tu-freiberg.de (S. Thümmmler), julian.bosch@intrapore.com (J. Bosch), alena.sevcu@tul.cz (A. Ševců).

¹ Present address: Intrapore UG, Katernberger Str. 107, 45327 Essen, Germany.

<https://doi.org/10.1016/j.ecoenv.2018.02.027>

Received 23 August 2017; Received in revised form 12 January 2018; Accepted 5 February 2018
0147-6513/ © 2018 Published by Elsevier Inc.

The overall impact of materials containing Fe(0) on aquatic ecosystems (introduced intentionally or accidentally) remains questionable (Bardos et al., 2015). Other nanomaterials also have the potential to seriously affect aquatic microorganisms such as microalgae, primary producers that play a key role in healthy ecosystems (Adeleye et al., 2016; Klaine et al., 2008). While iron is an essential nutrient in small amounts, increased loading of Fe(II)/Fe(III) ions can rapidly accumulate in the cells of aquatic organisms, resulting in oxidative stress due to the generation of oxide and hydroxide radicals via the Fenton reaction (Crane and Scott, 2012; Davies et al., 2000; Franqueira et al., 2000; Gillies et al., 2016). Moreover, ZVI particles show a strong affinity for cell surfaces; thus, they have the potential to physically damage bacterial or algal cells (Auffan et al., 2008; Lei et al., 2016).

A number of Fe-containing materials have been developed under the European FP7 project NanoRem (for more information see nanorem.eu) in order to provide new and improved materials for treatment of contaminated environments from a broader contaminant spectrum and to offer improved cost effectiveness and safety during transportation and application (Bardos et al., 2015). Up to now, nanoremediation using in-situ generation of permeable reactive barriers or zones through particle subsurface injection has been dominated by nanoiron-based materials. With the introduction of particles with different abilities, nanoremediation has been extended to support bioremediation, advanced oxidation and sorption-assisted clean-up strategies in permeable barriers.

During large-scale in-situ applications, such as those reported for ZVI injection for the treatment of chlorinated organic contaminants (Mueller et al., 2012; Soukupova et al., 2015), suspensions containing up to 10 g L^{-1} of particles are typically injected. Following migration of in-situ applied nanoscale ZVI (nZVI) suspensions within the treated aquifer or water body, Fe concentrations are expected to decline to mg L^{-1} levels or lower (Mueller et al., 2012); hence, ecotoxicological studies should be aimed at such concentrations.

The present study attempts to assess the biological effects of such Fe-containing materials on an aquatic microorganism commonly found in fresh water and soils, *Chlamydomonas* sp., using multiple biological end-points, i.e. growth rate, chlorophyll fluorescence, photosystem II (PSII) quantum efficiency, membrane integrity and intracellular reactive oxygen species (ROS) generation. The algal system was chosen as it is usually associated with contact effects to the cell wall rather than particle incorporation. In addition, behaviour of the Fe-containing materials in the exposure medium was characterised in terms of size, zeta-potential and effect on pH and oxidative reductive potential (ORP).

2. Material and methods

2.1. Fe-containing materials

Four newly developed Fe-containing materials intended for subsurface application as suspensions were examined (see Table 1 for particle descriptions and an overview of their constituents and intended use). The materials were received as dry powders and suspended according to the producers' instructions.

FerMEG12 are metallic ZVI particles that are produced mechanically using a two-stage top-down process and are one of the emerging particles for in-situ groundwater reduction (Köber et al., 2014). Particles of $< 40 \mu\text{m}$ were first generated by dry milling and then more finely ground by wet milling in bivalent alcohol. The milling process forms nanostructured flake-shaped particles.

Carbo-Iron[®] is a composite of ZVI-nanostructures embedded in activated carbon (AC) particles of about $1 \mu\text{m}$. *Carbo-Iron*[®] was synthesised carbothermally following a wet impregnation step, where the pores of the colloidal AC particles are filled with ferric nitrate (Fe(NO₃)₃) (Bleyl et al., 2012). Electron microscopy following reduction indicates nZVI clusters of predominantly $d_{\text{Fe}} \approx 50 \text{ nm}$ built into the AC grain (Mackenzie et al., 2012).

Fe-zeolites is a porous Fe-exchanged aluminosilicate mineral particles of the beta-zeolite type with 1.3 wt% total Fe (Gillies et al., 2017) that catalytically activate oxidising agents such as hydrogen peroxide (H₂O₂) (Gonzalez-Olmos et al., 2013). With a specific surface area of $602 \text{ m}^2 \text{ g}^{-1}$ (N₂-BET) and a water-filled pore effective density of $\rho \approx 1.7 \text{ g cm}^{-3}$, the particles show favourable sedimentation behaviour (i.e. $11\text{--}15 \text{ mm h}^{-1}$) for in-situ application (Gillies et al., 2016, 2017).

Nano-Goethite is produced using an industrial FeOOH precursor that undergoes ultrasonication and coating with a layer of a natural organic polymer that results in electro-steric stabilisation (Bosch et al., 2010; Braunschweig et al., 2013). A stable stock suspension of 100 g L^{-1} *Nano-Goethite* with a mean particle size of 400 nm can be generated in this way.

The shape and particle size of the Fe-containing materials were determined using a Zeiss Ultra Plus field-emission scanning electron microscope (FE SEM). Samples were fixed to aluminium stubs using double-sided carbon tape and cleaned with RF plasma (Evactron) for 10 min before image acquisition. For further details, see Supporting information Fig. S1.

Suspension stabilisers are added in order to generate suspensions stable enough to be injected without major agglomeration (Table 1), carboxymethyl cellulose being added to the *FerMEG12* and *Carbo-Iron*[®] suspensions and a humic-acid coating used for *Nano-Goethite*. No stabiliser was added to *Fe-zeolites*, as it forms a stable suspension.

2.2. Characterisation of Fe-containing materials in the algal exposure medium





The hydrodynamic diameter of each particle type was determined at a range of suspension concentrations (10 , 50 and 500 mg L^{-1}) in algal growth medium through dynamic light scattering (DLS) using a Malvern Zetasizer Nano ZS (Malvern Instruments, UK) with a 633 nm laser source and a detection angle of 173° . The same instrument was used to measure electrophoretic mobility, which was subsequently transformed to zeta potential using Smoluchowski's approximation. Each sample was measured in triplicate at 30 s intervals. At the beginning and end of each toxicity test, ORP and pH were measured using a standard multimeter (WTW, Germany).

2.3. Algal cultures and exposure conditions

The *Chlamydomonas* sp. used in this study (originally isolated from the Lipno reservoir, Czech Republic) was obtained from the Biology Centre of the Czech Academy of Sciences. The algae were cultivated in Guillard-Lorenzen medium (Guillard and Lorenzen, 1972) (Table S1) in an incubator (PlunoTech, Czech Republic) with a 150 rpm shaker and temperature set to $22 \pm 2^\circ\text{C}$, applying a light: dark regime of $16:8 \text{ h}$ with light intensity set to 1200 lux . The culture was harvested during its exponential growth phase and re-suspended in the exposure media to a cell density of $1 \times 10^6 \text{ cells mL}^{-1}$.

Based on preliminary experiments, where 5 mg L^{-1} of Fe-containing material showed no effect and 1000 mg L^{-1} interfered with measurement, toxicological effect was assessed through exposure to 10 , 50 and 500 mg L^{-1} for 2 and 24 h . The experiments were carried out in fully light-transmitting plastic vials containing 5 mL of *Chlamydomonas* sp. and the particle suspension. Negative controls without particles were run in parallel. Exposure experiments were performed under the same conditions (light, temperature and agitation regimes) as those described for the stock algal culture. Possible effects due to shading and particle sedimentation were also considered, particularly as high material concentrations produced a dark (*FerMEG12* and *Carbo-Iron*[®]; Figs. S2 and S3), skimmed milk-like (*Fe-zeolites*; Fig. S3) or light brown-red (*Nano-Goethite*; Fig. S3) suspension. After 2 h and 24 h exposure, $250 \mu\text{L}$ sub-samples were taken and examined through flow cytometry (FCM) in order to assess algal cell number, cellular membrane integrity and chlorophyll fluorescence. The effect on the ROS generation and

Table 1
New “nanoremediation” materials for in-situ application in groundwater treatment: summary of particle properties.

Particle type	FerMEG12	Carbo-Iron*	Trap-Ox* Fe-Zeolite	Nano-Goethite
Schematic presentation				
Brief description	Flake-like iron (Fe) nanoparticles formed by mechanical milling	Composite material of iron nanoclusters embedded in activated carbon (AC)	Fe-exchanged colloidal beta zeolite	Humic-acid coated nano-sized goethite particles
Composition	Fe metal with thin oxide shell	55 wt% porous AC, with 20 ± 1 wt% Fe(O) as nano-structures within the AC, 30.3 ± 1.5 wt% Fe _{total}	Porous aluminosilicate (Si ₃ Al ₂ O ₇ with 38% Si and 1.8% Al) with lattice sites exchanged with Fe (II/III)	FeOOH
Main Fe speciation	Fe(O) ≈ 80 wt%	Fe(O) ≈ 20 wt%	Fe(II/III) ≈ 1.3 wt%	Fe(III) ≈ 60 wt%
Other constituents	Remains of glycol from milling process	Remains of ≈ 10 wt% built-in Fe(II/III)-oxides		Humic acid coating
Mean particle size	< 40 μm, < 100 nm thick	1 μm	500 nm	400 nm
Specific surface area (N₂ BET)	13 – 18 m ² /g	550–650 m ² /g	600 m ² /g	135 m ² /g
Shape	flakes	sphere-like fragments	spheres	sphere-like fragments
Intended target application	<i>In-situ</i> application as reducing agent	<i>In-situ</i> application as combined adsorber and reducing agent	<i>In-situ</i> heterogeneous Fenton catalyst	<i>In-situ</i> material for metal adsorption and support of Fe-reducing bacteria
Additives during application for suppression of particle agglomeration	e.g. Carboxymethyl cellulose (CMC) as suspension stabiliser	CMC forming a layer around particles that washes off over time	Injection possible without stabiliser	Humic acid coating acts as stabiliser
Provider within the NanoRem project	UVR-FIA GmbH, Germany	SciDre GmbH, Germany	Helmholtz Centre for Environmental Research – UFZ, Germany	University of Duisburg-Essen
References for more information	Köber et al. (2014)	Bleyl et al. (2012), Mackenzie et al. (2012), Mackenzie et al. (2016)	Gillies et al. (2016), Gillies et al. (2017)	Bosch et al. (2010), Braunschweig et al. (2013)

algal PSII was also determined.

2.4. Determination of particle effect on membrane integrity and growth rate

A 250 μL aliquot of each sample was transferred to a Microtiter® 96-well flat-bottomed plate and Sytox Green or propidium iodide (PI) fluorescent probes (Life Technologies, Switzerland) were added to the sample at final concentrations of 1 μM and 7 μM , respectively. These probes stain the DNA of affected cells by penetrating impaired cell membranes. The plates were incubated in the dark for 20 min before FCM measurement. Each algal suspension was then passed through a BD Accuri C6 Flow Cytometer (BD Biosciences, USA) with a blue 488 nm excitation laser. Green fluorescence of Sytox Green was measured using the 533/30 nm FL1 channel, red fluorescence of PI using the 585/40 nm FL2 channel and red chlorophyll autofluorescence using the > 670 nm FL3 channel. Cells treated in hot water (100 °C) for 15 min were used as a positive control to test whether the Fe-containing materials interfered with probe staining (Fig. S4). Unexposed algae stained with a fluorescent probe were also included as a negative control. One vial was covered with aluminium foil to create dark conditions mimicking the shading effect caused by the dark colour of the Fe materials. Data were analysed using CFlow Plus software (BD Biosciences, USA). The percentage of autofluorescence, cell membrane integrity and PI (Cheloni et al., 2014, 2016) are all illustrated in the FCM analysis section (Figs. S5 and S6). Determination of algal growth rate (cells h^{-1}) = $(N_{24\text{h}} - N_{2\text{h}}) / (24 - 2\text{h})$; where $N_{2\text{h}}$ is the number of cells after 2 h exposure and $N_{24\text{h}}$ is the number of cells after 24 h exposure. *Chlamydomonas* produces a new generation approximately every 24 h; hence, the algal cell number at inoculation time (0h) and 2h was considered as similar.

2.5. Determination of the effect of particles on intracellular ROS generation

Sub-samples of 200 μL were taken after 2 h, 4 h and 24 h and stained with carboxy-H2DCFDA C-400 (Molecular Probes, Thermo Fisher Scientific Inc.). The intracellular ROS staining procedure used followed that detailed in Szivák et al. (2009). Cells were treated with H_2O_2 (final concentration 100 mM) in a preliminary test to verify the ROS staining procedure. An algal culture without particles was used as a negative control. Fluorescence was measured using a Synergy HTX plate reader (BioTek, USA) with excitation set at 485 nm and emission at 528 nm. The results are presented as the ratio between fluorescence units (FU) in the presence of particles (FU_E) versus FU for controls without particles (FU_0): FU_E/FU_0 .

2.6. Determination of particle effect on PSII

Suspensions of the all particle types were added to the same algal cultures (cell density approximately 1×10^6 cells mL^{-1}) in 30 mL glass flasks in order to achieve final concentrations of 50 and 100 mg L^{-1} of FerMEG12 and Carbo-Iron®, and 50, 100 and 500 mg L^{-1} of Fe-zeolites and Nano-Goethite. An algal culture without particles was used as a negative control and incubated in the dark, mimicking the dark colour of the materials. Aliquots (2.2 mL) of each sample were taken immediately and after 24 h incubation to determine their effect on the PSII quantum yield (PSII QY) using an AquaPen-C AP-C 100 fluorometer (PSI Ltd., Czech Republic). All measurements were dark-adapted for 5 min and undertaken in triplicate. QY, which represents the ratio of variable fluorescence ($F_v = F_m - F_0$) to maximum fluorescence (F_m): $\text{QY} = F_v/F_m$, is used as a proxy of photochemical quenching efficiency (Maxwell and Johnson, 2000). F_m was obtained by applying illumination (3000 $\mu\text{mol photons m}^{-2} \text{s}^{-1}$) at 680 nm for a few seconds, with minimal fluorescence (F_0 ; the initial measurement at minimum fluorescence levels in the absence of photosynthetic light) determined at 50 μs .

2.7. Optical microscopy

Untreated *Chlamydomonas* cells (negative control), hot-water treated cells (positive control) and cells exposed for 2 h and 24 h to the four Fe-containing materials (500 mg L^{-1}) were visualised using an AxioImager microscope (Zeiss, Germany) equipped with an AxioCam ICc1 digital camera and AxioVision SE64 software.

2.8. Statistical analysis

Differences in the effects observed for *Chlamydomonas* exposed to different particle concentrations and unexposed *Chlamydomonas* were tested using ANOVA and Dunnett's test (GraphPad PRISM, USA), with significance levels set at * $P < 0.05$, ** $P < 0.01$ and *** $P < 0.001$.

3. Results

3.1. Characterisation of Fe-containing materials in the algal exposure medium

Nano-Goethite had the smallest Z-average hydrodynamic size (207–288 nm) of all the materials tested, being about 3.5 times smaller than that of Fe-zeolites (Table 2). For Carbo-Iron® and FerMEG12, Z-average size ranged from 1289 to 2874 nm and 3726–4974 nm, respectively, with higher values for FerMEG12 being due to agglomeration. No significant difference in Z-average size was observed at 2 h and 24 h after dispersion in the algal exposure medium (Table 2). FerMEG12 and Nano-Goethite both displayed monomodal size distributions, while Carbo-Iron® and Fe-zeolites both showed bimodal number- and scattered light intensity-based size distributions (Fig. S7).

With the exception of FerMEG12, which showed positive zeta potential values (+ 5 mV) at high concentrations (500 mg L^{-1}), all other materials displayed negative Zeta potentials (- 8 to - 35 mV; Fig. 1), with no significant difference in Zeta potential at 2 h and 24 h for all materials. For all particle types, negative values increased slightly as the concentration increased.

Growth medium pH values ranged between 7 and 8 for all *Chlamydomonas* samples following dispersion of the Fe materials (Fig. S8A). In the presence of Carbo-Iron®, Fe-zeolites and Nano-Goethite, pH values were comparable with those in the absence of Fe-containing materials. The pH of algal medium containing FerMEG12, however, increased to 8 at highest concentrations (500 mg L^{-1}). ORP values for cultures without particles were in the range of + 80 to + 210 mV (Fig. S8B). In contrast, the ORP for FerMEG12 ranged between - 200 and - 300 mV at time 0, but was comparable with the other particle types at + 80 to + 180 mV at 24 h.

3.2. Effect of Fe-containing materials on growth rate and cell morphology

Growth rate in the presence of Fe-containing materials was not

Table 2
Z-averaged particle size determined in algal growth medium after 2 h and 24 h. The results represent the average of three replicated experiments.

Particles	Z-average size after 2 h (nm \pm SD)		
	10 mg L^{-1}	50 mg L^{-1}	500 mg L^{-1}
FerMEG12	4076 \pm 320	3726 \pm 580	4608 \pm 243
Carbo-Iron®	2874 \pm 1005	1515 \pm 183	1289 \pm 26
Fe-zeolites	845 \pm 114	810 \pm 88	789 \pm 41
Nano-Goethite	254 \pm 1	288 \pm 80	233 \pm 11
	Z-average size after 24 h (nm \pm SD)		
FerMEG12	4974 \pm 1426	4721 \pm 380	4426 \pm 340
Carbo-Iron®	2037 \pm 656	1643 \pm 174	1326 \pm 16
Fe-zeolites	977 \pm 420	798 \pm 114	856 \pm 58
Nano-Goethite	207 \pm 3	251 \pm 6	245 \pm 2

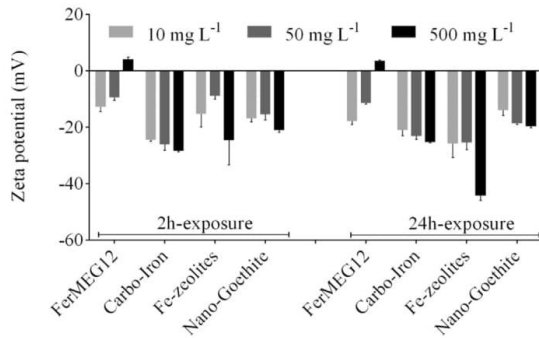


Fig. 1. Zeta-potential of particle surfaces at different concentrations after 2 h and 24 h dispersed in algal growth medium. Error bars = standard deviation of triplicate samples.

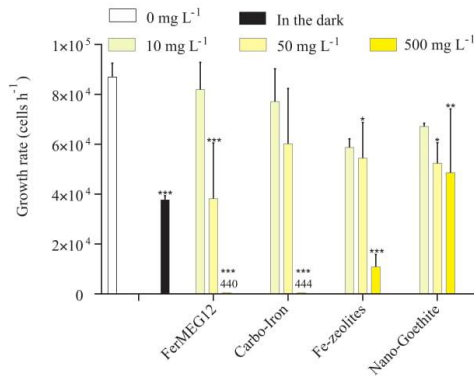


Fig. 2. Effect of four particle types on algal growth rate (cells h⁻¹) measured with FCM. Exposure conditions: FerMEG12, Carbo-Iron[®], Fe-zeolites and Nano-Goethite at concentrations of 10, 50, 500 mg L⁻¹. The error bars represent the standard deviation of triplicate samples. Significance levels * P < 0.05, ** P < 0.01, and *** P < 0.001.

reduced compared with growth rate in the dark without particles (3.8×10^4 cells h⁻¹, $P < 0.001$; Fig. 2). In general, growth rate decreased gradually as Fe-material concentration increased. At 500 mg L⁻¹, growth rate was reduced to 4.4×10^2 cells h⁻¹ for FerMEG12 and Carbo-Iron[®] ($P < 0.001$), 1.1×10^4 cells h⁻¹ for Fe-zeolites ($P < 0.001$) and 4.9×10^4 cells h⁻¹ for Nano-Goethite ($P < 0.01$) compared to the unexposed control (8.7×10^4 cells h⁻¹). When algal cells were grown in the presence of 50 mg L⁻¹ of FerMEG12, growth rate was reduced significantly ($P < 0.001$), while Fe-zeolite and Nano-Goethite both showed a slightly lower but still significant negative effect on growth rate ($P < 0.05$). The same concentration of Carbo-Iron[®], however, appeared to have no effect on growth rate. At the lowest particle concentration (10 mg L⁻¹), algal growth rate was comparable with that for the untreated control culture (Fig. 2) for all test materials.

Microscopic analysis revealed that algal cells were often associated with particle agglomerates following short-term (2 h) exposure with FerMEG12 and Carbo-Iron[®] but not with Fe-zeolites and Nano-Goethite (Fig. S9A, C, E, G). Interestingly, after 24 h exposure, all algal cells tended to detach from the agglomerates and revert to a dispersed single-cell state (Fig. S9).

3.3. Effect of Fe materials on algal chlorophyll fluorescence and PSII efficiency

The percentage of cells with altered chlorophyll fluorescence

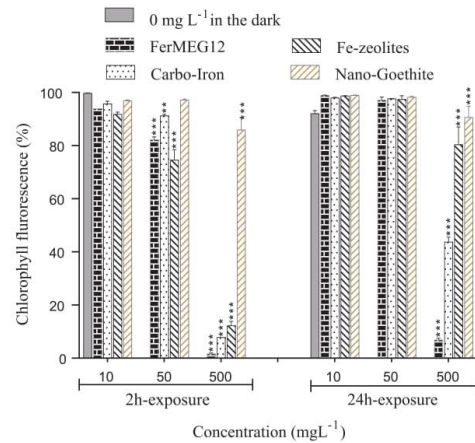


Fig. 3. Effect of Fe materials on chlorophyll fluorescence in *Chlamydomonas* cells. Exposure conditions: FerMEG12, Carbo-Iron[®], Fe-zeolites and Nano-Goethite at concentrations of 10, 50, 500 mg L⁻¹, duration 2 h and 24 h. The chlorophyll fluorescence of unexposed control represents 100%. The error bars represent the standard deviation of triplicate samples. Significance levels * P < 0.05, ** P < 0.01, and *** P < 0.001.

(extracted from FCM channel FL3; Fig. S6) increased significantly after 2 h exposure to FerMEG12, Carbo-Iron[®] and Fe-zeolites at concentrations of 50 and 500 mg L⁻¹, and to Nano-Goethite at concentrations of 500 mg L⁻¹ only (85.6%). Although less pronounced, the same trends were observed after 24 h exposure (Fig. 3).

The above observations were consistent with an effect on PSII QY, an indicator of photosynthetic efficiency. PSII QY values for *Chlamydomonas* exposed to 10 mg L⁻¹ of each material for 2 h and 24 h were comparable with those for unexposed controls (Fig. 4). In contrast, exposure to FerMEG12 for 24 h at 50 mg L⁻¹ resulted in a reduction of PSII QY. Fe-zeolites and Nano-Goethite at 500 mg L⁻¹ caused a significant increase in PSII QY after 2 h exposure but not after 24 h. The dark colour of FerMEG12 and Carbo-Iron[®] (500 mg L⁻¹) precluded reliable measurements of QY, thus control samples kept under dark

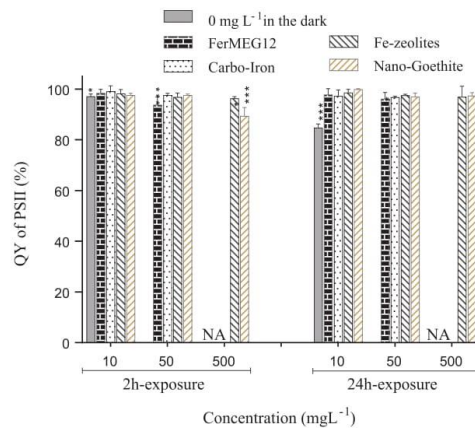


Fig. 4. Effect of Fe materials on the quantum yield (QY) of photosystem II (%) of *Chlamydomonas* after 2 h and 24 h exposure to Fe-NMs at 0, 10 and 50 mg L⁻¹ (FerMEG12, Carbo-Iron[®]) and 0, 10, 50 and 500 mg L⁻¹ (Fe-zeolites, Nano-Goethite). Grey bars are control algae grown without nanoparticles in the dark. The control without particles represents 100%. NA = not analysed as the dark colour induced by the particle suspensions interfered with measurement. The error bars represent the standard deviation of triplicate samples. Significance levels * P < 0.05, ** P < 0.01, and *** P < 0.001.

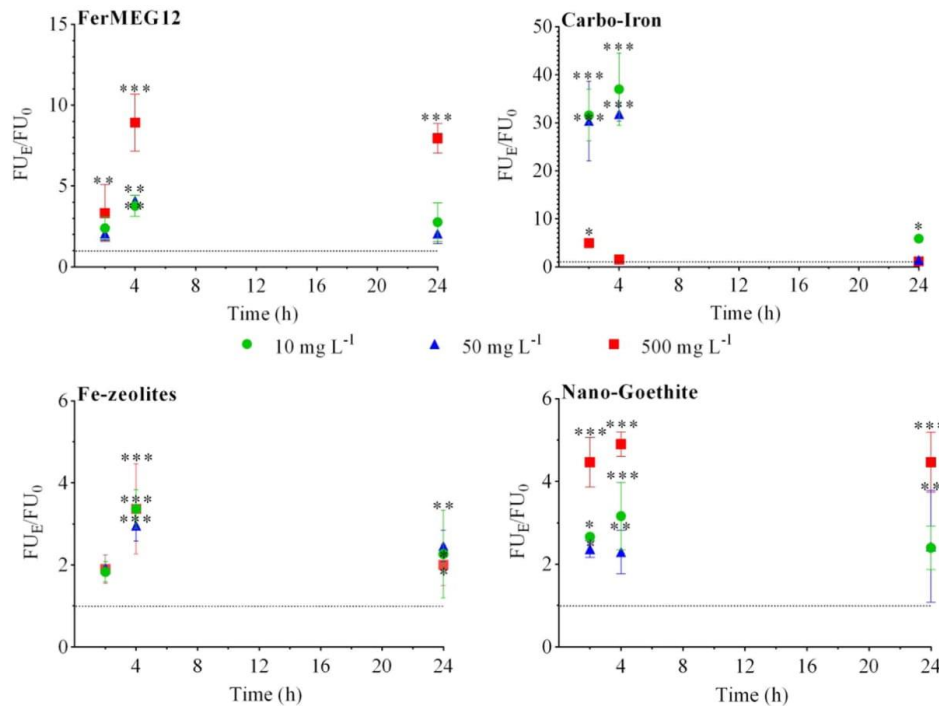


Fig. 5. Fluorescence unit (FU) ratios (FU_E/FU₀) of ROS production in *Chlamydomonas* cells after 2 h and 24 h exposure to FerMEG12, Carbo-Iron®, Fe-zeolites and Nano-Goethite at concentrations of 10 (green circle), 50 (blue up-triangle) and 500 (red square) mg L⁻¹. FU_E: fluorescence unit of exposed algae to Fe-NMs, FU₀: non-exposed *Chlamydomonas* cultures. The dotted line (—) represents the control and the error bars represent the standard deviation of triplicate samples. Note the different y-axis scales. Significance levels * P < 0.05, ** P < 0.01, and *** P < 0.001. (For interpretation of the references to color in this figure legend, the reader is referred to the web version of this article.)

conditions mimicked the shading effect. In the complete dark, algal chlorophyll fluorescence was progressively reduced to 92.0% (P < 0.001) over 24 h. Correspondingly, PSII QY was significantly reduced after 2 and 24 h (Fig. 4).

3.4. Effect of Fe materials on cellular ROS generation and membrane integrity

There was no clear trend in ROS production in the particle-treated *Chlamydomonas* sp. (Fig. 5). FerMEG12 caused a significant increase in ROS at 500 mg L⁻¹ after 2 h, and at all concentrations after 4 h. After 24 h, however, ROS formation was reduced at lower exposure concentrations (10, 50 mg L⁻¹) to levels comparable with untreated cells, but remained higher at 500 mg L⁻¹. Fe-zeolites, ROS generation was very low compared to FerMEG12 and Carbo-Iron®. While it increased slightly after 4 h it decreased again after 24 h, though remaining higher than the untreated control. Carbo-Iron® ROS levels increased rapidly when cells were exposed to 10 and 50 mg L⁻¹ of the material, attaining a maximum at 4 h. At the highest Carbo-Iron® concentrations (500 mg L⁻¹), however, enhanced ROS generation was not observed after 4 h or 24 h exposure. Nano-Goethite at 500 mg L⁻¹ resulted in elevated ROS levels at all exposure durations. At the lowest concentration (10 mg L⁻¹), enhanced ROS was observed after 2 h and increased after 4 h but was comparable with ROS in untreated cells after 24 h (Fig. 5).

Exposure to Fe-containing materials induced a relatively weak effect on algal membrane integrity. In agreement with the observed decrease in cell number and algal chlorophyll fluorescence, the percentage of cells with affected membrane integrity was higher after 2 h than after

24 h exposure for all the materials studied (Fig. 6). The percentage of unaffected cells should ideally be 100%; values ranged between 95% and 100%, however, due to the FCM gating strategy attempting to remove all particles. While the percentage of affected membranes was 30–40% for FerMEG12, 18% for Carbo-Iron®, 29% for Fe-zeolites and 10% for Nano-Goethite at concentrations of 10 and 50 mg L⁻¹ following exposure for 2 h, these percentages had all decreased to around 10% after 24 h exposure. Even at the highest concentration tested (500 mg L⁻¹), membrane integrity levels were moderate at 39% for FerMEG12, 25% for Carbo-Iron®, 25% for Fe-zeolites and 15% for Nano-Goethite. On the other hand, there was a significant difference in the proportion of damaged membranes after 2 h and 24 h exposure at high (500 mg L⁻¹) particle concentrations (Fig. 6).

4. Discussion

4.1. Main biological effects of Fe-containing materials

FerMEG12 appears to be most toxic to *Chlamydomonas* sp., as demonstrated by the significant effect on different biological endpoints at concentration higher than 50 mg L⁻¹. Note, however, that algal growth rate in the presence of FerMEG12 increased, and other effects were less pronounced, after 24 h. This observation is in agreement with an earlier study showing that FerMEG12 caused a decrease in chlorophyll fluorescence right after onset of acute effect on *Pseudomonas subcapitata* but after 48 h incubation, algal population recovered and the growth rate was similar or even higher than the non-exposed controls (Hjorth et al., 2017). Other reactive materials containing Fe(0), such as NANOFER STAR and NANOFER 25S, induced growth inhibition in marine

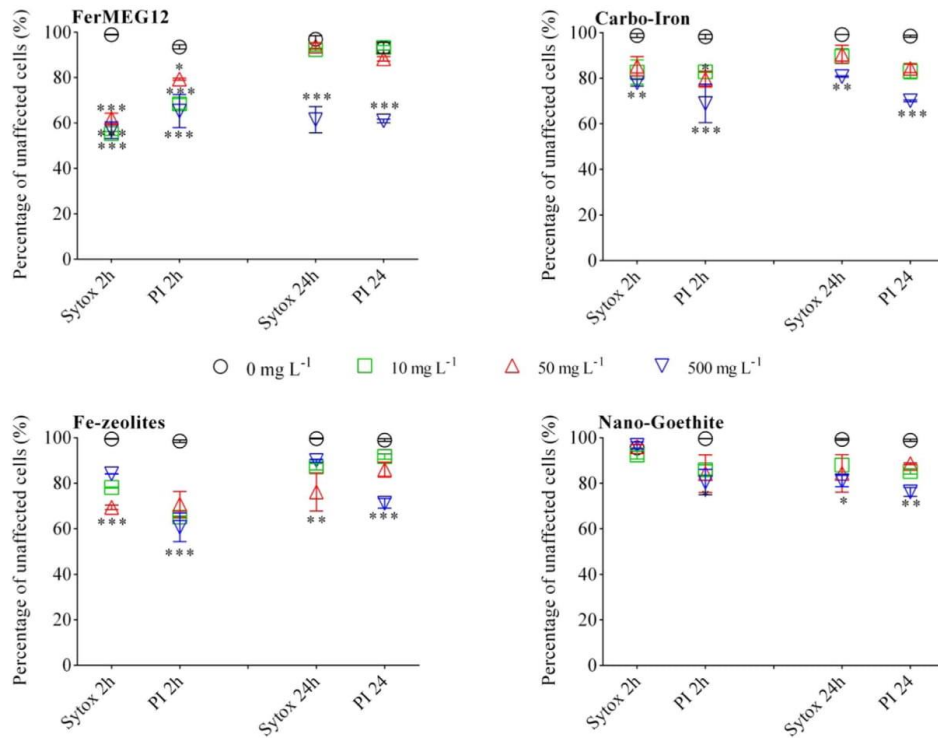


Fig. 6. Influence of the Fe materials on the membrane integrity of *Chlamydomonas* cells after 2h and 24h exposure to FerMEG12, Carbo-Iron®, Fe-zeolites and Nano-Goethite at concentrations of 10 (green square), 50 (red up-triangle) and 500 mg L⁻¹ (blue down-triangle). The error bars represent the standard deviation of triplicate samples. Significance levels * P < 0.05, ** P < 0.01, and *** P < 0.001. (For interpretation of the references to color in this figure legend, the reader is referred to the web version of this article.)

microalga *Isochrysis galbana* at 3 mg L⁻¹ (NANOFEAR 25S) or had no effect (NANOFEAR STAR up to 100 mg L⁻¹ or dissolved Fe at concentrations < 50 mg L⁻¹) (Keller et al., 2012). The lowest observed effect concentration of Fe(II) and Fe(III) exposed to *P. subcapitata* was 5 mg L⁻¹ and 25 mg L⁻¹, respectively, after 96 h (Keller et al., 2012). ZVI toxicity can also be influenced by corrosion and transformation processes, ferrous ion release and oxygen consumption (Chen et al., 2013; Zhu et al., 2012). Furthermore, transition metals (Fe) can participate in one-electron oxidation-reduction reactions producing ROS, which can have direct toxic effects on living organisms (Crane and Scott, 2012; Ševců et al., 2011; Schiwy et al., 2016). Surprisingly, the Carbo-Iron®-induced generation of elevated ROS in the present study was higher at lower concentrations (50 mg L⁻¹) than at higher concentration (500 mg L⁻¹). One explanation may be that, at 500 mg L⁻¹, embedded Fe(0) has a longer life-span as oxygen dissolved in the exposure medium would be 'caught', leading to reduced release of Fe(II) and lowered ROS at 24 h. Moreover, the activated carbon carrier could effectively scavenge any ROS-initiators. nZVI toxicity strongly depends on the percentage of ZVI used and on the surface coating (El-Temseh et al., 2016, 2017). FerMEG12, for example, with 80% Fe(0), was without surface passivation and displayed higher toxicity to *Chlamydomonas* sp. than the other Fe-containing materials. This could be due to higher release of Fe(II) followed by higher uptake by algal cells, causing oxidative stress via the classic Fenton reaction (Lee et al., 2008; Ševců et al., 2011). Active defence mechanisms against ROS are, however, a prerequisite for aerobic organisms such as algae (Schwab et al., 2011; Cheloni et al., 2014). Even though both Fe-zeolites and Nano-Goethite generated cellular ROS, their levels were considerably lower than those in FerMEG12 and Carbo-Iron® exposure reflecting the

significant role of ZVI in induction of oxidative stress in algal cultures. On the other side, modified Fe(III)-zeolite inhibited *Chlamydomonas vulgaris* growth, probably due to the formation of ROS (Pavíková et al., 2010). Of the studied materials Nano-Goethite weakly affected algal membranes, and affected chlorophyll fluorescence at the highest concentration (500 mg L⁻¹) only. At the micro-scale, goethite is commonly found in the natural environment and there have been no previous reports of toxicity to microorganisms (Cooper et al., 2003).

4.2. Other factors involved in ecotoxicity effects

Each of the Fe-containing materials tested has its own specific and unique properties for targeted application. Some of these characteristics should be taken into account, however, when undertaking ecotoxicity studies, e.g.:

- (1) The dark colour of FerMEG12 and Carbo-Iron®, and the colouration of Nano-Goethite at higher concentrations (500 mg L⁻¹), resulted in shading of the algal cells (Figs. S2 and S3). Algal toxicity tests have revealed that shading can considerably influence assessment of potential toxicity at high exposure concentrations (Hjorth et al., 2015; Sørensen et al., 2016). In one study, it was shown that ZVI shading reduced algal growth to a higher extent than other toxicity mechanisms (Schiwy et al., 2016). Shaded algal cells need more chlorophyll to acquire enough photons for photosynthesis (Nielsen and Jørgensen, 1968); hence, they rapidly synthesise chlorophyll as an adaptation to darker conditions (Schwab et al., 2011; Hjorth et al., 2015).
- (2) The larger size of FerMEG12 and Carbo-Iron® (whether in their

- original state or due to agglomeration) and consequent sedimentation could reduce their effect on *Chlamydomonas* sp. This is consistent with the increased toxicity of FerMEG12 agglomerates at higher Fe concentrations to oligochaeta *Lumbriculus variegatus* due to particle sedimentation compared with *Daphnia magna*, which can move in the water column (Hjorth et al., 2017).
- (3) Other constituents within the Fe-containing materials may also need to be considered in toxicity studies. FerMEG12, for example, had a lower Fe-mass referred surface than Carbo-Iron® and was more hydrophobic (due to glycol on its surface). It might be expected, therefore, that the amount of Fe-ions released in the vicinity of the particles will differ. With higher particle concentration, particle-algae-interactions are suspected to be more pronounced, with algae possibly attaching to the glycol-film on FerMEG12 and AC in Carbo-Iron® materials.
 - (4) Fe-zeolites have two phases of in situ application: a sorption phase following particle injection to the aquifer and, after sorption is complete, a flush of H₂O₂ is applied, which leads to hydroxyl radical formation (Fenton-like reaction), to regenerate the particles and oxidise contaminants. It is quite probable that some micro-organisms would be destroyed during this second phase. In this study, however, the Fe-zeolites were treated as representing an accidental introduction into the environment (e.g. by a spill reaching a waterbody), where the H₂O₂ oxidation phase does not play a role.
 - (5) Chemical-physical parameters: ORP values in algal cultures treated with FerMEG12 (50–500 mg L⁻¹) ranged from -300 mV to -200 mV (Fig. S8), suggesting that algal cells were subjected to unfavourable reducing conditions in the growth medium at the beginning of the experiment. These low ORP values could have negatively affected algal density (Wang et al., 2014). There is no evidence that pH affected the algal cells as it remained within the optimal growth range (pH 7 – 8, Fig. S8) for *Chlamydomonas* (Messerli et al., 2005). Nevertheless, the zeta-potential of FerMEG12 in exposure medium reached values close to zero mV, or positive values at concentrations of 500 mg L⁻¹, suggesting facilitated interaction of positively charged material surfaces with negatively charged algal cell surfaces.
 - (6) Even though there was no direct evidence that the shape of the Fe-containing materials affected algal cells, the percentage of membranes damaged by FerMEG12 was higher than that for other materials. It can thus be hypothesised that FerMEG12, having a flake-like appearance with rough, sharp edges on surface (Fig. S1), might impair cell membranes directly.

5. Conclusions

Investigation of four Fe-containing materials (FerMEG12, Carbo-Iron®, Fe-zeolites and Nano-Goethite) showed that biological effects on *Chlamydomonas* sp. were non-significant at low concentrations (10 and 50 mg L⁻¹), being similar or below those expected when such materials enter aquatic environments through accidental spills. Negative effects were observed at high concentration (500 mg L⁻¹), and especially for FerMEG12, which contained the highest proportion of reactive ZVI (80%). Overall, all effects tended to be less pronounced after 24 h at all concentrations, suggesting rapid recovery of the algal culture. High concentrations, in the exposure medium, however, caused problems when evaluating test endpoints, particularly as regards dark colouration resulting in a shading effect, agglomeration and sedimentation and consequent problem with assessment of concentration-based effects. On the other hand, agglomeration and sedimentation should be considered typical behaviour for these materials in the environment.

Acknowledgements

This research was supported by the European Union's Seventh

Framework Programme for research, technological development and demonstration under Grant Agreement no. 309517. Further support was provided to N. Nguyen and A. Ševců from the Ministry of Education, Youth and Sport (CZ project no. LO1201 and NanoEnvi project no. LM2015073) and from the Technology Agency of the Czech Republic (Project no. TE01010218). V. Slaveykova and N. von Moos received funding from the Swiss National Science Foundation (NRP 64: on the Opportunities and Risk of Nanomaterials, Project no. 406440-131280).

Conflict of interest

The authors declare that they have no conflict of interest.

Appendix A. Supporting information

Supplementary data associated with this article can be found in the online version at <http://dx.doi.org/10.1016/j.ecoenv.2018.02.027>.

References

- Adeleye, A.S., Stevenson, L.M., Su, Y., Nisbet, R.M., Zhang, Y., Keller, A.A., 2016. Influence of phytoplankton on fate and effects of modified zerovalent iron nanoparticles. *Environ. Sci. Technol.* 50, 5597–5605.
- Auffan, M., Achouak, W., Rose, J., Roncato, M.A., Chanéac, C., Waite, D.T., Masion, A., Woicik, J.C., Wiesner, M.R., Bottero, J.Y., 2008. Relation between the redox state of iron-based nanoparticles and their cytotoxicity toward *Escherichia coli*. *Environ. Sci. Technol.* 42, 6730–6735.
- Bardos, P., Bone, B., Černík, M., Elliott, D.W., Jones, S., Merly, C., 2015. Nanoremediation and international environmental restoration markets. *Remediat. J.* 26, 101–108.
- Bleyl, S., Kopinke, F.D., Mackenzie, K., 2012. Carbo-Iron-synthesis and stabilization of Fe (0)-doped colloidal activated carbon for in situ groundwater treatment. *Chem. Eng. J.* 191, 588–595.
- Bosch, J., Heister, K., Hofmann, T., Meckenstock, R.U., 2010. Nanosized iron oxide colloids strongly enhance microbial iron reduction. *Appl. Environ. Microbiol.* 76, 184–189.
- Braunschweig, J., Bosch, J., Meckenstock, R.U., 2013. Iron oxide nanoparticles in geo-microbiology: from biogeochemistry to bioremediation. *New Biotechnol.* 30, 793–802.
- Cheloni, G., Cosio, C., Slaveykova, V.I., 2014. Antagonistic and synergistic effects of light irradiation on the effects of copper on *Chlamydomonas reinhardtii*. *Aquat. Toxicol.* 155C, 275–282.
- Cheloni, G., Marti, E., Slaveykova, V.I., von Moos, N., Maillard, L., Slaveykova, V.I., Regier, N., Cosio, C., von Moos, N., Slaveykova, V.I., 2016. Interactive effects of copper oxide nanoparticles and light to green alga *Chlamydomonas reinhardtii*. *Aquat. Toxicol.* 170, 120–128.
- Chen, P.-J.J., Wu, W.-L.L., Wu, K.C.-W.W., 2013. The zerovalent iron nanoparticle causes higher developmental toxicity than its oxidation products in early life stages of medaka fish. *Water Res.* 47, 3899–3909.
- Cooper, D.C., Picardal, F.W., Schimmelmann, A., Coby, A.J., 2003. Chemical and biological interactions during nitrate and goethite reduction by *Shewanella putrefaciens* 200. *Appl. Environ. Microbiol.* 69, 3517–3525.
- Crane, R.A., Scott, T.B., 2012. Nanoscale zero-valent iron: future prospects for an emerging water treatment technology. *J. Hazard. Mater.* 211–212, 112–125.
- Davies, K.J., A Davies, K.J., Percy, E., 2000. Critical review oxidative stress, antioxidant defenses, and damage removal, repair, and replacement systems. *IUBMB Life* 50, 279–289.
- Nielsen, E.S., Jørgensen, E.G., 1968. The adaptation of plankton algae. *Physiol. Plant.* 21, 423–427.
- El-Temsah, Y.S., Sevcu, A., Bobcikova, K., Cernik, M., Joner, E.J., 2016. DDT degradation efficiency and ecotoxicological effects of two types of nano-sized zero-valent iron (nZVI) in water and soil. *Chemosphere* 144, 2221–2228.
- Franqueira, D., Orosa, M., Torres, E., Herrero, C., Cid A., 2000. Potential use of flow cytometry in toxicity studies with microalgae. *Sci. Total Environ.* 247, 119–126.
- Gillies, G., Mackenzie, K., Kopinke, F.D., Georgi, A., 2016. Fluorescence labelling as tool for zeolite particle tracking in nanoremediation approaches. *Sci. Total Environ.* 550, 820–826.
- Gillies, G., Rukmini, R., Kopinke, F.-D., Georgi, A., 2017. Suspension stability and mobility of Trap-Ox Fe-zeolites for in-situ nanoremediation. *J. Colloid Interface Sci.* 501, 311–320.
- Gonzalez-Olmos, R., Kopinke, F.D., Mackenzie, K., Georgi, A., 2013. Hydrophobic Fe-zeolites for removal of MTBE from water by combination of adsorption and oxidation. *Environ. Sci. Technol.* 47, 2353–2360.
- Guillard, R.R.L., Lorenzen, C.J., 1972. Yellow-green algae with chlorophyllide c. *J. Phycol.* 8, 10–14.
- Hjorth, R., Sørensen, S.N., Olsson, M.E., Baun, A., Hartmann, N.B., 2015. A certain shade of green: can algal pigments reveal shading effects of nanoparticles? *Integr. Environ. Assess. Manag.* 11, 719–728.
- Hjorth, R., Coutris, C., Nguyen, N., Sevcu, A., Baun, A., Joner, E., 2017. Ecotoxicity

- testing and environmental risk assessment of iron nanomaterials for sub-surface remediation – recommendations from the FP7 project NanoRem. *Chemosphere* 182, 525–531.
- Keller, A.A., Garner, K., Miller, R.J., Lenihan, H.S., 2012. Toxicity of nano-zero valent iron to freshwater and marine organisms. *PLoS One* 7, 1–10.
- Klaine, S.J., Alvarez, P.J.J., Batley, G.E., Fernandes, T.F., Handy, R.D., Lyon, D.Y., Mahendra, S., McLaughlin, M.J., Lead, J.R., 2008. Nanomaterials in the environment: behavior, fate, bioavailability, and effects. *Environ. Toxicol. Chem.* 27, 1825–1851.
- Köber, R., Hollert, H., Hornbruch, G., Jekel, M., Kamptner, A., Klaas, N., Maes, H., Mangold, K.-M., Martac, E., Matheis, A., Paar, H., Schäffer, A., Schell, H., Schiwy, A., Schmidt, K.R., Strutz, T.J., Thümmler, S., Tiehm, A., Braun, J., 2014. Nanoscale zero-valent iron flakes for groundwater treatment. *Environ. Earth Sci.* 72, 3339–3352.
- Lee, C., Kim, J.Y., Lee, W., Il, Nelson, K.L., Yoon, J., Sedlak, D.L., 2008. Bactericidal effect of zero-valent iron nanoparticles on *Escherichia coli*. *Environ. Pollut.* 13, 4927–4933.
- Lei, C., Zhang, L., Yang, K., Zhu, L., Lin, D., 2016. Toxicity of iron-based nanoparticles to green algae: effects of particle size, crystal phase, oxidation state and environmental aging. *Environ. Pollut.* 218, 505–512.
- Mackenzie, K., Bleyl, S., Georgi, A., Kopinke, F.D., 2012. Carbo-Iron - An Fe/AC composite - As alternative to nano-iron for groundwater treatment. *Water Res.* 46, 3817–3826.
- Mackenzie, K., Bleyl, S., Kopinke, F.D., Doose, H., Bruns, J., 2016. Carbo-Iron as improvement of the nanoiron technology: from laboratory design to the field test. *Sci. Total Environ.* 563–564, 641–648.
- Maxwell, K., Johnson, G.N., 2000. Chlorophyll fluorescence—a practical guide. *J. Exp. Bot.* 51, 659–668.
- Messerli, M.A., Amaral-Zettler, L.A., Zettler, E., Jung, S.-K., Smith, P.J.S., Sogin, M.L., 2005. Life at acidic pH imposes an increased energetic cost for a eukaryotic acidophile. *J. Exp. Biol.* 208, 2569–2579.
- Mueller, N.C., Braun, J., Bruns, J., Černík, M., Rissing, P., Rickerby, D., Nowack, B., 2012. Application of nanoscale zero valent iron (NZVI) for groundwater remediation in Europe. *Environ. Sci. Pollut. Res.* 19, 550–558.
- Pavliková, S., Šeršer, F., Jesenák, K., Gáplovská, K., Gabriel, Č., 2010. Efficacy of modified natural zeolites in the protection against the damaging effect of 4-chlorophenol on algal growth. *Fresenius Environ. Bull.* 19, 3055–3058.
- Ribas, D., Černík, M., Martí, V., Benito, J.A., 2016. Improvements in nanoscale zero-valent iron production by milling through the addition of alumina. *J. Nanopart. Res.* 18, 181.
- Schiwy, A., Maes, H.M., Koske, D., Flecken, M., Schmidt, K.R., Schell, H., Tiehm, A., Kamptner, A., Thümmler, S., Stanjek, H., Heggen, M., Dunin-Borkowski, R.E., Braun, J., Schäffer, A., Hollert, H., 2016. The ecotoxic potential of a new zero-valent iron nanomaterial, designed for the elimination of halogenated pollutants, and its effect on reductive dechlorinating microbial communities. *Environ. Pollut.* 216, 1–9.
- Schwab, F., Bucheli, T.D., Lukhele, L.P., Magrez, A., Nowack, B., Sigg, L., Knauer, K., 2011. Are carbon nanotube effects on green algae caused by shading and agglomeration? *Environ. Sci. Technol.* 45, 6136–6144.
- Ševců, A., El-Temsah, Y.S., Filip, J., Joneš, E.J., Bobčíková, K., Černík, M., 2017. Zero-valent iron particles for PCB degradation and an evaluation of their effects on bacteria, plants, and soil organisms. *Environ. Sci. Pollut. Res.* 24, 21191–21202.
- Ševců, A., El-Temsah, Y.S., Joneš, E.J., Černík, M., 2011. Oxidative stress induced in microorganisms by zero-valent iron nanoparticles. *Microbes Environ.* 26, 271–281.
- Sharma, V.K., Chen, L., Marsalek, B., Zboril, R., O'Shea, K.E., Dionysiou, D.D., 2016. Iron based sustainable greener technologies to treat cyanobacteria and microcystin-LR in water. *Water Sci. Technol. Water Supply* 17, 107–114.
- Sorensen, S.N., Engelbrekt, C., Lützhøft, H.H., Jiménez-Lamana, J., Noori, J.S., Alatrakch, F.A., Delgado, C.G., Slaveykova, V.I., Baun, A., 2016. A multi-method approach for disclosing algal toxicity of platinum nanoparticles. *Environ. Sci. Technol.* 19, 10635–10643.
- Soukupova, J., Zboril, R., Medrik, I., Filip, J., Safarova, K., Ledl, R., Mashlan, M., Nosek, J., Černík, M., 2015. Highly concentrated, reactive and stable dispersion of zero-valent iron nanoparticles: direct surface modification and site application. *Chem. Eng. J.* 262, 813–822.
- Szivač, I., Behra, R., Sigg, L., 2009. Metal-induced reactive oxygen species production in *Chlamydomonas reinhardtii* (Chlorophyceae). *J. Phycol.* 45, 427–435.
- Wang, G., Li, X., Fang, Y., Huang, R., 2014. Analysis on the formation condition of the algae-induced odorous black water agglomerate. *Saudi J. Biol. Sci.* 21, 597–604.
- Zhu, X., Tian, S., Cai, Z., 2012. Toxicity assessment of iron oxide nanoparticles in Zebrafish (*Danio rerio*) early life stages. *PLoS One* 7, 1–6.

Paper 3

Nhung H. A. Nguyen, Mohamed S. A. Darwish, Ivan Stibor, Pavel Kejzlar, and Alena Sevcu (2017). Magnetic Poly(N-isopropylacrylamide) nanocomposites: Effect of preparation method on antibacterial properties. *Nanoscale Research Letters*, 12, 571-582. **IF 2.833**

NANO EXPRESS

Open Access



Magnetic Poly(N-isopropylacrylamide) Nanocomposites: Effect of Preparation Method on Antibacterial Properties

Nhung H. A. Nguyen^{1,2}, Mohamed S. A. Darwish^{1,3}, Ivan Stibor¹, Pavel Kejzlar¹ and Alena Ševců^{1,2*}

Abstract

The most challenging task in the preparation of magnetic poly(N-isopropylacrylamide) (Fe_3O_4 -PNIPAAm) nanocomposites for bio-applications is to maximise their reactivity and stability. Emulsion polymerisation, in situ precipitation and physical addition were used to produce Fe_3O_4 -PNIPAAm-1, Fe_3O_4 -PNIPAAm-2 and Fe_3O_4 -PNIPAAm-3, respectively. Their properties were characterised using scanning electron microscopy (morphology), zeta-potential (surface charge), thermogravimetric analysis (stability), vibrating sample magnetometry (magnetisation) and dynamic light scattering. Moreover, we investigated the antibacterial effect of each nanocomposite against Gram-negative *Escherichia coli* and Gram-positive *Staphylococcus aureus*. Both Fe_3O_4 -PNIPAAm-1 and Fe_3O_4 -PNIPAAm-2 nanocomposites displayed high thermal stability, zeta potential and magnetisation values, suggesting stable colloidal systems. Overall, the presence of Fe_3O_4 -PNIPAAm nanocomposites, even at lower concentrations, caused significant damage to both *E. coli* and *S. aureus* DNA and led to a decrease in cell viability. Fe_3O_4 -PNIPAAm-1 displayed a stronger antimicrobial effect against both bacterial strains than Fe_3O_4 -PNIPAAm-2 and Fe_3O_4 -PNIPAAm-3. *Staphylococcus aureus* was more sensitive than *E. coli* to all three magnetic PNIPAAm nanocomposites.

Keywords: Magnetic poly(N-isopropylacrylamide), PNIPAAm, Bio-application, *Escherichia coli*, *Staphylococcus aureus*

Background

Magnetic thermoresponsive polymer nanocomposites have been used for a wide range of applications, including water treatment and nanomedicine [1–4]. Each nanocomposite is specifically designed to benefit from the combination of features inherent in both components, i.e. magnetic particles and temperature-responsive polymers, thus creating a nanocomposite that is more specific and controllable. Magnetite (Fe_3O_4) nanoparticles impart magnetic properties that allow for rapid and easy separation following application of an external magnetic field [5]. Poly(N-isopropylacrylamide) (PNIPAAm) forms a three-dimensional hydrogel that undergoes a reversible lower critical solution temperature (LCST) phase transition from a single coil with a swollen hydrated state to a collapsed and shrunken dehydrated

state [6] when heated in water above 32 °C. Capping of the magnetic nanoparticles with a PNIPAAm layer not only provides colloidal stability in water but also allows for surface functionality by binding with other molecules, such as drugs, proteins or enzymes [7]. Construction of dual responsive nanocomposites is achieved by combining two properties that respond simultaneously to a combination of temperature and magnetism. The most common methods used for synthesis of Fe_3O_4 -PNIPAAm nanocomposites are physical addition, in situ precipitation and emulsion polymerisation. Physical addition, the simplest method, requires the physical mixing of previously synthesised magnetic nanoparticles and PNIPAAm particles. The second method, in situ precipitation, involves precipitation of magnetic nanoparticles in the presence of the PNIPAAm nanopolymer [8]. The third (and most common) route, emulsion polymerisation, requires polymerisation of the (N-isopropylacrylamide) monomer in the presence of magnetic nanoparticles [9–11]. Fe_3O_4 -PNIPAAm nanocomposites have found widespread use in biomedical and

* Correspondence: alena.sevcu@tul.cz

¹Institute for Nanomaterials, Advanced Technologies and Innovation, Technical University of Liberec, 461 17 Liberec, Czech Republic

²Faculty of Mechatronics, Informatics and Interdisciplinary Studies, Technical University of Liberec, 461 17 Liberec, Czech Republic

Full list of author information is available at the end of the article



© The Author(s). 2017 **Open Access** This article is distributed under the terms of the Creative Commons Attribution 4.0 International License (<http://creativecommons.org/licenses/by/4.0/>), which permits unrestricted use, distribution, and reproduction in any medium, provided you give appropriate credit to the original author(s) and the source, provide a link to the Creative Commons license, and indicate if changes were made.

biotechnological applications. Highly stable, controlled and well-dispersed magnetic nanoparticles will be required in order to increase the suitability of such nanocomposites for future applications. One recent innovation involves an external magnetic field that creates a local heat source for self-heating particles, causing the PNIPAAm to shrink and in turn allowing release of encapsulated drugs [12]. This phenomenon, coupled with magnetic beads targeted on tumours, opens up other potential cancer therapies such as hyperthermia. Hyperthermia can be initiated by oscillating nanoparticles in an oscillating magnetic field at frequencies ranging from kilohertz to megahertz. Other Fe₃O₄-PNIPAAm nanocomposites have recently been synthesised to control the release of bio-active molecules, such as myoglobin or vitamin B12, and for drug delivery [13]. A recent study using PNIPAAm-coated superparamagnetic Fe₃O₄ nanoparticles was able to show that thermally induced aggregation of iron oxide nanoparticles greatly increases T2 contrast during magnetic resonance imaging [14]. Clearly, Fe₃O₄-PNIPAAm shows great promise for future developments in both biomedical and biotechnological applications. Consequently, it is important that further studies are undertaken on the biocompatibility of this material and its antibacterial effect.

In this study, we investigated the effect of three preparation methods on the physical-chemical properties of Fe₃O₄-PNIPAAm nanocomposites. In doing so, we aim to assess the most convenient preparation method for producing nanocomposites displaying enhanced properties for biological applications. For the first time, we also describe the antibacterial effects of the three Fe₃O₄-PNIPAAm nanocomposites using a multi-endpoint approach, bacterial growth rate, viability, cell morphology and level of DNA damage.

Methods

Chemicals

Iron(III) chloride hexahydrate (FeCl₃·6H₂O, ≥ 98%), Iron(II) chloride tetrahydrate (FeCl₂·4H₂O, ≥ 99%), ammonium hydroxide (26% NH₃ in H₂O), N-isopropylacrylamide (NiPAM, ≥ 99%), N,N-methylenebis(acrylamide) (BIS, ≥ 99%), sodium dodecyl sulphate (SDS, ≥ 99%) and ammonium persulphate (APS, ≥ 98.5%) were all purchased fresh from Sigma-Aldrich, Germany.

Preparation of PNIPAAm by Emulsion Polymerisation

NiPAM (4 g), BIS (0.2 g) and SDS (0.3 g) were dissolved in 350 ml of deionised water (DI) at 70 °C under atmospheric nitrogen. APS (0.0035 g) was dissolved in 1 ml of DI and added to the reaction vessel to start the reaction. After 4 h, the reaction was stopped and the prepared particles washed with DI water. Finally, the PNIPAAm nanoparticles were separated by centrifugation (12,000 rpm for 30 min) and used in further reactions.

Preparation of Magnetite (Fe₃O₄) Nanoparticles

FeCl₂·4H₂O (1.9 g) and FeCl₃·6H₂O (5.4 g) (molar ratio 1:2) were dissolved in DI (100 ml) and heated to 70 °C. Ammonium hydroxide (NH₄OH; 6 ml) was quickly added to the solution, which immediately produced a deep black magnetic precipitate. Finally, the Fe₃O₄ nanoparticle suspension was stirred for 30 min at 70 °C. The product was washed several times with DI, following which the Fe₃O₄ nanoparticles were dried in a rotary evaporator (25 mbar at 40 °C) until a fine powder was formed. This was used in all further reactions.

Preparation of Magnetic PNIPAAm Nanocomposite by Emulsion Polymerisation (Fe₃O₄-PNIPAAm-1)

NiPAM (0.4 g), freshly prepared Fe₃O₄ nanoparticles (0.2 g), BIS (0.2 g) and SDS (0.3 g) were dissolved in 350 ml of DI and heated to 70 °C under a nitrogen atmosphere. APS (0.0035 g) was then dissolved in 1 ml of DI and added to the reaction vessel to start the reaction. After 4 h, the reaction was stopped and the prepared nanocomposite washed with DI. Finally, Fe₃O₄-PNIPAAm-1 was separated out by centrifugation (12,000 rpm for 30 min) and then dried using a rotary evaporator (25 mbar at 40 °C). The powdered material was stored in the dark at room temperature.

Preparation of Magnetic PNIPAAm Nanocomposite

Through In Situ Precipitation (Fe₃O₄-PNIPAAm-2)

FeCl₂ (0.148 g), FeCl₃ (0.4 g) and 10 ml DI were mixed well and added to 1 g of PNIPAAm. NH₄OH (3 ml) was then quickly added to the solution, which immediately produced a deep black magnetic precipitate. The suspension was then stirred for 30 min at 70 °C. The prepared nanocomposite was washed with DI, following which the Fe₃O₄-PNIPAAm-2 was separated out by centrifugation (12,000 rpm for 30 min) and dried using a rotary evaporator (25 mbar at 40 °C). The resultant powder was stored in the dark at room temperature.

Preparation of Magnetic PNIPAAm Nanocomposite

Through Physical Addition (Fe₃O₄-PNIPAAm-3)

Freshly prepared PNIPAAm (1 g), freshly prepared Fe₃O₄ nanoparticles (0.5 g) and DI (5 ml) were mixed well, and the resultant suspension stirred for 30 min at 70 °C. The nanocomposite thus prepared was washed with DI, following which the Fe₃O₄-PNIPAAm-3 was separated out through centrifugation (12,000 rpm for 30 min) and dried using a rotary evaporator (25 mbar at 40 °C). The powdered material was stored in the dark at room temperature.

Nanocomposites Characterisation

The size and zeta potential of the Fe₃O₄-PNIPAAm nanocomposites were measured following complete

dissolution of the nanoparticles in DI (dispersal in DI followed by sonification for 2 min at room temperature). Zeta potential measurements were performed using a Zetasizer Nano analyser (Malvern Instruments, USA) at pH 7. A Zetasizer Nano dynamic light scattering (DLS) unit was employed to measure the hydrodynamic diameter of particle aggregates in DI. Thermogravimetric analysis (TGA) was undertaken in order to quantify the amount of coating and to determine the nanocomposite's thermal stability. Thermal studies were undertaken on 3–4 mg of dry sample at temperatures ranging from 25 to 900 °C, using a TGA Q500 (TA Instruments, USA) under a nitrogen atmosphere (heating rate 10 °C/min). The material's magnetic properties were measured using a MicroMag™ 2900 vibrating sample magnetometer (Princeton measurements corporation, USA). Microscopy images were obtained using a scanning electron microscope (SEM), the particles being first thoroughly dissolved in DI and a drop of the solution placed on the copper grid of a Zeiss ULTRA Plus field-emission SEM equipped with a Schottky cathode. All images were analysed using Smart SEM software v 5.05 (Zeiss, Germany) for imaging operated at 1.5 kV.

Bacterial Strains and Media

Gram-negative *Escherichia coli* CCM3954 and Gram-positive *Staphylococcus aureus* CCM 3953 (Brno, Czech Republic) were used for all experiments. Detailed information on the strains is provided on the web page of the 'Czech Collection of Microorganisms' (<http://www.sci.muni.cz/cem/>). Each bacterial culture was freshly prepared and held overnight in a soya nutrient broth (Sigma-Aldrich) before performing the biological experiments.

DNA Damage

Comet assays were performed following the methodology of Singh et al. [15] and Solanky et al. [16]. All chemicals were purchased from PENTA (Czech Republic) unless otherwise noted. A fresh bacterial culture (adjusted to 10^7 cells/ml) was grown overnight and then incubated with two concentrations (0.1 and 1 g/l) of PNIPAAm and each of the Fe₃O₄-PNIPAAm nanocomposites for 30 min at 37 °C.

A microgel was prepared by putting 100 ml of agarose onto the frosted surface of a slide and covering it with a 24 × 50 mm cover glass (ThermoFisher Scientific, USA). The slides were left at room temperature for 5 min, then the cover glasses were removed and the slides allowed to dry. This dried agarose layer (first layer) provided a firm base for subsequent layers. After exposing the bacteria to the PNIPAAm and Fe₃O₄-PNIPAAm nanocomposites for 30 min, 2 µl (containing approximately 10,000 exposed cells) was taken and mixed with 100 µl of freshly prepared 0.5% agarose. This mixture was pipetted onto

frosted slides and immediately covered with a cover glass (second layer). The slides were then cooled in a steel tray over ice. The cover glasses were removed after 1 min, and a third layer of 100 µl of lysis agarose (including 0.5% agarose with 5 µg/ml RNase A [Ameresco, USA], 0.25% sodium N-lauroylsarcosine and 0.5 mg/ml lysozyme) was produced, again using a cover glass. The slides were then left on ice for 10 min then placed into a humid chamber for 30 min at 37 °C. After removing the cover glass, the slides were immersed in a lysing solution containing 2.5 M of NaCl, 100 mM of EDTA tetrasodium salt, 10 mM tris buffer of pH 10, 1% sodium lauroyl sarcosine and 1% triton X-100. After 1 h of lysis at room temperature, the slides were transferred to an enzyme digestion solution containing 2.5 M of NaCl, 10 mM of EDTA and 10 mM tris pH 7. Four buffer with 1 mg/ml of proteinase K. The slides were then incubated at 37 °C for 2 h, following which they were placed on the horizontal slab of an electrophoretic unit (Scie-plas, UK) and equilibrated with 300 mM of sodium acetate and 100 mM pH 9 tris buffer for 20 min then electrophoresed at 12 V (0.4 V/cm, approximately 100 mA) for 30 min. Following electrophoresis, the slides were immersed in 1 M ammonium acetate in ethanol (5 ml of 10 M ammonium acetate and 45 ml of absolute ethanol) for 20 min, absolute ethanol for 0.5 h and 70% ethanol for 10 min, after which the slides were air-dried at room temperature. To achieve uniform staining, the slides were pretreated with 50 ml of a freshly prepared solution of 5% TE buffer and 10 mM of NaH₂PO₄. The slides were then stained with 50 µl of a freshly prepared 1 mM solution of SYBR stain (Sigma-Aldrich, USA) in TE buffer for 30 min. Migration of DNA strand breaks (comets) was visualised using an AxioImager fluorescence microscope at ×400 magnification and AxioVision v 4 software (Zeiss, Germany). Typically, a tail length of 50 comets was individually measured for each sample.

Bacterial Growth Rate, Cell Viability and Morphology

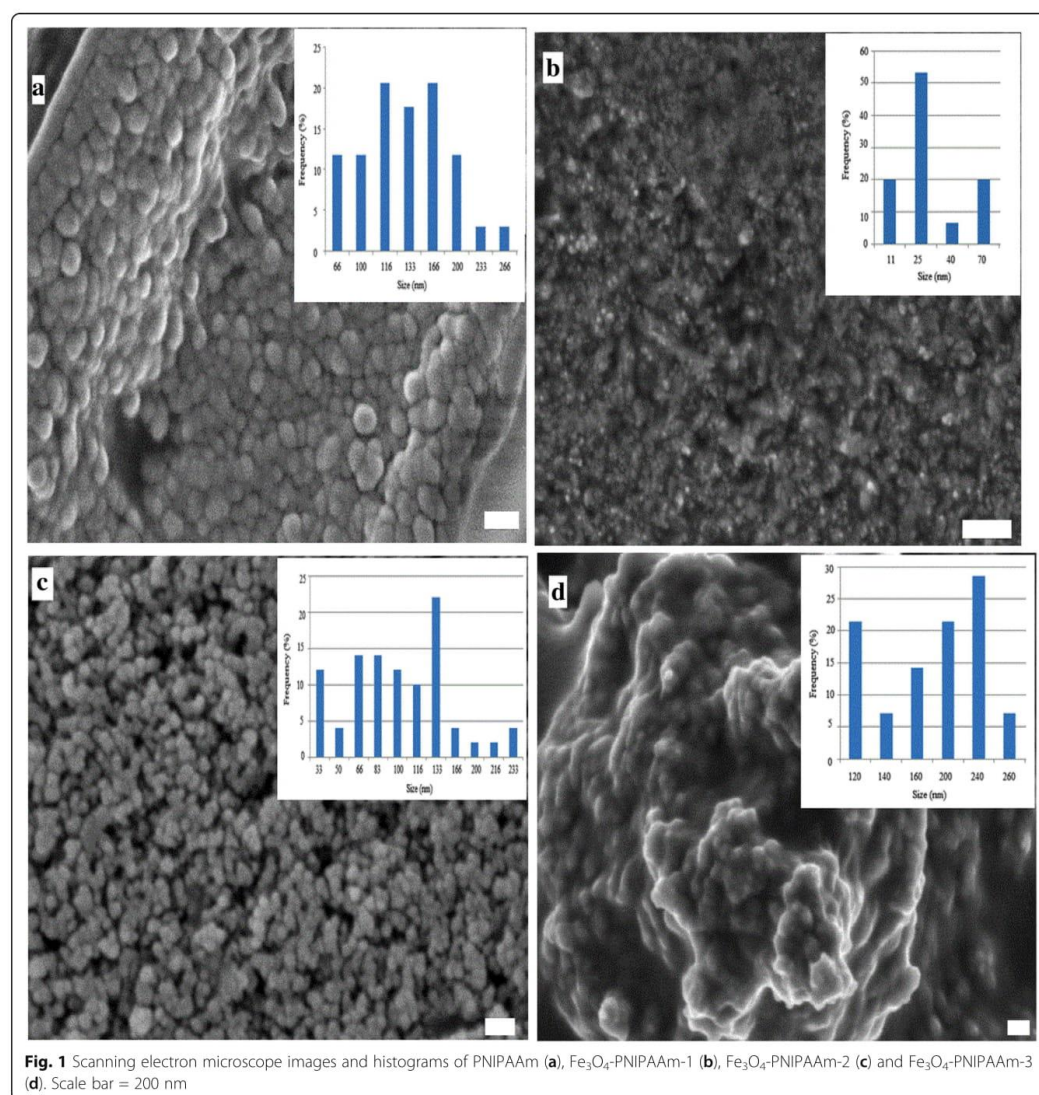
The experimental protocol followed that described in Darwish et al. [17]. Briefly, a Fe₃O₄-PNIPAAm nanocomposite stock suspension (10 g/l) was added to fresh bacterial culture in order to obtain final concentrations of 0.01, 0.05, 0.5 and 1 g/l. Each concentration was produced in triplicate in a 24-well plate. Negative controls, consisting of bacterial cells only in growth media and Fe₃O₄-PNIPAAm nanocomposite only in growth media, were run in parallel. The plate was then incubated at 37 °C, following which the sample's optical density was measured at 600 nm (OD600) every 2 h for 6 h using a Synergy™ HTX plate reader (Biotek, USA). Bacterial growth rate was defined as the R linear regression of the OD600 measurement (absorbance units, AU) versus

incubation time in hours. Preliminary measurements of nanocomposite samples without cells (6 h at 600 nm) showed constant absorbance values that did not interfere with absorbance values of nanocomposites measured with bacterial cells.

The effective concentration of nanocomposite at 10% inhibition (EC10) on bacterial growth rate (μ) was calculated for each form of Fe₃O₄-PNIPAAm based on the equation: $I(\%) = (\mu_C - \mu_T) / \mu_C \times 100$, where I is inhibition, μ_C

is the mean control growth rate value and μ_T is the growth rate of the culture affected by the nanocomposite [18].

After 24-h incubation, 100 μ l aliquots of each sample were stained using the L7007 Bacterial Viability Kit (Molecular Probes, Invitrogen, USA) in the dark for 15 min. Determination of the proportion of live (Ex/Em 485/528 nm) and dead cells (Ex/Em 485/645 nm) was performed using a Synergy™ HTX plate reader (Biotek, USA). The percentage of dead cells was calculated as the



ratio of dead to live cells. At the same time, images of *E. coli* and *S. aureus* were obtained using an AxioImager fluorescence microscope (Zeiss, Germany) with Ex/Em 470/490–700 nm. The length of *E. coli* cells and area of *S. aureus* cell clusters were determined at $\times 600$ magnification using AxioVision v 4 software (Zeiss, Germany).

Statistical Analysis

Differences between bacterial strains incubated in PNIPAAm, different Fe₃O₄-PNIPAAm nanocomposites and control samples without nanocomposites were tested using ANOVA and Dunnett’s test (GraphPad PRISM, USA).

Results

In this study, we synthesised Fe₃O₄-PNIPAAm nanocomposite employing three different protocols: emulsion polymerisation (Fe₃O₄-PNIPAAm-1), in situ precipitation (Fe₃O₄-PNIPAAm-2) and physical addition (Fe₃O₄-PNIPAAm-3). SEM imaging showed that the type of protocol used had a clear effect on sample morphology and particle size, with Fe₃O₄-PNIPAAm-1, Fe₃O₄-PNIPAAm-2 and Fe₃O₄-PNIPAAm-3 showing a broad size distribution, agglomeration due to high surface energy between nanoparticles and presence of magnetic dipolar interactions (Fig. 1).

TGA indicated that the Fe₃O₄-PNIPAAm samples became relatively stable at temperatures above 400 °C (Fig. 2). Overall, PNIPAAm nanoparticles showed lower residual content than the Fe₃O₄-PNIPAAm nanocomposites. Zeta potential values for surface charge were –1.58 mV for PNIPAAm, –15.6 mV for Fe₃O₄-PNIPAAm-

1, –16.4 mV for Fe₃O₄-PNIPAAm-2 and –1.8 mV for Fe₃O₄-PNIPAAm-3. Vibrating sample magnetometer values for magnetisation saturation were 50.4 emu/g for Fe₃O₄-PNIPAAm-1, 53.7 emu/g for Fe₃O₄-PNIPAAm-2 and 21.0 emu/g for Fe₃O₄-PNIPAAm-3. Dynamic light scattering above (45 °C) and below (25 °C) LCST indicated a hydrodynamic size for PNIPAAm of 50 nm at 25 °C and 27 nm at 45 °C; 412 nm at 25 °C and 197 nm at 45 °C for Fe₃O₄-PNIPAAm-1; 212 nm at 25 °C and 130 nm at 45 °C for Fe₃O₄-PNIPAAm-2 and 122 nm at 25 °C and 60 nm at 45 °C for Fe₃O₄-PNIPAAm-3 (Fig. 3).

Fe₃O₄-PNIPAAm Nanocomposite Effect on the Bacterial DNA

Following a short exposure of 30 min, DNA strand breaks were determined for both *E. coli* and *S. aureus* in cells treated with the Fe₃O₄-PNIPAAm nanocomposites, 40% EtOH (positive control) and untreated cells (negative control). All Fe₃O₄-PNIPAAm nanocomposites showed a similarly significant effect ($P < 0.001$) on mean *E. coli* and *S. aureus* comet tail length at all concentrations (Fig. 4), compared with control cells incubated without nanocomposites.

Fe₃O₄-PNIPAAm Nanocomposite Antibacterial Effect

Growth rates indicated that Gram-positive *S. aureus* was less resistant than Gram-negative *E. coli* to all nanocomposites after 6 h exposure. Fe₃O₄-PNIPAAm-1 and Fe₃O₄-PNIPAAm-2 both strongly inhibited bacterial growth, compared with PNIPAAm and Fe₃O₄-PNIPAAm-3, with *E. coli* growth rate significantly reduced from 0.08 to 0.028 ($P < 0.001$) with

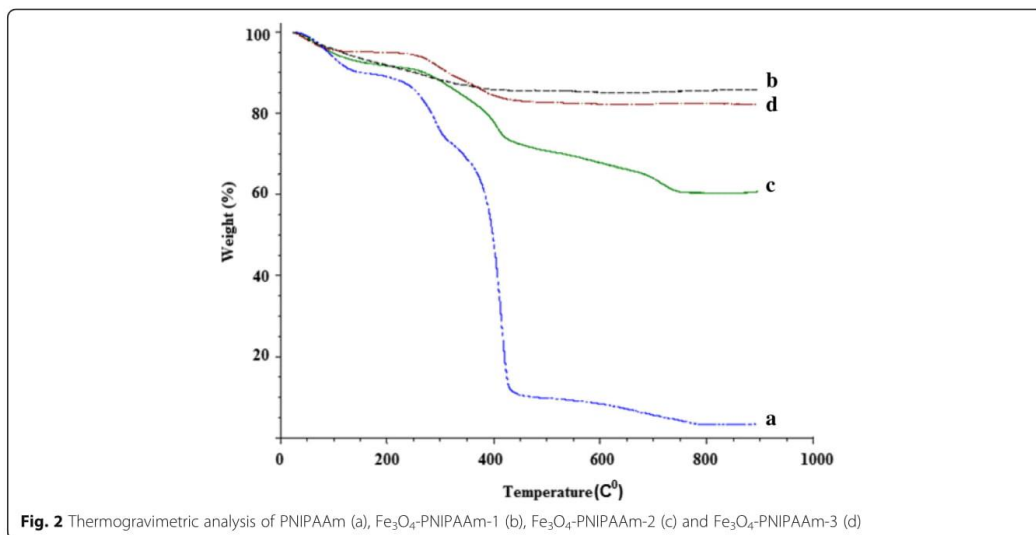


Fig. 2 Thermogravimetric analysis of PNIPAAm (a), Fe₃O₄-PNIPAAm-1 (b), Fe₃O₄-PNIPAAm-2 (c) and Fe₃O₄-PNIPAAm-3 (d)

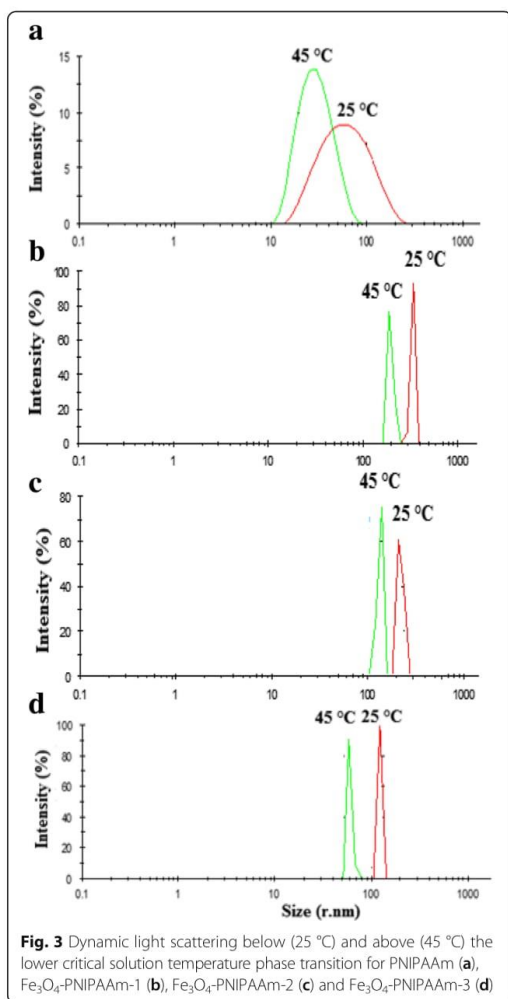


Fig. 3 Dynamic light scattering below (25 °C) and above (45 °C) the lower critical solution temperature phase transition for PNIPAAm (a), Fe₃O₄-PNIPAAm-1 (b), Fe₃O₄-PNIPAAm-2 (c) and Fe₃O₄-PNIPAAm-3 (d)

Fe₃O₄-PNIPAAm-2 and 0.005 ($P < 0.001$) with Fe₃O₄-PNIPAAm-1 (1 g/l). No effect was observed on *E. coli* growth rate by either PNIPAAm or Fe₃O₄-PNIPAAm-3 (Fig. 5a). In comparison, the growth rate of *S. aureus* was affected by all Fe₃O₄-PNIPAAm nanocomposites and by the PNIPAAm nanoparticles. At lower concentrations (0.01 g/l and 0.05 g/l), growth rate was only slightly reduced from 0.07 to 0.06 ($P < 0.05$). At higher concentrations (0.5 and 1 g/l), however, there was a significant reduction from 0.07 to 0.001 with PNIPAAm, 0.0 with Fe₃O₄-PNIPAAm-1, 0.01 with Fe₃O₄-PNIPAAm-2 and 0.009 with Fe₃O₄-PNIPAAm-3 (all $P < 0.001$; Fig. 5b). In addition, the EC10 for all Fe₃O₄-PNIPAAm nanocomposites and

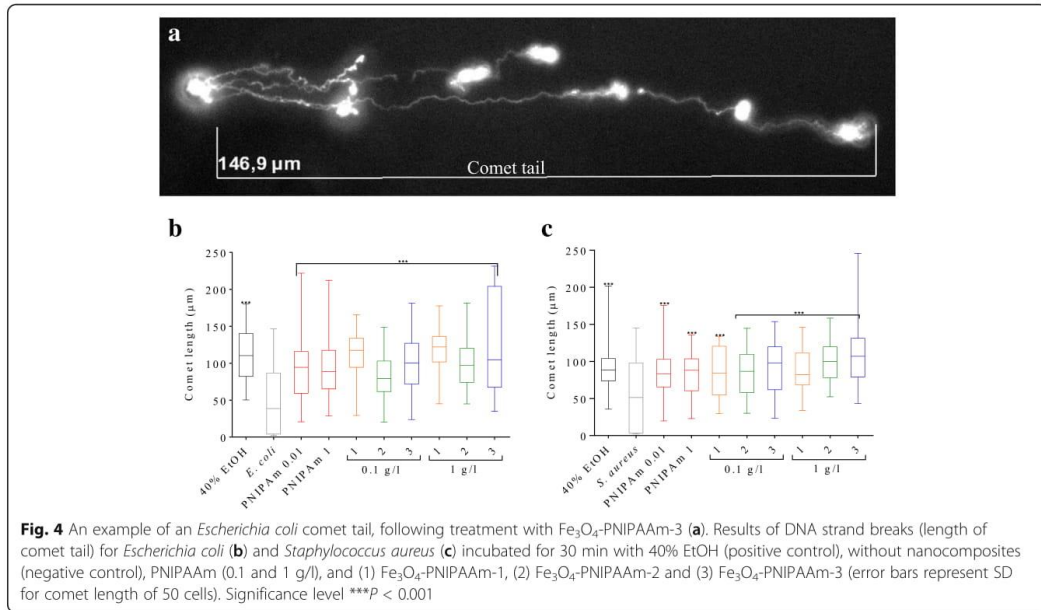
the PNIPAAm nanoparticle control was lower for *S. aureus* than that for *E. coli* (Table 1).

The percentage of dead *E. coli* cells increased with increasing concentration of Fe₃O₄-PNIPAAm nanocomposite after 24 h. PNIPAAm (0.5 and 1 g/l), for example, caused a significant increase in *E. coli* dead cells (20%) compared to cultures without Fe₃O₄-PNIPAAm nanocomposite (12%). Fe₃O₄-PNIPAAm-1 (0.5 g/l) resulted in up to 28% of dead *E. coli* cells and 32% at 1 g/l ($P < 0.001$). The effect of Fe₃O₄-PNIPAAm-2 was lower than that of Fe₃O₄-PNIPAAm-1 and Fe₃O₄-PNIPAAm-3, with the percentage of dead cells increasing from 13 to 25% when exposed to concentrations of 0.01 and 1 g/l, respectively ($P < 0.001$). At both 0.5 and 1 g/l, Fe₃O₄-PNIPAAm-3 resulted in around 25% dead cells ($P < 0.001$; Fig. 6a). The percentage of dead *S. aureus* cells was only significantly affected by 1 g/l Fe₃O₄-PNIPAAm-1 and Fe₃O₄-PNIPAAm-3, with dead cells reaching up to 50 and 48%, respectively ($P < 0.001$). The control without nanocomposites contained approximately 18% of dead cells while in lower concentrations of PNIPAAm, Fe₃O₄-PNIPAAm-1 and Fe₃O₄-PNIPAAm-3, the proportion of dead cells was even lower. PNIPAAm at concentrations of 0.5 and 1 g/l resulted in 25 and 30% ($P < 0.005$) dead cells, respectively. Fe₃O₄-PNIPAAm-2 had no effect on *S. aureus* cultures (Fig. 6b).

There was no difference in average *E. coli* cell length (5 μm) and average *S. aureus* cell cluster area (200 μm²) for any nanocomposite or the PNIPAAm control at lowest concentrations (0.1 g/l; Fig. 7). At higher concentrations, *E. coli* length did not change in the presence of Fe₃O₄-PNIPAAm-2, nor did *S. aureus* cell group area in the presence of Fe₃O₄-PNIPAAm-1. However, *E. coli* length was significantly increased in the presence of 1 g/l of PNIPAAm (5.4 μm, $P < 0.005$), Fe₃O₄-PNIPAAm-1 (6 μm, $P < 0.001$) and Fe₃O₄-PNIPAAm-3 (10 μm, $P < 0.001$) (Fig. 7a), while *S. aureus* formed larger clusters when exposed to PNIPAAm (1937 μm², $P < 0.001$), Fe₃O₄-PNIPAAm-2 (924 μm², $P < 0.001$) and Fe₃O₄-PNIPAAm-3 (1722 μm², $P < 0.001$) (Fig. 7b).

Discussion

Both the method of synthesis and the means by which magnetic nanoparticles were added to the polymer matrix had a clear effect on the intrinsic physical-chemical properties of the magnetic Fe₃O₄-PNIPAAm nanocomposites. Stepwise synthesis had a strong impact on nanocomposite properties, resulting in changes to particle shape, size distribution, size and surface chemistry, along with subsequent changes in magnetic properties [19, 20]. Emulsion polymerisation (Fe₃O₄-PNIPAAm-1), an easy and precise method, produced the stable nanocomposites with narrow particle size distribution and lowest aggregation tendency,



qualities particularly important in biomedical applications [17]. Produced as a result of both steric and coulombic repulsion, the particle dimensions were sufficiently small that precipitation was avoided [21]. The least effective method was physical addition (Fe₃O₄-PNIPAAm-3). Not only was it produced via three distinct steps, and hence took longer to prepare, the resulting nanocomposite showed higher aggregation than either of the other two production methods. Moreover, our results indicated that Fe₃O₄-PNIPAAm-3 produced in this way may have contained undesirable PNIPAAm and Fe₃O₄ nanoparticle residuals.

Polymers can become attached to magnetic nanoparticles by either physical (noncovalent) or covalent bonds, with the resulting hybrid material displaying specific properties depending on the synthetic route taken. Significant re-suspension of magnetic nanoparticles takes place when preparation proceeds in the solvent in which hybrid nanoparticle formation occurs, whereupon aggregation and segregation may become a problem. In this case, in situ formation of magnetic nanoparticles may be a better alternative in many cases. In addition, if the surfactant concentration is too low, coalescence will change the size of

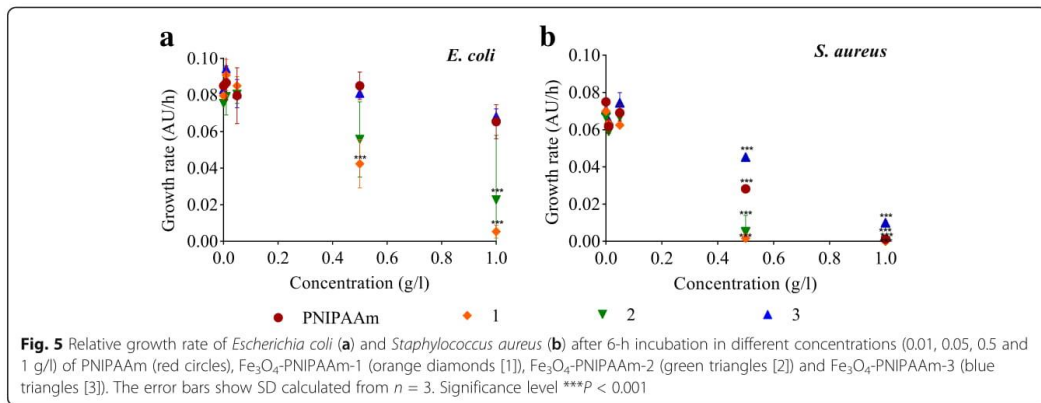


Table 1 The effective concentration of PNIPAAm, Fe₃O₄-PNIPAAm-1, Fe₃O₄-PNIPAAm-2 and Fe₃O₄-PNIPAAm-3 nanoparticles (g/l) at 10% growth inhibition (EC10) determined for Gram-negative *Escherichia coli* and Gram-positive *Staphylococcus aureus*

	PNIPAAm	Fe ₃ O ₄ -PNIPAAm-1	Fe ₃ O ₄ -PNIPAAm-2	Fe ₃ O ₄ -PNIPAAm-3
<i>E. coli</i>	0.43	0.11	0.14	0.67
<i>S. aureus</i>	0.10	0.05	0.04	0.06

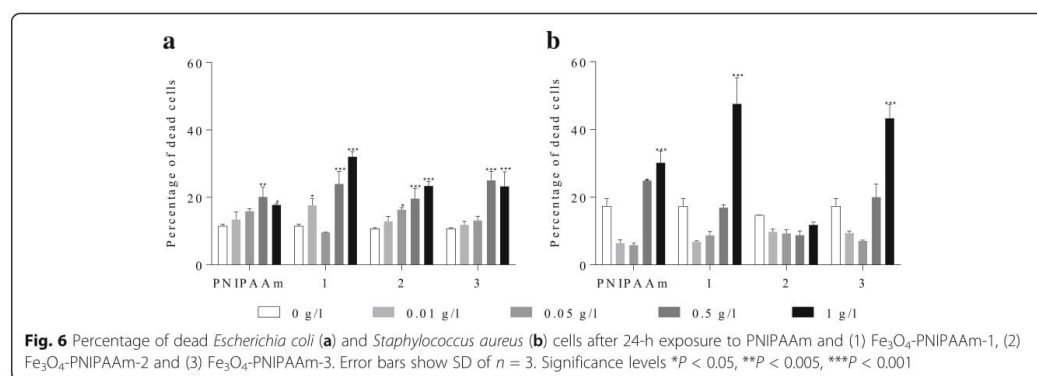
the droplets, whereas micelles can form if the concentration is too high, leading to micellar nucleation. In this respect, it is important that the surfactant concentration is chosen carefully based on precise characterisation of surface properties and extent of particle modification, in order to ensure the inorganic particle surface is compatible with the polymer matrix.

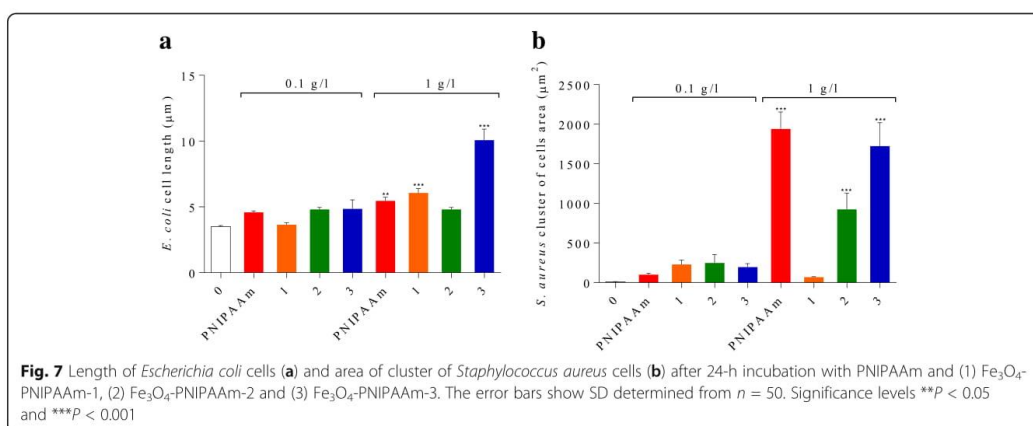
In order to evaluate the magnetic properties of Fe₃O₄-PNIPAAm nanocomposites, it is important to know the content of MNPs in the nanocomposite. TGA was employed to quantify amount of MNP and to investigate thermal stability of Fe₃O₄-PNIPAAm nanocomposites compared with PNIPAAm nanoparticles alone. All three Fe₃O₄-PNIPAAm nanocomposites displayed higher thermal stability than PNIPAAm nanoparticles, presumably due to the presence of Fe₃O₄ particles in the matrix (Fig. 2). Higher residues in magnetic nanocomposites could be attributed to the presence of inorganic Fe₃O₄ compounds in the samples, which were sustained even at higher temperatures.

Fe₃O₄-PNIPAAm-1 showed highest thermal nanocomposite stability, along with the lowest weight lost. Up to 200 °C, the main source of weight loss was through loss of water and physical adsorption of the polymer layer [22]; above 200 °C, however, losses were mainly due to decomposition of the chemical layer bonding the PNIPAAm. The sample residue, which became stable above 400 °C, represented 87%

of the original weight, which corresponds with the amount of magnetic nanoparticles in the nanocomposite. One aim of this preparation process was to produce a nanocomposite with magnetic properties preventing aggregation and enabling it to re-disperse rapidly as soon as the magnetic field is turned off. Such properties would allow its use in a range of different fields, including hyperthermic treatment of tumours, as contrasting agents in magnetic resonance imaging, in tissue repair, biomedical device coating, immunoassay, cell separation and biomagnetic separation of biomolecules [18, 23–26]. We tested our nanomaterials through magnetisation saturation, which assesses the maximum possible magnetisation of the substance beyond which no further change takes place despite an increase in the magnetic field. Our results showed Fe₃O₄-PNIPAAm-2 to have the highest magnetisation saturation level of the three nanocomposites tested. Our values were lower (53.7 emu/g) than those previously reported for uncoated Fe₃O₄ nanoparticles (92 emu/g) [27], however, presumably due to surface order/disorder interactions in the magnetic spin moment and an increase in nanocomposite weight and volume due to the presence of the PNIPAAm polymer layer.

Of special interest as regards biomedical application is the behaviour of polymer-water solutions stable below a LCST [28]. After heating the prepared Fe₃O₄-PNIPAAm nanomaterials above the transition temperature, a coil-to-globule transition occurred, followed by intermolecular association. All three Fe₃O₄-PNIPAAm nanomaterials displayed very similar behaviour, with all shrinking as temperature increased. PNIPAAm is widely used as a thermoresponsive polymer due to the proximity of its LCST (~30–32 °C) to physiological temperature. Furthermore, the thermo-responsibility of PNIPAAm has proved useful for drug release in vivo [28]. Nanoscale magnetic hydrogels based on PNIPAAm





have now been developed for theranostic application, with those embedded with low concentrations of Fe₃O₄ magnetic nanostructures resulting in an LCST of ~40 °C, making Fe₃O₄-PNIPAAm of especial interest for controlled drug release application [29].

SEM nanoparticle histograms displayed a broader size distribution than those using DLS (Fig. 1). Interpretation of DLS data involves the interplay of multiple parameters, however, including the size, concentration, shape, polydispersity and surface properties of the particles. Measurement of the hydrodynamic size of thermoresponsive samples in relation to temperature is a common method of characterising LCST behaviour, with nanoparticles shrinking as temperatures increase, soluble polymers precipitating and particle size increasing. As expected, PNIPAAm had a lower hydrodynamic size than the Fe₃O₄-PNIPAAm nanocomposites. Of the nanocomposites, Fe₃O₄-PNIPAAm-3 displayed the lowest hydrodynamic size and a narrow size distribution.

Table 2 Summary of the antimicrobial effect of PNIPAAm and three nanocomposites on *Escherichia coli* and *Staphylococcus aureus*

Endpoint	PNIPAAm	Fe ₃ O ₄ -PNIPAAm-1	Fe ₃ O ₄ -PNIPAAm-2	Fe ₃ O ₄ -PNIPAAm-3
Growth rate				
<i>E. coli</i>	0	--	-	0
<i>S. aureus</i>	-	--	--	-
Viability				
<i>E. coli</i>	--	--	--	--
<i>S. aureus</i>	--	--	0	--
DNA damage				
<i>E. coli</i>	-	--	--	--
<i>S. aureus</i>	-	--	--	--

0 no effect, - significant negative effect, -- strong negative effect

Variability in hydrodynamic size is likely to be due to the presence of Fe₃O₄ nanoparticles in the PNIPAAm matrix, which increases both the particle dimension and aggregation in water (Fig. 3) [8].

All Fe₃O₄-PNIPAAm nanocomposites displayed antimicrobial properties (Table 2), with both Gram-negative and Gram-positive bacteria negatively affecting *E. coli* growth rate in the order Fe₃O₄-PNIPAAm-1 > Fe₃O₄-PNIPAAm-2 > Fe₃O₄-PNIPAAm-3 = PNIPAAm and *S. aureus* growth rate as Fe₃O₄-PNIPAAm-1 > Fe₃O₄-PNIPAAm-2 > Fe₃O₄-PNIPAAm-3 > PNIPAAm. Similarly, the antibacterial properties desired for medical applications such as biomedical device coatings and wound dressing materials have been confirmed for a number of new PNIPAAm composites, including ZnO-PNIPAAm, Ag-PNIPAAm and chitosan-PNIPAAm [23–26].

In comparison with the modified Fe₃O₄ nanomaterials described in our earlier studies, the PNIPAAm-1, PNIPAAm-2 and PNIPAAm-3 nanocomposites all showed a stronger effect on both *E. coli* and *S. aureus*, with *S. aureus* EC10 growth inhibition ranging from 0.04 to 0.06 g/l for the three nanomaterials, while modified APTS-, PEG- and TEOS-MNPs ranged between 0.1 and 0.25 g/l [17], and polymer-coated Fe₃O₄ (PEI-mC-, PEI- and OA-MNPs) had a value of 0.15 g/l [18]. Inhibition of bacterial growth could have been caused by several factors, including cell membrane damage, oxidative stress and cell elongation, resulting in the production of lethal cells. The cells could, on the other hand, survive such unfavourable conditions by employing repair enzymes, antioxidants and/or transient growth arrest. This could partly explain the phenomenon that in lower concentrations (0.01 and 0.05 g/l) of PNIPAAm, Fe₃O₄-PNIPAAm-1 and Fe₃O₄-PNIPAAm-3, the proportion of dead cells of *S. aureus* was lower after 24-h incubation than in control where no such factor inducing mobilisation of the

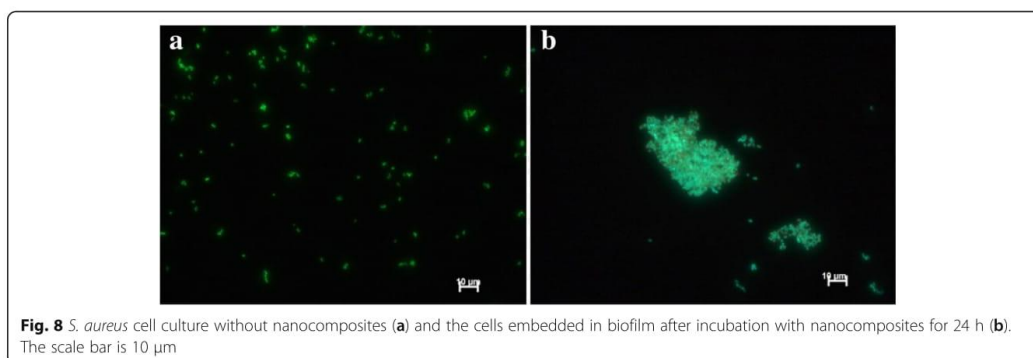


Fig. 8 *S. aureus* cell culture without nanocomposites (a) and the cells embedded in biofilm after incubation with nanocomposites for 24 h (b). The scale bar is 10 µm

defence/repair system was present. Higher concentrations of PNIPAAm and nanocomposites caused indeed significant increase in dead cells of *E. coli* and *S. aureus* corresponding well with significant decrease in growth rate of the cell cultures.

Exposure to 1 g/l of the nanocomposite resulted in changes to bacterial cell morphology, with greatest change to *E. coli* cell length caused by Fe_3O_4 -PNIPAAm-3 > Fe_3O_4 -PNIPAAm-1 > PNIPAAm > Fe_3O_4 -PNIPAAm-2, and Fe_3O_4 -PNIPAAm-3 > Fe_3O_4 -PNIPAAm-2 > PNIPAAm > Fe_3O_4 -PNIPAAm-1 for *S. aureus* clustering. This effect was also observed previously when the same bacteria were exposed to different functional magnetic nanoparticles [17]. Elongation of *E. coli* cells in the presence of nanocomposites is indicative of transient growth arrest and is evidence of an adaptive response to oxidative stress or DNA damage [30]. In the case of *S. aureus*, which is a biofilm formation species, the cells became embedded over a larger area than the nanocomposite-free control when exposed to PNIPAAm, Fe_3O_4 -PNIPAAm-2 and Fe_3O_4 -PNIPAAm-3 (Fig. 8). No *S. aureus* biofilm was produced when in contact with Fe_3O_4 -PNIPAAm-1, possibly due to its stronger antibacterial properties. *S. aureus* usually produces a biofilm in harsh environments to protect the cells [31]; however, this could also have an adverse effect on the bacteria as nanocomposites can integrate through the biofilm and harm the cells, as has already been described for *Pseudomonas* sp. [32].

Iron could lead to DNA damage in bacterial cells as described in previous reviews [33, 34]; hence, we attempted to test whether our MNPs caused DNA damage to bacteria. The presence of Fe_3O_4 -PNIPAAm nanocomposites at both low and high concentrations (0.01 or 1 g/l) caused significant damage to *E. coli* and *S. aureus* DNA, even after short exposures (30 min). To the best of our knowledge, this is the first acute genotoxicity study of magnetic composites on bacteria; as a result, we cannot compare our results with those of other authors directly. Previous

studies have shown no genotoxicity attributable to PNIPAAm nanoparticles, however, and no decrease in cell viability when tested against two kinds of mammalian cell at nanoparticle concentrations of up to 800 mg/l [30]. On the other hand, previous genotoxicity studies on MNPs ($\gamma\text{-Fe}_3\text{O}_4$) have shown a negative effect on human fibroblast cells at 100 mg/l [35]. Studies performed with mammalian cell lines, however, cannot be directly compared to studies done with bacterial cells, due to significant differences in eukaryotic and prokaryotic cells.

Conclusions

Magnetic poly(N-isopropyl-acrylamide) nanocomposites were prepared through emulsion polymerisation (Fe_3O_4 -PNIPAAm-1), in situ precipitation (Fe_3O_4 -PNIPAAm-2) and physical addition (Fe_3O_4 -PNIPAAm-3). Both Fe_3O_4 -PNIPAAm-1 and Fe_3O_4 -PNIPAAm-2 showed higher values for surface charge and thermal stability, indicating a stable colloidal system. At room temperature, Fe_3O_4 -PNIPAAm-3 displayed highest magnetisation saturation. Presence of Fe_3O_4 -PNIPAAm nanocomposites at both low and high concentrations caused significant damage to both *E. coli* and *S. aureus* DNA, even after short exposure, and led to a decrease in cell viability. Overall, we suggest that Fe_3O_4 -PNIPAAm-1, prepared through emulsion polymerisation, is the most appropriate method for producing a magnetic nanocomposite with high antimicrobial activity towards Gram-negative *E. coli* and Gram-positive *S. aureus*.

Abbreviations

Fe_3O_4 -PNIPAAm: Magnetic poly(N-isopropylacrylamide); MNPs: Magnetite nanoparticles

Acknowledgements

We thank Dr. Kevin Roche for helping us with English language correction.

Funding

This research was supported through the Centre of Competence project 'Nanobiowat' no. TE01020218. Further support was provided by MSMT within the framework of targeted support under the projects: 'National Programme

for Sustainability I' project no. LO1201 and 'Centre for Nanomaterials, Advanced Technologies and Innovation' project no. CZ.1.05/2.1.00/01.0005. The work of M. Darwish was supported through 'Development for Research Teams of R&D Projects' project no. CZ.1.07/2.3.00/30.0024. The work of N. Nguyen was partly supported by MŠMT under SGS project no. 21176/115 of the Technical University of Liberec and by 'Research Infrastructure NanoEnvicZ' under project no. LM2015073.

Authors' Contributions

NHAN designed and performed the antimicrobial tests and wrote the majority of the manuscript. MSAD performed the synthesis and characterisation of magnetite composites and participated on the manuscript text. PK assisted with SEM analysis. AS and IS supervised the conceptual framework and corrected the manuscript. All authors read and approved the final manuscript.

Ethics Approval and Consent to Participate

Not applicable.

Competing Interests

The authors declare that they have no competing interests.

Publisher's Note

Springer Nature remains neutral with regard to jurisdictional claims in published maps and institutional affiliations.

Author details

¹Institute for Nanomaterials, Advanced Technologies and Innovation, Technical University of Liberec, 461 17 Liberec, Czech Republic. ²Faculty of Mechatronics, Informatics and Interdisciplinary Studies, Technical University of Liberec, 461 17 Liberec, Czech Republic. ³Egyptian Petroleum Research Institute, 1 Ahmed El-Zomor Street, El Zohour Region, Nasr City, Cairo 11727, Egypt.

Received: 6 June 2017 Accepted: 10 October 2017

Published online: 19 October 2017

References

- Schwall CT, Banerjee I a. (2009) Micro- and nanoscale hydrogel systems for drug delivery and tissue engineering. *Materials* 2:577–612
- Hu X, Hao X, Wu Y et al (2013) Multifunctional hybrid silica nanoparticles for controlled doxorubicin loading and release with thermal and pH dual response. *J Mater Chem B* 1:1109–1118
- Cooperstein MA, Canavan HE (2013) Assessment of cytotoxicity of (N-isopropyl acrylamide) and poly(N-isopropyl acrylamide)-coated surfaces. *Biointerphases* 8:19
- Philippova O, Barabanova A, Molchanov V, Khokhlov A (2011) Magnetic polymer beads: recent trends and developments in synthetic design and applications. *Eur Polym J* 47:542–559
- Elaissari A (2009) Magnetic latex particles in nanobiotechnologies for biomedical diagnostic applications: state of the art. *Macromol Symp* 281:14–19
- Lee C-F, Lin C-C, Chien C-A, Chiu W-Y (2008) Thermosensitive and control release behavior of poly(N-isopropylacrylamide-co-acrylic acid)/nano-Fe₃O₄ magnetic composite latex particle that is synthesized by a novel method. *Eur Polym J* 44:2768–2776
- Afrassiabi A, Hoffman AS, Cadwell LA (1987) Effect of temperature on the release rate of biomolecules from thermally reversible hydrogels. *J Memb Sci* 33:191–200
- Macková H, Horák D (2006) Effects of the reaction parameters on the properties of thermosensitive poly(N-isopropylacrylamide) microspheres prepared by precipitation and dispersion polymerization. *J Polym Sci Part A Polym Chem* 44:968–982
- Macková H, Králová D, Horák D (2009) Magnetic poly(N-isopropylacrylamide) microspheres by dispersion and inverse emulsion polymerization. *J Polym Sci* 47:4289–4301
- Mu J, Zheng S (2007) Poly(N-isopropylacrylamide) nanocrosslinked by polyhedral oligomeric silsesquioxane: temperature-responsive behavior of hydrogels. *J Colloid Interface Sci* 307:377–385
- Zhang X, Zhou L, Zhang X, Dai H (2009) Synthesis and solution properties of temperature-sensitive copolymers based on NIPAM. *J Appl Phys* 113: 1763–1772
- Hoare T, Timko BP, Santamaria J et al (2011) Magnetically triggered nanocomposite membranes: a versatile platform for triggered drug release. *Nano Lett* 11:1395–1400
- Dionigi C, Lungaro L, Goranov V et al (2014) Smart magnetic poly(N-isopropylacrylamide) to control the release of bio-active molecules. *J Mater Sci Mater Med* 25:2365–2371
- Balasubramaniam S, Pothayee N, Lin Y et al (2011) Poly(N-isopropylacrylamide)-coated superparamagnetic iron oxide nanoparticles: relaxometric and fluorescence behavior correlate to temperature-dependent aggregation. *Chem Mater* 23:3348–3356
- Singh NP, Stephens RE, Singh H, Lai H (1999) Visual quantification of DNA double-strand breaks in bacteria. *Mutat Res - Fundam Mol Mech Mutagen* 429:159–168
- Singh NP, Stephens RE (1997) Microgel electrophoresis: sensitivity, mechanisms, and DNA electrostretching. *Mutat Res* 383:167–175
- Darwish MSA, Nguyen NHA, Ševců A, Stibor I (2015) Functionalized magnetic nanoparticles and their effect on *Escherichia coli* and *Staphylococcus aureus*. *J Nanomater* 2015. doi 10.1155/2015/416012.
- Darwish MSA, Nguyen NHA, Ševců A et al (2016) Dual-modality self-heating and antibacterial polymer-coated nanoparticles for magnetic hyperthermia. *Mater Sci Eng C* 63:88–95
- Lee Y, Lee J, Bae CJ et al (2005) Large-scale synthesis of uniform and crystalline magnetite nanoparticles using reverse micelles as nanoreactors under reflux conditions. *Adv Funct Mater* 15:503–509
- Wormuth K (2001) Superparamagnetic latex via inverse emulsion polymerization. *J Colloid Interface Sci* 241:366–377
- Akbarzadeh A, Samiei M, Davaran S (2012) Magnetic nanoparticles: preparation, physical properties, and applications in biomedicine. *Nanoscale Res Lett* 7:144
- Kurzahls S, Zirbs R, Reimhult E (2015) Synthesis and magneto-thermal actuation of iron oxide core-PNIPAM shell nanoparticles. *ACS Appl Mater Interfaces* 7:19342–19352
- Yu Q, Cho J, Shivapooja P et al (2013) Nanopatterned smart polymer surfaces for controlled attachment, killing, and release of bacteria. *ACS Appl Mater Interfaces* 5:9295–9304
- Schwartz VB, Thétiot F, Ritz S et al (2012) Antibacterial surface coatings from zinc oxide nanoparticles embedded in poly(N-isopropylacrylamide) hydrogel surface layers. *Adv Funct Mater* 22:2376–2386
- Spasojević J, Radosavljević A, Krstić J et al (2015) Dual responsive antibacterial Ag-poly(N-isopropylacrylamide/itaconic acid) hydrogel nanocomposites synthesized by gamma irradiation. *Eur Polym J* 69:168–185
- Kong M, Chen XG, Xing K, Park HJ (2010) Antimicrobial properties of chitosan and mode of action: a state of the art review. *Int J Food Microbiol* 144:51–63
- Fajaro F, Setyawan H, Widiyastuti W, Winardi S (2012) Synthesis of magnetite nanoparticles by surfactant-free electrochemical method in an aqueous system. *Adv Powder Technol* 23:328–333
- Akbarzadeh A, Samiei M, Davaran S. (2012). Magnetic nanoparticles: preparation, physical properties, and applications in biomedicine. *Nanoscale Res Lett* 7:144
- Jaiswal MK, De M, Chou SS et al (2014) Thermoresponsive magnetic hydrogels as theranostic nanoconstructs. *ACS Appl Mater Interfaces* 6:6237–6247
- Tamarit J, Cabisco E, Joaquim R. (1998) Identification of the Major Oxidatively Damaged Proteins in *Escherichia coli* Cells Exposed to Oxidative Stress. *J Biol Chem* 273:3027–3032
- Chien CC, Lin BC, Wu CH (2013) Biofilm formation and heavy metal resistance by an environmental *Pseudomonas* sp. *Biochem Eng J* 78:132–137
- Mahmoudi M, Serpooshan V (2012) Silver-coated engineered magnetic nanoparticles are promising for the success in the fight against antibacterial resistance threat. *ACS Nano* 6:2656–2664
- Henle ES, Linn S (1997) Formation, prevention, and repair of DNA damage by iron/hydrogen peroxide. *J Biol Chem* 272:19095–19098
- Ševců A, El-Temshah YS, Joner EJ, Cerník M (2011) Oxidative stress induced in microorganisms by zero-valent iron nanoparticles. *Microbes Environ* 26:271–281
- Auffan M, Decome L, Rose J et al (2006) In vitro interactions between DMSA-coated maghemite nanoparticles and human fibroblasts: a physicochemical and cyto-genotoxicity study. *Environ Sci Technol* 40:4367–4373

Paper 4

Rune Hjorth, Claire Coutris, **Nhung H. A. Nguyen**, Alena Sevcu, Julian Alberto Gallego-Urrea, Anders Baun, and Erik J. Joner (2017). Ecotoxicity testing and environmental risk assessment of iron nanomaterials for sub-surface remediation – Recommendations from the FP7 project
NanoRem. *Chemosphere*, 182, 525-531. **IF 4.208**



Ecotoxicity testing and environmental risk assessment of iron nanomaterials for sub-surface remediation – Recommendations from the FP7 project NanoRem



Rune Hjorth^{a,*}, Claire Coutris^b, Nhung H.A. Nguyen^c, Alena Sevcu^c, Julián Alberto Gallego-Urrea^{d,1}, Anders Baun^a, Erik J. Joner^b

^a Department of Environmental Engineering, Building 115, Technical University of Denmark, Kgs. Lyngby, 2800, Denmark

^b Department for Environment and Natural Resources, Norwegian Institute of Bioeconomy Research, Høyskoleveien 7, 1431 Ås, Norway

^c Institute for Nanomaterials, Advanced Technologies and Innovations, Technical University of Liberec, Studentská 2, 461 17, Liberec, Czech Republic

^d Department of Environmental Sciences, Norwegian University of Life Sciences, Fougnerbakken 3, 1430 Ås, Norway

HIGHLIGHTS

- This study summarizes the outcome of nanoecotoxicity testing in NanoRem.
- We assessed four novel engineered nanomaterials in an ecotoxicological test battery.
- Only one of the tested materials gave rise to toxicity below 100 mg/L.
- Standardized testing is inadequate to inform site-specific risk assessment.

ARTICLE INFO

Article history:

Received 17 February 2017

Received in revised form

1 May 2017

Accepted 10 May 2017

Available online 13 May 2017

Handling Editor: Tamara S. Galloway

Keywords:

Nanoremediation

Iron nanomaterials

Ecotoxicology

nZVI

Environmental risk assessment

NanoRem

ABSTRACT

Nanoremediation with iron (Fe) nanomaterials opens new doors for treating contaminated soil and groundwater, but is also accompanied by new potential risks as large quantities of engineered nanomaterials are introduced into the environment. In this study, we have assessed the ecotoxicity of four engineered Fe nanomaterials, specifically, Nano-Goethite, Trap-Ox Fe-zeolites, Carbo-Iron[®] and Fer-MEG12, developed within the European FP7 project NanoRem for sub-surface remediation towards a test battery consisting of eight ecotoxicity tests on bacteria (*V. fischeri*, *E. coli*), algae (*P. subcapitata*, *Chlamydomonas* sp.), crustaceans (*D. magna*), worms (*E. fetida*, *L. variegatus*) and plants (*R. sativus*, *L. multiflorum*). The tested materials are commercially available and include Fe oxide and nanoscale zero valent iron (nZVI), but also hybrid products with Fe loaded into a matrix. All but one material, a ball milled nZVI (FerMEG12), showed no toxicity in the test battery when tested in concentrations up to 100 mg/L, which is the cutoff for hazard labeling in chemicals regulation in Europe. However it should be noted that Fe nanomaterials proved challenging to test adequately due to their turbidity, aggregation and sedimentation behavior in aqueous media. This paper provides a number of recommendations concerning future testing of Fe nanomaterials and discusses environmental risk assessment considerations related to these.

© 2017 Elsevier Ltd. All rights reserved.

1. Introduction

Innovation in nanotechnology introduces new treatment

options for environmental remediation of organic compounds (notably chlorinated solvents) and heavy metals in soil and groundwater (Karn et al., 2009; Mueller et al., 2012). Especially iron (Fe) based nanomaterials have shown a potential for remediation due to a larger specific surface area and corresponding increased reactivity compared to micro-scale and larger Fe materials traditionally used for remediation of contaminated sites (Wang and Zhang, 1997). Nanoscale zerovalent iron (nZVI) has received most

* Corresponding author.

E-mail address: ruhj@env.dtu.dk (R. Hjorth).

¹ Present address: Department of marine sciences, University of Gothenburg, Box 100, SE-405, 30 Gothenburg, Sweden.

of the attention as it is highly reactive compared to the bulk ZVI used in permeable reactive barriers (Henderson and Demond, 2007). Remediation with nZVI has been claimed to represent a faster, cheaper and a potentially more effective treatment option than current *ex situ* and *in situ* methods (Yan et al., 2013). However, nanomaterials engineered to remediate polluted soil and groundwater may constitute a risk to the environment as they are injected into the subsurface in large quantities (Grieger et al., 2010). As such this could represent a worst case scenario when considering possible negative environmental effects of manufactured nanomaterials. Nanoremediation in general seems associated with high uncertainty both in relation to its potential environmental risks, but also towards its field scale efficacy (Grieger et al., 2015). Uncertainty with regards to the potential environmental impacts of Fe nanomaterials hampers their use and has partly been the reason for the limited implementation of Fe nanomaterials in remediation (Bardos et al., 2014), although no major environmental impacts have been reported in the first decade of field deployments with Fe nanomaterials (Mueller et al., 2012).

Several publications in recent years have evaluated the ecotoxicity of Fe nanomaterials, particular nZVI materials, with NANOFE STAR, NANOFE 25 and 25s being the most common commercially available particles. In these publications the focus has been on aquatic and terrestrial ecotoxicity (Keller et al., 2012; Marsalek et al., 2012; Saccà et al., 2014; El-Temsah et al., 2016) and in general effect concentrations as low as 0.5 mg/L to above 2.5 g/L have been reported, demonstrating considerable variation in ecological response to Fe nanomaterials.

A range of Fe nanomaterials has been developed in the European FP7 project NanoRem (Taking Nanotechnological Remediation Processes from Lab Scale to End User Applications for the Restoration of a Clean Environment, for more information see nanorem.eu) in order to extend the spectrum of treatable soil and groundwater contaminants from halogenated organics to non-halogenated substances and non-reducible metals. Contrary to the three materials mentioned above, the potential ecotoxicity of the materials developed in NanoRem have not previously been tested. These materials are currently available on the international market (see Table 1). Common for all materials is that if they are to be used in field-scale remediation, their production volume will easily reach 1 metric ton per year (Mueller et al., 2012). In this case, they will have to be registered under the European chemical legislation REACH, which will be accompanied with data requirements on ecotoxicity. The data generated will feed into the general hazard identification of the nanomaterials and form the basis for a generic risk assessment (i.e. a hazard classification according to the classification, labeling and packaging (CLP

regulation). It is important to emphasize that this risk assessment does not directly relate to the safety of injecting said material into an aquifer or a contaminated soil. Such a task is done in a site-specific risk assessment, which is outside the scope of this study.

Test organisms and endpoints in the ecotoxicology test battery were chosen to include representatives for both terrestrial and aquatic environments as Fe nanomaterials may spread, in worst case scenarios, to both terrestrial and aquatic habitats (Grieger et al., 2010). The ecotoxicity tests were also selected to include standardized tests to ensure general regulatory acceptance of test results as well as non-standardized tests to broaden the test basis with respect to modes of exposure and modes of action, and to enhance the likelihood of seeing biological responses within the range of particles and concentrations tested. The aim of the paper is to provide ecotoxicity data for four newly developed Fe nanomaterials and the paper also highlights current challenges in doing adequate hazard identification and environmental risk assessment of Fe nanomaterials. Finally, recommendations for future ecotoxicity testing of Fe nanomaterials are provided.

2. Materials and methods

2.1. Nanomaterials

Samples of Fe nanomaterials for ecotoxicity testing were obtained directly from the manufacturers within the NanoRem project. A full list and characterization of the nanomaterials is seen in Table 1.

2.1.1. Dispersion of nanomaterials for toxicity testing

Dispersions of powder Fe nanomaterials were made according to the description provided by the manufactures. Due to testing constraints (e.g. infeasibility to degas exposure media) for the aquatic standard tests (on *V. fischeri*, *P. subcapitata* and *D. magna*), all nanomaterial powders were dispersed as described for magnetite.

2.1.1.1. Carbo-Iron®. For 100 mL of a stock suspension at 10 g/L, 20 mL of a 10 g/L carboxymethyl cellulose (CMC) solution was added to 80 mL of test medium and degassed with N₂ for an hour. Then, 1 g of test material was added to the solution under N₂ flow, and mixed for 10 min with a high-shear mixer. Dilution series were prepared under regular aerobic conditions and used right away.

2.1.1.2. Trap-Ox Fe-zeolites. A stock suspension with a zeolite concentration of 25 g/L was prepared by dissolving 2.5 g CMC in 50 mL deionized water by heating the mixture to 70 °C with stirring for an

Table 1

Characterization of the pristine Fe nanomaterials. Magnetite is not used for remediation in NanoRem but was chosen as a control in this study. The listed information is obtained from the manufacturer.

Name	Description	Development Status	Mode of remediation	Form	Chemical composition	Average primary particle size (nm)	Specific surface area (m ² /g)
FerMEG12	Zero-valent Fe mechanically ground through ball milling	Field tested and commercially available	Reduction	Suspension	15–30% Fe 70–85% monoethylene glycol	–	12–18
Carbo-Iron®	Composite of activated carbon and zero-valent Fe	Field tested and commercially available	Adsorption + Reduction	Powder	30.3% Fe _{tot} 20.5% Fe ⁰ 13.1% Fe ₂ O ₄ 55 ± 1% C _{tot}	13440 ± 20	594
Magnetite	Fe oxides (Fe ₂ O ₄)	Precursor for NANOFE STAR	–	Powder	Fe ₂ O ₄	–	–
Nano-Goethite	Fe oxides stabilized with humic acids	Field tested and commercially available	Adsorption + Oxidation	Suspension	'pure' FeOOH with organic coating	220 ± 20	140
Trap-Ox Fe-zeolites	Nanoporous aluminosilicate loaded with Fe(III)	Premarket	Adsorption + Oxidation	Powder	4% Al 92% Si 3% Fe	1000	600

hour. Then, 2.5 g Fe-zeolite in 50 mL deionized water was sonicated for 15 min and the CMC solution and zeolite suspension were mixed and sonicated for additional 15 min.

2.1.1.3. Magnetite. Magnetite, received as powder, was suspended in deionized water and mixed for 10 min with a high-shear mixer. Subsequent dilutions series in exposure media were prepared and used right away.

2.1.1.4. Suspensions. Nano-Goethite was provided as a stable suspension and was diluted directly from the sample into the exposure media. However, the FerMEG12 were additionally sonicated for 15 min due to sedimentation.

2.2. Characterization of stock suspensions

Dynamic Light Scattering (DLS) measurements of aqueous suspensions (deionized water) from 10 mg/L to 10 g/L test material were performed on a Malvern Zetasizer ZS (Malvern instruments Ltd, Worcestershire, UK) equipped with a laser source at a wavelength of 633 nm. Zeta-averaged hydrodynamic diameters and size distributions were determined using the “multiple narrow modes (high resolution)” algorithm supplied by Malvern. Measurements were done in triplicates of 5 runs with autocorrelation functions of 10 s. The same instrument was used for the measurements of electrophoretic mobility and the Smoluchowski approximation was used for determining zeta-potentials. Three measurements with 5 runs per measurement were obtained.

Nanoparticle Tracking Analysis (NTA) measurements of the hydrodynamic diameter of individual particles suspended in deionized water at a concentration of 10 mg/L to 10 g/L were done on a Nanosight LM10 (NanoSight Ltd, Amesbury, UK).

The light source was a solid-state, single-mode laser diode (radiation output max power <50 μ W, 635 nm continuous wave, max power < 35 mW). The standard camera Marlin F-033B (Allied Vision Technologies GmbH, Stadtroda, Germany) was used. All data were analyzed using the instrument software (NanoSight™ version 2.2). The analysis with NTA was done on 7 videos with 1 min length each. The solution oxidation-reduction potential and pH were measured in all exposure suspensions at the beginning and the end of the tests. Total Fe concentration in stock suspensions was measured by ICP-OES (Perkin Elmer, Optima 5300 DV) following microwave assisted digestion under acidic conditions (3.7% HCl).

2.3. Ecotoxicological test battery

A test battery of eight tests (see Table 2) was used to assess and rank the nanomaterials listed in Table 1. Dilutions series were made from stock suspensions and tested in concentrations up to 1 g/L. For some tests, higher concentrations were assessed, including the root elongation test with radish *Raphanus sativus*, ryegrass *Lolium*

multiflorum (up to 10 g/L) and the earthworm mortality test with *Eisenia fetida* (up to 25 g/L). Full tests protocols are enclosed in the Supplementary Information.

3. Results

3.1. Characterization

Table 3 provides an overview of the characterization of the Fe nanomaterials in deionized water. Differences in size distribution were observed, with NTA generally finding a lower average size than DLS. Based on zeta potential measurements, Nano-Goethite and Trap-Ox Fe-zeolites showed higher aqueous stability than FerMEG12 and Carbo-Iron®, however sedimentation of the Trap-Ox Fe-zeolites was also observed. In the more complex aquatic test media, DLS measurements proved difficult due to particle sedimentation of all tested materials. This violates the principle behind DLS for size distribution measurements as the particles are affected by gravitational movement and not just Brownian movement and no reliable estimation of size distribution could be made. Characterization with DLS also revealed that all particle suspensions had a very broad size distribution with polydispersity indexes around 1, which also undermines the use of DLS measurements to characterize the suspensions.

3.2. Ecotoxicity

Almost all of the tests conducted showed no toxicity of the tested Fe nanomaterials at concentrations up to 100 mg/L, which is the cutoff value for hazard labeling in the EU. Only FerMEG12 gave rise to toxicity at concentrations below 100 mg/L. Effects were seen in the 6 h growth inhibition test with *E. coli* (Fig. 1), the 6 d root elongation test with *R. sativus* (Fig. 2) and 96 h mortality test with *L. variegatus* (Fig. 3).

The growth rate (h^{-1}) of Gram-negative *E. coli* was not significantly affected in the presence of Carbo-Iron®, Nano-Goethite and Trap-Ox Fe-zeolites at any of the tested concentrations (Fig. 1). A significant effect on *E. coli* growth rate was observed for FerMEG12, from concentrations as low as 50 mg/L ($P < 0.001$), and for magnetite at the highest concentration tested (1000 mg/L, $P < 0.05$).

The root elongation of *R. sativus* was reduced by 33% by FerMEG12 particles at a nominal Fe concentration as low as 10 mg/L. Root elongation was increasingly reduced in a concentration-dependent manner and completely inhibited at 10 g/L (Fig. 2, left). The root elongation of *L. multiflorum* was significantly reduced at nominal Fe concentrations >1 g/L, and completely inhibited at 10 g/L (Fig. 2, right). The pH of the exposure suspensions at the beginning of the experiment was 6.0 ± 0.5 over the whole concentration range. In contrast, the oxidation reduction potential, measured in exposure suspensions at the beginning of the

Table 2
Organisms and testing endpoints of the eight ecotoxicity tests in the test battery.

Organism	Species	Duration	Endpoint	Reference
Bacteria	<i>Vibrio fischeri</i>	15 min	Decrease in bioluminescence	ISO11348-3
Bacteria	<i>Escherichia coli</i>	6 h/24 h	Growth/Cell viability	–
Algae	<i>Pseudokirchneriella subcapitata</i>	48 h	Growth rate inhibition	OECD 201
Algae	<i>Chlamydomonas</i> sp.	48 h	Photosynthesis efficiency	–
Crustacean	<i>Daphnia magna</i>	48 h	Immobilization	OECD 202
Earthworm	<i>Eisenia fetida</i>	48 h	Mortality	OECD 207
Oligochaete	<i>Lumbriculus variegatus</i>	96 h	Mortality	OECD 225 ^a
Plant	<i>Raphanus sativus</i> , <i>Lolium multiflorum</i>	6 d	Root elongation	OECD 208

^a Modified to short term water-phase exposure.

Table 3

Characterization of the four tested nanomaterials dispersed in deionized water at 100 mg/L. Samples were characterized 2 and 144 h after dispersion and analyzed by DLS for hydrodynamic diameter and zeta-potential. NTA analysis was performed in samples 2 h after dispersion.

Nanomaterial	DLS Hydrodynamic diameter (z-average; nm)		Zeta-potential (mV)		NTA Average size (mode average; nm)
	2 h	144 h	2 h	144 h	
FerMEG12	480	720	12	1.5	210
Carbo-Iron®	1300	500	-15	-17	120
Nano-Goethite	230	270	-41	-44	–
Trap-Ox	780*	780*	-65	-60	250
Fe-zeolites					

–: No data.

*: sedimentation after suspension in deionized water occurred.

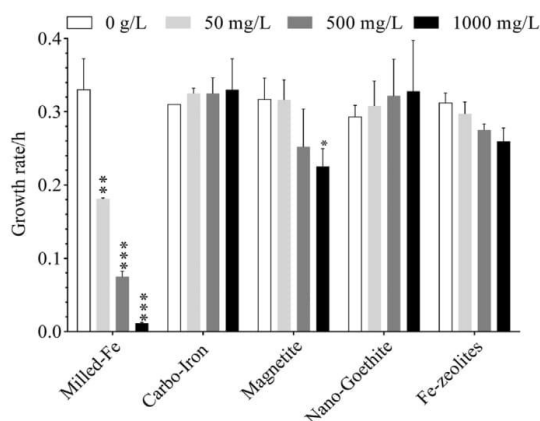


Fig. 1. Growth rate of *E. coli* after 6 h exposure to FerMEG12, Carbo-Iron®, magnetite, Nano-Goethite and Trap-Ox Fe-zeolites at 0, 50, 500 and 1000 mg/L. Asterisks indicate treatments that differ significantly from controls (ANOVA and Dunnett's test, $n = 3$). Significance levels were set at $P < 0.05$ (*), $P < 0.001$ (**) and $P < 0.0001$ (***).

experiment, was dramatically different among concentrations and ranged from +250 mV (control), +50 mV (0.01–0.1 g/L), to -590 mV (5 and 10 g/L).

For the *L. variegatus* test, no toxicity was observed at 1 mg/L, however more than 50% mortality was observed at 5 mg/L and 100% at 10 mg/L. Mortality was observed already after 24 h, together with a rapid decrease in the dissolved oxygen concentration in test beakers containing FerMEG12 (see Fig. 3).

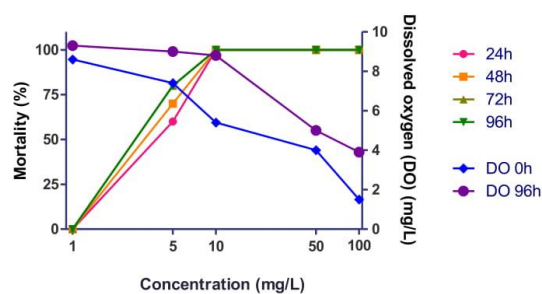


Fig. 3. Mortality of *L. variegatus* after 24–96 h exposure to FerMEG12 (left axis) and dissolved oxygen (DO) concentration in test beakers after 0–96 h (right axis).

3.3. Technical challenges of ecotoxicity testing of Fe nanomaterials

The higher concentrations of Fe nanomaterials did in several cases influence the measurement principles or assumptions behind the tests. Especially the turbidity of the suspensions caused issues with limited light transmission through the suspensions. In the *V. fischeri* test, the quantification of the bioluminescence could be influenced by quenching of the emitted light before it reaches the detector. This can easily be measured in a double vial setup that ensures no actual bacterial exposure to the suspension, with the inner vial containing the bacteria. A way to account for this is by spiking the suspension with *V. fischeri* emitting a known amount of bioluminescence. In this way, the added bacteria can act as an internal standard and the effect of quenching can be estimated and corrected for. Using this method, it was clear that the tested materials did quench light emission, giving rise to potential erroneous

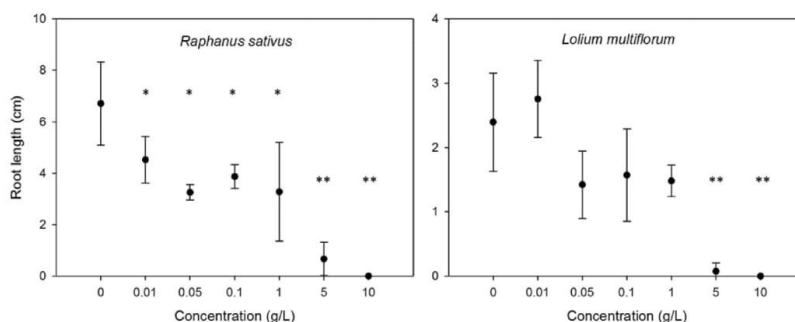


Fig. 2. Root length of radish (*Raphanus sativus*) and ryegrass (*Lolium multiflorum*) exposed to various nominal Fe concentrations from FerMEG12 particles for 6 d. Asterisks indicate treatments that differ significantly from controls (Holm-Sidak, $n = 3$, $P < 0.05$ (*), $P < 0.0001$ (**)).

conclusions if unaccounted for.

For the algal growth inhibition, issues with the quantification of algal biomass also started to appear at higher concentrations (>100 mg/L). At high Fe concentrations the fluorescence spectrum was altered significantly and obfuscated the presence and the size of the chlorophyll peak. During the testing, the turbidity can also prevent the algae to obtain sufficient light for exponential growth, a shading effect that can be difficult to account for (Hjorth et al., 2015).

In the tests with *D. magna* and *L. variegatus*, oxidation, aggregation, precipitation and ultimately sedimentation of Fe resulted in a change of exposure route (which was intended to be through the water phase alone) directly affecting the mobility of *D. magna*. Due to the described stratification of Fe particles, *L. variegatus* was exposed to an increased concentration, as both the particles and the oligochaeta stay at the bottom of the beaker.

4. Discussion

4.1. Ecotoxicity of Fe nanomaterials

Based on the performed ecotoxicity tests in the present study, only the FerMEG12 particles would be classified as toxic to aquatic organisms in accordance to the CLP regulation. As none of the other tested materials showed toxicity below 100 mg/L, none of them would receive any environmental hazard classification. The highest toxicity of the FerMEG12 particles was observed towards the oligochaeta *L. variegatus*. However particle sedimentation during the test consequently exposed *L. variegatus* to higher Fe concentrations than what was initially dispersed, which could explain why toxicity was observed for *L. variegatus* and not e.g. for *D. magna* which spends more time in the water column. Ageing the particles for 1 h in media alleviated the toxicity, which is in agreement with an earlier study on milled particles reporting low toxicity after oxidation (Köber et al., 2014). Similarly, a recent study on zebrafish found no adverse effects of aged Carbo-Iron® (Weil et al., 2015).

The FerMEG12 particles were also tested in the standard algal test with *P. subcapitata* with acute effects evidenced by a decrease in fluorescence right after the onset of the test (data not shown). However, during the incubation period the algal population recovered and exhibited growth rates similar (or higher) than the non-exposed controls. As the only material out of the four tested, FerMEG12 was dispersed in a solvent (ethylene glycol) and although ethylene glycol in itself showed no toxicity when tested, it seems to have preserved the reactivity of FerMEG12's elemental iron. Other studies confirm the toxicity of freshly prepared, non-oxidized nZVI. For instance, Keller et al. (2012) studied the response of microalgae and *D. magna* exposed to NANOFE STAR and 25S. *D. magna* proved the most sensitive with LOEC values of 0.5 mg/L for the NANOFE STAR and NANOFE 25s, compared to a LOEC of 1 mg/L for Fe²⁺. Whereas the growth of the marine microalga *I. galbana* was inhibited after exposure to NANOFE 25s starting at 3 mg/L (Keller et al., 2012), no effect was observed for NANOFE STAR at concentrations up to 100 mg/L and effects from dissolved Fe did not occur at concentrations lower than 50 mg/L. For the freshwater microalgae, *P. subcapitata*, Fe²⁺ exposure proved the most toxic with a LOEC value of 5 mg/L, which was lower than for any of the particles or Fe³⁺ (Keller et al., 2012).

NANOFE 25s has also been found to affect the growth of the nematode *C. elegans* at 0.5 mg/L, whereas at 5 mg/L a decrease in survival and reproduction occurred. However, when tested in soil, no toxicity to *C. elegans* was observed for NANOFE 25s at concentrations up to 17 mg/g. On the contrary, their growth and reproduction increased (Saccà et al., 2014). Similarly, the survival of the earthworm, *E. fetida*, was not affected by nZVI even at 3 g/kg,

although DNA damage and lipid oxidation was observed (Yirsaw et al., 2016).

Chen et al. (2011) investigated continuous exposure of carboxymethyl cellulose stabilized nZVI (CMC-nZVI) towards medaka fish larvae and concluded that the toxicity was caused by hypoxia, Fe²⁺ toxicity, and ROS-mediated oxidative damage. In their experiment Fe²⁺ proved the most acutely toxic with 100% mortality at 75 mg/L. In a similar study, Chen et al. (2012) reported Fe²⁺ being the most toxic form of Fe tested, followed by CMC-nZVI, nZVI and lastly the aged nZVI. Yet in Chen et al. (2013) CMC-nZVI had a higher acute toxicity than both Fe²⁺ and aged nZVI.

Marsalek et al. (2012) have reported low aquatic toxicity for NANOFE 25 with EC₅₀ > 1 g/L for *D. magna* and >2.5 g/L for fish (*P. reticulata*) and similar values for willows (*S. alba*), duckweed (*L. minor*), and microalgae (*D. subspicatus*). Effects on the cyanobacteria *M. aeruginosa* were observed at the lowest concentrations in the test battery and with an EC₅₀-value of 50 mg/L.

Although there are signs of increased ecotoxicity of nZVI compared to Fe²⁺, which seems rational due to the additional oxidative capacity of Fe⁰, the opposite is also sometimes the case. However none of the studies in the scientific literature on Fe nanomaterials have reported a higher toxicity than what has been shown for dissolved Fe (Johnson et al., 2007). It seems likely that varying, and generally lower, bioavailability of nZVI in media has the potential to offset any increase in toxicity compared to dissolved Fe.

4.2. Environmental risk assessment of Fe in surface water

Whereas hazard and risk assessment of Fe nanomaterials is a novel task, the toxic effects of Fe and Fe salts on aquatic life is well described. Fe²⁺ is generally considered bioavailable and can induce toxicity in aquatic organisms, whereas when oxidized to Fe³⁺ it hydrolyses and precipitates out of solution as hydroxides at normal pH, which then can give rise to indirect, physical effects (Vuori, 1995). Ecotoxicity testing of Fe has traditionally made a distinction between total Fe and dissolved Fe, ideally signifying Fe²⁺, however in practice meaning anything that passes through a 0.45 µm filter, which includes colloidal Fe(II) stabilized mostly by organic material (Vuori, 1995) and Fe(III) complexed by organic ligands. In this way, many tests have already, indirectly, assessed the toxicity of suspended Fe in the nano range. Even for Fe, hazard and risk assessment as well as setting appropriate environmental quality standards (EQS) has been difficult for decades due to this redox cycling, inorganic speciation, complexation and precipitation.

As an example, the company American Electric Power (AEP) argued in 1983 that the USEPA water quality standard of 1 mg/L for Fe was too low, stating that field data showed that Fe concentrations "need to be far over 1 mg/L to adversely affect" aquatic life, and that toxicity testing is not fit to assess Fe toxicity (Loeffelman et al., 1985). AEP also called for a use of Fe²⁺, and not total Fe, as the foundation for setting the water quality standard, based on the fact that Fe²⁺ is the bioavailable fraction of Fe.

More recently, Linton et al. (2007) acknowledged that the USEPA "metal policy" generally is to derive "aquatic life criteria" based on the dissolved metal and therefore Fe should be regulated based on Fe²⁺ toxicity. Yet, it makes sense to use field data on total Fe, as lab-based toxicity testing of Fe is poor at assessing colloidal and indirect effects such as the impact on respiration and food consumption. With reference to a review by Vuori (1995) who states "the effect of Fe on aquatic animals and their habitats are mainly indirect", Linton et al. (2007) argue that field studies therefore would do a better job of assessing the overall environmental impact of Fe. Accordingly, the assessment still has a foundation in field observations partly

due to this issue of indirect effects (Linton et al., 2007). Based on additional field data, Linton et al. (2007) however proposed a new and differentiated EQS of 0.21 mg/L for sensitive groups and 1.74 mg/L for “slight to moderate changes” in the aquatic community.

In Europe, the Environment Agency in England proposed a new EQS for Fe in 2007 under the Water Framework Directive (Johnson et al., 2007). A long term PNEC of 16 µg/L was derived, based on a NOEC value of 0.16 mg/L obtained in a 21-d study on *D. magna*. Similarly, a 96 h study on brook trout (*S. fontinalis*) with a LC₅₀ value of 0.41 mg/L gave rise to a short term PNEC of 41 µg/L. They rationalized the use of the considerably lower PNEC values with the emergence of new data as well as the fact that the old EQS was based on field data and not on standardized toxicity tests.

In response to this, Crane et al. (2007) stated that 16 µg/L was “substantially below concentrations associated with impaired invertebrate assemblages in the field”. Based on their analysis of data from 253 sites in England and Wales, Crane et al. (2007) proposed an EQS between 43 and 250 µg/L based on dissolved Fe. In 2012, the UK Technical Advisory Group proposed an EQS of 0.73 mg/L total Fe, based on field data, in a very thorough review (Peters et al., 2012). The suggested EQS from the Environment Agency of 16 µg/L was described as well below background levels and therefore “not adopted for regulatory use”.

In accordance with Linton et al. (2007), Peters et al. (2012) state that the effects of Fe are difficult to isolate and, in contrast to most metals, we cannot just focus on the dissolved fraction as there is also a physical effect from the total Fe, which perhaps could even be dominating. This line of reasoning also advocates for the use of total Fe as the dose metric for ecotoxicity studies on Fe nanomaterials.

4.3. Applicability of standardized ecotoxicity tests for hazard identification of Fe nanomaterials

As shown above, the current consensus seems to move away from using standardized ecotoxicity tests on Fe for risk assessment purposes; rather the use of field data and mesocosm studies are encouraged. Peters et al. (2012) point towards the issue of Fe solubility as well as the issue with assessing physical effects as the key points against using standardized ecotoxicity testing of Fe. West (2015) also questions the adequacy of ecotoxicity tests on Fe to inform risk assessment as they fail to uphold various criteria for assessing causation, e.g. issues with establishing dose response relationships and incoherence with field data. If these ecotoxicity tests are not suitable for Fe salts due to precipitation and exposure control issues, then clearly they are not suitable to assess Fe nanomaterials, which by definition are not dissolved entities.

However, having the test limitations and challenges in mind, such as the ones mentioned in section 3.3, as well as the general testing considerations in nanoeotoxicology (Petersen et al., 2014; Skjolding et al., 2016) and indirect physical effects (Sørensen et al., 2015), standardized ecotoxicity tests can still provide valuable information, as a screening and ranking tool for hazard identification. Trying to overcome these limitations will sometimes result in deviations from the standard tests, which at times are necessary to obtain meaningful data. Additionally, the information generated from standardized ecotoxicity tests is still required by regulatory agencies to achieve market access.

On the other hand, as shown for Fe salts, standardized ecotoxicity tests are challenged in terms of their usefulness and accuracy for site-specific and case oriented risk assessments, and it is recommended to rely more on field data when assessing the environmental impact of Fe (EC, 2011). The relevance of standard organisms for site-specific risk assessment is questionable for remediation cases, as the extrapolation value from these organisms

to ecosystems may be low. In addition, the transformation of the pristine material to the oxidized form expected in the environment and the corresponding change in toxicity is also better assessed in the field. As such, it makes sense to rely less on laboratory ecotoxicity testing and instead incorporate mesocosm and field data into site-specific risk assessment of Fe nanomaterials.

5. Conclusion and recommendations

Ecotoxicity testing of four nanomaterials engineered for subsurface remediation revealed low toxicity for all Fe oxides materials as well as Carbo-Iron®, and the results do not lead to any hazard classification according to current EU regulation. FerMEG12 was the only material exhibiting toxicity towards bacteria and plants at 50 mg/L and oligochaetes at 5 mg/L. Standard ecotoxicity testing of nanoparticles has in general proven technically difficult and it may be questioned whether proper hazard identification of engineered nanoparticles needed for environmental risk assessment is currently feasible. Aggregation, agglomeration, sedimentation, shading, and other physical effects are known to confound the measuring principles behind the tests and these interferences were also observed for the tested particles. This was pronounced for tests on algae, bacteria, and crustaceans and requires inclusion of additional controls to ensure a correct data interpretation. While Fe⁰ nanomaterials have the potential to be toxic at low concentrations, a potential environmental impact downstream of the injection of Fe nanomaterials seems more likely to originate from the large amount of Fe injected in *in-situ* remediation, than from novel particle related effects, especially since Fe is abundant in nature as particulate matter. In conclusion we recommend:

- Testing concentrations up to 100 mg/L is relevant for hazard identification and classification purposes. Testing Fe nanoparticles at higher concentrations not only decreases the environmental relevance, but also increases the influence of physical effects such as turbidity and concentration-dependent agglomeration. Therefore, the main focus in testing should be on concentrations <100 mg/L, and care should be taken when conducting ecotoxicological testing of Fe nanomaterials at higher concentrations.
- For Fe nanomaterials, agglomeration and sedimentation challenge the validity of the standard test setups for which a constant exposure during incubation is required. These issues are currently under scrutiny in the OECD WPMN and in several EU projects (Lynch, 2016). We recommend the use of these tests for hazard identification and ranking, where these tests still provide valuable information.
- We recommend studying the effects of Fe nanomaterials in more environmentally realistic conditions to support site-specific hazard assessment. E.g. through testing of relevant organisms, media and more complex testing systems closer related to the field, as the scope of standardized ecotoxicity testing is limited and not designed to assess the indirect effects of Fe exposure.

Acknowledgements

This project has received funding from the European Union's Seventh Framework Programme for research, technological development and demonstration under grant agreement no 309517 (NanoRem). RH is also funded by the project ‘Integrated water technology’ - an initiative between the Korea Advanced Institute of Science and the Technical University of Denmark. NN and AÅ acknowledge the assistance provided by the Research Infrastructure NanoEnvicZ, supported by the Ministry of Education, Youth

and Sports (CZ) under project No. LM2015073. The authors are also grateful to E. Maremonti for her help during plant growth testing.

Appendix A. Supplementary data

Supplementary data related to this article can be found at <http://dx.doi.org/10.1016/j.chemosphere.2017.05.060>.

References

- Bardos, P., Bone, B., Daly, P., Elliott, D., Jones, S., Lowry, G., Merly, C., 2014. A Risk/Benefit Appraisal for the Application of Nano-scale Zero Valent Iron (nZVI) for the Remediation of Contaminated Sites. WP9 NanoRem. Available at: http://www.nanorem.eu/Stream.aspx?p=/App_Data/docs/user7Gallery/NANOREM%20NZVI%20risk%20benefit%20issues%20paper%20FINAL_2.0.pdf.
- Chen, P.-J., Su, C.-H., Tseng, C.-Y., Tan, S.-W., Cheng, C.-H., 2011. Toxicity assessments of nanoscale zerovalent iron and its oxidation products in medaka (*Oryzias latipes*) fish. *Mar. Pollut. Bull.* 63 (5–12), 339–346.
- Chen, P.-J., Tan, S.-W., Wu, W.-L., 2012. Stabilization or oxidation of nanoscale zerovalent iron at environmentally relevant exposure changes bioavailability and toxicity in medaka fish. *Environ. Sci. Technol.* 46 (15), 8431–8439.
- Chen, P.-J., Wu, W.-L., Wu, K.C.-W., 2013. The zerovalent iron nanoparticle causes higher developmental toxicity than its oxidation products in early life stages of medaka fish. *Water Res.* 47 (12), 3899–3909.
- Crane, M., Kwok, K.W.H., Wells, C., Whitehouse, P., Lui, G.C.S., 2007. Use of field data to support European Water Framework Directive quality standards for dissolved metals. *Environ. Sci. Technol.* 41 (14), 5014–5021.
- EC, 2011. Common Implementation Strategy for the Water Framework Directive (2000/60/EC). Guidance Document No. 27. Technical Guidance for Deriving Environmental Quality Standards. European Commission, Brussels, Belgium.
- El-Temsah, Y.S., Sevcu, A., Bobcikova, K., Cernik, M., Joner, E.J., 2016. DDT degradation efficiency and ecotoxicological effects of two types of nano-sized zerovalent iron (nZVI) in water and soil. *Chemosphere* 144, 2221–2228.
- Grieger, K.D., Fjordbøge, A., Hartmann, N.B., Eriksson, E., Bjerg, P.L., Baun, A., 2010. Environmental benefits and risks of zero-valent iron nanoparticles (nZVI) for in situ remediation: risk mitigation or trade-off? *Journal of contaminant hydrology*, 118 (3–4), 165–183.
- Grieger, K.D., Hjorth, R., Rice, J., Kumar, N., Bang, J., 2015. Nano-remediation: Tiny Particles Cleaning up Big Environmental Problems. Blog entry for the International Union for Conservation of Nature (IUCN). Available at: <http://cmsdata.iucn.org/downloads/nanoremediation.pdf>.
- Henderson, A.D., Demond, A.H., 2007. Long-term performance of zero-valent iron permeable reactive barriers: a critical review. *Environ. Eng. Sci.* 24 (4), 401–423.
- Hjorth, R., Sørensen, S.N., Olsson, M.E., Baun, A., Hartmann, N.B., 2015. A certain shade of green: can algal pigments reveal shading effects of nanoparticles? *Integr. Environ. Assess. Manag.* 15 (1), 200–202.
- Johnson, I., Sorokin, N., Atkinson, C., Rule, K., Hope, S.-J., Agency, E., 2007. Pre-consultation Report: Proposed EQS for Water Framework Directive Annex VIII Substances: Iron (Total Dissolved). Environment Agency, Bristol, UK.
- Karn, B., Kuiken, T., Otto, M., 2009. Nanotechnology and in situ remediation: a review of the benefits and potential risks. *Environ. Health Perspect.* 117 (12), 1813–1831.
- Keller, A.A., Garner, K., Miller, R.J., Lenihan, H.S., 2012. Toxicity of nano-zero valent iron to freshwater and marine organisms. *PLoS one* 7 (8), 1–10.
- Köber, R., Hollert, H., Hornbruch, G., Jekel, M., Kamptner, A., Klaas, N., Maes, H., Mangold, K.M., Martac, E., Matheis, A., Paar, H., Schäffer, A., Schell, H., Schiwy, A., Schmidt, K.R., Strutz, T.J., Thümmel, S., Tiehm, A., Braun, J., 2014. Nanoscale zero-valent iron flakes for groundwater treatment. *Environ. Earth Sci.* 72 (9), 3339–3352.
- Linton, T., Pacheco, M., McIntyre, D., Clement, W., Goorich-Mahoney, J., 2007. Development of bioassessment-based benchmarks for iron. *Environ. Toxicol.* 26 (6), 1291–1298.
- Loeffelman, P.H., Van Hassel, J.H., Arnold, T.E., Hendricks, J.C., 1985. A new approach for regulating iron in water quality standards. In: *Aquatic Toxicology and Hazard Assessment: Eight Symposium*. ASTM STP 891, pp. 137–152.
- Lynch, I., 2016. *Compendium of Projects in the European NanoSafety Cluster. 2016 Edition*. Available at: <http://www.nanosafetycluster.eu/www.nanosafetycluster.eu/home/european-nanosafety-cluster-compendium.html>.
- Marsalek, B., Jancula, D., Marsalkova, E., Mashlan, M., Safarova, K., Tucek, J., Zboril, R., 2012. Multimodal action and selective toxicity of zerovalent iron nanoparticles against cyanobacteria. *Environ. Sci. Technol.* 46 (4), 2316–2323.
- Mueller, N.C., Braun, J., Bruns, J., Cernik, M., Rissing, P., Rickerby, D., Nowack, B., 2012. Application of nanoscale zero valent iron (NZVI) for groundwater remediation in Europe. *Environ. Sci. Pollut. Res. Int.* 19 (2), 550–558.
- Peters, A., Merrington, G., Simpson, P., Crane, M., 2012. Proposed Quality Standards for Iron in Freshwaters Based on Field Evidence. Water Framework Directive – United Kingdom Technical Advisory Group (WFD-UKTAG), Edinburgh, Scotland.
- Petersen, E.J., Henry, T.B., Zhao, J., Maccuspie, R.L., Kirschling, T.L., Dobrovolskaia, M.A., Hackley, V., Xing, B., White, J.C., 2014. Identification and avoidance of potential artifacts and misinterpretations in nanomaterial ecotoxicity measurements. *Environ. Sci. Technol.* 48, 4226–4246.
- Saccà, M.L., Fajardo, C., Costa, G., Lobo, C., Nande, M., Martin, M., 2014. Integrating classical and molecular approaches to evaluate the impact of nanosized zerovalent iron (nZVI) on soil organisms. *Chemosphere* 104, 184–189.
- Skjoldung, L.M., Sørensen, S.N., Hartmann, N.B., Hjorth, R., Hansen, S.F., Baun, A., 2016. A critical review of aquatic ecotoxicity testing of nanoparticles – the quest for disclosing nanoparticle effects. *Angew. Chem. Int. Ed.* 55 (49), 15224–15239.
- Sørensen, S.N., Hjorth, R., Delgado, C.G., Hartmann, N.B., Baun, A., 2015. Nanoparticle toxicity – physical and/or chemical effects? *Integr. Environ. Assess. Manag.* 11 (4), 722–724.
- Vuori, K.-M., 1995. Direct and indirect effects on iron on river ecosystems. *Ann. Zool. Fenn.* 32, 317–329.
- Wang, C.-B., Zhang, W., 1997. Synthesizing nanoscale iron particles for rapid and complete dechlorination of TCE and PCBs. *Environ. Sci. Technol.* 31 (7), 2154–2156.
- Weil, M., Meißner, T., Busch, W., Springer, A., Kühnel, D., Schulz, R., Duis, K., 2015. The oxidized state of the nanocomposite Carbo-Iron® causes no adverse effects on growth, survival and differential gene expression in zebrafish. *Sci. Total Environ.* 530–531, 198–208.
- Wess, R.A., 2015. The question of causation and adequacy – iron as an example of intrinsic toxicity and other effects. *Integr. Environ. Assess. Manag.* 12 (1), 202–204.
- Yan, Weile, Lien, Hsing-Lung, Koel, Bruce E., Zhang, Wei-xian, 2013. Iron nanoparticles for environmental clean-up: recent developments and future outlook. *Environ. Sci. Process. Impacts* 15 (1), 63–77.
- Yirsaw, B.D., Mayilswami, S., Megharaj, M., Chen, Z., Naidu, R., 2016. Effect of zero valent iron nanoparticles to *Eisenia fetida* in three soil types. *Environ. Sci. Pollut. Res.* 23 (10), 9822–9831.

Paper 5

Mohamed S. A. Darwish, **Nhung H. A. Nguyen**, Alena Sevcu, Ivan Stibor, and Stoyan K Smoukov (2016). Dual-modality self-heating and antibacterial polymer-coated nanoparticles for magnetic hyperthermia. *Materials Science and Engineering: C*, 63, 88-95. **IF 4.164**



Dual-modality self-heating and antibacterial polymer-coated nanoparticles for magnetic hyperthermia



Mohamed S.A. Darwish^{a,b,c}, Nhung H.A. Nguyen^a, Alena Ševců^a, Ivan Stibor^a, Stoyan K. Smoukov^c

^a Institute for Nanomaterials, Advanced Technologies and Innovation, Technical University of Liberec, Studentská 2, 461 17 Liberec, Czech Republic

^b Egyptian Petroleum Research Institute, 1 Ahmed El-Zomor Street, El Zohour Region, Nasr City, 11727 Cairo, Egypt

^c Department of Materials Science and Metallurgy, 27 Charles Babbage Road, University of Cambridge, CB3 0FS, United Kingdom

ARTICLE INFO

Article history:

Received 23 November 2015

Received in revised form 28 January 2016

Accepted 17 February 2016

Available online 18 February 2016

Keywords:

Magnetic

Hyperthermia

Self-heating

Antibacterial properties

ABSTRACT

Multifunctional nanoparticles for magnetic hyperthermia which simultaneously display antibacterial properties promise to decrease bacterial infections co-localized with cancers. Current methods synthesize such particles by multi-step procedures, and systematic comparisons of antibacterial properties between coatings, as well as measurements of specific absorption rate (SAR) during magnetic hyperthermia are lacking. Here we report the novel simple method for synthesis of magnetic nanoparticles with shells of oleic acid (OA), polyethyleneimine (PEI) and polyethyleneimine-methyl cellulose (PEI-mC). We compare their antibacterial properties against single gram-positive (*Staphylococcus aureus*) and gram-negative (*Escherichia coli*) bacteria as well as biofilms. Magnetite nanoparticles (MNPs) with PEI-methyl cellulose were found to be most effective against both *S. aureus* and *E. coli* with concentration for 10% growth inhibition (EC10) of <150 mg/l. All the particles have high SAR and are effective for heat-generation in alternating magnetic fields.

© 2016 Published by Elsevier B.V.

1. Introduction

Magnetite nanoparticles (MNPs) have attracted broad interest for hyperthermic cancer treatment because they are non-toxic, biocompatible, and can be remotely heated by alternating magnetic fields [1–2]. The magnetic induction heating behavior also provides a benefit for biomedical applications, such as targeted drug delivery, and magnetic separation [3–6]. MNP can transform the energy of an alternating magnetic field into heat through two kinds of relaxation: Neel relaxation and the Brownian relaxation. Neel relaxation is caused by the reorientation of the magnetization, which is caused by the reorientation of the magnetization vector inside the magnetic core against an energy barrier [7]. Brownian relaxation is due to the rotational diffusion of the whole particle in the carrier liquid [8–11].

The size of nanoparticles influences the number of their magnetic domains, where small nanoparticles are composed of a single domain and the larger ones are composed of multiple domains minimizing the magnetostatic energy. Conversion of dissipated magnetic energy into thermal energy in magnetic nanoparticles shows promising applications in hyperthermic cancer treatment. Artificially induced hyperthermia, by locally raising the temperature of an affected region of the body to 42–46 °C, has the power to kill cancer cells without affecting the nearby healthy tissue [12–13].

The most common methods used for the synthesis of magnetite nanoparticles are co-precipitation process, thermal decomposition, and hydrothermal synthesis [14–18]. Co-precipitation process is considered one of the easier procedures for preparation of magnetic nanoparticles by precipitation of magnetic nanoparticles in solution media. The size and the morphology of the prepared magnetic nanoparticles strongly depend on the type of iron salts used, the reaction temperature, pH and speed of stirring [14]. Heat dissipation, morphological and magnetic properties are important for hyperthermia response.

Magnetic nanoparticles tend to aggregate due to the presence of high surface energy of nanoparticles and their strong van der Waals interactions. In situ formation of an organic or polymer layer on their surface is one of the efficient methods for decreasing nanoparticle aggregation, as well as providing functional groups on the surface and allowing further functionalization with drugs and therapeutic agents. The co-precipitation method used here is an easy method to produce such coatings [15–16]. Several types of organic layer capped superparamagnetic iron oxide nanoparticles have been prepared with cinnamaldehyde, citric acid, starch and oleic acid [17–21]. It was reported that poly(N-isopropylacrylamide) (PNIPAm), polyvinylpyrrolidone (PVP), polyvinyl alcohol (PVA), polyethylene glycol (PEG), polyethyleneimine (PEI) and chitosan have also been used to stabilize magnetic nanoparticles [22–25].

It is highly desired to have new hyperthermic agents that are also antibacterial, which would decrease bacterial infections co-localized with cancers [26–28]. Gold nanorods capped with toluidine blue O (TBO) have been used as dual-function agents for photodynamic

E-mail address: sks46@cam.ac.uk (S.K. Smoukov).

inactivation and hyperthermia against methicillin resistant *Staphylococcus aureus* [26]. Recent studies have focused on dual-action nanoparticles, Fe₃O₄-ZnO nanocomposite were prepared for inactivation of bacterial pathogens under magnetic hyperthermia [27]. In another report a rapid drug release system was designed with a near-infrared (NIR) light-activated molecular switch for dual-mode photothermal/antibiotic treatments of subcutaneous abscesses [28]. A graphene-based photothermal agent was used for rapid and effective killing of bacteria [29].

The aim of the present work, is the fabrication of magnetic nanoparticles coated with a functional layer having dual-action self-heating and antibacterial effects. Magnetic fields have full penetration in the human body, and by directly heating the particles themselves, no damage is incurred on the surrounding tissues. The multi-functional particles could also be conveniently guided from a convenient injection site to the site of internal infection without additional incisions and risks for re-infection.

2. Materials and methods

2.1. Materials

Iron (III) chloride hexahydrate (FeCl₃·6H₂O), iron (II) chloride tetrahydrate (FeCl₂·4H₂O), ammonium hydroxide (26% NH₃ in H₂O), oleic acid, methylcellulose (M.W. 88,000), poly(ethyleneimine) solution ~50% in H₂O (M.W. 600,000–1,000,000) were all commercial products from Sigma–Aldrich, Germany.

2.2. Preparation of magnetite coated with oleic acid (OA-MNP), polyethyleneimine (PEI-MNP) and polyethyleneimine-methyl cellulose (PEI-mC-MNP)

1.9 g FeCl₂·4H₂O and 5.4 g FeCl₃·6H₂O (molar ratio of 1:2) are dissolved in 100 ml distilled water with mechanical stirrer for 1 h. This sample is named as *mixture 1*. Magnetite coated with oleic acid (OA-MNP) was prepared by addition 6 ml of ammonium hydroxide to *mixture 1* at 70 °C for 30 min. Particles are transferred into a mixture of dichloromethane 50 ml and oleic acid 1 ml to form OA-MNPs. The product was washed with water (to remove impurities, such as ammonium salt). Magnetite coating with polyethyleneimine (PEI-MNP) and polyethyleneimine-methyl cellulose (PEI-mC-MNP) was carried out by addition of (4 g PEI in 50 ml distilled water) and (5 g PEI and 5 g methyl cellulose in 50 ml distilled water) to *mixture 1*, respectively. PEI-MNP and PEI-mC-MNP were prepared by addition 6 ml of ammonium hydroxide to two solutions at 70 °C for 1 h. The product was washed several times with distilled water and after that, OA-MNP, PEI-MNP and PEI-mC-MNP were dried in a rotary evaporator at 40 °C (25 mbar, 80 rpm), until forming the fine powder.

2.3. Characterization

Fourier Transform Infrared (FTIR) was performed by Bruker Tensor 27 Infrared Spectrometer. Thermogravimetric Analysis (TGA) was measured by TA Instruments Q500, while zeta potential measurements were performed using a Zetasizer Nano analyzer (Malvern Instruments, USA) at pH = 7. Dynamic Light Scattering (DLS) analysis was employed to measure the hydrodynamic diameters of magnetic nanoparticle aggregates in DI water using a Zetasizer Nano DLS unit. Microscopy images were obtained through scanning electron microscopy (SEM) using a Zeiss ULTRA Plus field-emission SEM equipped with a Schottky cathode. The images were analyzed using Smart SEM software v5.05 (Zeiss, Germany) for imaging operated at 1.5 kV. Magnetic properties were measured by vibrating sample magnetometer (VSM), heating properties of the samples were measured by Cheltenham induction heating limited with constant frequency (142 kHz) and power (1, 0.7,

0.5, 0.3, 0.1 kW) and the temperature was measured by infrared thermometer.

2.4. Bacterial strains

Bacterial strains of Gram-negative *Escherichia coli* CCM 3954 and Gram-positive *S. aureus* CCM 3953 were obtained from the Czech Collection of Microorganisms, Masaryk University, Brno, Czech Republic. The bacterial inocula were always prepared fresh from a single colony growing overnight in a soya nutrient broth (Sigma Aldrich) at 37 °C. The culture was diluted to achieve optical density OD = 0.01–0.02 at 600 nm (OD₆₀₀). The growth rate was monitored by using a UV–Vis spectrophotometer (Hach Lange DR6000, Germany) to measure the increased scattering.

2.5. Bacterial growth rate exposed to MNPs

The freshly prepared bacterial cultures were transferred to 30 ml of soya broth and kept in 200 ml conical flasks. The MNPs stock suspensions (10 g/l) were added to the bacterial culture at a range of final concentrations, i.e. 50, 500 and 1000 mg/l. A 250 µl was then transferred to each well of 96-well plate. Negative controls: bacterial cells only in growth media and magnetic nanoparticles only in growth media were run in parallel. Each sample was prepared in duplicates. The plate was incubated at 37 °C and optical density of the samples was measured at 600 nm (OD₆₀₀) every 2 h by using a Multi-Mode Microplate Reader (Synergy™ HT, Biotek). The bacterial growth rate (h⁻¹) was defined by a linear regression of cell density measurement (OD₆₀₀) versus incubation time (hours).

As an earlier publication, the effect of nanoparticle concentration on bacterial growth rate (μ) was calculated for each nanoparticle type, based on Eq. (1):

$$I(\%) = (\mu_c - \mu_T) / \mu_c \times 100 \quad (1)$$

[30] where I is inhibition, μ_c is the mean value of growth rate of the control, and μ_T value is the growth rate of the culture affected by the nanoparticles. The EC10 value (effective concentration for 10% inhibition) was obtained by plotting $I\%$ versus concentration of nanoparticle tested.

2.6. Cell viability

In parallel with the determination of bacterial growth rate, bacterial viability test was carried out in the same MNP concentrations as described above. Each bacteria-MNP sample was prepared in replicates and cultures without nanoparticles were cultivated in growth media as controls. Bacterial samples, including MNP were centrifuged at 5000 rpm for 5 min after 24 h incubation at 37 °C. The cell pellet was washed and resuspended in physiological solution (0.85% of NaCl). After that, the cells were stained (Live/Dead BacLight kit L7007, Life Technologies) for 15 min in dark to distinguish viable and non-viable cells. Viable cells showed green fluorescence and non-viable cells were of red fluorescence. The viable and non-viable cells were observed in fluorescence microscope (Axiomager, Zeiss, Germany) with excitation 470 nm, emission 490–700 nm and counted by Zeiss AxioVision software. A range of 200 *E. coli* cells or *S. aureus* clusters (colonies) was inspected to get the ratio of dead cells versus live cells.

2.7. Determination of *S. aureus* biofilm

The biofilm assay with crystal violet staining was previously described [31]. *S. aureus* culture exposed to MNP as described for the growth rate test was further incubated for 24 h in 96-well plate. The growth media solution was then removed followed by drying the 96-well plate on air for 10 min. The formed biofilms were fixed with methanol and stained with 0.1% of crystal violet aqueous solution for 15 min. The staining solution

was washed out using sterile ultra-pure water and air-dried. The wells were then filled with 100 μ l of 30% (v/v) acetic acid aqueous solution for 5 min to solubilize the dye. The sample (biofilm) absorbance was read at 490 nm in microplate reader. The background values of MNPs in the dye (without bacteria) were subtracted to stained biofilm values (MNPs with *S. aureus*). The replicated treated samples were compared with untreated samples of *S. aureus* alone in growth media only.

2.8. Statistical analysis

One-way ANOVA and the Mann–Whitney test (GraphPad Prism software; CA, USA) were used to compare differences between means of bacterial growth rate for OA-MNP, PEI-MNP, PEI-mC-MNP on *E. coli* and *S. aureus*.

The results were analyzed by ordinary ANOVA and the significance level was shown with an asterisk * $P < 0.02$, ** $P < 0.006$, *** $P < 0.0002$, **** $P < 0.0001$.

3. Results and discussion

3.1. Characterization of MNPs

Magnetic nanoparticles of OA-MNP, PEI-MNP and PEI-mC-MNP were prepared through co-precipitation of magnetite nanoparticles in

the presence of oleic acid, polyethyleneimine or polyethyleneimine-methyl cellulose, respectively as shown in (Fig. 1).

The surface functionality of the magnetite nanoparticles was detected by IR (Fig. S1), with an absorption peak at 580 cm^{-1} confirming the presence of a Fe–O bond related to the magnetite phase of magnetite nanoparticles. The bands at 1430 cm^{-1} and 1590 cm^{-1} correspond to the symmetric and asymmetric stretching vibrations of oleate ($-\text{COO}$). This indicates that oleic acid bond with iron oxide, which is consistent with the literature value [21]. The absorption bands at 1040 cm^{-1} of C–O, 3440 cm^{-1} of $-\text{OH}$ (methyl cellulose) is probably overlapped by the vibration band of $-\text{NH}$. The absorption contribution bands appeared at 3350 cm^{-1} and 1650 cm^{-1} from $-\text{NH}$ symmetric and deformation respectively, and assignable for PEI in PEI-MNP and PEI-mC-MNP.

SEM indicated slight differences in the morphology between functionalized magnetic nanoparticles (Fig. 2) showed a broader size distribution. Nanoparticles were usually agglomerated due to the high surface energy between the nanoparticles and dipole–dipole interactions [32].

Dynamic Light Scattering (DLS) displays a wide size-range for the prepared samples. The average sizes of 132, 174 and 242 nm have been measured for OA-MNP, PEI-MNP and PEI-mC-MNP, respectively. DLS shows that the average size of magnetite coated with PEI-methyl cellulose is higher than with PEI only due to the presence of methyl cellulose particles in the layer (Fig. S2).

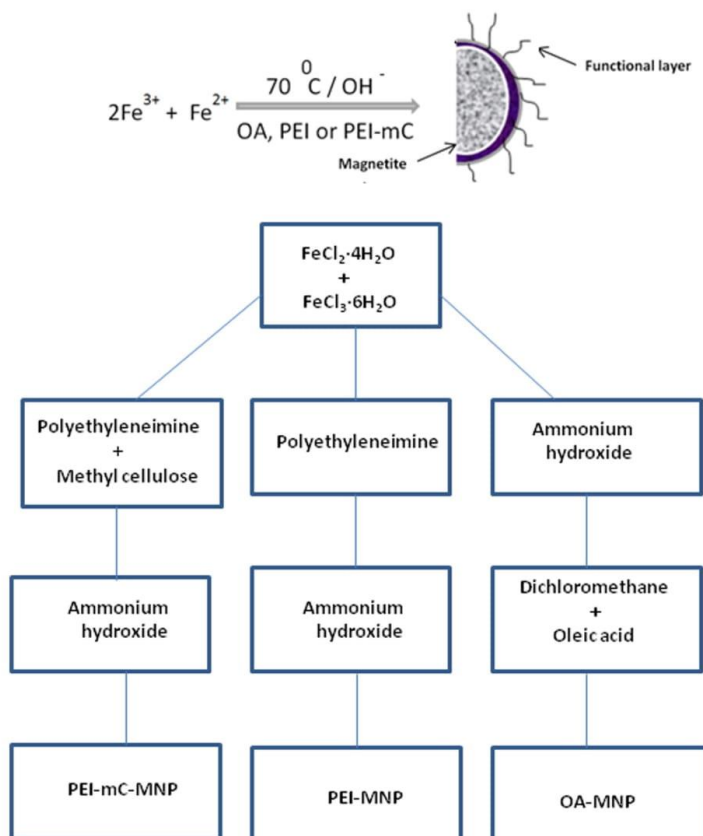


Fig. 1. 1.9 g $\text{FeCl}_2 \cdot 4\text{H}_2\text{O}$ and 5.4 g $\text{FeCl}_3 \cdot 6\text{H}_2\text{O}$ are dissolved in 100 ml distilled water and stirring for 1 h at $70\text{ }^\circ\text{C}$. 6 ml of NH_4OH is added to the resulting solution. 1 ml oleic acid, 4 g polyethyleneimine, 5 g polyethyleneimine and 5 g methyl cellulose to produce 132 nm OA-MNP, 174 nm PEI-MNP and 242 nm PEI-mC-MNP, respectively.

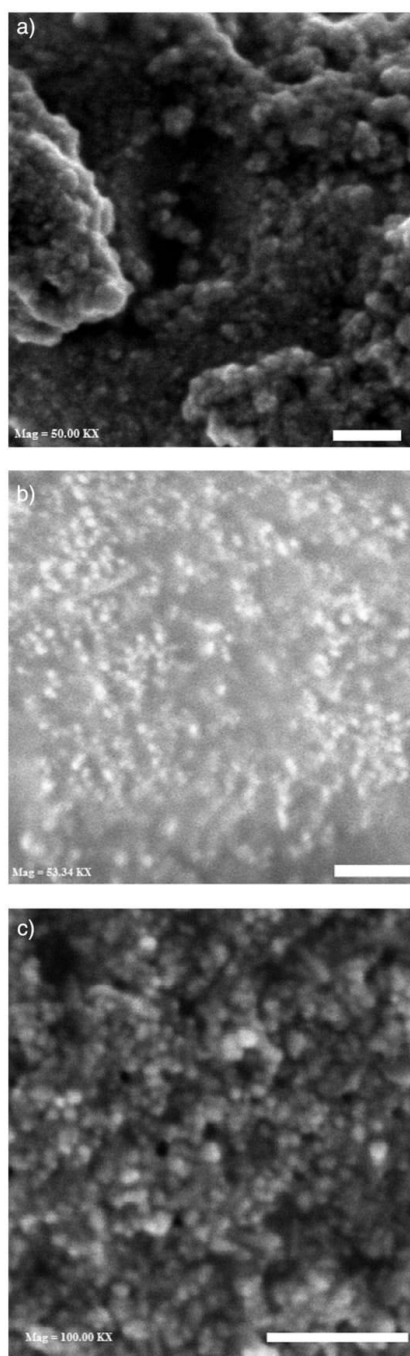


Fig. 2. Scanning electron microscopy pictures of a) OA-MNP b) PEI-MNP c) PEI-mC-MNP. scale bars = 200 nm.

The zeta potential for functionalized magnetite nanoparticles were 32.6 mV, 35.3 mV and 10.3 mV for OA-MNP, PEI-MNP and PEI-mC-MNP, respectively. The nanoparticle's zeta potential (surface charge) indicates how effectively nanoparticles form stable or aggregated colloids during the colloidal phase. It was reported that, at low zeta potentials (close to zero), particles are no longer repelled strongly and colloids will aggregate due to attractive surface forces. Conversely, stable dispersions are formed at high zeta potentials (above ~ 30 mV) [30]. This is of particular importance in biomedical applications where stable colloidal systems are required (Fig. S3).

The stability of the prepared nanoparticles coated with oleic acid, PEI and PEI-methyl cellulose was measured as a function of temperature by the TGA (Fig. S4). OA-MNP show higher stability than those coated with PEI-MNP and PEI-mC-MNP. Weight loss until 200 °C is mainly related to loss of water and physically adsorbed layers of oleic acid, or PEI or PEI-methyl cellulose. Above 200 °C the decomposition of chemical layer bound to iron oxide occurs. Above 600 °C samples residue becomes stable and the rest of the samples was 53.95%, 45.34% and 42.89%, which correspond to amount of iron in MNP.

The magnetic properties of the prepared magnetite nanoparticles were investigated with VSM at room temperature. Magnetization saturation (M_s) is the maximum possible magnetization, whereby a further increase in magnetic field, has no effect to enhance changing in magnetization and become saturated. The values of M_s (emu/g) are 14.8, 10.7 and 9 for OA-MNP, PEI-MNP and PEI-mC-MNP, respectively. The values are less than the values for uncoated magnetite nanoparticles ($M_s = 92$ emu/g) [33–34]. The decreased M_s for nanoparticles is attributed to the disordered surface spins [35–36]. It is obvious that by decreasing the particle size, the surface-to-volume ratio of a particle will increase, which leads to a reduction in magnetization of the particles [37].

3.2. Heating properties

The heat generated from samples was examined by exposing 20% magnetic particle suspension dispersed in distilled water to an alternating current (AC) magnetic field for certain time. It was an obvious rise of temperature by increasing in strength of applied magnetic field (1, 0.7, 0.5, 0.3, 0.1 kW) and by the exposure time (1–5 min) as shown in (Fig. 3). In induction heating curves of nanoparticles it is seen that the heating temperature increases with increasing time until reaching equilibrium after 3 min, where the heating rate become equal to the cooling rate. It was observed that the saturated temperature of OA-MNP, PEI-MNP and PEI-mC-MNP is 55.8, 75 and 65.4 °C, respectively at 5 min under 1 kW of strength of applied magnetic field. Where 0.1 kW was applied magnetic field the saturated temperature for OA-MNP, PEI-MNP and PEI-mC-MNP is 29.6, 44.2 and 37.5 °C, respectively at 5 min. So, for example for PEI-MNP at 2 min under 0.3 kW of strength of applied magnetic field temperature can reach to 45 °C, which is sufficient for cancer treatment. In addition, shorter rise time gives the benefits of less sample weight loss and faster treatment. For hyperthermia applications the temperature of cancerous tissue needs to reach 42–45 °C for effective therapy, whereas temperatures above 50 °C cause damage to cancer cells via thermoablation (necrosis) [38].

3.3. Specific absorption rate (SAR)

SAR describes the energy amount converted into heat per unit time and mass (e.g. Watts per gram) [39–40]. The SAR value was calculated using Eq. (2):

$$\text{SAR} = (C/m) * (dT/dt) \quad (2)$$

[40] where dT/dt is the slope of the time-dependent temperature curve and, C is the volumetric specific heat capacity of the sample solution

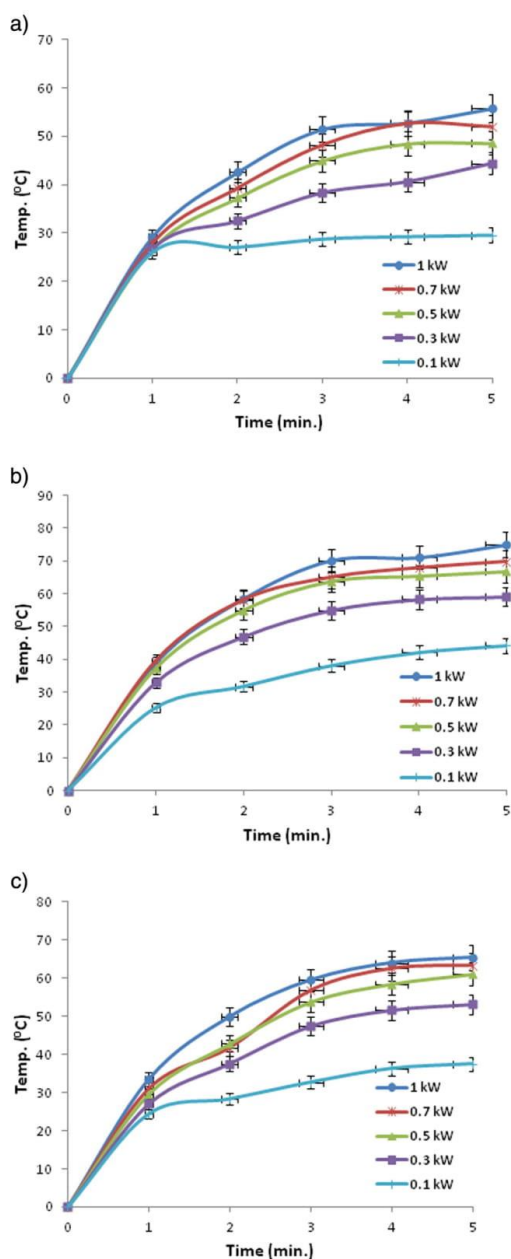


Fig. 3. Heating curves of a) OA-MNP b) PEI-MNP c) PEI-mC-MNP by exposing 20% MNPs suspension dispersed in distilled water in a glass tube with Cheltenham induction heating limited with copper coil and constant frequency (142 kHz) and power (1, 0.7, 0.5, 0.3, 0.1 kW).

($4.186 \text{ J}/(\text{g} \cdot ^\circ\text{C})$ for water) and m is the mass of magnetic material in the sample (0.2 g). We use the data in the initial linear region of 0–3 min for calculating the SAR before heat-saturation and diffusion cause flattening of the curve. In Fig. 4 we plot the specific absorption rate (SAR) as a function of the strength of the applied magnetic field and show that

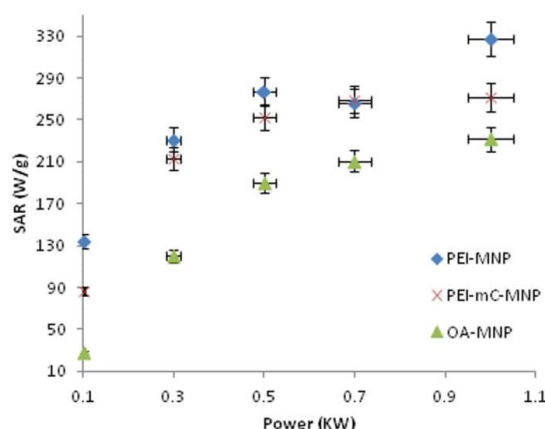


Fig. 4. SAR values of OA-MNP, PEI-MNP and PEI-mC-MNP were calculated from Cheltenham induction heating limited with copper coil and constant frequency (142 kHz) and power (1, 0.7, 0.5, 0.3, 0.1 kW).

the SAR values increase with increasing the power applied. The efficiency of the transformation of energy is dependent on the strength and frequency of the magnetic field and the properties of the magnetic particles like mean size, width of size distribution, particle shape and crystallinity [11–13]. The SAR of magnetite particles in an external AC magnetic field can be attributed to two kinds of power loss mechanisms; one is hysteresis loss and other is relaxation loss. The relaxation time depends on the particle diameter and when the particles are small and the relaxation time is comparable to the frequency, large amount of heat is generated [41]. It was reported that for particles with diameters less than 9 nm, Neel relaxation is dominant. For larger particles, heating is primarily due to Brownian rotation [42–44]. For the OA-MNP, PEI-MNP and PEI-mC-MNP particles we report the highest absorption rates of 231.99, 327.08 and 271.7 W g^{-1} , respectively.

3.4. Antibacterial properties of magnetic nanoparticles on bacteria

The growth rate (h^{-1}) of Gram-negative *E. coli* was not significantly changed in the presence of OA-MNP, PEI-MNP and PEI-mC-MNP within all tested concentrations. However, it was notably affected when *E. coli* grew in 1000 mg/l of PEI-mC-MNP ($P = 0.001$). Surprisingly, *S. aureus* was more susceptible toward all MNPs at high concentrations, concretely in 500 and 1000 mg/l. *S. aureus* growth rate dramatically decreased from 0.1 (only *S. aureus* culture) to 0.02 ($P < 0.0001$) (Fig. 5).

The first results of the bacterial growth rate investigation implied that *S. aureus* was more susceptible to MNPs than *E. coli*. The effective concentration at 10% EC10 (mg/l) for growth inhibition of OA-MNP, PEI-MNP and PEI-mC-MNP with Gram-positive *S. aureus* was shown more significant than with Gram-negative *E. coli* ($P = 0.04$). Precisely, PEI-MNP and PEI-mC-MNP displayed the highest effectiveness on *S. aureus* (EC10 = 77.4 and 146.7 mg/l) and *E. coli* (EC10 = 520 and 145.7 mg/l), while OA-MNP showed the least effect on both bacteria, *S. aureus* (EC10 = 200 mg/l) and *E. coli* (EC10 > 1000 mg/l) (Table 1).

After 24 h-exposure of bacteria to MNPs, the percentage of *E. coli* dead cells only slightly increased from 1.3% (*E. coli* alone) to 21% ($P = 0.03$) and 24% ($P = 0.02$) when it was grown with PEI-mC-MNP 500, 1000 mg/l, respectively. By contrast, *S. aureus* dead cells significantly increased from 7.5% (*S. aureus* without MNPs) to a range of 33–39% ($P < 0.0001$) when in contact with all MNPs materials at concentrations of 500 and 1000 mg/l (Fig. 6). This result was confirmed by the trend of non-affected or affected cultures of either *E. coli* or *S. aureus* during growth rate tests.

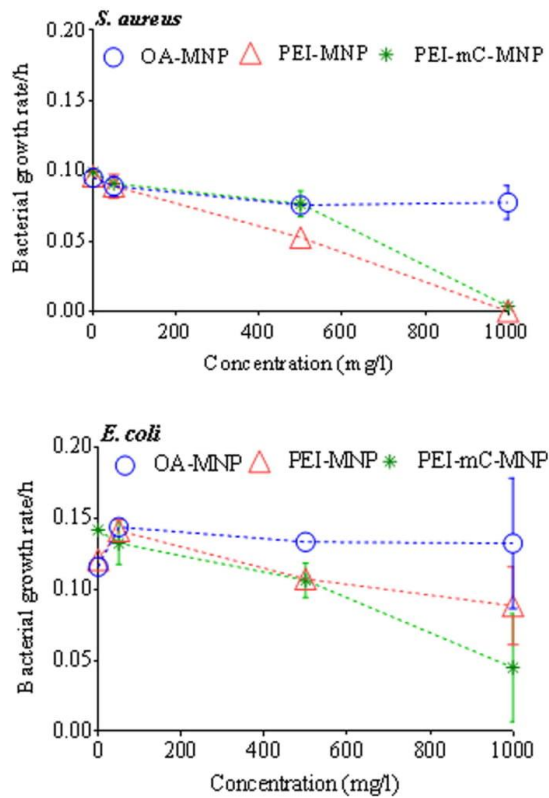


Fig. 5. Bacterial growth rate (h^{-1}) of *E. coli* and *S. aureus* after 6 h incubation with MNPs: OA-MNP, PEI-MNP and PEI-mC-MNP in a range of different concentration. Bacterial growth rate determined in Soya broth medium served as negative controls (0 mg/l). The error bars were determined from $n = 2$.

The strength of the biofilm formation of *S. aureus* was significantly reduced by all MNPs at concentration of 50 mg/l ($P < 0.002$). Interestingly, the absorbance at 490 nm of biofilm was dramatically decreased from 2 to 1.1, 0 and 0.3 ($P < 0.0001$) when *S. aureus* was cultivated with 1000 mg/l of OA-MNP, PEI-MNP and PEI-mC-MNP, respectively (Fig. 7).

The effect of MNPs on Gram-negative *E. coli* and Gram-positive *S. aureus* presented by bacterial growth rate (h^{-1}), percentage of bacterial dead cells and biofilm formation showed that all three types of MNPs have promising antibacterial properties.

To make sure that the effect is solely due to the MNPs, we measured pH and ORP as chemical indicators of the medium which may contribute to bacterial stress. In this research, both *E. coli* or *S. aureus* in the presence of MNPs show similar pH values to the negative control (bacteria alone in a medium), namely pH 7 at time 0 and pH = 5 after 6 h incubation. The case of *S. aureus* grown with PEI-MNP was an exception, where pH remained at pH = 7 after 6 h exposure, likely

Table 1

The effective concentration at 10% inhibition, EC10 (mg/l) of MNPs determined for Gram-negative *Escherichia coli* and Gram-positive *Staphylococcus aureus*.

	OA-MNP	PEI-MNP	PEI-mC-MNP
<i>E. coli</i>	>1000	520	145.7
<i>S. aureus</i>	200	77.4	146.7

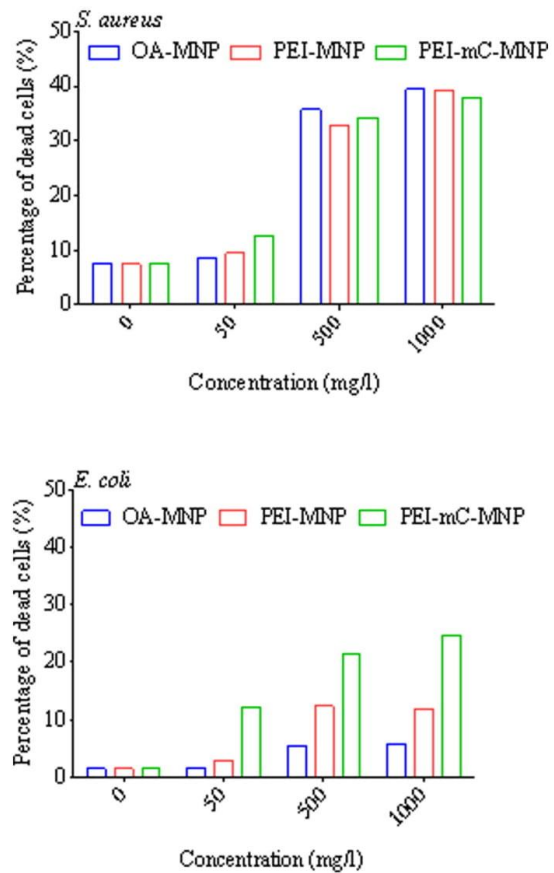


Fig. 6. Percentage of *E. coli* and *S. aureus* dead cells after 24 h incubated with OA-MNP, PEI-MNP and PEI-mC-MNP. Bacterial growth in Soya broth medium alone was the negative control.

caused by a complete lack of grow, and confirmed by the reduction in growth rate from 0.1 to 0.02 h^{-1} (Fig. S5). It is known that ORP is a measurement of oxidizing or reducing ability in a solution and can in principle contribute to stress experienced by the bacteria. Our measured ORP values, however, show that the medium without the MNPs ($0 < \text{ORP} < +200$) falls in the range of normal condition for bacterial growth ($-200 < \text{ORP} < +200$) (Fig. S6) [45–47].

The highest effectiveness against bacteria was obtained for PEI-mC-MNP following by PEI-MNP and OA-MNP at 1000 mg/l. The EC10 of 77.4 mg/l (*S. aureus*) and 145.7 mg/l (*E. coli*) in our results were an improvement on the antibacterial properties of surface-modified magnetite with EC10 of 108 mg/l toward *S. aureus* and 170 mg/l toward *E. coli* recently measured by Darwish et al. [30]. Moreover, compared to a previous study of superparamagnetic iron oxide (SPION), 25% cell mortality was shown when *S. epidermidis* was grown in the presence of 2 mg/ml of superparamagnetic iron oxide after 48 h [48]. One year later, Tran et al. proved that 3 mg/ml IO/PVA nanoparticles added to *S. aureus* culture possess bactericidal effect where the ratio of live/dead cells was 40% after 4 h incubation and decreased to 25% after 24 h [49]. Based on our results, carried out in the same conditions at 1000 mg/l, while 24 h exposure to OA-, PEI- and PEI-mC-MNPs results in 39% ($P < 0.0001$) dead *S. aureus* cells, same exposures resulted in

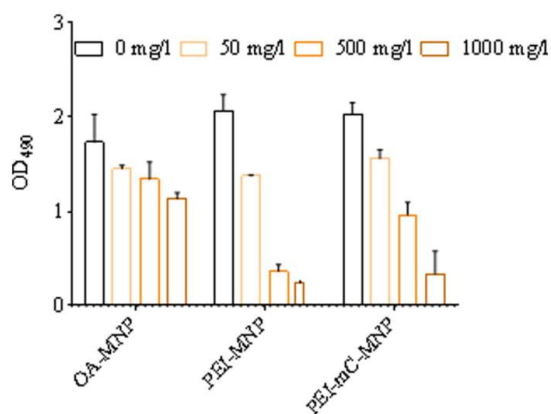


Fig. 7. Biofilm of *S. aureus* cells after 24 h incubation with OA-MNP, PEI-MNP and PEI-mC-MNP. A negative control was *S. aureus* growth in Soya broth medium. The OD490 was presented by OD490 MNP, PEI-MNP and PEI-mC-MNP. A negative control was *S. aureus* growth in Soya broth medium. The OD490 was presented by OD490 values of stained biofilm values (MNPs with *S. aureus*) subtracted to OD490 values of MNPs in the dye (without bacteria).

25% ($P = 0.02$) of dead *E. coli* cells for PEI-mC-MNPs, 12% ($P = 0.2$) for PEI-MNPs and only 5% ($P = 0.8$) for OA-MNPs.

Taylor et al., has also demonstrated that *S. aureus* biofilm formation can be inhibited by SPION doses as small as 10 $\mu\text{g}/\text{ml}$ after 12 h [48]. The biofilm formation of *S. aureus* was also reduced significantly in this study by exposure to 50 $\mu\text{g}/\text{ml}$ of all MNPs. It has been proven that the biofilm formation strongly contributes to bacterial survival in exposure to antibacterial drugs or NPs (e.g. *S. aureus* or *Pseudomonas aeruginosa*) [50–51]. In this study, we show that in addition to the antibacterial activity against single cells, our fictionalized MNPs also inhibit the formation of biofilms of *S. aureus*.

4. Conclusions

Bi-functional self-heating and antibacterial magnetite nanoparticles were successfully prepared by coating magnetite with oleic acid (OA-MNP), polyethyleneimine (PEI-MNP), and polyethyleneimine-methyl cellulose (PEI-mC-MNP) using a co-precipitation process. The magnetic heating specific absorption rates (SARs) and antibacterial properties were measured for the three sets of nanoparticles. Though all the magnetic nanoparticles (MNPs) were found to be antibacterial, those coated with PEI-mC were found most effective. Concentrations necessary for 10% growth inhibition (EC10) of both *E. coli* and *S. aureus* were both $<150 \mu\text{g}/\text{l}$. The functionalized magnetite nanoparticles are promising agents for hyperthermia, as well as for further work toward hyperthermic drug release.

Supplementary data to this article can be found online at <http://dx.doi.org/10.1016/j.msec.2016.02.052>.

Acknowledgments

The results of this project LO1201 were obtained through the financial support of the Ministry of Education, Youth and Sports in the framework of the targeted support of the "National Programme for Sustainability I", the OPR&DI project Centre for Nanomaterials, Advanced Technologies and Innovation CZ.1.05/2.1.00/01.0005 and the Project Development of Research Teams of R&D Projects at the Technical university of Liberec CZ.1.07/2.3.00/30.0024.

This work was funded by the ERC grant EMATTER (#280078).

References

- [1] A. Hervault, N.T.K. Thanh, Magnetic nanoparticle-based therapeutic agents for thermo-chemotherapy treatment of cancer, *Nanoscale* 6 (2014) 11553–11573.
- [2] J.Q. Cao, Y.X. Wang, J.F. Yu, J.Y. Xia, C.F. Zhang, D.Z. Yin, Urs O. Häfeli, Preparation and radiolabeling of surface-modified magnetic nanoparticles with rhenium-188 for magnetic targeted radiotherapy, *J. Magn. Magn. Mater.* 277 (2004) 165–174.
- [3] J. Wang, B. Zhang, L. Wang, M. Wang, F. Gao, One-pot synthesis of water-soluble superparamagnetic iron oxide nanoparticles and their MRI contrast effects in the mouse brains, *Mater. Sci. Eng. C* 48 (2015) 416–423.
- [4] N. Ye, Y. Xie, P. Shi, T. Gao, J. Ma, Synthesis of magnetite/graphene oxide/chitosan composite and its application for protein adsorption, *Mater. Sci. Eng. C* 5 (2014) 8–14.
- [5] Q.A. Pankhurst, J. Connolly, S.K. Jones, J. Dobson, Applications of magnetic nanoparticles in biomedicine, *J. Phys. D: Appl. Phys.* 36 (2003) R167–R181.
- [6] P. Tartaj, M.P. Morales, S. Veintemillas-Verdaguer, T. Gonzalez-Carreño, C.J. Serna, The preparation of magnetic nanoparticles for applications in biomedicine, *J. Phys. D: Appl. Phys.* 36 (2003) R182–R197.
- [7] L. Néel, Théorie du trainage magnétique des ferromagnétiques en grains fins avec application aux terres cuites, *Ann. Geophys.* 5 (1949) 99.
- [8] P. Debye, *Polar Molecules*, Chemical Catalog Company, New York, 1929.
- [9] M. Ma, Y. Wu, J. Zhou, Y. Sun, Y. Zhang, N. Gu, Size dependence of specific power absorption of Fe_3O_4 particles in AC magnetic field, *J. Magn. Magn. Mater.* 268 (2004) 33–39.
- [10] S. Maenosono, S. Saita, Theoretical assessment of FePt nanoparticles as heating elements for magnetic hyperthermia, *IEEE Trans. Magn.* 42 (2006) 1638–1642.
- [11] F. Gazeau, M. Lévy, C. Wilhelm, Optimizing magnetic nanoparticle design for nanothermotherapy, *Nanomedicine* 3 (2008) 831–844.
- [12] N.L. Rosi, C.A. Mirkin, Nanostructures in diagnostics, *Chem. Rev.* 105 (2005) 1547–1562.
- [13] N. Kawai, D. Kobayashi, T. Yasui, Y. Umemoto, K. Mizuno, A. Okada, K. Tozawa, T. Kobayashi, K. Kohri, Evaluation of side effects of radiofrequency capacitive hyperthermia with magnetite on the blood vessel walls of tumor metastatic lesion surrounding the abdominal large vessels: an agar phantom study, *Vasc. Cell* 6 (2014) 15.
- [14] A.H. Lu, E.L. Salabas, F. Schüth, Magnetic nanoparticles: synthesis, protection, functionalization, and application, *Angew. Chem. Int. Ed. Engl.* 46 (2007) 1222–1244.
- [15] M.S. Islam, Y. Kusumoto, J. Kurawaki, M.D. Abdulla-Al-Mamun, H. Manaka, A comparative study on heat dissipation, morphological and magnetic properties of hyperthermia suitable nanoparticles prepared by co-precipitation and hydrothermal methods, *Bull. Mater. Sci.* 35 (2012) 1047–1053.
- [16] H. Sadeghi-Aliabadi, M. Mozaffari, B. Behdadfar, M. Raesizadeh, H. Zarkesh-Esfahani, Preparation and cytotoxic evaluation of magnetite (Fe_3O_4) nanoparticles on breast cancer cells and its combinatory effects with doxorubicin used in hyperthermia, *Avicenna J. Med. Biotechnol.* 5 (2013) 96–103.
- [17] K.D. Wani, B.S. Kadu, P. Mansara, P. Gupta, A.V. Deore, R.C. Chikate, P. Poddar, S.D. Dhole, R. Kaul-Ghanekar, Synthesis, characterization and in vitro study of biocompatible cinnamaldehyde functionalized magnetite nanoparticles (CPGF Nps) for hyperthermia and drug delivery applications in breast cancer, *PLoS One* 9 (2014), <http://dx.doi.org/10.1371/journal.pone.0107315>.
- [18] N.V. Jadhav, A.I. Prasad, A. Kumar, R. Mishra, S. Dhara, K.R. Babu, C.L. Prajapat, N.L. Misra, R.S. Ningthoujam, B.N. Pandey, Synthesis of oleic acid functionalized Fe^{30} 4 magnetic nanoparticles and studying their interaction with tumour cells for potential hyperthermia applications, *Colloids Surf. B: Biointerfaces* 108 (2013) 158–168.
- [19] E. Cheraghpour, S. Javadpour, A.R. Mehdizadeh, Citrate capped superparamagnetic iron oxide nanoparticles used for hyperthermia therapy, *J. Biomed. Sci. Eng.* 5 (2012) 715–719.
- [20] P.H. Linh, P.V. Thach, N.A. Tuan, Magnetic fluid based on Fe_3O_4 nanoparticles: preparation and hyperthermia application, *J. Phys. Conf. Ser.* 187 (2009) 012069.
- [21] M.S.A. Darwish, S. Machunsky, U. Peuker, U. Kunz, T. Turek, Magnetite core-shell nano-composites with chlorine functionality: preparation by miniemulsion polymerization and characterization, *J. Polym. Res.* 18 (2011) 79–88.
- [22] S. Ota, N. Yamazaki, A. Tomitaka, T. Yamada, Y. Takemura, Hyperthermia using antibody-conjugated magnetic nanoparticles and its enhanced effect with cryptotanshinone, *Nanomaterials* 4 (2014) 319–330.
- [23] S.R. Deka, A. Quarta, R.D. Corato, A. Riedinger, R. Cingolani, T. Pellegrino, Magnetic nanobeads decorated by thermo-responsive PNIPAM shell as medical platforms for the efficient delivery of doxorubicin to tumour cells, *Nanoscale* 3 (2011) 619–629.
- [24] Y. Ding, S.Z. Shen, H. Sun, K. Sun, F. Liu, Y. Qi, J. Yan, Design and construction of polymerized-chitosan coated Fe_3O_4 magnetic nanoparticles and its application for hydrophobic drug delivery, *Mater. Sci. Eng. C* 48 (2015) 487–498.
- [25] C. Fleesch, Y. Unterfinger, E. Bourgeat-Lami, E. Duguet, C. Delaite, P. Dumas, Poly(ethylene glycol) surface coated magnetic particles, *Macromol. Rapid Commun.* 26 (2005) 1494–1498.
- [26] W.S. Kuo, C.N. Chang, Y.T. Changa, C.S. Yeh, Antimicrobial gold nanorods with dual-modality photodynamic inactivation and hyperthermia, *Chem. Commun.* 32 (2009) 4853–4855.
- [27] S. Singha, K.C. Barickb, D. Bahadur, Inactivation of bacterial pathogens under magnetic hyperthermia using Fe_3O_4 -ZnO nanocomposite, *Powder Technol.* 269 (2015) 513–519.
- [28] W.L. Chiang, T.T. Lin, R. Sureshbabu, W.T. Chia, H.C. Hsiao, H.Y. Liu, C.M. Yang, H.W. Sung, A rapid drug release system with a NIR light-activated molecular switch for dual-modality photothermal/antibiotic treatments of subcutaneous abscesses, *J. Control. Release* 199 (2015) 53–62.

- [29] M.C. Wu, A.R. Deokar, J.H. Liao, P.Y. Shih, Y.C. Ling, Graphene-based photothermal agent for rapid and effective killing of bacteria, *ACS Nano* 7 (2013) 1281–1290.
- [30] M.S.A. Darwish, N.H.A. Nguyen, A. Ševcu, I. Stibor, Functionalized magnetic nanoparticles and their effect on *Escherichia coli* and *Staphylococcus aureus*, *J. Nanomater.* (2015), <http://dx.doi.org/10.1155/2015/416012>.
- [31] E. Burton, N. Yakandawala, K. LoVetri, M.S. Madhyastha, A microplate spectrofluorometric assay for bacterial biofilms, *J. Ind. Microbiol. Biotechnol.* 34 (2007) 1–4.
- [32] D.L. Zhao, P. Teng, Y. Xu, Q.S. Xia, J.T. Tang, Magnetic and inductive heating properties of Fe₃O₄/polyethylene glycol composite nanoparticles with core-shell structure, *J. Alloys Compd.* 502 (2010) 392–395.
- [33] F. Fajaro, H. Setyawan, Synthesis of magnetite nanoparticles by surfactant-free electrochemical method in an aqueous system, *Adv. Powder Technol.* 23 (2012) 328–333.
- [34] B. Li, D. Jia, Y. Zhou, Q. Hu, W. Cai, In situ hybridization to chitosan/magnetite nanocomposite induced by the magnetic field, *J. Magn. Magn. Mater.* 306 (2006) 223–227.
- [35] J. Qu, G. Liu, Y. Wang, R. Hong, Preparation of Fe₃O₄-chitosan nanoparticles used for hyperthermia, *Adv. Powder Technol.* 21 (2010) 461–467.
- [36] C.Y. Kim, L. Xu, E.H. Lee, Self-heating of magnetite nanoparticles for a potential hyperthermia application, *J. Korean Phys. Soc.* 65 (2014) 261–266.
- [37] G. Kong, M.W. Dewhirst, Review hyperthermia and liposomes, *Int. J. Hyperth.* 15 (1999) 345–370.
- [38] A.A. Elsherbini, M. Saber, M. Aggag, A. El-Shahawy, H.A. Shokier, Magnetic nanoparticle-induced hyperthermia treatment under magnetic resonance imaging, *Magn. Reson. Imaging* 29 (2011) 272–280.
- [39] M. Babincova, D. Leszcznska, P. Sourivong, P. Čičmanec, P. Babinec, Superparamagnetic gel as a novel material for electromagnetically induced hyperthermia, *J. Magn. Magn. Mater.* 225 (2001) 109–112.
- [40] J.H. Lee, J.T. Jang, J.S. Choi, S.H. Moon, S.H. Noh, J.W. Kim, J.G. Kim, I.S. Kim, K.I. Park, J. Cheon, Exchange-coupled magnetic nanoparticles for efficient heat induction, *Nat. Nanotechnol.* 6 (2011) 418–422.
- [41] J.P. Fortin, F. Gazeau, C. Wilhelm, Intracellular heating of living cells through Néel relaxation of magnetic nanoparticles, *Eur. Biophys. J.* 37 (2008) 223–228.
- [42] C. Fannin, B.K. Scaife, S.W. Charles, On the permittivity of magnetic colloids subject to a strong external magnetic field over the frequency range 50 kHz to 1 MHz, *J. Magn. Magn. Mater.* 122 (1993) 168–171.
- [43] M.I. Shliomis, Y. Raikher, Experimental investigation of magnetic fluids, *IEEE Trans. Magn.* 16 (1980) 237–250.
- [44] N. Ramachandran, K. Mazuruk, Magnetic microspheres and tissue model studies for therapeutic applications, *Ann. N. Y. Acad. Sci. Trans. Phenom. Microgravity* 1027 (2004) 99–109.
- [45] T. Bastian, J. Brondum, Do traditional measures of water quality in swimming pools and spas correspond with beneficial oxidation reduction potential, *Public Health Rep.* 124 (2009) 255–261.
- [46] T.V. Suslow, Oxidation reduction potential (ORP) for water disinfection monitoring, control and documentation, *J. ANR Publication* 8149 2004, pp. 1–15.
- [47] K. Victorin, K.G. Hellstrom, R. Rylander, Redox potential measurements for determining the disinfecting power of chlorinated water, *J. Hyg.* 70 (1972) 313–323.
- [48] E.N. Taylor, T.J. Webster, The use of superparamagnetic nanoparticles for prosthetic biofilm prevention, *Int. J. Nanomedicine* 4 (2009) 145–152.
- [49] N. Tran, A. Mir, D. Mallik, A. Sinha, S. Nayar, Bactericidal effect of iron oxide nanoparticles on *Staphylococcus aureus*, *Int. J. Nanomedicine* 5 (2010) 277–283.
- [50] H. Park, H.J. Park, J.A. Kim, S.H. Lee, J.H. Kim, J. Yoon, T.H. Park, Inactivation of *Pseudomonas aeruginosa* PAO1 biofilms by hyperthermia using superparamagnetic nanoparticles, *J. Microbiol. Methods* 84 (2011) 41–45.
- [51] M. Mahmoudi, V. Serpooshan, Silver-coated engineered magnetic nanoparticles are promising for the success in the fight against antibacterial resistance threat, *ACS Nano* 6 (2012) 2656–2664.

Paper 6

Mohamed S. A. Darwish, **Nhung H.A. Nguyen**, Alena Sevcu, and Ivan Stibor (2015).
Functionalized magnetic nanoparticles and their effect on *Escherichia coli* and *staphylococcus aureus*. *Journal of Nanomaterials*, Article ID 416012, doi:10.1155/2015/416012. **IF 1.871**

Research Article

Functionalized Magnetic Nanoparticles and Their Effect on *Escherichia coli* and *Staphylococcus aureus*

Mohamed S. A. Darwish,^{1,2} Nhung H. A. Nguyen,¹ Alena Ševců,¹ and Ivan Stibor¹

¹Institute for Nanomaterials, Advanced Technologies and Innovation, Technical University of Liberec, Studentská 2, 461 17 Liberec, Czech Republic

²Egyptian Petroleum Research Institute, 1 Ahmed El-Zomor Street, El Zohour Region, Nasr city, Cairo 11727, Egypt

Correspondence should be addressed to Mohamed S. A. Darwish; msa.darwish@gmail.com and Ivan Stibor; ivan.stibor@tul.cz

Received 8 December 2014; Accepted 1 March 2015

Academic Editor: Piaoping Yang

Copyright © 2015 Mohamed S. A. Darwish et al. This is an open access article distributed under the Creative Commons Attribution License, which permits unrestricted use, distribution, and reproduction in any medium, provided the original work is properly cited.

Magnetite (Fe_3O_4) nanoparticles were prepared using coprecipitation and subsequently surface-functionalized with 3-aminopropyltriethoxysilane (APTS), polyethylene glycol (PEG), and tetraethoxysilane (TEOS). Nanoparticle morphology was characterized using scanning electron microscopy, while structure and stability were assessed through infrared spectroscopy and zeta potential, respectively. Average size of the nanoparticles analysed by dynamic light scattering was 89 nm, 123 nm, 109 nm, and 130 nm for unmodified magnetite and APTS-, PEG-, and TEOS-modified magnetite nanoparticles, respectively. Biological effect was studied on two bacterial strains: Gram-negative *Escherichia coli* CCM 3954 and Gram-positive *Staphylococcus aureus* CCM 3953. Most of modified magnetite nanoparticles had a significant effect on *S. aureus* and not on *E. coli*, whereas PEG-magnetite nanoparticles displayed no significant effect on the growth rate of either bacteria.

1. Introduction

Surface functionalized magnetic nanoparticles have been widely used in a range of biological applications [1–3]. Magnetite (Fe_3O_4) is easily degradable and is useful, therefore, in bioseparation and catalytic processes. Magnetite nanoparticles have also been extensively studied in biomedicine [4, 5] due to their superparamagnetic properties, high biocompatibility, and lack of toxicity to humans. Magnetite nanoparticles possess high surface energy and thus tend to quickly aggregate. Such strong aggregation, however, may alter their adsorption properties and magnetic efficiency; hence the nanoparticles are frequently coated with an organic or inorganic layer to prevent aggregation. Such coatings not only stabilize the magnetite nanoparticles but can be easily used for further functionalization. Uncoated magnetite nanoparticles are also known to be highly susceptible to leaching under acidic conditions; hence several methods have been developed for the preparation of magnetic nanoparticles coated with a polymer, such as polyethylene glycol (PEG) and silica-containing organic material [6–8] in the form of a core/shell structure, with the silica/PEG shell coated onto

magnetic nanoparticles [9, 10]. Described coating enhances hydrophilicity and improves biocompatibility [11, 12]; the core/shell structure [13] has a number of attractive properties, including high adsorption capacity and chemical and thermal stability [14]. As the shell provides active groups on its surface that make available binding sites for enzymes, proteins, or drugs [15], magnetic nanoparticles have the potential to serve as drug carriers that can selectively target cancer cells, for example, and provide controlled release of chemotherapeutics [16, 17]. Magnetite nanoparticles coated with aminopropyltriethoxysilane (APTS) have many applications as adsorbent layers for removal of aqueous heavy metals during waste water treatment [18, 19]. Finally, the nontoxic nature of PEG-modified nanoparticles may be useful for more efficient biotechnology application [20].

Coprecipitation, sol-gel, and microemulsion are some of the most common methods for superparamagnetic magnetite nanoparticle synthesis, with coprecipitation being the most simple and economic method [21, 22]. It is based on the mixing of probably Fe^{3+} and Fe^{2+} at a 2:1 molar ratio in a highly basic solution, with the size and shape of the magnetite nanoparticles produced depending on the type of salt used,

the reaction temperature, pH, and ionic strength of the media. A common method for coating magnetite nanoparticles with a uniform silica shell is the sol-gel process. This process makes use of base-catalyzed hydrolysis and condensation of tetraethoxysilane (TEOS) [23]. The shell thickness of these silica-coated magnetite nanoparticles can be adjusted by controlling the amount of TEOS used [24].

The use of nanoscale materials has also attracted increasing concern due to the potential for environmental risk of toxicity. Several studies have been performed to evaluate the toxicity of magnetite nanoparticles on eukaryotic organisms, with surfactant-modified magnetite nanoparticles displaying negligible toxicity [25, 26]. Few studies have been published on the toxicity of magnetite nanoparticles to bacteria [27–33]; hence it is important to study the toxic effects of modified magnetite nanoparticles on more bacterial strains in order to fill gaps in our knowledge.

In this study, we prepared a range of magnetite nanoparticles with different surface functionality by modifying the nanoparticle surface with either APTS, PEG, or TEOS. The functional groups, surface charge, diameter, and morphology of the nanoparticles were characterized, together with their biological effect on Gram-negative *Escherichia coli* and Gram-positive *Staphylococcus aureus*.

2. Materials and Methods

2.1. Chemicals and Characterization. Iron (III) chloride hexahydrate ($\text{FeCl}_3 \cdot 6\text{H}_2\text{O}$, $\geq 98\%$), iron (II) chloride tetrahydrate ($\text{FeCl}_2 \cdot 4\text{H}_2\text{O}$, $\geq 99\%$), ammonium hydroxide (26% NH_3 in H_2O), PEG (PEG6000, $\geq 95\%$), APTS ($\geq 97\%$), and TEOS ($\geq 99\%$) were purchased from Sigma-Aldrich and used as received. Nanoparticle structure and stability were assessed through infrared spectroscopy and zeta potential, respectively. Fourier transform infrared spectroscopy (FT-IR) was performed using the Tensor 27 Infrared Spectrometer (Bruker, USA), while zeta potential measurements were performed using a Zetasizer Nano analyzer (Malvern Instruments, USA) at pH 7. Dynamic light scattering (DLS) analysis was employed to measure the hydrodynamic diameters of magnetic nanoparticle aggregates in DI water using a Zetasizer Nano DLS unit. Microscopy images were obtained through scanning electron microscopy (SEM) using a Zeiss ULTRA Plus field-emission SEM equipped with a Schottky cathode. The images were analyzed using Smart SEM software v5.05 (Zeiss, Germany) for imaging operated at 1.5 kV.

2.2. Synthesis of Unmodified Magnetite Nanoparticles. The unmodified magnetite nanoparticles were produced from an aqueous solution of $\text{FeCl}_3 \cdot 6\text{H}_2\text{O}$ and $\text{FeCl}_2 \cdot 4\text{H}_2\text{O}$ using the coprecipitation method [21, 22]. $\text{FeCl}_2 \cdot 4\text{H}_2\text{O}$ (1.9 g) and $\text{FeCl}_3 \cdot 6\text{H}_2\text{O}$ (5.4 g) at an $\text{Fe}^{3+}/\text{Fe}^{2+}$ molar ratio of 2:1 were dissolved in deionized water (DI; 100 mL) and heated to 70°C. Ammonium hydroxide (6 mL) was quickly added to the solution, which immediately produced a deep black magnetite precipitate. The suspension was stirred for 30 min at 70°C. The product was washed several times with distilled water, following which the magnetite nanoparticles were

dried in a rotary evaporator at 40°C (25 mbar) until a powder was formed. The powdered nanomaterial was stored in the dark at room temperature prior to modification.

APTS-modified magnetite nanoparticles were prepared according to Ming et al. [34, 35], with minor modification. A 0.0128 M of magnetite solution (25 mL), which was prepared from first experiment, was diluted to 150 mL with ethanol (absolute) and 1 mL DI water. This solution was then treated in an ultrasonic bath (28 kHz at 25°C) for 1 h, whereupon APTS (35 μL) was added and stirred rapidly for 2 h. The resulting liquid was washed with ethanol five times and then dried in a vacuum at room temperature until a powder was formed.

PEG-modified magnetite nanoparticles were prepared by dissolving 1.99 g of $\text{FeCl}_2 \cdot 4\text{H}_2\text{O}$ and 3.24 g of $\text{FeCl}_3 \cdot 6\text{H}_2\text{O}$ in 50 mL of DI water (Beaker I) and 30 mL of ammonium hydroxide in 50 mL of DI water (Beaker II). Subsequently, 2.5 g of PEG 6000 was dissolved in 100 mL of DI water and the liquid stirred at room temperature. The PEG solution (25 mL) was added to both beakers (I and II) and stirred in order to obtain a homogenous solution. The contents of Beaker II were added dropwise to Beaker I until pH 9 was reached. Formation of the magnetic nanoparticles was confirmed through a color change in the solution [36, 37]. The nanoparticles were separated out by centrifuging (28 kHz for 30 minutes) and the resultant precipitate was dried for 24 hours at room temperature. The dried powder was then redissolved in the remaining 50 mL of PEG solution and placed in an ultrasonic bath for about 30 minutes, whereupon it was again centrifuged to obtain the magnetic PEG-nanoparticles, which were then washed several times with DI water and dried to a powder under vacuum at room temperature.

TEOS-modified magnetite nanoparticles were prepared by dispersing approximately 30 mg of freshly prepared magnetite nanoparticles in 30 mL of ethanol and 6 mL of DI water, with the dispersion then being homogenized in an ultrasonic bath (28 kHz at 25°C) for about 10 minutes. TEOS (3.3 mmol) was then added to the mixture and sonicated for a further 20 minutes. Finally, aqueous ammonia (30 mmol) was added and the mixture again was placed in an ultrasonic bath for 60 minutes. The magnetic nanoparticles were magnetically separated and washed several times with DI water and then dried to a powder under vacuum at room temperature [38–41].

2.3. Dispersion of Magnetite Nanoparticles. To assess the effect of functionalized magnetite nanoparticles on bacteria, stock solutions (10 g/L) of unmodified magnetite and APTS-, PEG-, TEOS-modified magnetite nanoparticles were prepared from powdered material (see above) by dispersing in sterilized DI water in a sterile glass tube and vortexing (IKA vortex3, Germany) for five minutes. Each suspension was prepared freshly before testing for toxicity.

2.4. Bacterial Strains and Culture Media. Bacterial strains of Gram-negative *E. coli* CCM 3954 and Gram-positive *S. aureus* CCM 3953 were obtained from the Czech Collection of

Microorganisms, Masaryk University, Brno, Czech Republic. The bacterial inocula were always prepared freshly from a single colony growing overnight in a soya nutrient broth (Sigma Aldrich) at 37°C. The culture was adjusted to 0.01–0.02 optical density (OD) at 600 nm (OD_{600}) using the DR6000 UV-Vis spectrophotometer (Hach Lange, Germany), immediately before performing the antibacterial experiments.

2.5. Bacterial Growth Rate. The freshly prepared bacterial cultures were transferred to 30 mL of soya broth and kept in 200 mL conical flasks. The magnetite suspensions (unmodified and APTS-, PEG-, TEOS-modified) were added to the bacterial culture at a range of final concentrations (0.05, 0.3, 0.6, and 1 g/L), each sample being prepared in replicate. Negative (bacterial cells only in growth media) and positive (magnetic nanoparticles only in growth media) controls were run in parallel. All samples were incubated for six hours at 37°C. Subsamples were taken every two hours for OD_{600} measurement. To prevent cross contamination, each bacterial strain was tested on different days. Oxidative/reductive potential (ORP) and pH were measured during the experiments using a WTW multimeter (Germany).

Effect of nanoparticle concentration on bacterial growth rate (μ) was calculated for each nanoparticle type based on the equation: $I(\%) = (\mu_C - \mu_T) / \mu_C \times 100$, where I is inhibition, μ_C is mean value of growth rate (μ) of the control, and μ_T value is the growth rate of the culture affected by the nanoparticles. The bacterial growth rate was defined by R linear regression of cell density (OD_{600}) versus incubation time (hour). The EC_{10} value (effective concentration at 10% inhibition) was obtained by plotting $I\%$ versus concentration of nanoparticle tested.

2.6. Determination of Colony Forming Units (CFU). Number of *E. coli* and *S. aureus* CFU was determined using the same unmodified and APTS-, PEG-, and TEOS-modified magnetite (1 g/L) samples used for growth rate measurement. The bacterial strains were exposed to the nanoparticles in the dark for six hours at 37°C. Following incubation, 1 mL of the culture was transferred to a sterile agar plate and incubated for 24 h under the same conditions as the liquid cultures. All samples were prepared in duplicate and cultures without nanoparticles were cultivated in growth media as controls.

2.7. Bacterial Cell Morphology. Cell morphology of *E. coli* and *S. aureus* was determined using the same unmodified and APTS-, PEG-, and TEOS-modified magnetite (1 g/L) bacterial samples used for determination of growth rate. Cells with nanoparticles (1 g/L) were stained using 4',6-diamidino-2-phenylindole (DAPI) and observed under an AxioImager fluorescence microscope (Zeiss, Germany) at 365/461 nm excitation/emission. Length of *E. coli* cells was measured for samples with nanoparticles (incubated for six hours) and for a control without nanoparticles.

2.8. Statistical Analysis. All results were analysed using ANOVA (GraphPad Prism software; CA, USA). Dunnett's multicomparison test was used to compare differences

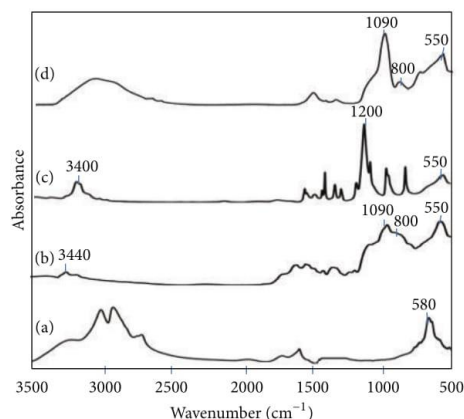


FIGURE 1: Infrared spectroscopic scans of (a) unmodified magnetite nanoparticles, (b) APTS-magnetite, (c) PEG-magnetite, and (d) TEOS-magnetite.

between the means of *E. coli* and *S. aureus* growth rate, while values for CFU and bacterial cell length were compared using Sidak's multicomparison test.

3. Results and Discussion

3.1. Characterization of Magnetic Nanoparticles. In each case, functional groups on the surface of the magnetite nanoparticles were detected by IR (Figure 1), with absorption peak at 580 cm^{-1} confirming the presence of an Fe–O bond related to the magnetite phase of magnetite nanoparticles [42]. Bands at 800 cm^{-1} and 1090 cm^{-1} were due to symmetric and asymmetric linear vibrations of Si–O–Si, indicative of formation of a silica shell with APTS- and TEOS-modified magnetite. The absorption contribution from the free $-\text{NH}_2$ group of APTS-modified magnetite appeared at 3440 cm^{-1} . Absorption bands at 3400 cm^{-1} and 1200 cm^{-1} were assignable to O–H stretching and C–O of PEG-modified magnetite.

DLS indicated that unmodified magnetite nanoparticles display a wider size range than modified magnetite nanoparticles. Presence of an APTS, PEG, or TEOS layer on the nanoparticle surface increased average particle size (Figure 2), with an average increase of 89 nm for unmodified nanoparticles and 123 nm, 109 nm, and 130 nm for APTS-, PEG-, and TEOS-modified magnetite nanoparticles, respectively.

The zeta potential for unmodified magnetite nanoparticles was 36.9 mV and 12.2 mV, 23.1 mV, and 36.2 mV for APTS-, PEG-, and TEOS-modified magnetite nanoparticles, respectively. The nanoparticle's zeta potential (surface charge) indicates how effectively nanoparticles form stable or aggregated colloids during the colloidal phase. At low zeta potentials (close to zero), particles are no longer repelled strongly and colloids will aggregate due to attractive surface forces. Conversely, stable dispersions are formed at high zeta

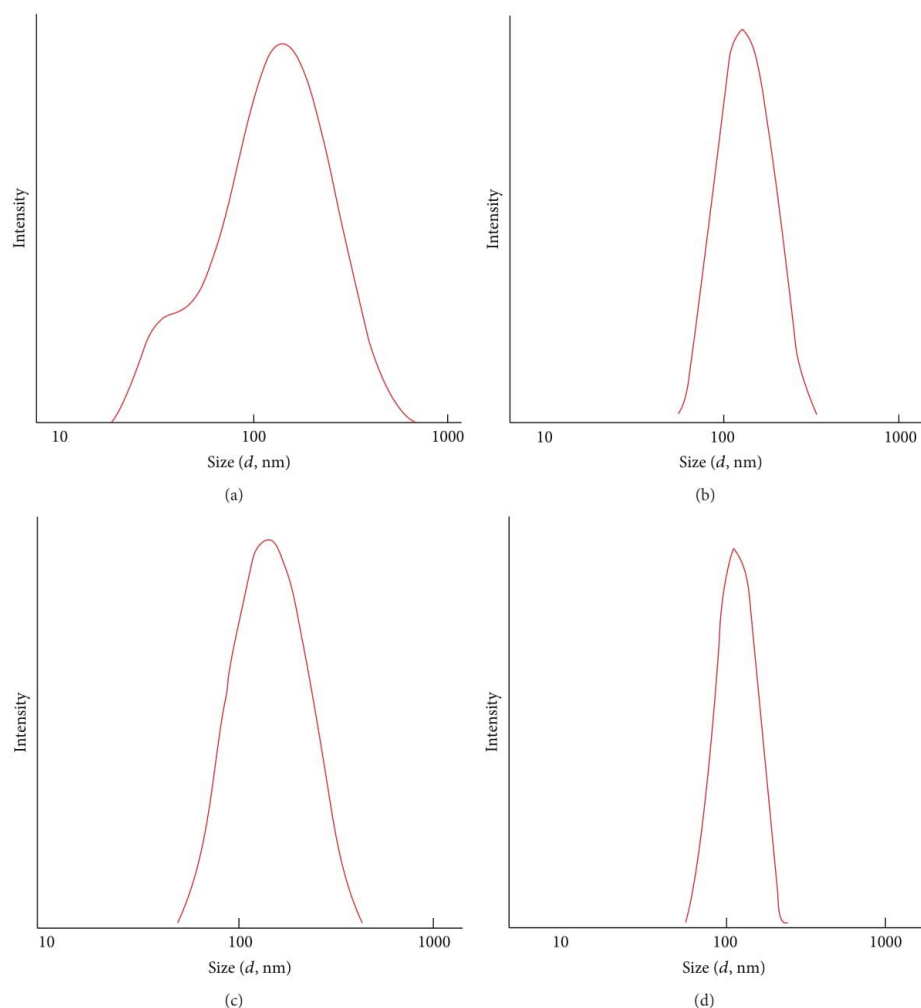


FIGURE 2: Hydrodynamic diameters of (a) unmodified magnetite nanoparticles, (b) APTS-magnetite, (c) PEG-magnetite, and (d) TEOS-magnetite.

potentials (above ~ 30 mV). This is of particular importance in water treatment and biomedicine applications where stable colloidal systems are required.

SEM indicated slight differences in the morphology of unmodified and modified magnetite nanoparticles (Figure 3). Unlike modified magnetite nanoparticles, unmodified nanoparticles, which showed a broader size distribution, were usually agglomerated due to the high surface energy between the nanoparticles and dipole-dipole interactions. In addition, we detected a higher number of modified magnetite nanoparticles, providing further evidence for insertion of a surface layer on the magnetite.

3.2. Effect of Surface-Modified Magnetite on Bacteria. The growth rates of Gram-negative *E. coli* and Gram-positive *S. aureus* control solutions (nutrient broth without nanoparticles) were 0.24 and 0.18 doublings/h, respectively. Unmodified magnetite nanoparticles had no significant effect on the growth rate of either bacteria. Interestingly, however, the growth rates of both bacteria were negatively correlated with suspension concentration (0.05, 0.3, 0.6, and 1 g/L) in APTS-, PEG-, and TEOS-modified nanoparticle solutions (Figure 4).

E. coli growth rate dropped to 0.15 doublings/h when incubated with APTS-magnetite (1 g/L), while growth rates for PEG- and TEOS-magnetite (1 g/L) were 0.22 and

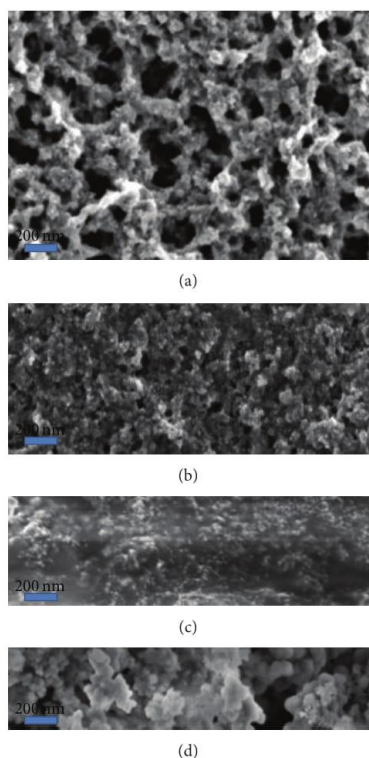


FIGURE 3: Scanning electron microscope images of (a) unmodified magnetite nanoparticles, (b) APTS-magnetite, (c) PEG-magnetite, and (d) TEOS-magnetite. Scale bar = 200 nm.

0.18 doublings/h, respectively. At all concentrations, APTS-magnetite had a greater effect on *E. coli* growth rate than the other modified magnetite nanoparticles (Figure 4). Growth rates of *S. aureus* exposed to APTS-, PEG-, and TEOS-magnetite were 0.09, 0.13, and 0.1 doublings/h, respectively (Figure 4).

The EC10 for growth inhibition on both *E. coli* and *S. aureus* in unmodified and modified nanoparticle solutions indicated that modified nanoparticles had a greater effect on *S. aureus* than *E. coli*, with PEG-magnetite nanoparticles having the least effect on growth rate of either bacteria (Table 1). Both APTS-magnetite and TEOS-magnetite (1 g/L) had a significant negative effect (ANOVA; $P < 0.0001$) on both *E. coli* and *S. aureus* growth.

The effect of modified magnetite on bacterial growth rate was further supported by results obtained from the colony-forming assay. Compared to control samples with no nanoparticles, *E. coli* CFU declined to 73% with APTS-magnetite and 63.6% with TEOS-magnetite, whilst that for *S. aureus* declined to 27% with APTS-magnetite and 38% with TEOS-magnetite, after six hours of exposure (Figure 5). This confirms a similar effect determined for growth rate in both

TABLE 1: The effective concentration at 10% inhibition, EC10 (g/L) of unmodified and modified magnetite nanoparticles determined for Gram-negative *Escherichia coli* and Gram-positive *Staphylococcus aureus*.

	Unmodified magnetite	APTS-magnetite	PEG-magnetite	TEOS-magnetite
<i>E. coli</i>	0.60	0.170	0.509	0.325
<i>S. aureus</i>	NOEC < 1	0.108	0.259	0.128

bacterial strains. Comparison of viable cells using ANOVA indicated that APTS-magnetite had a greater impact on *S. aureus* ($P = 0.0019$) than TEOS-magnetite ($P = 0.0086$). On the other hand, both APTS- and TEOS-magnetite had no significant effect on *E. coli* ($P = 0.2$ and $P = 0.13$).

In order to elucidate these results further, we compared bacterial cell morphology using fluorescence microscopy after DAPI staining. Notably, *E. coli* showed rapid cell elongation ($3.8 \pm 0.12 \mu\text{m}$ to $6.5 \pm 0.5 \mu\text{m}$ after six hours; $P = 0.0001$) when exposed to APTS-magnetite in soya broth media (Figure 6). Moreover, *E. coli* cells were clearly attached to the APTS-magnetite particles while the grape-like clusters of *S. aureus* were irregularly grouped with more single cells than cell clusters.

3.3. Factors Affecting Biological Stress. Our results indicate that APTS-, TEOS-, and PEG-magnetite nanoparticles had a significantly greater biological effect on *S. aureus* than on *E. coli*. Many variables may impact on biological effect, including both biological (e.g., bacterial cell structure, cell growth rate, biofilm formation, stress/toxicity mechanisms) and chemical parameters (e.g., pH, ORP). Bacterial cell walls (peptidoglycan layers) are designed to protect the intracellular matrix while allowing for nutrient transport. In doing so they help to maintain the structural strength of the cell and stabilize the osmotic pressure of the cytoplasm and they are involved in binary fission during bacterial cell reproduction [43, 44]. Gram-positive cells possess a thick peptidoglycan layer of 20–50 nm [45], while Gram-negative cells contain a thin peptidoglycan layer. Notably, in our study, *E. coli* cells in contact with APTS-magnetite were unable to divide as the cells had increased in length from $3.8 \mu\text{m}$ to $6.5 \mu\text{m}$. Further, Gram-negative cell walls comprise an outer membrane, which covers the surface membrane and is often resistant to compounds such as detergents, and a lipopolysaccharide layer, which is essential for cell viability and contributes to the negative charge of the membrane [46]. An increased negative surface charge could reduce the likelihood of *E. coli* interacting with nanoparticles, as reflected in the lowered effect on Gram-positive *S. aureus* in this study.

Bacterial growth rate is a good method for indicating tolerance of bacteria to nanoparticles. Fast-growing bacteria, for example, are more susceptible to antibiotics and nanoparticles than slow-growing bacteria [47, 48]. The hindered growth observed in *E. coli* and *S. aureus* in this study could be related to expression of stress-response genes [49, 50]. Gram-positive bacteria have the ability to form a biofilm to protect

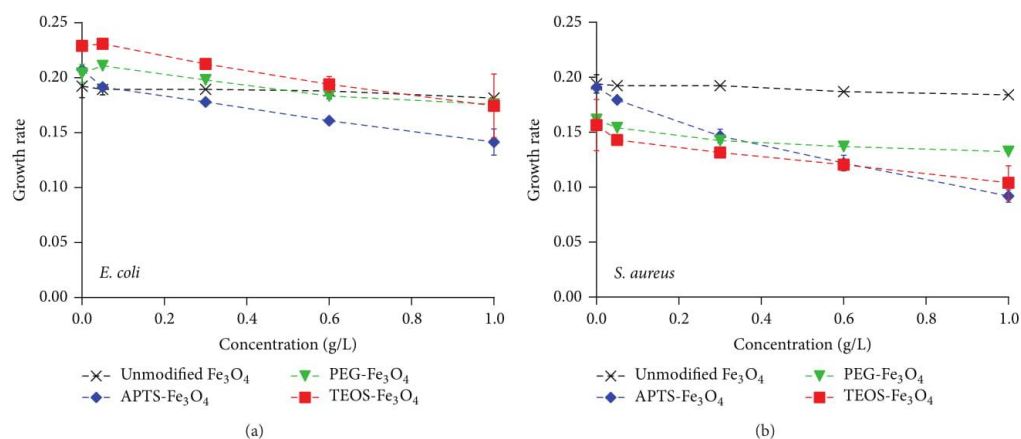


FIGURE 4: Growth rate (doublings/h) of *Escherichia coli* (a) and *Staphylococcus aureus* (b) after six hours of incubation with unmodified and modified APTS-, PEG-, and TEOS-magnetite. The error bars were determined from $n = 2$.

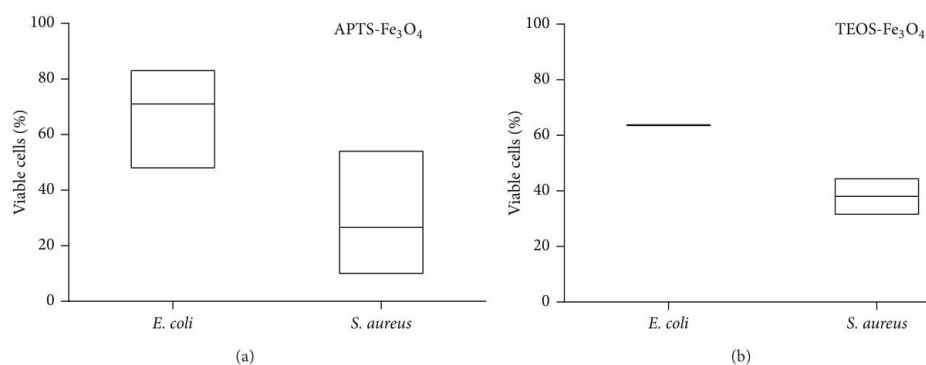


FIGURE 5: Proportion of viable cells (colony forming units) after six hours of exposure to 1 g/L APTS-magnetite (a) and 1 g/L TEOS-magnetite (b) comparing to control (without nanoparticles) = 100%.

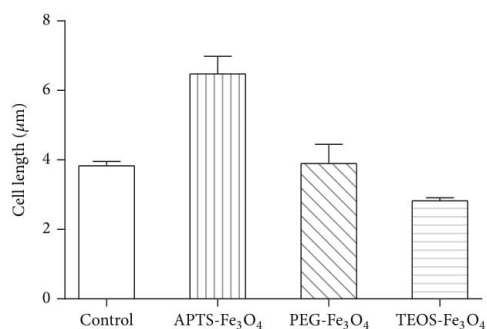


FIGURE 6: Length of *Escherichia coli* cells after six hours of exposure to surface-modified magnetite nanoparticles. The error bars show standard error of the mean.

themselves under stressful conditions (*Pseudomonas* sp., e.g., develop a biofilm in the presence of heavy metals) [51]. In our study, Gram-positive *S. aureus* aggregated into large grape-like clusters after six hours of incubation with unmodified and APTS-, TEOS-, and PEG-modified magnetite. Previous studies have also reported that magnetite nanoparticles have a considerable capacity to penetrate biofilms [52, 53]. By interacting with the outer membrane, nanoparticles may cause loss of membrane integrity in bacteria and change the cell's structure. Such damage could lead to an increase in membrane permeability and leakage of intracellular constituents [54–56] and, indirectly, generate reactive oxidation species (ROS) through the Fenton reaction [57]. Zero-valent iron, for example, causes cell membrane disruption in *E. coli* [54] and adsorption on cells and ROS generation in *Bacillus subtilis* var. *niger* and *Pseudomonas fluorescens* [58]. In this study, magnetite nanoparticles are likely to have created

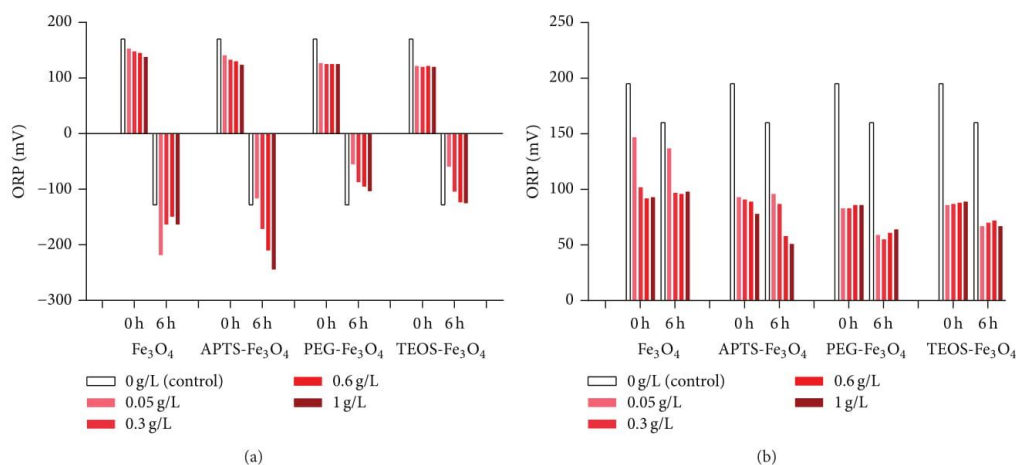


FIGURE 7: Oxidation/reduction potential (ORP) of (a) *Escherichia coli* and (b) *Staphylococcus aureus* cultures at time zero and after six hours of incubation with modified magnetite nanoparticles.

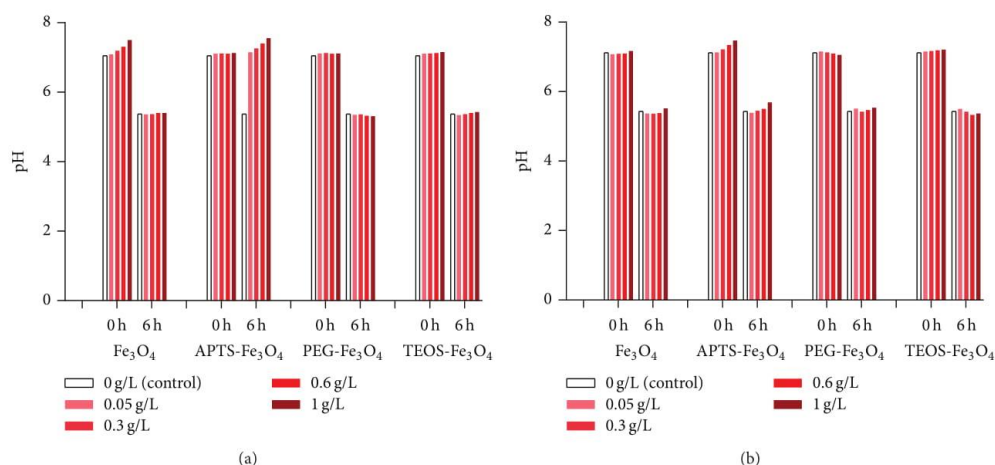


FIGURE 8: pH values for *Escherichia coli* (a) and *Staphylococcus aureus* (b) cultures at time zero and after six hours of incubation with modified magnetite nanoparticles.

stressful conditions via ROS generation, which significantly inhibited *S. aureus* growth. Additionally, pH values obtained in parallel with bacterial growth experiments at the start and end of the experiment were similar to those of the controls (*E. coli* or *S. aureus* culture alone), with initial pH being neutral and dropping to around pH 5 after six hours, with or without the presence of magnetic nanoparticles (Figure 7). Only in the case of *E. coli* cultured with APTS-magnetite did the neutral pH remain unchanged after six hours, remaining within the optimum pH range of 6-7 for *E. coli* growth [59]. Furthermore, the negative ORP of *E. coli* and positive ORP of *S. aureus* both showed similar trends in both treated and untreated cultures (Figure 8). In our biological effect tests, therefore, pH and ORP could not be considered

as indicators for stressed bacterial states (Figures 7 and 8).

In summary, magnetite nanoparticles surface-functionalized with APTS and TEOS had a significant biological effect on Gram-positive *S. aureus*, while PEG-nanoparticles did not. In contrast, none of the functionalized magnetite nanoparticles showed any statistically significant effect on Gram-negative *E. coli*.

4. Conclusion

Functionalized modified magnetite nanoparticles (TEOS-, PEG-, and APTS-magnetite) were prepared using coprecipitation and characterized with SEM and IR. Testing for

biological effect indicated that PEG-magnetite can be considered as safe nontoxic material. TEOS-magnetite showed stronger effect only towards *S. aureus*. APTS-magnetite nanoparticles display a degree of antimicrobial activity, allowing for their use in bioapplications such as drug nanocarriers, where bacterial growth is undesirable.

Conflict of Interests

The authors declare that there is no conflict of interests regarding the publication of this paper.

Acknowledgments

The results of this project (LO1201) were obtained through the financial support of the Ministry of Education, Youth and Sports under the framework of targeted support from the “National Programme for Sustainability I”, the OPR&DI project Centre for Nanomaterials, Advanced Technologies and Innovation (CZ.1.05/2.1.00/01.0005), and “Project Development for Research Teams of R&D Projects” at the Technical university of Liberec (CZ.1.07/2.3.00/30.0024).

References

- [1] S. Mondini, S. Cenedese, G. Marinoni et al., “One-step synthesis and functionalization of hydroxyl-decorated magnetite nanoparticles,” *Journal of Colloid and Interface Science*, vol. 322, no. 1, pp. 173–179, 2008.
- [2] K. G. Paul, T. B. Frigo, J. Y. Groman, and E. V. Groman, “Synthesis of ultrasmall superparamagnetic iron oxides using reduced polysaccharides,” *Bioconjugate Chemistry*, vol. 15, no. 2, pp. 394–401, 2004.
- [3] J. Namanga, J. Foba, D. T. Ndinteh, D. M. Yufanyi, and R. W. M. Krause, “Synthesis and magnetic properties of a superparamagnetic nanocomposite ‘pectin-magnetite nanocomposite,’” *Journal of Nanomaterials*, vol. 2013, Article ID 137275, 8 pages, 2013.
- [4] C. C. Gonzalez, C. A. M. Pérez, A. M. Martínez et al., “Development of antibody-coated magnetite nanoparticles for biomarker immobilization,” *Journal of Nanomaterials*, vol. 2014, Article ID 978284, 7 pages, 2014.
- [5] X. Cao, B. Zhang, F. Zhao, and L. Feng, “Synthesis and properties of MPEG-coated superparamagnetic magnetite nanoparticles,” *Journal of Nanomaterials*, vol. 2012, Article ID 607296, 6 pages, 2012.
- [6] D. K. Yi, S. S. Lee, and J. Y. Ying, “Synthesis and applications of magnetic nanocomposite catalysts,” *Chemistry of Materials*, vol. 18, no. 10, pp. 2459–2461, 2006.
- [7] D. K. Yi, S. S. Lee, G. C. Papaefthymiou, and J. Y. Ying, “Nanoparticle architectures templated by SiO₂/Fe₃O₄ nanocomposites,” *Chemistry of Materials*, vol. 18, no. 3, pp. 614–619, 2006.
- [8] D. C. Lee, F. V. Mikulec, J. M. Pelaez, B. Koo, and B. A. Korgel, “Synthesis and magnetic properties of silica-coated FePt nanocrystals,” *Journal of Physical Chemistry B*, vol. 110, no. 23, pp. 11160–11166, 2006.
- [9] C. R. Vestal and Z. J. Zhang, “Synthesis and magnetic characterization of Mn and Co spinel ferrite-silica nanoparticles with tunable magnetic core,” *Nano Letters*, vol. 3, no. 12, pp. 1739–1743, 2003.
- [10] T.-J. Yoon, K. N. Yu, E. Kim et al., “Specific targeting, cell sorting, and bioimaging with smart magnetic silica core-shell nanomaterials,” *Small*, vol. 2, no. 2, pp. 209–215, 2006.
- [11] S. M. Moghimi, A. C. Hunter, and J. C. Murray, “Long-circulating and target-specific nanoparticles: theory to practice,” *Pharmacological Reviews*, vol. 53, no. 2, pp. 283–318, 2001.
- [12] W. Wu, Q. He, and C. Jiang, “Magnetic iron oxide nanoparticles: synthesis and surface functionalization strategies,” *Nanoscale Research Letters*, vol. 3, no. 11, pp. 397–415, 2008.
- [13] H. Xuemei and Y. Hao, “Fabrication of polystyrene/detonation nanographite composite microspheres with the core/shell structure via pickering emulsion polymerization,” *Journal of Nanomaterials*, vol. 2013, Article ID 751497, 8 pages, 2013.
- [14] R. T. Yang, *Adsorbents: Fundamentals and Applications*, John Wiley & Sons, 2003.
- [15] W. Zhao, J. Gu, L. Zhang, H. Chen, and J. Shi, “Fabrication of uniform magnetic nanocomposite spheres with a magnetic core/mesoporous silica shell structure,” *Journal of the American Chemical Society*, vol. 127, no. 25, pp. 8916–8917, 2005.
- [16] S. D. Steichen, M. Calderera-Moore, and N. A. Peppas, “A review of current nanoparticle and targeting moieties for the delivery of cancer therapeutics,” *European Journal of Pharmaceutical Sciences*, vol. 48, no. 3, pp. 416–427, 2013.
- [17] D. D. Herea and H. Chiriac, “One-step preparation and surface activation of magnetic iron oxide nanoparticles for bio-medical applications,” *Optoelectronics and Advanced Materials—Rapid Communications*, vol. 2, no. 9, pp. 549–552, 2008.
- [18] J. Wang, S. Zheng, Y. Shao, J. Liu, Z. Xu, and D. Zhu, “Amino-functionalized Fe₃O₄@SiO₂ core-shell magnetic nanomaterial as a novel adsorbent for aqueous heavy metals removal,” *Journal of Colloid and Interface Science*, vol. 349, no. 1, pp. 293–299, 2010.
- [19] H. Hu, Z. Wang, and L. Pan, “Synthesis of monodisperse Fe₃O₄@silica core-shell microspheres and their application for removal of heavy metal ions from water,” *Journal of Alloys and Compounds*, vol. 492, no. 1–2, pp. 656–661, 2010.
- [20] A. K. Gupta and S. Wells, “Surface-modified superparamagnetic nanoparticles for drug delivery: preparation, characterization, and cytotoxicity studies,” *IEEE Transactions on Nanobioscience*, vol. 3, no. 1, pp. 66–73, 2004.
- [21] M. S. A. Darwish, U. Peuker, U. Kunz, and T. Turek, “Bilayered polymer-magnetite core/shell particles: synthesis and characterization,” *Journal of Materials Science*, vol. 46, no. 7, pp. 2123–2134, 2011.
- [22] M. S. A. Darwish, U. Kunz, and U. Peuker, “Preparation and catalytic use of platinum in magnetic core/shell nanocomposites,” *Journal of Applied Polymer Science*, vol. 129, no. 4, pp. 1806–1811, 2013.
- [23] W. Stöber, A. Fink, and E. Bohn, “Controlled growth of monodisperse silica spheres in the micron size range,” *Journal of Colloid and Interface Science*, vol. 26, no. 1, pp. 62–69, 1968.
- [24] Y. Lu, Y. Yin, B. T. Mayers, and Y. Xia, “Modifying the surface properties of superparamagnetic iron oxide nanoparticles through a sol-gel approach,” *Nano Letters*, vol. 2, no. 3, pp. 183–186, 2002.
- [25] M. Mahmoudi, M. A. Shokrgozar, S. Sardari et al., “Irreversible changes in protein conformation due to interaction with superparamagnetic iron oxide nanoparticles,” *Nanoscale*, vol. 3, no. 3, pp. 1127–1138, 2011.
- [26] J. Raheb, M. E. Kafayati, M. T. Angazi, S. Alizadeh, and H. Bardania, “The effect of magnetic Fe₃O₄ nanoparticles on the growth of genetically manipulated bacterium, *Pseudomonas*

- aeruginosa (PTSOX4)," *Iranian Journal of Biotechnology*, vol. 11, no. 1, pp. 41–46, 2013.
- [27] E. N. Taylor and T. J. Webster, "The use of superparamagnetic nanoparticles for prosthetic biofilm prevention," *International journal of nanomedicine*, vol. 4, pp. 145–152, 2009.
- [28] N. Tran, A. Mir, D. Mallik, A. Sinha, S. Nayar, and T. J. Webster, "Bactericidal effect of iron oxide nanoparticles on *Staphylococcus aureus*," *International Journal of Nanomedicine*, vol. 5, no. 1, pp. 277–283, 2010.
- [29] M. Senthil and C. Ramesh, "Biogenic synthesis of Fe₃O₄ nanoparticles using tridax procumbens leaf extract and its antibacterial activity on *Pseudomonas aeruginosa*," *Digest Journal of Nanomaterials and Biostructures*, vol. 7, no. 4, pp. 1655–1661, 2012.
- [30] S. S. Behera, J. K. Patra, K. Pramanik, N. Panda, and H. Thatoi, "Characterization and evaluation of antibacterial activities of chemically synthesized iron oxide nanoparticles," *World Journal of Nano Science and Engineering*, vol. 2, pp. 196–200, 2012.
- [31] S. L. Iconaru, A. M. Prodan, P. Le Coustumer, and D. Predoi, "Synthesis and antibacterial and antibiofilm activity of iron oxide glycerol nanoparticles obtained by coprecipitation method," *Journal of Chemistry*, vol. 2013, Article ID 412079, 6 pages, 2013.
- [32] B. Stephen Inbaraj, T.-Y. Tsai, and B.-H. Chen, "Synthesis, characterization and antibacterial activity of superparamagnetic nanoparticles modified with glycol chitosan," *Science and Technology of Advanced Materials*, vol. 13, no. 1, Article ID 015002, 2012.
- [33] D. E. Mihaiescu, M. Horja, I. Gheorghie et al., "Water soluble magnetite nanoparticles for antimicrobial drugs delivery," *Letters in Applied NanoBioScience*, vol. 1, pp. 45–49, 2012.
- [34] M. Ming, Y. Zhang, W. Yu, H.-Y. Shen, H.-Q. Zhang, and N. Gu, "Preparation and characterization of magnetite nanoparticles coated by amino silane," *Colloids and Surfaces A: Physicochemical and Engineering Aspects*, vol. 212, no. 2–3, pp. 219–226, 2003.
- [35] A. M. Demin, M. A. Uimin, N. N. Shchegoleva, A. E. Yermakov, and V. P. Krasnov, "Surface modification of Fe₃O₄ magnetic nanoparticles with (S)-naproxen," *Nanotechnologies in Russia*, vol. 7, no. 3–4, pp. 132–139, 2012.
- [36] S. A. Jayanthi, D. Sukanya, A. J. Pragasam, and P. Sagayaraj, "The influence of PEG 20,000 concentration on the size control and magnetic properties of functionalized bio-compatible magnetic nanoparticles," *Der Pharma Chemica*, vol. 5, pp. 90–102, 2013.
- [37] J. Sun, S. Zhou, P. Hou et al., "Synthesis and characterization of biocompatible Fe₃O₄ nanoparticles," *Journal of Biomedical Materials Research Part A*, vol. 80, no. 2, pp. 333–341, 2007.
- [38] S. C. Pang, S. Y. Kho, and S. F. Chin, "Fabrication of magnetite/silica/Titania core-shell nanoparticles," *Journal of Nanomaterials*, vol. 2012, Article ID 427310, 6 pages, 2012.
- [39] H.-S. Yang, S.-Y. Choi, S.-H. Hyun, H.-H. Park, and J.-K. Hong, "Ambient-dried low dielectric SiO₂ aerogel thin film," *Journal of Non-Crystalline Solids*, vol. 221, no. 2–3, pp. 151–156, 1997.
- [40] M. Mahdavi, M. B. Ahmad, M. J. Haron, Y. Gharayebi, K. Shameli, and B. Nadi, "Fabrication and characterization of SiO₂/(3-aminopropyl)triethoxysilane-coated magnetite nanoparticles for lead(II) removal from aqueous solution," *Journal of Inorganic and Organometallic Polymers and Materials*, vol. 23, no. 3, pp. 599–607, 2013.
- [41] K. D. Kim, S. S. Kim, Y. Choa, and H. T. Kim, "Formation and surface modification of Fe₃O₄ nanoparticles by co-precipitation and sol-gel method," *J. Ind. Eng. Chem*, vol. 13, no. 7, pp. 1137–1141, 2007.
- [42] P. E. García Casillas, C. A. Rodriguez Gonzalez, and C. A. Martínez Pérez, *Infrared Spectroscopy of Functionalized Magnetic Nanoparticles, Infrared Spectroscopy—Materials Science, Engineering and Technology*, edited by T. Theophile, 2012.
- [43] J. R. Scott and T. C. Barnett, "Surface proteins of gram-positive bacteria and how they get there," *Annual Review of Microbiology*, vol. 60, pp. 397–423, 2006.
- [44] F. Van den Ent, L. A. Amos, and J. Löwe, "Prokaryotic origin of the actin cytoskeleton," *Nature*, vol. 413, no. 6851, pp. 39–44, 2001.
- [45] F. van den Ent, C. M. Johnson, L. Persons, P. de Boer, and J. Löwe, "Bacterial actin MreB assembles in complex with cell shape protein RodZ," *The EMBO Journal*, vol. 29, no. 6, pp. 1081–1090, 2010.
- [46] I. S. Roberts, "The biochemistry and genetics of capsular polysaccharide production in bacteria," *Annual Review of Microbiology*, vol. 50, pp. 285–315, 1996.
- [47] M. R. W. Brown, D. G. Allison, and P. Gilbert, "Resistance of bacterial biofilms to antibiotics: a growth-rate related effect?" *Journal of Antimicrobial Chemotherapy*, vol. 22, no. 6, pp. 777–780, 1988.
- [48] T.-F. C. Mah and G. A. O'Toole, "Mechanisms of biofilm resistance to antimicrobial agents," *Trends in Microbiology*, vol. 9, no. 1, pp. 34–39, 2001.
- [49] C. Lu, M. J. Brauer, and D. Botstein, "Slow growth induces heat-shock resistance in normal and respiratory-deficient yeast," *Molecular Biology of the Cell*, vol. 20, no. 3, pp. 891–903, 2009.
- [50] P. S. Stewart, "Mechanisms of antibiotic resistance in bacterial biofilms," *International Journal of Medical Microbiology*, vol. 292, no. 2, pp. 107–113, 2002.
- [51] C.-C. Chien, B.-C. Lin, and C.-H. Wu, "Biofilm formation and heavy metal resistance by an environmental *Pseudomonas* sp," *Biochemical Engineering Journal*, vol. 78, pp. 132–137, 2013.
- [52] M. Mahmoudi and V. Serpooshan, "Silver-coated engineered magnetic nanoparticles are promising for the success in the fight against antibacterial resistance threat," *ACS Nano*, vol. 6, no. 3, pp. 2656–2664, 2012.
- [53] H. Park, H.-J. Park, J. A. Kim et al., "Inactivation of *Pseudomonas aeruginosa* PA01 biofilms by hyperthermia using superparamagnetic nanoparticles," *Journal of Microbiological Methods*, vol. 84, no. 1, pp. 41–45, 2011.
- [54] M. Auffan, W. Achouak, J. Rose et al., "Relation between the redox state of iron-based nanoparticles and their cytotoxicity toward *Escherichia coli*," *Environmental Science & Technology*, vol. 42, no. 17, pp. 6730–6735, 2008.
- [55] D. B. Zorov, C. R. Filburn, L. O. Klotz, J. L. Zweier, and S. J. Sollott, "Reactive oxygen species (ROS)-induced ROS release: a new phenomenon accompanying induction of the mitochondrial permeability transition in cardiac myocytes," *The Journal of Experimental Medicine*, vol. 192, no. 7, pp. 1001–1014, 2000.
- [56] D. B. Zorov, M. Juhaszova, and S. J. Sollott, "Mitochondrial ROS-induced ROS release: an update and review," *Biochimica et Biophysica Acta*, vol. 1757, no. 5–6, pp. 509–517, 2006.
- [57] A. Ševců, Y. S. El-Temsah, E. J. Joner, and M. Černík, "Oxidative stress induced in microorganisms by zero-valent iron nanoparticles," *Microbes and Environments*, vol. 26, no. 4, pp. 271–281, 2011.

- [58] M. Diao and M. Yao, "Use of zero-valent iron nanoparticles in inactivating microbes," *Water Research*, vol. 43, no. 20, pp. 5243–5251, 2009.
- [59] P. M. Desmarchelier and N. Fegan, "Enteropathogenic *Escherichia coli*," in *Foodborne Microorganisms of Public Health Significance*, A. D. Hocking, Ed., chapter 9, pp. 267–310, Australian Institute of Food Science and Technology (NSW Branch), Sydney, Australia, 6th edition, 2003.

Paper 7 (Technical report in NanoREM project)

Claire Coutris, **Nhung H. A. Nguyen** and Rune Hjorth (2015). Environmental impact of reactive nanoparticles - Dose response relationships, Matrix effects on Ecotox. Report number: EU 7th FP NanoRem, Project Nr. 309517, Deliverable 5.1. NANOREM - Nanotechnology for Contaminated Land Remediation.



**Taking Nanotechnological Remediation Processes
from Lab Scale to End User Applications
for the Restoration of a Clean Environment**

Project Nr.: 309517
EU, 7th FP, NMP.2012.1.2

**WP5:
Environmental Impact of Reactive Nanoparticles**

**DL-5.1:
Dose reponse relationships, Matrix effects
on Ecotox**

Claire Coutris, Nhung Nguyen, Rune Hjorth

May 29, 2015



[Downloaded from www.nanorem.eu/toolbox](http://www.nanorem.eu/toolbox)

The research leading to these results has received funding from the European Union Seventh Framework Programme (FP7/2007-2013) under grant agreement n° [309517]

Table of Contents

Executive summary	1
1 Introduction	2
2 Ecotoxicity test protocols	2
2.1 <i>Ecotoxicity tests on aquatic species</i>	2
2.1.1 Algal growth test (OECD 201)	2
2.1.2 Algal assimilation test	3
2.1.3 Algal photosynthesis efficiency test	3
2.1.4 Daphnia immobilization test (OECD 202)	4
2.1.5 Lumbriculus variegatus mortality test	4
2.2 <i>Ecotoxicity tests on bacteria</i>	4
2.2.1 Bacterial luminescence bioassay (ISO 11348-3)	4
2.2.2 Escherichia coli growth test	4
2.2.3 Escherichia coli viability cell test	5
2.2.4 Clostridium perfringens growth test	5
2.3 <i>Ecotoxicity tests on soil species</i>	5
2.3.1 Earthworm survival test (OECD 207)	5
2.3.2 Seed germination and root elongation test (OECD 208)	6
3 Test materials: sample preparation for toxicity testing	7
3.1 <i>Particles from WP2</i>	7
3.1.1 NanoFer STAR (Nanolron)	7
3.1.2 Nano-magnetite (UPOL)	7
3.1.3 Milled Fe particles (UVR-FIA)	7
3.2 <i>Particles from WP3</i>	7
3.2.1 Nano-goethite (HMGU)	7
3.2.2 Fe zeolite (UFZ)	8
3.2.3 Carbo-Iron and associated (UFZ)	8
3.2.4 Bio-nanomagnetite (UMAN)	8
4 Methods for characterization of exposure suspensions	9
4.1 <i>Hydrodynamic diameter, size distribution and zeta-potential</i>	9
4.2 <i>Oxidation reduction potential and pH</i>	9
4.3 <i>Total iron concentration</i>	9
4.4 <i>Electron microscopy</i>	9
5 Results	10
5.1 <i>Results for direct exposure to organisms</i>	10
5.1.1 NanoFer STAR (Nanolron)	10
5.1.2 Nano-magnetite (UPOL)	16

5.1.3	Milled Fe particles (UVR-FIA).....	18
5.1.4	Nano-goethite (HMGU).....	25
5.1.5	Fe zeolite (UFZ).....	31
5.1.6	Carbo-Iron and associated (UFZ).....	37
5.1.7	Bio-nanomagnetite (UMAN)	39
5.2	<i>Matrix effects on Ecotox</i>	39
5.2.1	Bacterial growth test	40
5.2.2	Algal assimilation test.....	42
6	Conclusions	43
7	List of References	43

5.2.1 Bacterial growth test

Characterization of the exposure media

The zeta potential of milled Fe particles KKM 14 and positive control nZVI are presented in Figure 33; the average hydrodynamic diameter (by Dynamic Light Scattering, DLS) in Figure 34, and the average particles size (by Differential Centrifugal Sedimentation, DCS) in Figure 35.

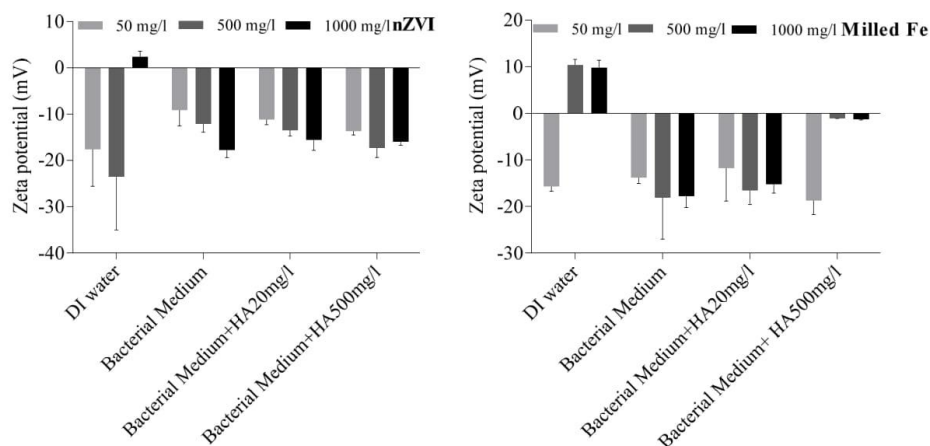


Figure 33 Zeta potential (mV) of positive control nZVI (left) and milled Fe particles (right) suspended in DI water, bacterial medium and bacterial medium with humic acids (20 and 500 mg/L). Each measurement was done in triplicated runs.

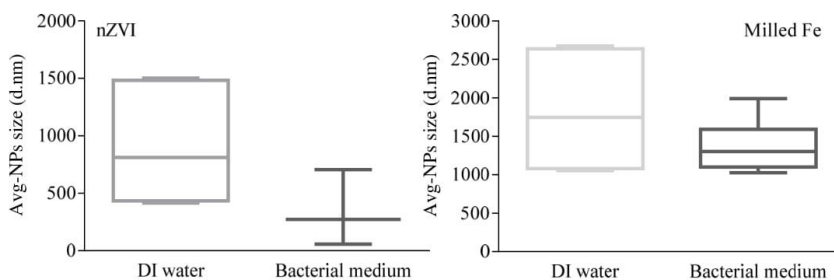


Figure 34 Average hydrodynamic diameter (determined by DLS) of positive control nZVI (left) and milled Fe particles (right) suspended in DI water and bacterial medium. Each measurement was done in triplicated runs.

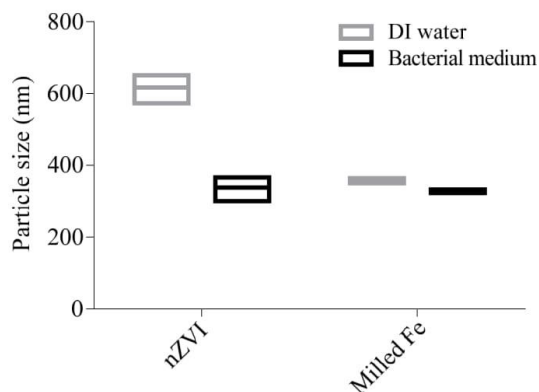


Figure 35 Average particle size (determined by DCS) of positive control nZVI (left) and milled Fe particles (right) suspended in DI water and bacterial medium. Each measurement was done in triplicated runs.

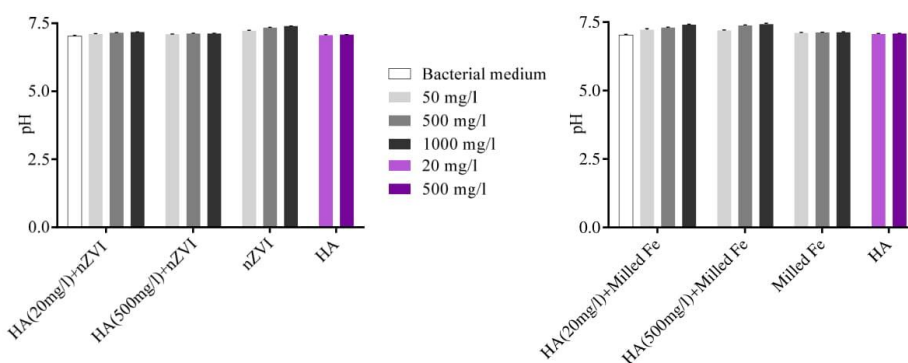


Figure 36 pH values of positive control nZVI (left) and milled Fe particles (right) suspended in bacterial growth medium, with and without humic acids (HA).

Bacterial growth test results

The growth rate of anaerobic bacteria *C. perfringens* exposed to milled Fe particles or positive control nZVI in presence/absence of humic acid was followed over a 24h period. No change in toxicity was observed in the presence of humic acid (Fig. 37). The positive control nZVI was more toxic to *C. perfringens* than the milled Fe particles, as expected.

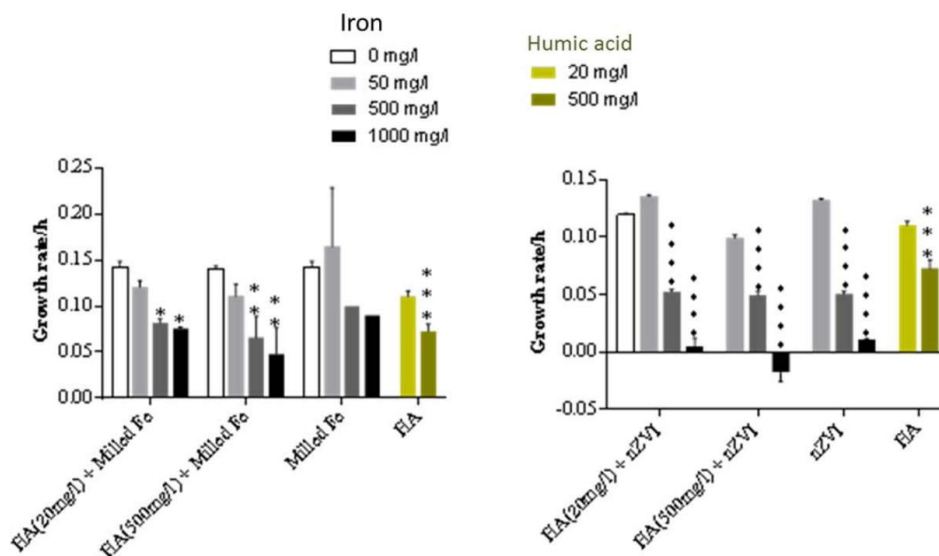


Figure 37 Growth rate of *C. perfringens* after 24h exposure to milled Fe particles (left) and positive control nZVI (right) in the presence/absence of humic acid (HA).

5.2.2 Algal assimilation test

Characterization of the exposure media

Determination of particle size distribution, hydrodynamic diameter and zeta potential of the milled Fe particles and the positive control nZVI suspended in algal media (ISO 8692, 2012) with and without 20 mg/L humic acid (Suwannee river NOM) was attempted by DLS. It revealed that all particle suspensions had a very broad size distribution with polydispersity indexes around 1, which undermines the use of DLS measurements.

Algal assimilation test results

In general, no change in toxicity was observed with or without the addition of humic acid, as the tested particles did not significantly inhibit the biomass assimilation of ^{14}C compared to controls (data not shown). On the contrary, most tested concentrations of both particles with and without humic acid showed higher rates of assimilation than controls, as the abundance of iron can be a stimulating factor for photosynthesis.

6 Conclusions

The results of ecotoxicity tests using the particles developed during the first two years of the project did not show any toxicity to organisms. The only exception was the milled Fe particles KKM 03-06. However, bacterial and algal tests performed on another (newer) batch of milled Fe particles (batch KKM 14) did not show the same high toxicity as found with batch KKM 03-06. The producer UVR-FIA told us that these batches were supposed to be similar, since they were produced following the same protocol. The reasons for the difference in toxicity between the two batches are therefore still unknown.

The low toxicities found in the standard organisms do not lead to any hazard classification according to EU regulation for any of the tested particles and the results indicate that the particles, except the milled ZVI particles, can be considered non-toxic.

In the absence of intrinsic toxicity of most of the particles, the second part of the deliverable was limited to tests on milled Fe particles. The presence of humic acid did not change the outcome of the ecotox tests, contrary to what was expected.

7 List of References

- ISO (2007). ISO 11348-3. Water quality - determination of the inhibitory effect of water samples on the light emission of *Vibrio fischeri* (luminescent bacteria test), Geneva, Switzerland.
- ISO (2012). ISO 8692. Water quality - Fresh water algal growth inhibition test with unicellular green algae, Geneva, Switzerland.
- Water quality -- Fresh water algal growth inhibition test with unicellular green algae
- Lien HL and Zhang WX (2001). Nanoscale iron particles for complete reduction of chlorinated ethenes. *Colloid and Surfaces A*, 191:97-105.
- Mayer P, Cuhel R, Nyholm N (1997). A simple in vitro fluorescence method for biomass measurements in algal growth inhibition. *Water Research*, 31(10):2525-2531
- OECD (1984). OECD guideline 207 for testing of chemicals. Earthworm, acute toxicity tests. Paris, France.
- OECD (2004). OECD guideline 202 for testing of chemicals. *Daphnia sp.*, Acute Immobilisation. Paris, France.
- OECD (2006). OECD guideline 208 for testing of chemicals. Terrestrial Plant Test: Seedling Emergence and Seedling Growth Test. Paris, France.
- OECD (2008). OECD guideline 315 for testing of chemicals. Bioaccumulation in Sediment-dwelling Benthic Oligochaetes. Paris, France.
- OECD (2011). OECD guideline 201 for testing of chemicals. Freshwater Alga and Cyanobacteria, Growth Inhibition. Paris, France.
- Raghupathi KR, Koodali RT, Manna AC. (2011). Size-dependent bacterial growth inhibition and mechanism of antibacterial activity of zinc oxide nanoparticles. *Langmuir*, 27(7):4020-8.
- Sørensen SN and Baun A. (2014). Controlling silver nanoparticle exposure in algal toxicity testing - A matter of timing. *Nanotoxicology*, 5390:1-9.
- USEPA (1996). OPPTS 850.4200 Seed Germination/Root Elongation Toxicity Test. USA.

7. Conclusions

This work aimed to establish and evaluate different methods to study the biological effect of iron-based NMs/NPs. This included basic as well as advance methods, namely: optical density (OD), cultivation, fluorescence microscopy, comet assay, optical microscopy, fluorometry (QY), flow cytometry and next-generation sequencing. A multiple-endpoint approach is recommended to reliably evaluate the biological effect of the tested materials. It is also fruitful to study a wider range of representative (micro)organisms to obtain a broad view of material toxicity. Moreover, the physical interaction effects should be clearly included in studies of toxic mechanisms. The bacterial or algal growth rate endpoint was commonly used when following other biological effects (cell length, biofilm formation, membrane integrity, ROS generation, DNA damage). Importantly, the interfering factors caused by iron materials should be taken into account, e.g. colour, aggregation and sedimentation. It is recommended that the toxicity assessment should be set up in relevant concentrations and target application conditions.

The toxicity study on single prokaryotic strains found that Gram-positive *S. aureus* was more sensitive to the tested functionalized Fe₃O₄ NMs/NPs compared to Gram-negative *E. coli* using multiple endpoints such as growth rate, cell length, biofilm formation, as well as DNA damage. *S. aureus* biofilm formation was inhibited by PEI-Fe₃O₄ while it was formed in the presence of PNIPAAm and PNIPAAm-3. *E. coli* cell length was prolonged by APTS-Fe₃O₄ and Fe₃O₄-PNIPAAm-3. The magnetic NPs coated with APTS and PEI had an antibacterial potential. The Fe₃O₄-PNIPAAm was synthesised by an emulsion polymerisation method and displayed a strong antibacterial property.

Gram-positive *C. perfringens* was exposed to ZVI in anaerobic conditions, which was similar to the environmental conditions. The nZVI was in low-oxygen concentrations, which prolongs its reactivity. Therefore, nZVI affected the growth of *C. perfringens* more than aerobic bacteria tested in oxic conditions.

Alga *Chlamydomonas* sp. was sensitive to iron-based materials in short-exposure (2h) compared to longer-exposure (24h) based on its multiple endpoints including algal growth rate, membrane integrity, ROS formation and photosynthesis efficiency. The effects on

Chlamydomonas sp. decreased in the order FerMEG12 > Carbo-Iron® > Fe-zeolite > Nano-Goethite. The ecotoxicological experiments were challenged due to various particle properties, namely dark colour, the effect of constituents and a tendency to agglomerate, especially at high concentrations. All particles exhibited the potential to induce significant toxicity at high concentrations (500 mg/L), although such concentrations would rapidly decrease to mg or µg/L in natural aquatic environments, at levels harmless to *Chlamydomonas* sp. The presented findings contribute to the practical use of particle-based nanoremediation.

With planktonic microorganisms in freshwater, nZVI showed stronger effect than mZVI, due to its higher reactivity, which caused a rapid decrease in ORP and dissolved oxygen, and possibly the generation of intracellular ROS, leading to cell damage. nZVI significantly stimulated the growth of cultivable bacteria and iron-oxidising bacteria, but slightly inhibited the growth of algae. Phagotrophic flagellates and ciliates were affected by low dissolved oxygen concentrations, and such conditions released bacteria from grazing pressure and shifted the community from small grazing-resistant prokaryotes to fast-growing opportunists. In support of this hypothesis, nZVI strongly favoured the growth of the facultative anaerobe *Limnohabitans* and other opportunist bacteria that can come to dominate in bacterivore-free treatments, whereas the LD12 cluster and *Verrucomicrobia*, with slow-growing life strategies, were depleted. mZVI caused an unexpectedly positive effect on cyanobacteria, which could be explained by a surplus of iron in its non-toxic form. Further *in-situ* studies that more realistically mimic reservoir conditions could well reveal more information on the influence of ZVI on natural microbial communities, including parts of the microbial food web not covered here, such as heterotrophic flagellates and viruses.

Table 4. Summary of endpoints, microorganisms, materials/particles and results investigated and discussed in this thesis.

Iron-based NMs/NPs	Endpoint(s)	Microorganism(s)	Results	Article No.
nZVI, milled nZVI, nZVI + humic acid	Bacterial growth rate	Gram-positive <i>C. perfringens</i>	No toxicity was observed in the presence of humic acid. The nZVI was more toxic to <i>C. perfringens</i> than the milled Fe particles.	7
APTS- Fe ₃ O ₄ , PEG- Fe ₃ O ₄ , TEOS- Fe ₃ O ₄	(1) Bacterial growth rate (2) Viability (3) <i>E. coli</i> cell length	Gram-negative <i>E. coli</i> and Gram-positive <i>S. aureus</i>	All magnetic materials affected <i>S. aureus</i> and not <i>E. coli</i> , whereas APTS-Fe ₃ O ₄ displayed antibacterial property.	6
OA-Fe ₃ O ₄ , PEI-Fe ₃ O ₄ , PEI-mC-Fe ₃ O ₄	(1) Bacterial growth rate (2) Cell viability (3) <i>S. aureus</i> biofilm formation	Gram-negative <i>E. coli</i> and Gram-positive <i>S. aureus</i>	PEI-Fe ₃ O ₄ was found to be most effective against both <i>S. aureus</i> and <i>E. coli</i> .	5

<p>Fe₃O₄-PNIPAAm-1, Fe₃O₄-PNIPAAm-2, Fe₃O₄-PNIPAAm-3</p>	<p>(1) Bacterial growth rate (2) Cell viability (3) Cell morphology (4) DNA damage</p>	<p>Gram-negative <i>E. coli</i> and Gram-positive <i>S. aureus</i></p>	<p>Fe₃O₄-PNIPAAm caused significant damage to both <i>E. coli</i> and <i>S. aureus</i> DNA and led to a decrease in cell viability. Fe₃O₄-PNIPAAm-1 displayed a stronger antimicrobial effect against both bacterial strains than Fe₃O₄-PNIPAAm-2 and Fe₃O₄-PNIPAAm-3. <i>S. aureus</i> was more sensitive than <i>E. coli</i> to all three magnetic PNIPAAm.</p>	<p>3</p>
<p>Nano-Goethite, Trap-Ox[®] Fe-zeolites, Carbo-Iron[®], Fer- MEG12</p>	<p>Growth rate</p>	<p><i>E. coli</i>, <i>Chlamydomonas</i> sp.</p>	<p>All tested materials, except for FerMEG12 showed no toxicity up to 100 mg/L.</p>	<p>4</p>
<p>FerMEG12, Carbo-Iron[®], Fe-zeolite, Nano-Goethite</p>	<p>(1) Algal growth rate (2) Chlorophyll fluorescence (3) Efficiency of photosystem II (4) Membrane integrity ROS generation</p>	<p><i>Chlamydomonas</i> sp.</p>	<p>Effects on <i>Chlamydomonas</i> sp. decreased in the order FerMEG12 > Carbo-Iron[®]> Fe-zeolite> Nano-Goethite</p>	<p>2</p>

nZVI mZVI	(1) Number of bacteria, cyanobacteria and algae. (2) Diversity of bacterial communities	Phytoplankton microorganisms in freshwater	Both nZVI and mZVI showed negative effects on phytoplankton microorganisms. nZVI stimulated growth bacteria but reduced algal growth. mZVI notably reduced cyanobacterial growth.	1
--------------	--	--	--	---

To summarise, in 2013, I started to research the toxicity of iron-based NMs/NPs, at that time there have been only several publications on the toxicity of iron-based materials/particles, while several more papers mentioned the applications and benefits of iron-based NPs. It was therefore exciting to exploring this relatively new field. During course of my PhD study my research has contributed valuable data on the toxicity of various new iron-based materials as well as other materials on a broad spectrum of microorganisms (Table 5). The latest results of my study of iron-based NMs/NPs have made a significant contribution to field of eco(nano)toxicity, specifically in freshwater.

Table 5. Summary of tasks and outcomes of this thesis.

YEARS	Tasks and outcomes
2013	<ul style="list-style-type: none"> - Setting up the bacterial growth rate method. - Working on Fe₃O₄ materials (group 1).
2014	<ul style="list-style-type: none"> - Improving the method and working on other methods (viability, cell length). - Continuing to work with Fe₃O₄ materials (group 2). - Writing manuscript of Fe₃O₄ (group 1). - Working on ZVI with bacterial growth rate method with aerobic and anaerobic conditions.

<p>2015</p>	<ul style="list-style-type: none"> - Publishing the article on Fe₃O₄ (group 1) (paper 6). - Writing manuscript on Fe₃O₄ (group 2). - Working on Fe₃O₄ materials (group 3). - Passing four exams in PhD study. - Finishing technical report for NanoREM project (paper 7). - Learning flow cytometry in Geneva. - Working on ZVI materials with alga (<i>Chlamydomonas</i> sp.)
<p>2016</p>	<ul style="list-style-type: none"> - Publishing the article on Fe₃O₄ (group 2) (paper 5). - Writing manuscript on Fe₃O₄ materials (group 3). - Writing manuscript on ZVI effect on algae. - Writing manuscript on ZVI effect on bacterial growth rate. - Passing the state exam. - Experiment of ZVI and complex microbial community.
<p>2017</p>	<ul style="list-style-type: none"> - Publishing articles on Fe₃O₄ (group 3) (paper 3) - Publishing articles on ZVI effect on bacterial growth rate of 2014 (paper 4) - Writing manuscript on ZVI and complex microbial community.
<p>2018</p>	<ul style="list-style-type: none"> - Publishing article on ZVI effect on alga (<i>Chlamydomonas</i> sp.) - Publishing article on nZVI and mZVI and complex microbial community. - Writing thesis.

8. References

- Ali, A., Zafar, H., Zia, M., ul Haq, I., Phull, A.R., Ali, J.S., Hussain, A., 2016. Synthesis, characterization, applications, and challenges of iron oxide nanoparticles. *Nanotechnol. Sci. Appl.* 9, 49–67. doi:10.2147/NSA.S99986
- Arakha, M., Pal, S., Samantarrai, D., Panigrahi, T.K., Mallick, B.C., Pramanik, K., Mallick, B., Jha, S., 2015. Antimicrobial activity of iron oxide nanoparticle upon modulation of nanoparticle-bacteria interface. *Sci. Rep.* 5, 1–12. doi:10.1038/srep14813
- Auffan, M., Achouak, W., Rose, J., Roncato, M.-A., Chanéac, C., Waite, D.T., Masion, A., Woicik, J.C., Wiesner, M.R., Bottero, J.-Y., 2008. Relation between the redox state of iron-based nanoparticles and their cytotoxicity toward *Escherichia coli*. *Environ. Sci. Technol.* 42, 6730–6735. doi:10.1021/es800086f
- Barnes, R.J., van der Gast, C.J., Riba, O., Lehtovirta, L.E., Prosser, J.I., Dobson, P.J., Thompson, I.P., 2010. The impact of zero-valent iron nanoparticles on a river water bacterial community. *J. Hazard. Mater.* 184, 73–80. doi:10.1016/j.jhazmat.2010.08.006
- Baselga-Cervera, B., Costas, E., Bustillo-Avenidaño, E., García-Balboa, C., 2016. Adaptation prevents the extinction of *Chlamydomonas reinhardtii* under toxic beryllium. *PeerJ* 4, 1–24. doi:10.7717/peerj.1823
- Bayer, F., 1989. Resistance of bacterial biofilm to antibiotics: a growth-rate related effect? *J. Antimicrob. Chemother.* s3-1, 777–783. doi:10.1136/bmj.s3-1.23.497
- Blaney, L., 2007. Magnetite syntheses from room temperature to 150°C with and without microwaves. *Lehigh Perserve* 15, 33–81. doi:10.1016/j.ceramint.2011.11.027
- Carlos, L., Einschlag, F.S.G., González, M.C., Mártire, D.O., 2013. Applications of magnetite nanoparticles for heavy metal removal from wastewater. *INTECH* 2013, 64–78. doi:http://dx.doi.org/10.5772/54608
- Cheloni, G., Marti, E., Slaveykova, V.I., 2016. Interactive effects of copper oxide nanoparticles and light to green alga *Chlamydomonas reinhardtii*. *Aquat. Toxicol.* 170, 120–128. doi:10.1016/j.aquatox.2015.11.018

- Cotelle, S., Fe, J.F., 1999. Review comet assay in genetic ecotoxicology : A Review. *Environ. Mol. Mutagen.* 255, 246–255.
- Coutris, C., Nguyen, N., Hjorth, R., 2015. Environmental impact of reactive nanoparticles - Dose reponse relationships , matrix effects on ecotox taking nanotechnological remediation processes from lab scale to end user applications dose reponse relationships , matrix effects on ecotox. *Tech. Rep.* 1–43.
- Darwish, M.S.A., Nguyen, N.H.A., Ševcu, A., Stibor, I., 2015. Functionalized magnetic nanoparticles and their effect on escherichia coli and *Staphylococcus aureus*. *J. Nanomater.* 2015, 1–10. doi:org/10.1155/2015/416012
- Darwish, M.S.A., Nguyen, N.H.A., Ševců, A., Stibor, I., Stoyan K. Smoukov, 2016. Dual-modality self-heating and antibacterial polymer-coated nanoparticles for magnetic hyperthermia. *Mater. Sci. Eng. C* 63, 88–95. doi:10.1016/j.msec.2016.02.052
- Diao, M., Yao, M., 2009. Use of zero-valent iron nanoparticles in inactivating microbes. *Water Res.* 43, 5243–5251. doi:10.1016/j.watres.2009.08.051
- El-Temsah, Y.S., Joner, E.J., 2012. Ecotoxicological effects on earthworms of fresh and aged nano-sized zero-valent iron (nZVI) in soil. *Chemosphere* 89, 76–82. doi:10.1016/j.chemosphere.2012.04.020
- El-Temsah, Y.S., Sevcu, A., Bobcikova, K., Cernik, M., Joner, E.J., 2016. DDT degradation efficiency and ecotoxicological effects of two types of nano-sized zero-valent iron (nZVI) in water and soil. *Chemosphere* 144, 2221–2228. doi:10.1016/j.chemosphere.2015.10.122
- Fajardo, C., Ortíz, L.T., Rodríguez-Membibre, M.L., Nande, M., Lobo, M.C., Martin, M., 2012. Assessing the impact of zero-valent iron (ZVI) nanotechnology on soil microbial structure and functionality: A molecular approach. *Chemosphere* 86, 802–808. doi:10.1016/j.chemosphere.2011.11.041
- Fajardo, C., Saccà, M.L., Martinez-Gomariz, M., Costa, G., Nande, M., Martin, M., 2013. Transcriptional and proteomic stress responses of a soil bacterium bacillus cereus to nanosized zero-valent iron (nZVI) particles. *Chemosphere* 93, 1077–1083. doi:10.1016/j.chemosphere.2013.05.082
- Gaharwar, U.S., Paulraj, R., 2015. Iron oxide nanoparticles induced oxidative damage in peripheral blood cells of rat. *Biomed. Sci. Eng.* 8, 274–286.

- Gerloff-Elias, A., Spijkerman, E., Pröschold, T., 2005. Effect of external pH on the growth, photosynthesis and photosynthetic electron transport of *Chlamydomonas acidophila* Negoro, isolated from an extremely acidic lake (pH 2.6). *Plant, Cell Environ.* 28, 1218–1229. doi:10.1111/j.1365-3040.2005.01357.x
- Ghosh, M., J, M., Sinha, S., Chakraborty, A., Mallick, S.K., Bandyopadhyay, M., Mukherjee, A., 2012. In vitro and in vivo genotoxicity of silver nanoparticles. *Mutat. Res. - Genet. Toxicol. Environ. Mutagen.* 749, 60–69. doi:10.1016/j.mrgentox.2012.08.007
- Guillard, R.R.L., J.Lorenzen, C., 1972. Yellow-green algae with chlorophyllid C. *J. Phycol.*
- Hjorth, R., Coutris, C., Nguyen, N., Sevcu, A., Baun, A., Joner, E., 2017. Ecotoxicity testing and environmental risk assessment of iron nanomaterials for sub-surface remediation – Recommendations from the FP7 project NanoRem. *Chemosphere* 182, 525–531. doi:10.1016/j.chemosphere.2017.05.060
- Iconaru, S.L., Prodan, A.M., Le Coustumer, P., Predoi, D., 2013. Synthesis and antibacterial and antibiofilm activity of iron oxide glycerol nanoparticles obtained by coprecipitation method. *J. Chem.* 2013, 1–6. doi:10.1155/2013/412079
- Ismail, R.A., Sulaiman, G.M., Abdulrahman, S.A., Marzoog, T.R., 2015. Antibacterial activity of magnetic iron oxide nanoparticles synthesized by laser ablation in liquid. *Mater. Sci. Eng. C* 53, 286–297. doi:10.1016/j.msec.2015.04.047
- Jiang, C., Xu, X., Megharaj, M., Naidu, R., Chen, Z., 2015. Inhibition or promotion of biodegradation of nitrate by *Paracoccus* sp. in the presence of nanoscale zero-valent iron. *Sci. Total Environ.* 530–531, 241–246. doi:10.1016/j.scitotenv.2015.05.044
- Jung, S.-K., Qu, X., Aleman-Meza, B., Wang, T., Celeste, R., Zheng, L., Zhong, W., 2013. A multi-endpoint, high-throughput study of nanomaterial toxicity in *Caenorhabditis elegans*. *Environ. Sci. Technol.* 31, 1713–1723. doi:10.1109/TMI.2012.2196707.Separate
- Karlsson, H.L., 2010. The comet assay in nanotoxicology research. *Anal. Bioanal. Chem.* 398, 651–666. doi:10.1007/s00216-010-3977-0
- Keller, A.A., Garner, K., Miller, R.J., Lenihan, H.S., 2012. Toxicity of nano-zero valent iron to freshwater and marine organisms. *PLoS One* 7, 1–10. doi:10.1371/journal.pone.0043983
- Kim, J.Y., Park, H.J., Lee, C., Nelson, K.L., Sedlak, D.L., Yoon, J., 2010. Inactivation of *Escherichia coli* by nanoparticulate zerovalent iron and ferrous ion. *Appl. Environ. Microbiol.*

76, 7668–7670. doi:10.1128/AEM.01009-10

- Kirschling, T.L., Gregory, K.B., Minkley, E.G., Lowry, G. V., Tilton, R.D., 2010. Impact of nanoscale zero valent iron on geochemistry and microbial populations in trichloroethylene contaminated aquifer materials. *Environ. Sci. Technol.* 44, 3474–3480. doi:10.1021/es903744f
- Kocur, C.M.D., 2015. Field scale application of nanoscale zero valent iron: mobility, contaminant degradation, and impact on microbial communities. *Electron. Thesis Diss. Repos.* 3068, 1–300.
- Kocur, C.M.D., Lomheim, L., Molenda, O., Weber, K.P., Austrins, L.M., Sleep, B.E., Boparai, H.K., Edwards, E.A., O’Carroll, D.M., 2016. Long-term field study of microbial community and dechlorinating activity following carboxymethyl cellulose-stabilized nanoscale zero-valent iron injection. *Environ. Sci. Technol.* 50, 7658–7670. doi:10.1021/acs.est.6b01745
- Lefevre, E., Bossa, N., Wiesner, M.R., Gunsch, C.K., 2015. A review of the environmental implications of in situ remediation by nanoscale zero valent iron (nZVI): Behavior, transport and impacts on microbial communities. *Sci. Total Environ.* 565, 889–901. doi:10.1016/j.scitotenv.2016.02.003
- Lei, C., Zhang, L., Yang, K., Zhu, L., Lin, D., 2016. Toxicity of iron-based nanoparticles to green algae: Effects of particle size, crystal phase, oxidation state and environmental aging. *Environ. Pollut.* 218, 505–512. doi:10.1016/j.envpol.2016.07.030
- Li, L., Fan, M., Brown, R.C., Van Leeuwen, J., Wang, J., Wang, W., Song, Y., Zhang, P., 2006. Synthesis, properties, and environmental applications of nanoscale iron-based materials: A review. *Crit. Rev. Environ. Sci. Technol.* 36, 405–431. doi:10.1080/10643380600620387
- Liu, G., Gao, J., Ai, H., Chen, X., 2013. Applications and potential toxicity of magnetic iron oxide nanoparticles. *Small* 9, 1533–1545. doi:10.1002/sml.201201531
- Lowry, G. V., Gregory, K.B., Apte, S.C., Lead, J.R., 2012. Transformations of nanomaterials in the environment. *Environ. Sci. Technol.* 46, 6893–6899. doi:10.1021/es300839e
- Mah, T.C., Toole, G.A.O., 2001. Mechanisms of biofilm resistance to antimicrobial agents. *Trends Microbiol.* 9, 34–39.
- Mahdavi, M., Ahmad, M. Bin, Haron, M.J., Namvar, F., Nadi, B., Ab Rahman, M.Z., Amin, J., 2013. Synthesis, surface modification and characterisation of biocompatible magnetic iron oxide nanoparticles for biomedical applications. *Molecules* 18, 7533–7548. doi:10.3390/molecules18077533

- Melegari, S.P., Perreault, F., Costa, R.H.R., Popovic, R., Matias, W.G., 2013. Evaluation of toxicity and oxidative stress induced by copper oxide nanoparticles in the green alga *Chlamydomonas reinhardtii*. *Aquat. Toxicol.* 142–143, 431–440. doi:10.1016/j.aquatox.2013.09.015
- Mohammed, L., Gomaa, H.G., Ragab, D., Zhu, J., 2017. Magnetic nanoparticles for environmental and biomedical applications: A review. *Particuology* 30, 1–14. doi:10.1016/j.partic.2016.06.001
- Mueller, N.C., Braun, J., Bruns, J., Černík, M., Rissing, P., Rickerby, D., Nowack, B., 2012. Application of nanoscale zero valent iron (NZVI) for groundwater remediation in Europe. *Environ. Sci. Pollut. Res.* 19, 550–558. doi:10.1007/s11356-011-0576-3
- Naik, S.K., Mohanty, S., Padhi, A., Pati, R., Sonawane, A., 2014. Evaluation of antibacterial and cytotoxic activity of *Artemisia nilagirica* and *Murraya koenigii* leaf extracts against mycobacteria and macrophages. *BMC Complement. Altern. Med.* 14, 87. doi:10.1186/1472-6882-14-87
- Němeček, J., Pokorný, P., Lhotský, O., Knytl, V., Najmanová, P., Steinová, J., Černík, M., Filipová, A., Filip, J., Cajthaml, T., 2015. Combined nano-biotechnology for in-situ remediation of mixed contamination of groundwater by hexavalent chromium and chlorinated solvents. *Sci. Total Environ.* 563–564, 822–834. doi:10.1016/j.scitotenv.2016.01.019
- Nguyen, N.H.A., Darwish, M.S.A., Stibor, I., Kejzlar, P., Ševců, A., 2017. Magnetic Poly(N-isopropylacrylamide) nanocomposites: Effect of preparation method on antibacterial properties. *Nanoscale Res. Lett.* 12, 571. doi:10.1186/s11671-017-2341-0
- Nguyen, N.H.A., Roman, S., Kasalicky, V., Ribas, D., Vlkova, D., Rehakova, H., Kejzlar, P., Sevcu, A., 2018a. Different effects of nano-scale and micro-scale zero-valent iron particles on planktonic microorganisms from natural reservoir water. *Environ. Sci. Nano* Accepted.
- Nguyen, N.H.A., Von Moos, N.R., Slaveykova, V.I., Mackenzie, K., Meckenstock, R.U., Thümmler, S., Bosch, J., Ševců, A., 2018b. Biological effects of four iron-containing nanoremediation materials on the green alga *Chlamydomonas* sp. *Ecotoxicol. Environ. Saf.* 154, 36–44. doi:10.1016/j.ecoenv.2018.02.027
- Omidkhoda, A., Mozdarani, H., Movasaghpoor, A., Fatholah, A.A.P., 2007. Study of apoptosis in labeled mesenchymal stem cells with superparamagnetic iron oxide using neutral comet assay. *Toxicol. In Vitro* 21, 1191–1196. doi:10.1016/j.tiv.2007.03.010
- Oukarroum, A., Polchtchikov, S., Perreault, F., Popovic, R., 2012. Temperature influence on silver

- nanoparticles inhibitory effect on photosystem II photochemistry in two green algae, *Chlorella vulgaris* and *Dunaliella tertiolecta*. *Environ. Sci. Pollut. Res.* 19, 1755–1762. doi:10.1007/s11356-011-0689-8
- Phenrat, T., Long, T.C., Lowry, G. V., Veronesi, B., 2009. Partial oxidation (“Aging”) and surface modification decrease the toxicity of nanosized zerovalent Iron. *Environ. Sci. Technol.* 43, 195–200. doi:10.1021/es801955n
- Prabhu, Y.T., Rao, K.V., Kumari, B.S., Kumar, V.S.S., Pavani, T., 2015. Synthesis of Fe₃O₄ nanoparticles and its antibacterial application. *Int. Nano Lett.* 5, 85–92. doi:10.1007/s40089-015-0141-z
- Ralph, P.J., Smith, R.A., MacInnis-Ng, C.M.O., Seery, C.R., 2007. Use of fluorescence-based ecotoxicological bioassays in monitoring toxicants and pollution in aquatic systems: Review. *Toxicol. Environ. Chem.* 89, 589–607. doi:10.1080/02772240701561593
- Ribas, D., Cernik, M., Martí, V., Benito, J.A., 2016. Improvements in nanoscale zero-valent iron production by milling through the addition of alumina. *J. Nanoparticle Res.* 18, 181–192. doi:10.1007/s11051-016-3490-2
- Saccà, M.L., Fajardo, C., Nande, M., Martín, M., 2013. Effects of nano zero-valent iron on *Klebsiella oxytoca* and stress response. *Microb. Ecol.* 66, 806–812. doi:10.1007/s00248-013-0269-1
- Semerád, J., Cajthaml, T., 2016. Ecotoxicity and environmental safety related to nano-scale zerovalent iron remediation applications. *Appl. Microbiol. Biotechnol.* 100, 9809–9819. doi:10.1007/s00253-016-7901-1
- Ševců, A., El-Temsah, Y.S., Filip, J., Joner, E.J., Bobčíková, K., Černík, M., 2017. Zero-valent iron particles for PCB degradation and an evaluation of their effects on bacteria, plants, and soil organisms. *Environ. Sci. Pollut. Res.* 24, 21191–21202. doi:10.1007/s11356-017-9699-5
- Ševců, A., El-Temsah, Y.S., Joner, E.J., Černík, M., 2011. Oxidative stress induced in microorganisms by zero-valent iron nanoparticles. *Microbes Environ.* 26, 271–281. doi:10.1264/jsme2.ME11126
- Sørensen, S.N., Engelbrekt, C., Lützhøft, H.H., Jiménez-Lamana, J., Noori, J.S., Alatrakch, F.A., Delgado, C.G., Slaveykova, V.I., Baun, A., 2016. A multi-method approach for disclosing algal toxicity of platinum nanoparticles. *Environ. Sci. Technol.* 19, 10635–10643. doi:10.1021/acs.est.6b01072

- Tilston, E.L., Collins, C.D., Mitchell, G.R., Princivalle, J., Shaw, L.J., 2013. Nanoscale zerovalent iron alters soil bacterial community structure and inhibits chloroaromatic biodegradation potential in Aroclor 1242-contaminated soil. *Environ. Pollut.* 173, 38–46. doi:10.1016/j.envpol.2012.09.018
- von Moos, N., Maillard, L., Slaveykova, V.I., 2015. Dynamics of sub-lethal effects of nano-CuO on the microalga *Chlamydomonas reinhardtii* during short-term exposure. *Aquat. Toxicol.* 161, 267–275. doi:10.1016/j.aquatox.2015.02.010
- Wacławek, S., Chronopoulou, L., Papini, M.P., V.T.P, V., Palocci, C., Kupčík, J., Černík, M., 2017. Enhancement of stability and reactivity of nanosized zero-valent iron with polyhydroxybutyrate. *Desalin. Water Treat.* 69, 302–307. doi:10.5004/dwt.2017.0704
- Yan, W., Lien, H.-L., Koel, B.E., Zhang, W., 2013. Iron nanoparticles for environmental clean-up: recent developments and future outlook. *Environ. Sci. Process. Impacts* 15, 63–77. doi:10.1039/c2em30691c